I. Synthetic Progress Towards the Total Synthesis of Rhodojaponin III
II. Design and Synthesis of Novel ENT Inhibitors

by

Caroline Grace Webster

Department of Chemistry
Duke University

Date:_____
Approved:

_____
Jiyong Hong, Supervisor

_____
Steven W. Baldwin

_____
Cynthia Kuhn

_____
Qiu Wang

Dissertation submitted in partial fulfillment of
the requirements for the degree of Doctor
of Philosophy in the Department of
Chemistry in the Graduate School
of Duke University

2022

ABSTRACT

I. Synthetic Progress Towards the Total Synthesis of Rhodojaponin III
II. Design and Synthesis of Novel ENT Inhibitors

by

Caroline Grace Webster

Department of Chemistry
Duke University

Date:_____
Approved:

_____
Jiyong Hong, Supervisor

_____
Steven W. Baldwin

_____
Cynthia Kuhn

_____
Qiu Wang

An abstract of a dissertation submitted in partial
fulfillment of the requirements for the degree
of Doctor of Philosophy in the Department of
Chemistry in the Graduate School of
Duke University

2022

Copyright by
Caroline Webster
2022

Abstract

Affecting 1 in 5 Americans, chronic pain has become the most common reason individuals seek out medical care. Those suffering from daily pain often endure mobile restrictions, anxiety, depression, and an overall reduced quality of life. Currently, pain management relies heavily on non-steroidal anti-inflammatory drugs (NSAIDs) and opioid analgesics, but these options only provide relief for ~25% of patients. Opioids, which are considered the most effective at relieving pain, are associated with very serious side effects such as addiction, dependence, and tolerance. As a result of their addictive properties, we now face an epidemic of opioid overdose. Since 1999 the number of deaths resulting from opioid overdose has steadily increased with ~70,000 deaths in 2020. Consequently, the discovery of safe, effective, and non-addictive analgesics is imperative to end this epidemic and treat those suffering from daily pain.

As natural products have had a long-standing role in the identification of bioactive compounds for drug development, they may provide an excellent starting point for the development of non-opioid analgesics. Grayanane-type natural products are diterpenoids extracted from the plants of the Ericaceae family. They exhibit a unique 5/7/6/5 ring system and a wide variety of bioactivities. Among them, rhodojaponin III has recently been reported to possess potent analgesic activity in an acute, inflammatory, and diabetic neuropathic pain model. Notably, rhodojaponin III does not affect the endogenous opioid peptidergic system but it's mechanism of action has yet to be established. As the total synthesis of rhodojaponin III has yet to be reported, we aim

to develop an efficient route to access rhodojaponin III for further development as an analgesic and a chemical probe for mechanistic studies.

Our synthetic strategy relies on a convergent approach in which two fragments are synthesized separately and then coupled together to provide the skeleton of grayanane-type natural products. Herein, the synthesis of the two fragments will be discussed with an emphasis on the enantioselective construction of the key bicyclo[3.2.1]octane fragment. Synthesis of the bicycle is centered around a copper(I)-mediated conjugate addition to a shielded enoate, cyclization of an alkynyl ketone via Mn(III)-mediated radical cyclization and a stereoselective ketone reduction with SmI_2.

In addition to natural product synthesis, our efforts towards the development of non-opioid analgesics includes the structure-guided design of adenosine reuptake inhibitors (AdoRIs). The analgesic effect of adenosine has gained recent attraction as an alternative approach for pain-relief. One tactic for increasing extracellular adenosine is to inhibit the intracellular transport by equilibrative nucleoside transporters (ENTs). Consequently, our work takes advantage of the co-crystal structure of hENT1 in complex with two known inhibitors, dilazep and NBMPR, to rationally design novel inhibitors with improved potency, selectivity, and pharmacological properties. Herein, the generation of a small library of hENT1 inhibitors with promising analgesic activity in a streptozotocin (STZ) induced diabetic neuropathic pain model will be reviewed. Additionally, the design and synthetic progress towards a macrocyclic inhibitor and hENT3 selective compounds will be discussed.

Contents

Abstract iv

List of Tables ix

List of Figures x

Acknowledgements xiii

1. Introduction 2

1.1 Pain Prevalence and the Opioid Overdose Crisis 2

2. Synthetic Progress Towards the Total Synthesis of Rhodojaponin III 8

2.1 Introduction 8

2.1.1 Grayanane-type Natural Products 8

2.1.2 Isolation and Analgesic Activity of Rhodojaponin III 11

2.1.3 Synthesis of Structurally Related Diterpenoids 16

2.1.3.1 Total Synthesis of (−)- Grayanotoxin III 16

2.1.3.2 Highly Functionalized B-homo-C-nor Grayanotoxin 19

2.1.3.3 Synthetic Approach towards Pierisformaside C 20

2.1.3.4 Total Synthesis of Principinol D 22

2.1.3.4 Total Syntheses of Rhodomolleins XX and XXII 25

2.1.3.4 Total Synthesis of Glaucocalyxin A 28

2.1.3.4 Luo's Total Syntheses of Grayanane Diterpenoids 30

2.2 Results and Discussion 32

2.2.1 Retrosynthetic Analysis 32

2.2.2 Synthesis of the 5-membered Ring Fragment 34

2.2.3 Formation of the Bicyclo[3.2.1]octane Fragment 36

2.2.3.1 Formation of the Alkynyl Ketone Substrate 36

2.2.3.2 Conia-ene Type Cyclizations 37

2.2.3.3 Mn(III)-mediated Radical Cyclization 44

2.2.4 Formation of the Equatorial Alcohol 46

2.2.4.1 PMB Protected γ-hydroxyl Ketone 46

2.2.4.2 *β*-keto Ester Substrate 49

2.2.4.3 *β*-hydroxy Ketone 55

2.2.5 Enantioselective Synthesis of the Bicyclo[3.2.1]octane Fragment 57

2.2.5.1 Asymmetric Conjugate Addition with Maduit-type Ligand 57

2.2.5.2 Rhodium Catalyzed Conjugate Addition 60

2.2.5.3 ACA with Helmchen's Auxiliary 62

2.3 Conclusion 65

2.4 Experimental 66

3. Design and Synthesis of Novel ENT Inhibitors 89

3.1 Introduction 89

3.1.1 Equilibrative Nucleoside Transporters 89

3.2 Results and Discussion 100

3.2.1 Development of Novel ENT1 Inhibitors 100

3.2.1.1 Hybrid Analog Design 100

3.2.1.2 JH-ENT-01 Synthesis and Bioactivity 102

3.2.1.3 Design and Synthesis of ENT1 Inhibitor Library 105

3.2.2 Efforts Towards a Macrocyclic ENT Inhibitor 118

3.2.2.1 Macrocyclic Design 118

3.2.2.2 First Approach Towards Macrocyclization 121

3.2.2.3 Second Approach Towards Macrocyclization.....127

3.2.2.4 Third Approach Towards Macrocyclization 131

3.2.3 Design and Synthesis of ENT3 Selective Inhibitors 134

3.2.3.1 Design of ENT3 Selective Inhibitors 134

3.2.3.2 Synthesis of ENT3 Selective Inhibitors.....137

3.3 Conclusion.....141

3.4 Experimental.....142

4. Conclusion 173

Appendix A. Spectral Data for Chapter 2 176

Appendix B. Spectral Data for Chapter 3 192

References 211

Biography.....219

List of Tables

Table 1. Gold-catalyzed Conia-ene cyclization 41

Table 2. Gold-catalyzed conia-ene cyclization of TMS-protected alkyne.....43

Table 3. Direct reduction of PMB protected γ-hydroxyl ketone.....46

Table 4. SmI_2 reduction of *β*-keto ester substrate 51

Table 5. Direct reduction of *β*-keto ester substrate 54

Table 6. Inversion of *β*-keto ester substrate.....55

Table 7. Attempts to invert *β*-hydroxy ketone 57

Table 8. Asymmetric conjugate addition attempts 59

Table 9. Attempts at rhodium catalyzed conjugate addition 61

Table 10. Removal of Helmchen's chiral auxiliary.....64

Table 11. Equilibrative Nucleoside Transporter Family. Adapted from ref 54 91

Table 12. Attempts towards cyclization with Grubbs II 127

Table 13. CM attempts with 3.072 and 3.058.....128

Table 14. Attempts for oxidation of 3.103.....133

Table 15. Iodopyridine coupling conditions.....138

Table 16. Imidazole coupling conditions.....139

Table 17. Methoxy deprotection attempts.....140

List of Figures

Figure 1. Pain pathway involving transduction, transmission, perception, and modulation. Figure adapted from ref 3. 3

Figure 2. Selected analgesic therapeutics 4

Figure 3. National overdose death involving any opioids. Figure adapted from ref 9. 6

Figure 4. Natural product derived therapeutics 8

Figure 5. Biosynthetic pathway of grayanane-type & related diterpenoids. Figure adapted from ref 17 9

Figure 6. Grayanoid-Activity Relationship Data. Figure adapted from ref 17. 11

Figure 7. Grayanane-type diterpenoids extracted from the roots of *Rhododendron molle.* Figure adapted from ref 19. 12

Figure 8. Analgesic activity of extracted diterpenoids. 13

Figure 9. Further evaluation of rhodojaponin III & VI analgesic activity. 14

Figure 10. X-ray crystallographic data of 2.162 37

Figure 11. Conia-ene cyclization. 37

Figure 12. ^{1}HNMR ($CDCl_3$, 500 MHz) of 6-*endo-dig* product 2.179 42

Figure 13. ^{1}H NMR ($CDCl_3$, 500 MHz) of 5-*exo-dig* product 2.197 46

Figure 14. Stereochemical model of 2.198 and 2.199 47

Figure 15. ^{1}H-NMR ($CDCl_3$, 500 MHz) spectrum of axial alcohol 2.199 48

Figure 16. ^{1}H-NMR ($CDCl_3$, 500 MHz) spectrum of axial alcohol 2.212 52

Figure 17. ^{1}H-NMR ($CDCl_3$, 500 MHz) spectrum of equatorial alcohol 2.211 53

Figure 18. HPLC data for ACA reaction. (Top) racemic (bottom) attempt with maduit-type ligand 60

Figure 19. Examples of purine and pyrimidine-based nucleosides 90

Figure 20. Antiviral and antineoplastic nucleoside analog therapeutics. Figure adapted from ref 58 92

Figure 21. Selected ENT1 Inhibitors 93

Figure 22. Analgesic effect of AR receptor activation. Figure adapted from ref. 59 94

Figure 23. AR activation by ENT inhibition. Figure adapted from ref 62. 95

Figure 24. A) Co-crystal structure of hENT1 in complex with dilazep and NBMPR. B) 6 + 5 structural topology of hENT1. Figure reprinted with permission from ref 69. 97

Figure 25. Dilazep and NBMPR binding sites within ENT1 binding pocket. Figure reprinted with permission from ref 69. 98

Figure 26. Dilazep and NBMPR bound hENT1. Figure reprinted with permission from ref 69. 99

Figure 27. Hybrid analog design for ENT1 inhibitors 101

Figure 28. Cold-competition Scintillation Proximity Assay (SPA) 104

Figure 29. Overlay of JH-ENT-01's (white) binding pose with dilazep (left) and NBMPR (right) 105

Figure 30. ENT1 inhibitor library 106

Figure 31. Cold-competition SPA for JH-ENT-01, 02 & 03 114

Figure 32. Analgesic activity of JH-ENT-01 to 07 115

Figure 33. Further analysis of JH-ENT-01 & 07. A) experimental design B) mechanical pain C) mechanical allodynia D) cold related pain 116

Figure 34. Rotarod test for motor function assessment 117

Figure 35. Evaluation of JH-ENT-07 binding pose. NBMPR (white)/JH-ENT-07 (pink) 118

Figure 36. Docking result for the macrocyclic design. dilazep (yellow) macrocycle (green) 119

Figure 37. ^{1}H NMR ($CDCl_3$, 500 MHz) of racemic Mosher ester 124

Figure 38. ^{1}H NMR ($CDCl_3$, 500 MHz) of Mosher esters 3.068 & 3.069 125

Figure 39. Overlay of ENT1 and ENT3 binding pockets 135

Figure 40. Key binding interactions of candidate 1 and 2 136

Acknowledgements

I would like to express my sincerest gratitude towards my research advisor, Professor Jiyong Hong for his consistent support and helpful advice. Working under his guidance has been a wonderful experience and one that has helped me grow as a person and a scientist. Additionally, to my committee members, Professor Steven W. Baldwin, Professor Cynthia Kuhn and Professor Qiu Wang for their insightful academic feedback.

I would like to thank current and past lab members, Yunju Oh, Hyejin Lee, Yiquan Zhao, Patrick Dome, Amanda Ennis, Dr. Hongjun Jang, Dr. Pyeongwa Jeong, Dr. Won Young Lim, Dr. Iljin Shin, Dr. Seung-hwa Kwak, Dr. Hyunji Lee, and Dr. Hyeri Park for their support, advice and most importantly, friendship. I would also like to thank the departmental instrument staff, Dr. Peter Silinski and Dr. Benjamin Bobay for their assistance in Mass spectrometry and NMR experiments. Lastly, to my family whom I can not thank enough for their unconditional love, support, and encouragement.

1. Introduction

1.1 Pain Prevalence and the Opioid Overdose Crisis

In 1994, the International Association for the study of Pain (IASP) defined pain as "an unpleasant sensory and emotional experience associated with actual or potential tissue damage or described in terms of such damage."[1] Although pain is subjective and can be caused by a variety of stimuli, the mechanism for detection and perception follows a consistent path. Put simply, the pain mechanism involves four major processes: transduction, transmission, perception, and modulation (Figure 1).[2]

When a painful stimulus (mechanical, heat or chemical) causes damage to the peripheral tissue, inflammatory mediators such as substance P, serotonin, bradykinin, prostaglandins, and others, sensitize primary afferent nociceptors (transduction). The signal is then transmitted from the periphery to the central nervous system through the dorsal root ganglia, up the spinal cord to the brain stem and thalamus. Finally, the signal reaches the somatosensory cortex, and the painful stimuli is perceived. Perception is subjective as it integrates many sensory messages and is influenced by attention, expectation, and interpretation. Lastly, modulation refers to the process by which transmission of the pain signal is reduced by the release of neurotransmitters such as

opioid peptides, norepinephrine, glycine, or GABA.[2, 3]

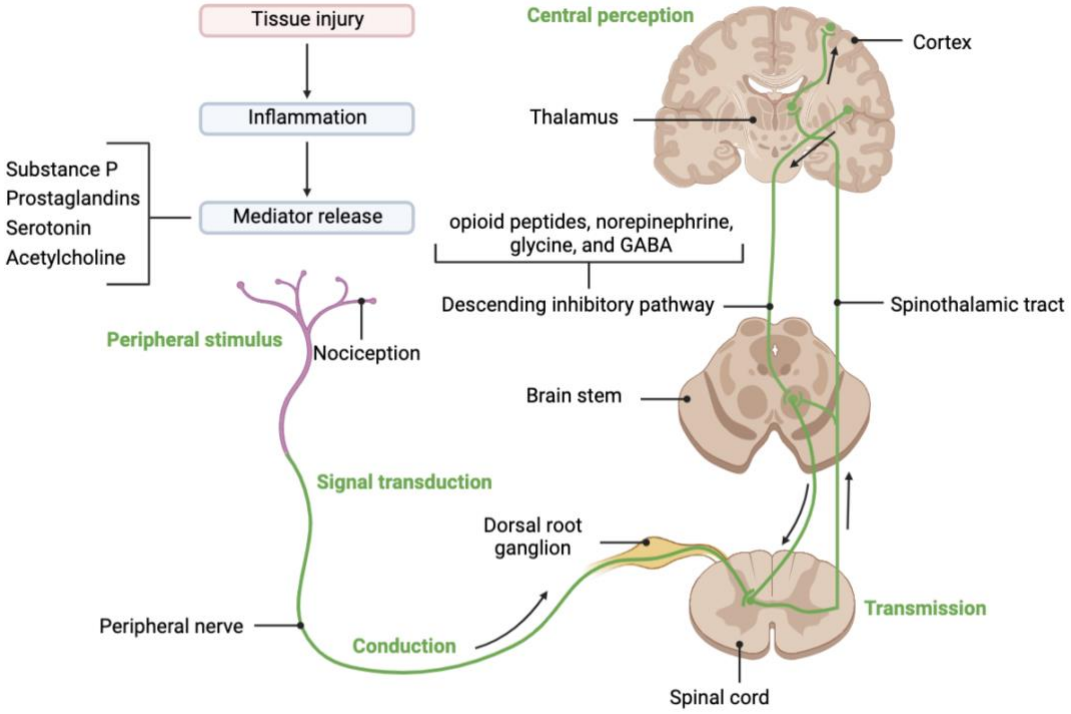

Figure 1. Pain pathway involving transduction, transmission, perception, and modulation. Figure adapted from ref 3.

Pain is broadly classified under two categories, acute or chronic. Acute pain is a physiological response to noxious stimuli (i.e., laceration or broken bone), typically at a well-defined location, and although it can be quite severe, it recedes relatively quickly. Whereas chronic pain generally exceeds 3 months and does not resolve with treatment and/or normal tissue healing.[4] Chronic pain can further be classified by the source of pain including, nociceptive, neuropathic, visceral, or mixed pain.[5]

Chronic pain affects roughly 1 in 5 Americans and has become the most common reason individuals seek out medical care.[4] Patients with chronic pain often suffer from

mobile restrictions, anxiety, depression, and an overall reduced quality of life.[6] Pain management options rely heavily on analgesic therapeutics such as non-narcotic analgesics, non-steroidal anti-inflammatory drugs (NSAIDS) and narcotics (opioids), with ~65% of the total market share attributable to NSAIDs and opioids.[5] Examples of analgesics therapeutics are depicted in Figure 2. Disappointingly, ~25% of patients with daily pain find relief from these therapeutic treatments.[5]

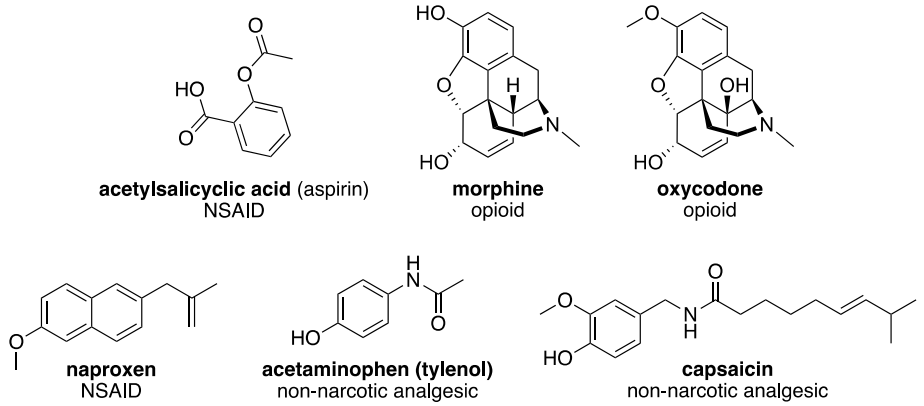

Figure 2. Selected analgesic therapeutics

Mechanistically, NSAIDs reduce inflammation by inhibiting the cyclooxygenase isoenzymes COX1 and COX2 from converting arachidonic acid to prostaglandins, which are key mediators in promoting signal transduction. While NSAIDs provide relief for many patients, serious side effects such as gastrointestinal bleeding and cardiovascular risks make them unsuitable for some and preclude them from long-term use.[7] Contrastingly, opioids produce an analgesic effect by preventing the release of neurotransmitters such as substance P, glutamate, and calcitonin gene-related peptide (CGRP) in the dorsal horn of the spinal cord, which prevents transmission of the pain

impulse to the brain stem. Although opioids are considered most effective for relieving pain, they too are accompanied by very serious side effects such as addiction, dependence, and tolerance.[8]

As a result of their addictive properties, we now face an epidemic of opioid overdose. As seen in Figure 3, since 1999 the number of deaths resulting from opioid overdose has steadily increased with ~70,000 deaths in 2020.[9] This has also placed a huge economic burden on society with an estimated $1.02 trillion spent in 2017 on costs for opioid use disorder and fatal opioid overdose.[10] Ongoing efforts to combat this crisis include an initiative launched by NIH in 2018 termed "Helping to End Addiction Long-term (HEAL)" in order to aid in scientific research for preventing opioid misuse and addiction and enhance pain management.[11] Additionally, the CDC's "Overdose Data to Action (OD2A)" program is working to identify outbreaks, collect data, respond to overdoses, provide care, and increase public awareness.[12] Importantly, significant research efforts are being made towards analgesics with novel strategies such as targeting ion channels, enzymes, and G-protein-coupled receptors (GPCRs).[13]

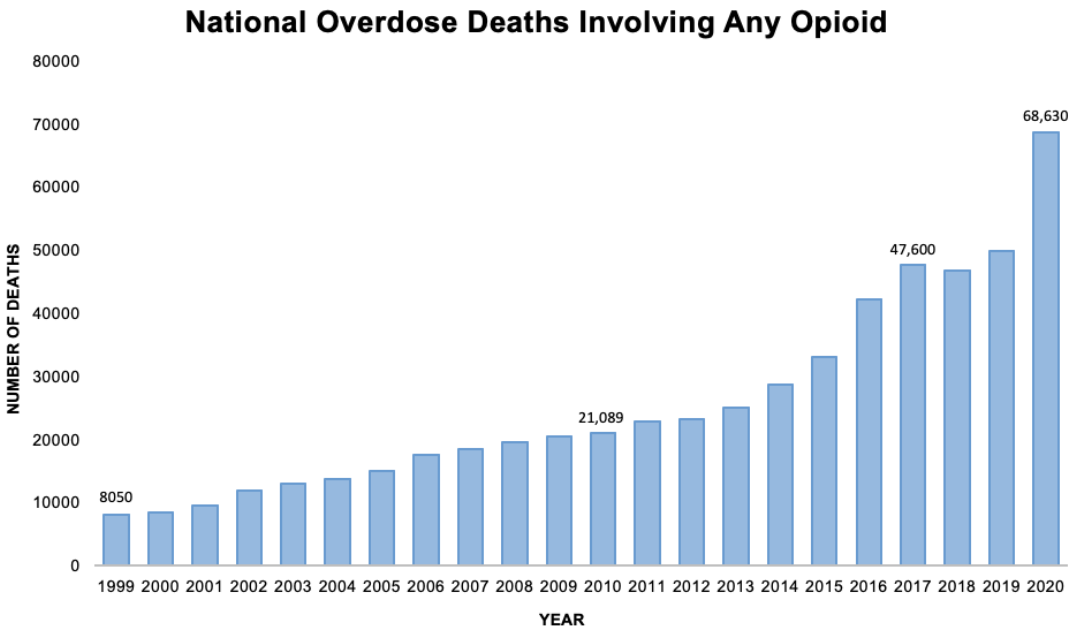

Figure 3. National overdose death involving any opioids. Figure adapted from ref 9.

Although considerable efforts have been made to overcome the opioid overdose crisis, identifying safe, effective, and non-addictive analgesics is paramount to end this epidemic and treat those suffering from daily pain. In this regard, the focus of this dissertation will be on the development of analgesic compounds for the development of non-opioid therapeutics. In the second chapter, our efforts towards the total synthesis of rhodojaponin III, a grayanane-type natural product with potent antinociceptive properties will be discussed. Our synthetic strategy is based on a convergent approach that relies on the enantioselective construction of a key bicyclo[3.2.1]octane fragment, which will be the primary goal of this chapter. The third chapter describes the role of equilibrative nucleoside transporters (ENTs) in analgesia and our progress towards the

rational design and synthesis of ENT inhibitors with promising activity in a streptozotocin (STZ)-induced diabetic neuropathic pain model.

2. Synthetic Progress Towards the Total Synthesis of Rhodojaponin III

2.1 Introduction

2.1.1 Grayanane-type Natural Products

Natural products (NPs) have a long-standing role in medicine; dating back to 2600 B.C. Mesopotamia where oils from *Cupressus sempervirens* (Cypress) and *Commiphora* (myrrh) were used to treat coughs, colds, and inflammation. NPs are secondary metabolites that are uniquely produced by an organism as an adaptation to the surrounding environment and are generally not essential for growth, development, or reproduction.[14] They have immense scaffold diversity, structural complexity, and are 'optimized' to serve a biological function, which makes them advantageous in the drug discovery process.[15]

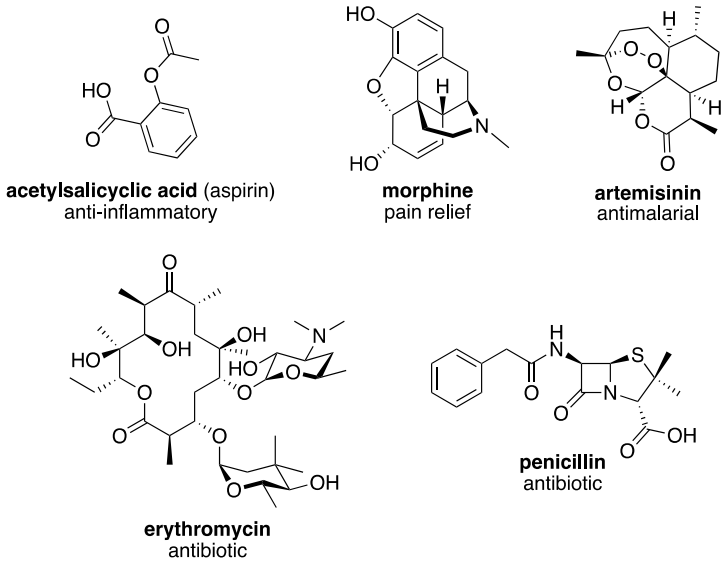

Figure 4. Natural product derived therapeutics

In addition to traditional herbal remedies, NPs and NP-derived compounds have had a key contribution in FDA approved drugs from 1981 to 2019, having key roles in cancer, infectious disease, cardiovascular disease, and multiple sclerosis therapeutics, including many widely recognized drugs (Figure 4).[16] As many novel NPs continue to be isolated and characterized with potent biological activity, NPs maintain a promising role in drug development.

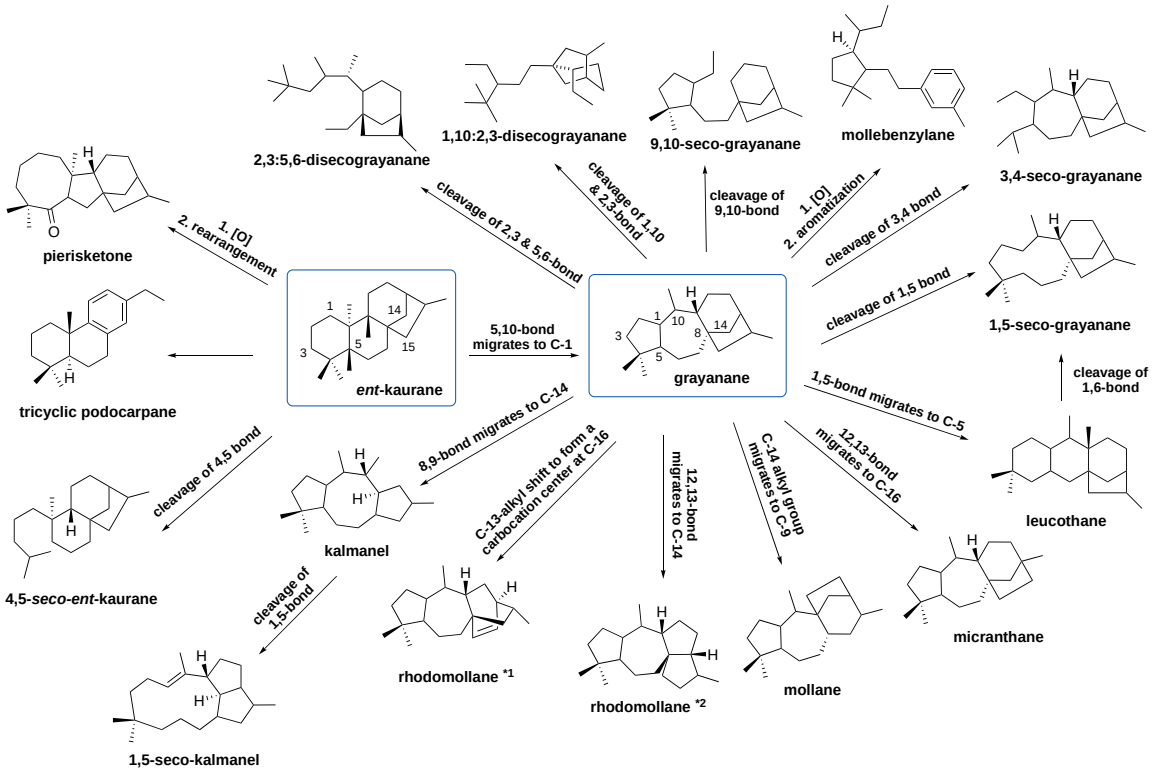

Figure 5. Biosynthetic pathway of grayanane-type & related diterpenoids. Figure adapted from ref 17

The plants of the Ericaceae family are a rich source of terpenoids, especially grayanane-type diterpenoids, which possess a unique 5/7/6/5 tetracyclic core derived

from rearrangement of the *ent*-kaurane skeleton (Figure 5).[17] Over 290 grayanoids have been isolated and characterized with 18 different carbon skeletons. Biologically, they have shown a plethora of activities, including analgesic, PTP1B inhibition, antitumor, antiviral, antinociceptive, anti-inflammatory, insecticidal, immunomodulatory and ion channel activities.[17] Many of these, termed grayanotoxins, have also shown severe toxicity due to their ability to bind to the group II receptor site in voltage-gated sodium channels, preventing channel inactivation and resulting in hyperpolarization.[18] Additionally, limited structure activity relationship data for these compounds is available and is outlined in Figure 6.[17]

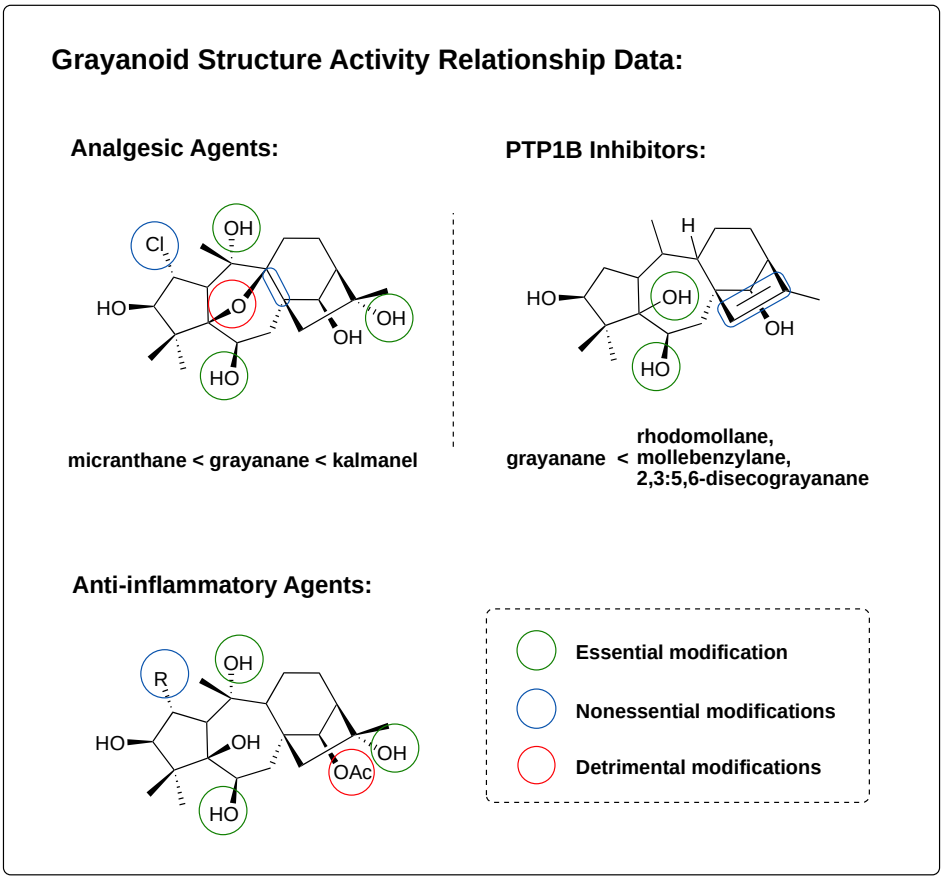

Figure 6. Grayanoid-Activity Relationship Data. Figure adapted from ref 17.

2.1.2 Isolation and Analgesic Activity of Rhodojaponin III

In traditional Chinese medicine, plants belonging to the Ericaceae family have been used to relieve pain clinically for thousands of years. In particular, the flowering plant *Rhododendron molle* G. Don has been shown to be one of the most potent herbal remedies. Motivated by its potent activity and lack of defined analgesic components, Yu and co-workers extracted 20 grayanane-type diterpenoids (Figure 7), 9 new and 11 known, from the roots of *Rhododendron molle* and assessed their antinociceptive

properties. The structures of the 9 new diterpenoids were determined via HRESIMS, 1D and 2D NMR data.[19]

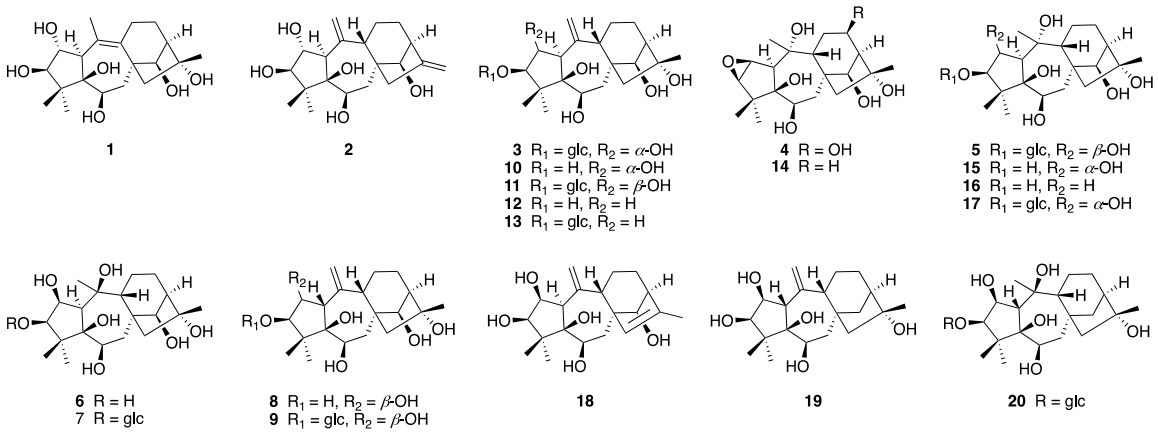

Figure 7. Grayanane-type diterpenoids extracted from the roots of *Rhododendron molle*. Figure adapted from ref 19.

To begin their assessment of the diterpenoids' antinociceptive properties, Yu and co-workers utilized an acetic acid-induced writhing test for an acute pain model. As shown in Figure 8, two diterpenoids rhodojaponin III (**14**) and rhodojaponin VI (**15**) were even more potent than morphine at reducing writhing events even at a lower dose (0.08 mg/kg vs. 0.8 mg/kg). Excited by these results, rhodojaponin III & VI were assessed further at three doses (0.02, 0.04 and 0.08 mg/kg) in respect to both chemical and thermal stimuli. As shown in Figure 8B, rhodojaponin III & VI reduced acetic acid induced writhes in a dose-dependent manner. In response to thermal stimuli, only rhodojaponin III showed licking latency at the highest dose of 0.08 mg/kg (Figure 8C).

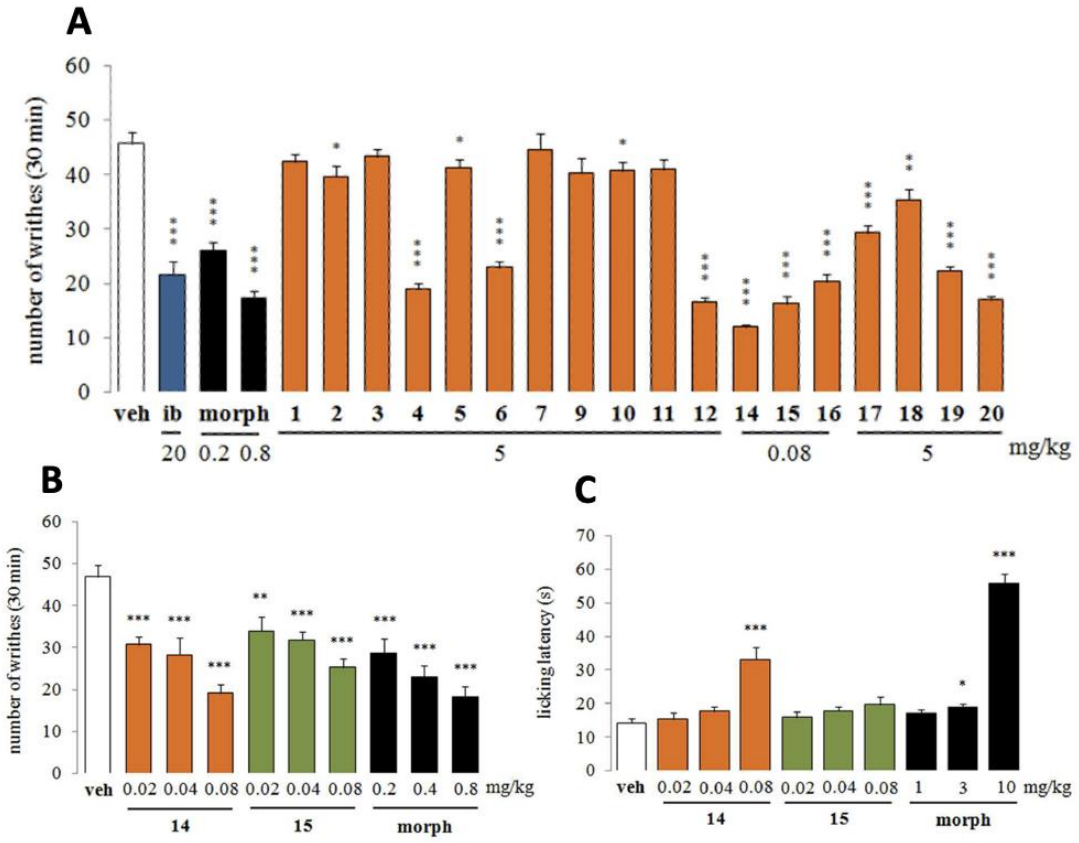

Figure 8. Analgesic activity of extracted diterpenoids.

A) acetic acid-induced writhing test of the 20 extracted diterpenoids. B) acetic acid-induced writhing test of rhodojaponin III & VI at three doses. C) licking latency in response to thermal stimuli. Figure reprinted with permission from ref 19.

Next, Yu and co-workers were interested in rhodojaponin III & VI's analgesic activity in response to inflammatory pain. Therefore, a formalin assay was designed to induce a biphasic pain response to assess both acute and persistent inflammatory pain. While ibuprofen (a nonsteroidal anti-inflammatory (NSAID)) only decreased behavioral activity in phase II, morphine (opioid) showed activity in both phase I and phase II

(Figure 9A). Comparatively, rhodojaponin III & VI showed a dose-dependent response in both phases, similar to that of morphine, but at a lower dose.

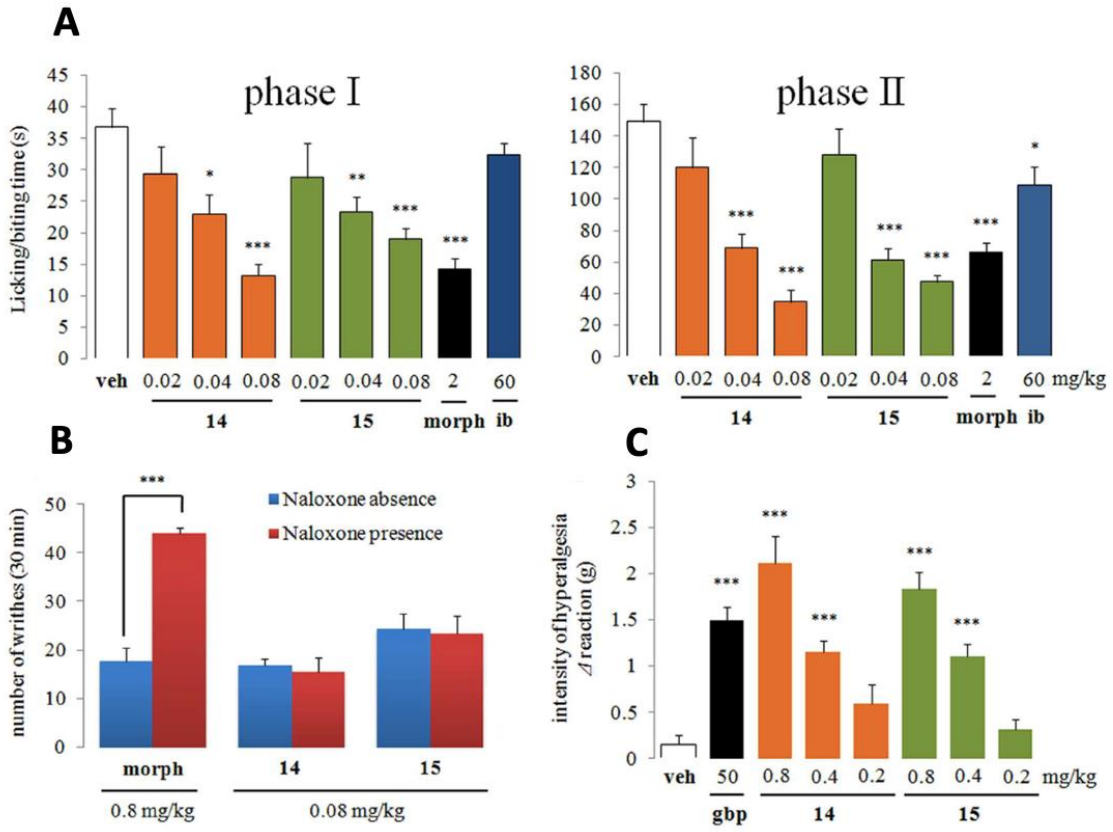

Figure 9. Further evaluation of rhodojaponin III & VI analgesic activity.

A) biphasic response in the formalin assay. B) analgesic activity in the presence of naloxone. C) response to neuropathic pain in (STZ)-induced diabetic mouse model. Figure reprinted with permission from ref 19.

The final pain model used by Yu and co-workers was a streptozotocin (STZ)-induced diabetic mouse model to study diabetic peripheral neuropathic pain. For this

study, they compared rhodojaponin III & VI's activity to gabapentin, a first line agent for neuropathic pain. As shown in Figure 9C, rhodojaponin III & VI showed comparable potency to gabapentin but at a much lower dose.

Lastly, the effect of naloxone, a non-selective opioid antagonist, on rhodojaponin III & VI's analgesic activity was examined. When naloxone was co-administered in an acetic acid-induced writhing test with rhodojaponin III & VI, there was no significant effect on analgesic activity. Whereas the presence of naloxone reversed the effect produced by morphine. These results suggest that rhodojaponin III and VI do not affect the endogenous opioid peptidergic system and may provide an alternative mechanism of action for pain relief.

Taken together, these studies identify two compounds (rhodojaponin III & VI) to be more potent than morphine in acute and inflammatory pain models and 100-fold more potent than gabapentin in a diabetic neuropathic pain model. Excitingly, they do not affect the endogenous opioid peptidergic system and may provide a novel mechanism of action for pain-relieving therapeutics. With such promising analgesic activity and unique structural complexity, rhodojaponin III is an excellent target for total synthesis. Therefore, in this chapter we aim to develop an enantioselective route to access key fragments in the total synthesis of rhodojaponin III.

2.1.3 Synthesis of Structurally Related Diterpenoids

Due to their various skeletons, unique structural features, and diverse biological activities there has been long standing interest in synthesizing grayanane-type diterpenoids. Although synthetic efforts began in 1972 with the partial synthesis of grayanotoxin II by Hamanaka and Matsumote, the first total synthesis wasn't published until 1994 when Shirahama and co-workers published the first total synthesis of grayanotoxin III.[20, 21] Since then, an advanced intermediate of kalmanol (tetracyclic 7-oxy-5,6-dioxykalmanol), a synthetic approach for pierisformaside C, and the total synthesis of principinol D and E, rhodomolleins XX and XXII, and glaucocalyxin A have been published. Herein, each of these synthetic accomplishments will be briefly discussed.

2.1.3.1 Total Synthesis of (–)- Grayanotoxin III

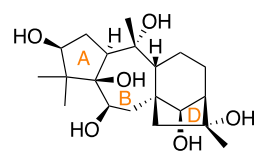

Grayanotoxin III
(2.001)

Shirahama and co-workers accomplished the first total synthesis of (–)-grayanotoxin III in 1994. This was accomplished via a linear approach in 38 steps and a 0.05% overall yield. Their synthetic strategy was creatively centered around three stereoselective SmI_2-mediated radical cyclizations to form the A, B and D rings of grayanane diterpenoids. Their synthetic efforts are outlined in Scheme 1 and 2.[21]

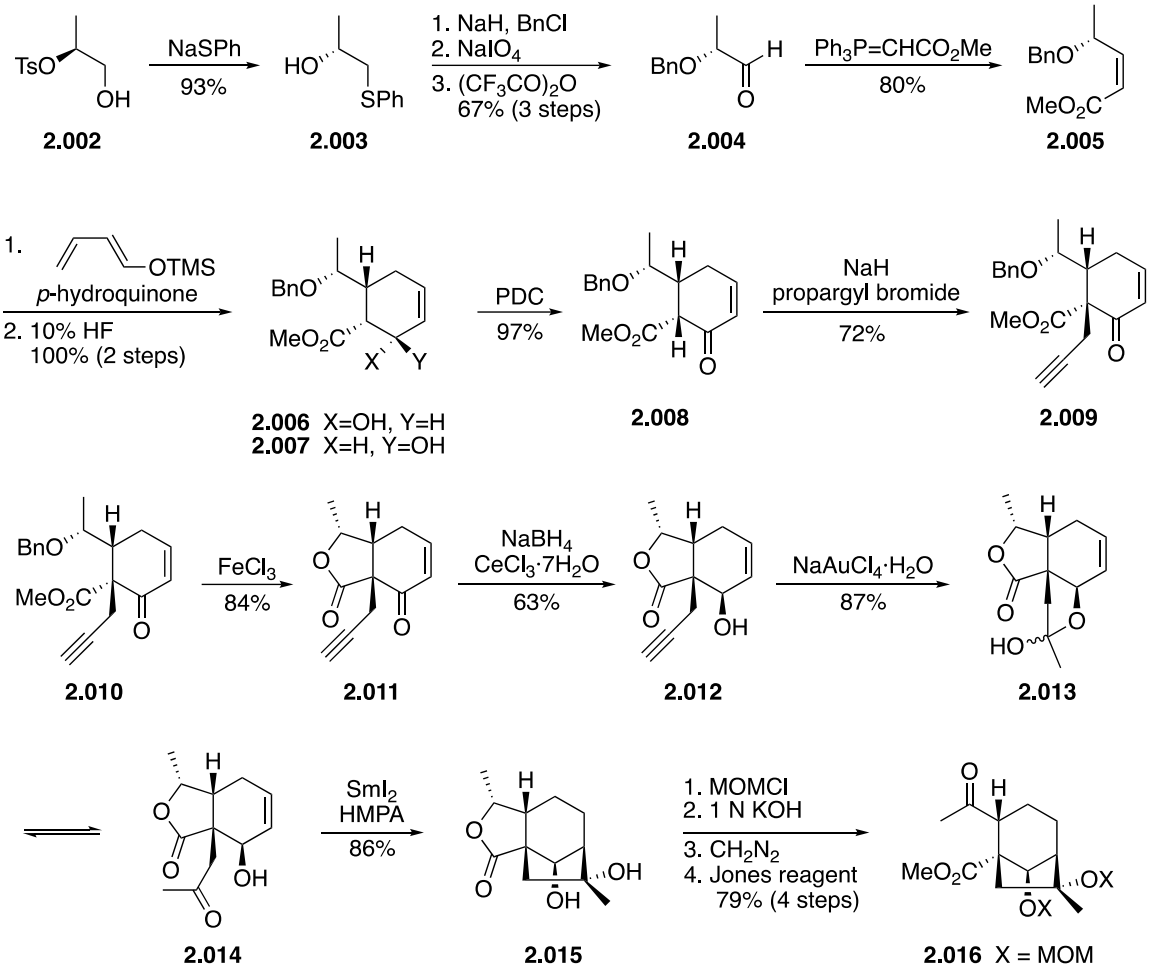

Scheme 1. Synthesis of the 5/6 bicycle of grayanotoxin III

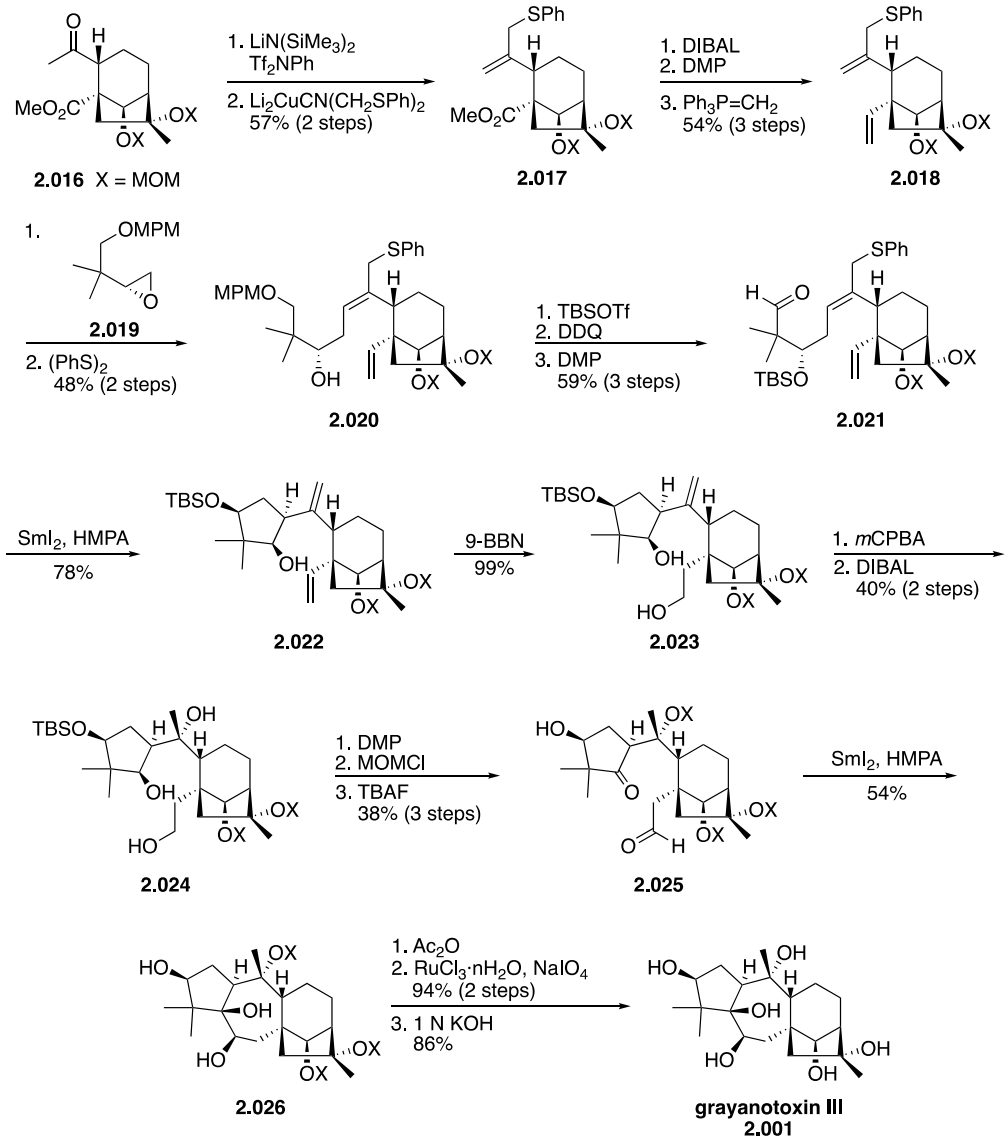

Scheme 2. Total synthesis of grayanotoxin III

2.1.3.2 Highly Functionalized B-homo-C-nor Grayanotoxin

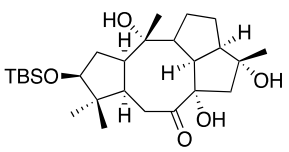

2.027

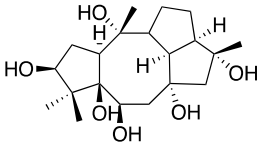

kalmanol
2.028

In 1995, Paquette and Borrelly reported the synthesis of highly functionalized B-homo-C nor grayanotoxin (**2.027**), which is structurally related to kalmanol (**2.028**). Their work establishes an enantioselective route to a key bicyclic diquinane subunit and demonstrates the viability of a Tebbe–Claisen sequence for building the backbone of kalmanol. Their synthetic efforts are outlined in Scheme 3.[22]

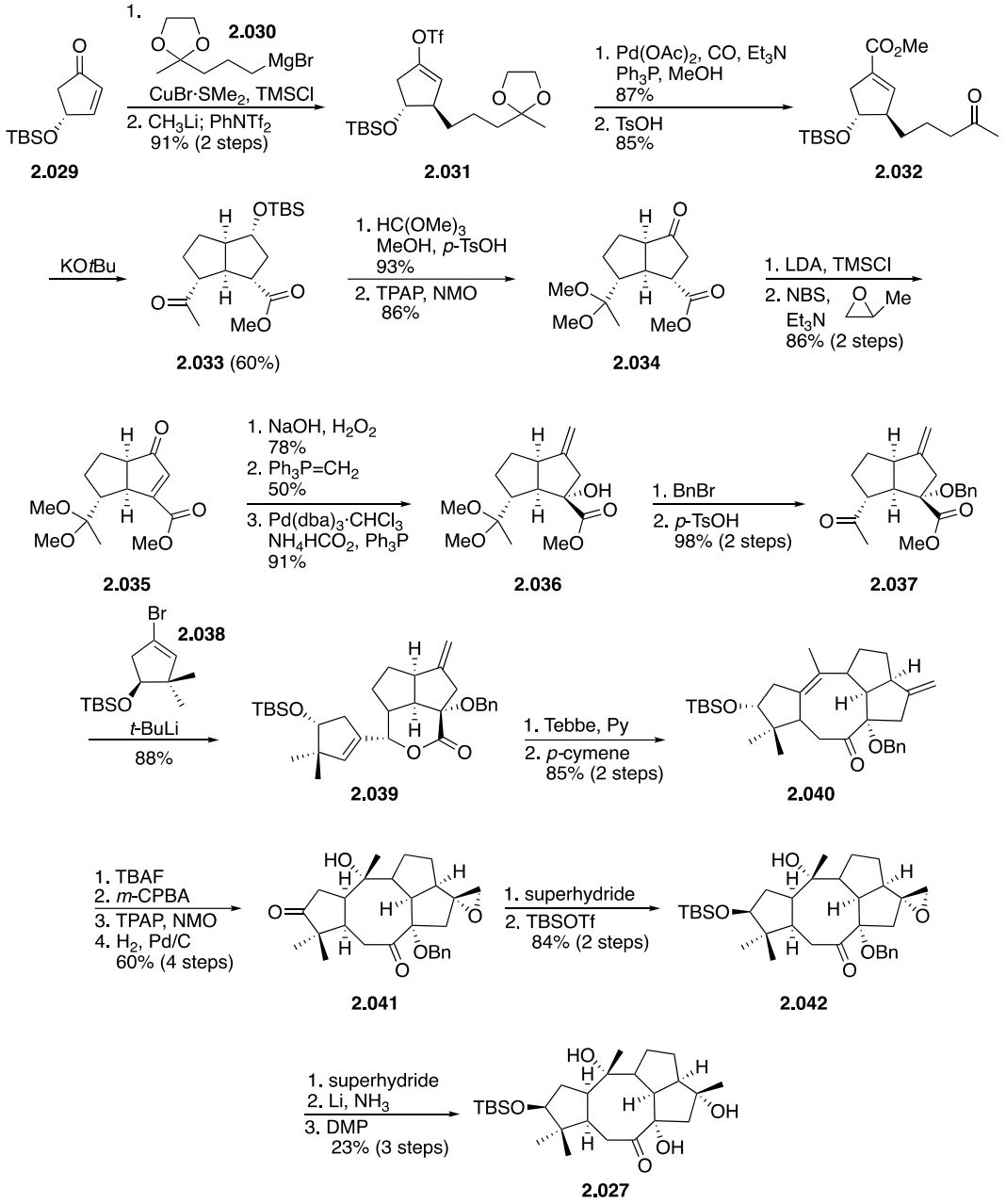

Scheme 3. Synthesis of highly functionalized b-homo-c-nor grayanotoxin

2.1.3.3 Synthetic Approach towards Pierisformaside C

In 2011, Williams and co-workers were interested in developing a synthetic route to pierisformaside C, as it was the first grayanane-type diterpene to possess three central

double bonds. Retrosynthetically, they proposed pierisformaside C could be obtained by late-stage construction of the central seven-membered ring **2.044** (Scheme 4), which they would access via an aldol or Claisen cyclization, controlled by the *cis*-double bond of **2.045**. **2.045** accessed by a Sonogashira coupling of a bicyclo[3.2.1]octane fragment (**2.046**) and five-membered ring fragment **2.047**. From their synthetic efforts (outlined in Scheme 5 and 6), Williams and co-workers successfully synthesized an advanced intermediate (**2.060**) of pierisformaside C in 15 steps. This work will pave the way for the asymmetric total synthesis of pierisformaside C and structurally related diterpenes.[23]

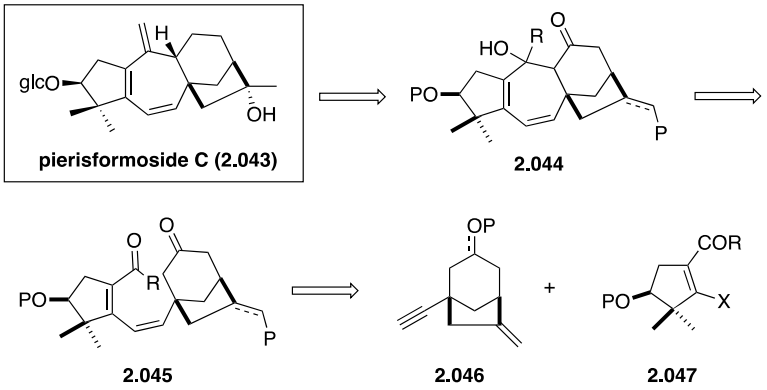

Scheme 4. Williams' retrosynthetic analysis of pierisformaside C

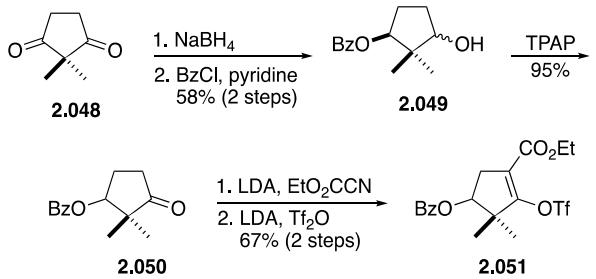

Scheme 5. Williams' synthesis of fragment 2.051

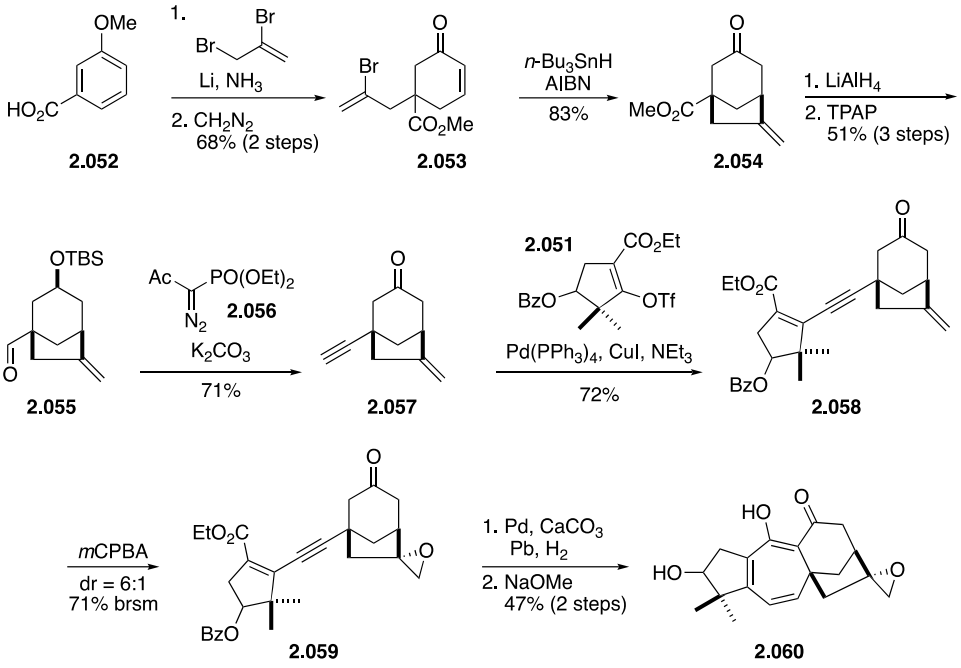

Scheme 6. Williams' synthesis of an advanced intermediate of pierisformaside C

2.1.3.4 Total Synthesis of Principinol D

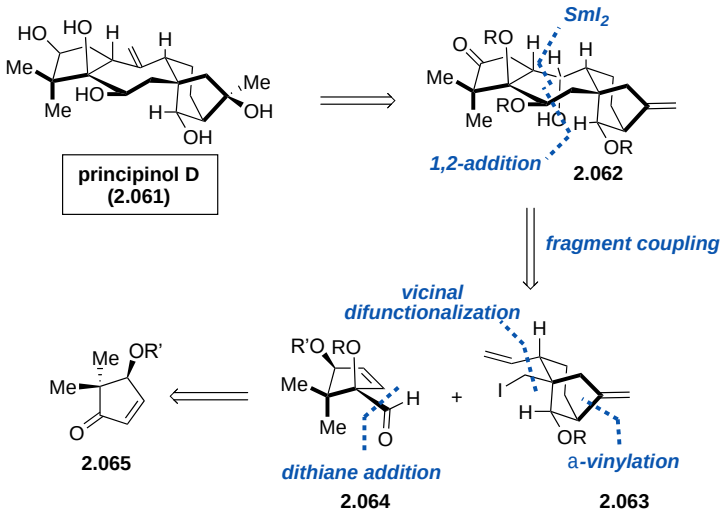

Scheme 7. Newhouse's retrosynthetic analysis of principinol D

Newhouse and co-workers contributed to the synthetic progress of grayanane-type diterpenes with their report on the total synthesis of principinol D in 2019. They

were interested in developing a synthetic route that would enable efficient synthesis of structurally diverse analogs. Previous synthetic efforts towards this class of compounds followed linear cyclization strategies to introduce the stereochemical complexities but Newhouse envisioned that a convergent approach would be better suited towards analog development. Therefore, two major fragments would be joined together via two C–C bond-forming reactions, a 1,2-addition between **2.064** and the bicyclo[3.2.1]octane fragment **2.063** and a reductive cyclization using SmI_2 (Scheme 7) . As outlined in Scheme 8, the total synthesis of principinol D was accomplished in 19 steps following this strategy.[24]

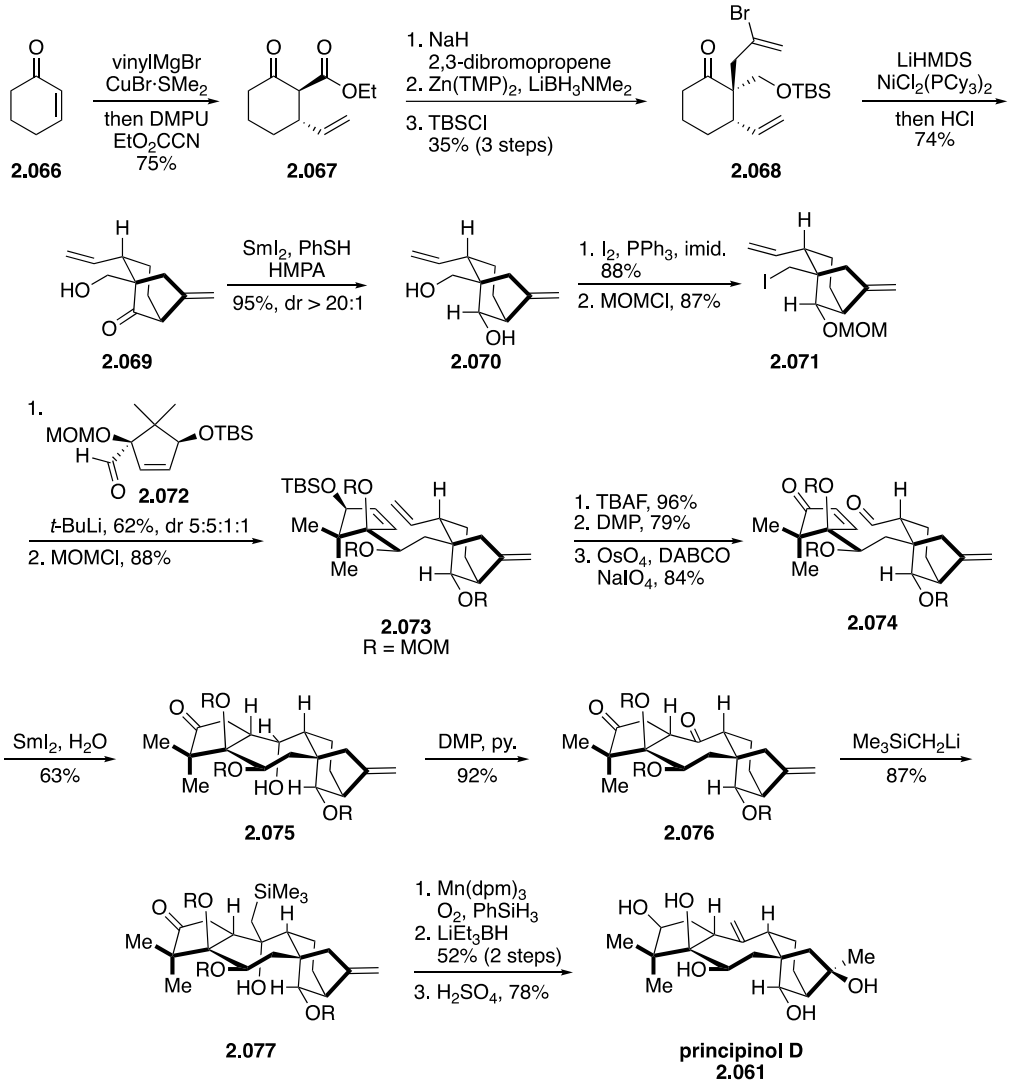

Scheme 8. Newhouse's synthesis of principinol D

2.1.3.4 Total Syntheses of Rhodomolleins XX and XXII

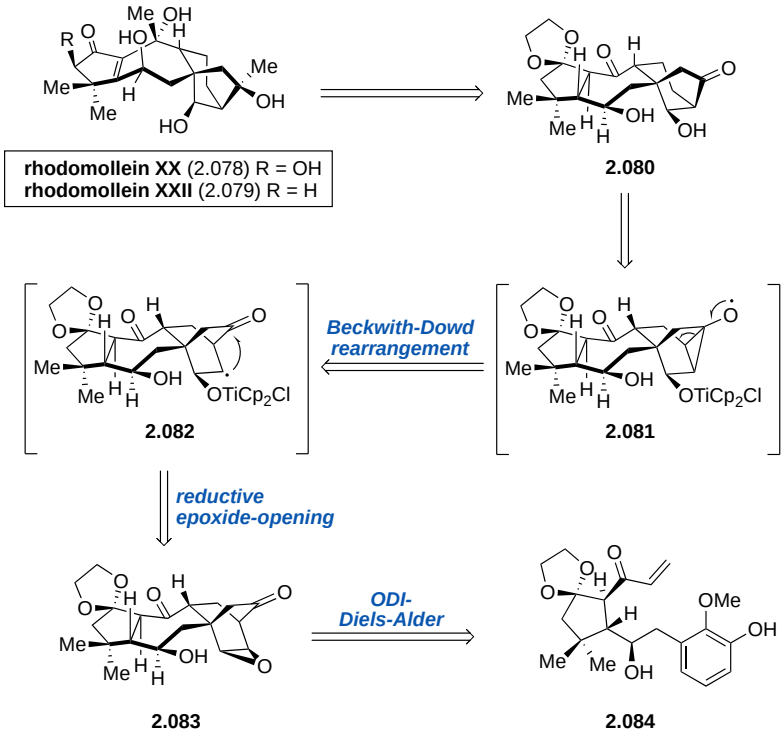

Scheme 9. Ding's retrosynthetic analysis of rhodomollein XX & XXII

Prompted by previously reported synthetic routes that were lengthy and required many functional group manipulations to access the [3.2.1] bicyclic skeletons of tetracyclic diterpenoids, Ding and co-workers sought to develop a more versatile route to access the [3.2.1] bicyclic motif. To achieve this goal, a new titanium(III)-mediated reductive epoxide-opening/Beckwith–Dowd rearrangement process was developed (Scheme 9). As shown in Scheme's 10 and 11, this methodology was utilized in the first total synthesis of rhodomolleins XX (**2.078**) and XXII (**2.079**).[25]

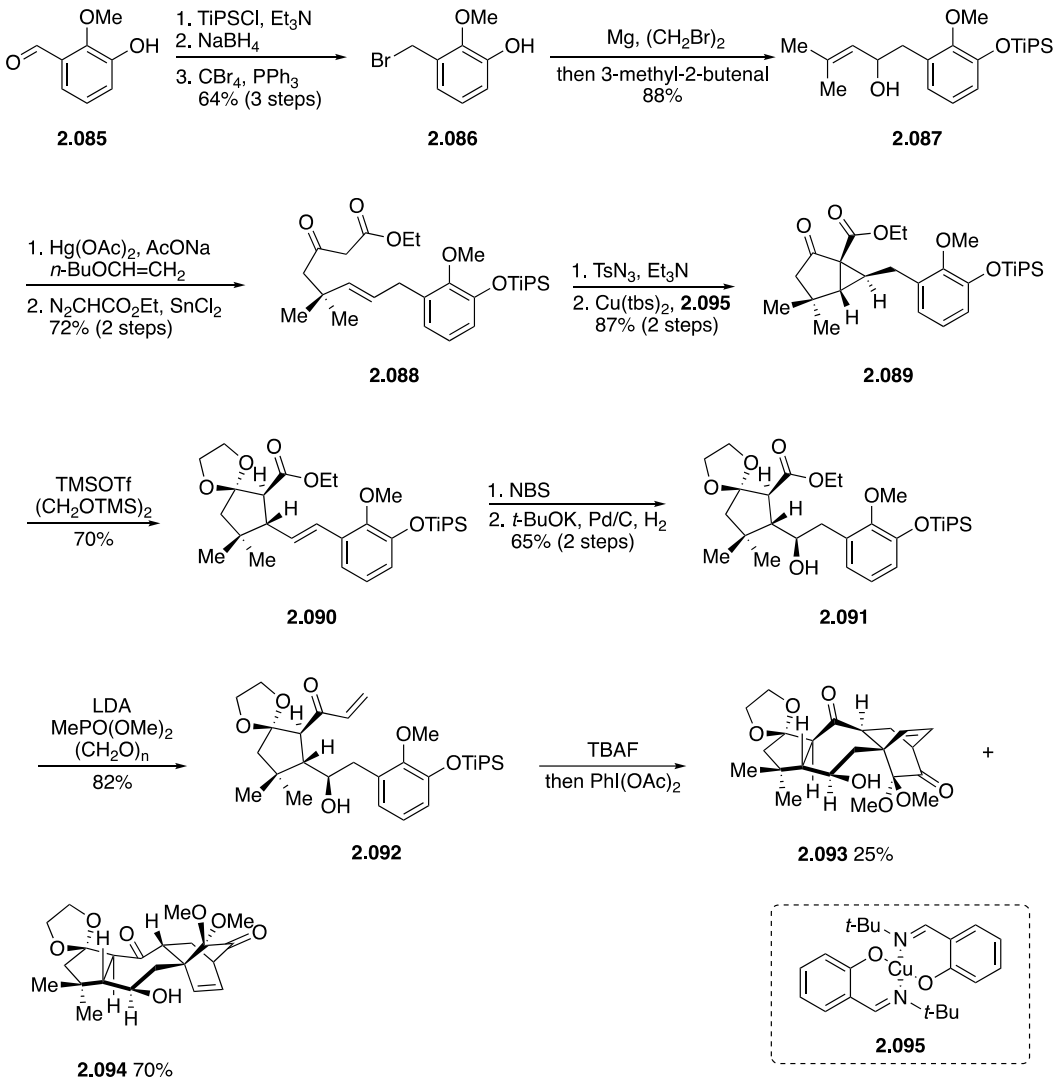

Scheme 10. Ding's synthesis of tetracycle 2.094

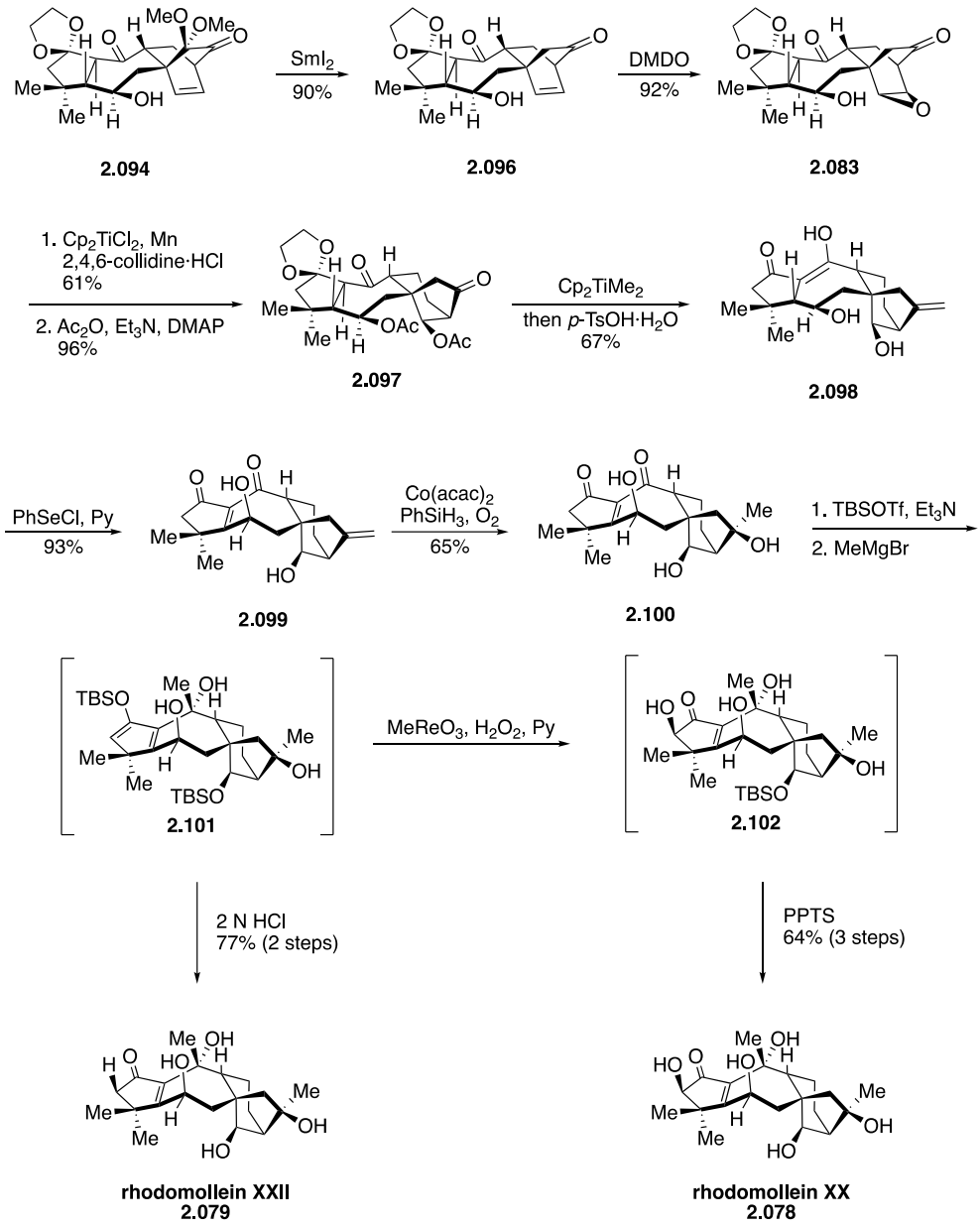

Scheme 11. Ding's synthesis of rhodomollein XX & XXII

2.1.3.4 Total Synthesis of Glaucocalyxin A

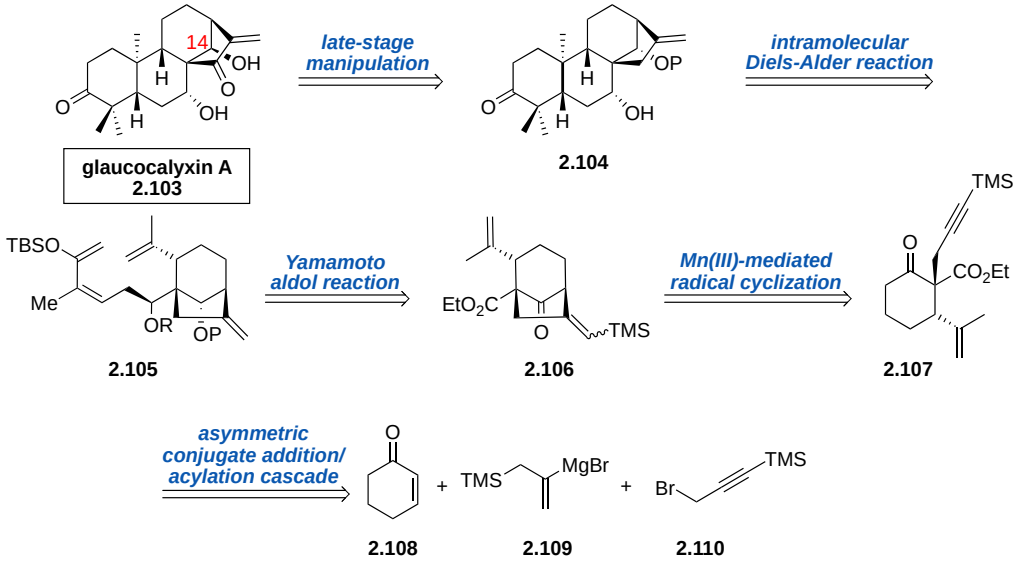

Scheme 12. Jia's retrosynthetic analysis of glaucocalyxin A

Among the naturally produced diterpenes, about half contain the 14(*β*)-oxygenation pattern for the bicyclo[3.2.1]octane fragment. As this motif has been notoriously difficult to introduce employing previous strategies, Jia and co-workers set out to develop a practical method for the formation of the C14 oxygenated bicyclo[3.2.1]octane moiety and complete the total synthesis of glaucocalyxin A. They envisioned glaucocalyxin A could be generated by late-stage manipulation of **2.104**, which would be assembled by an intramolecular Diels–Alder (IMDA) of intermediate **2.105**. The Diels–Alder substrate obtainable from the 14-oxygenated bicycle **2.106** via a Yamamoto aldol reaction. The 5/6 bicycle **2.106** introduced by Mn(III)-mediated radical cyclization of **2.107**, which will be synthesized from readily available compounds. Through their efforts, they accomplished the total synthesis of glaucocalyxin A via a

Mn(III)-mediated oxidative cyclization to access the key oxygenated bicyclo[3.2.1]octane ring system (Scheme 13).[26]

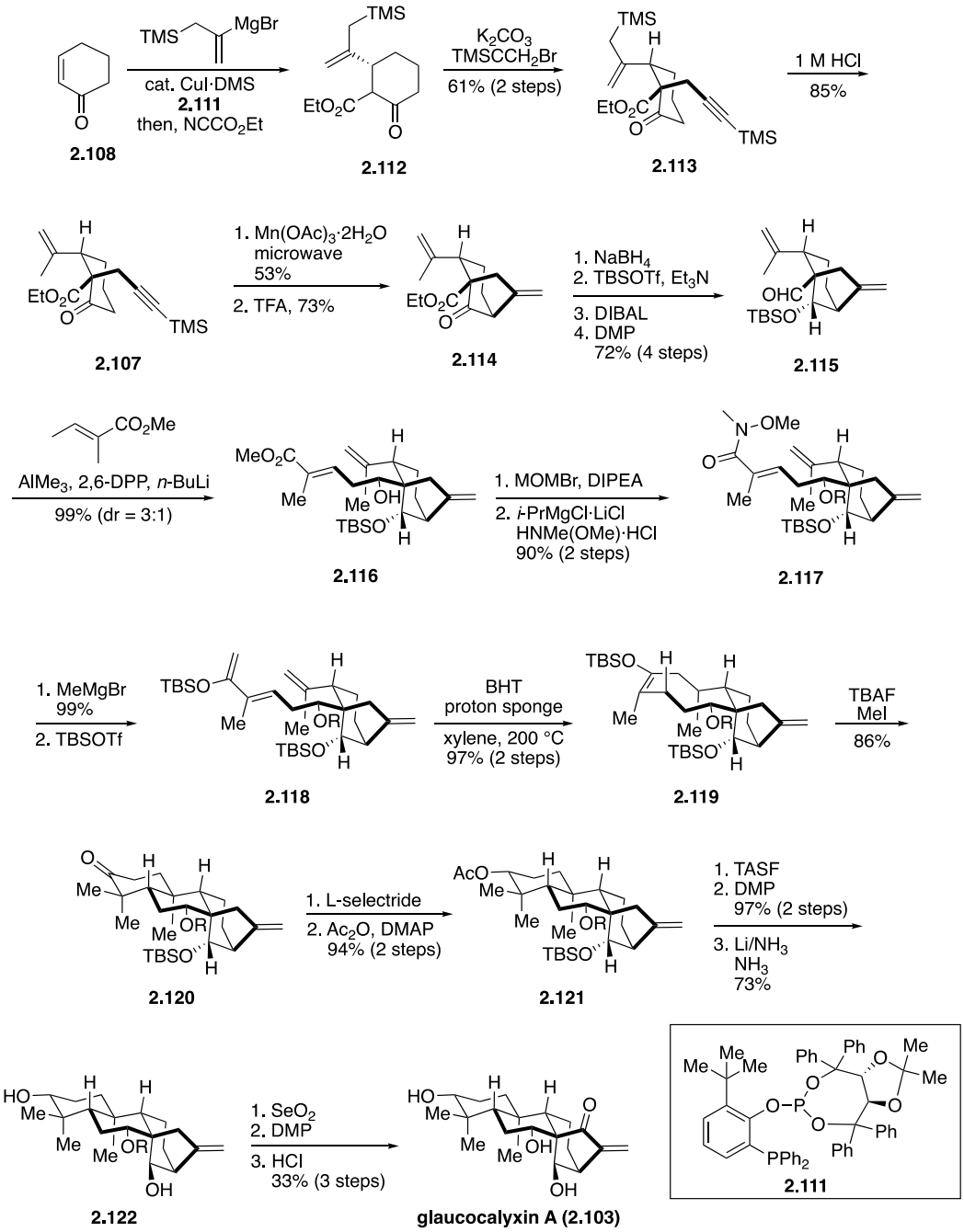

Scheme 13. Jia's synthesis of glaucocalyxin A

2.1.3.4 Luo's Total Syntheses of Grayanane Diterpenoids

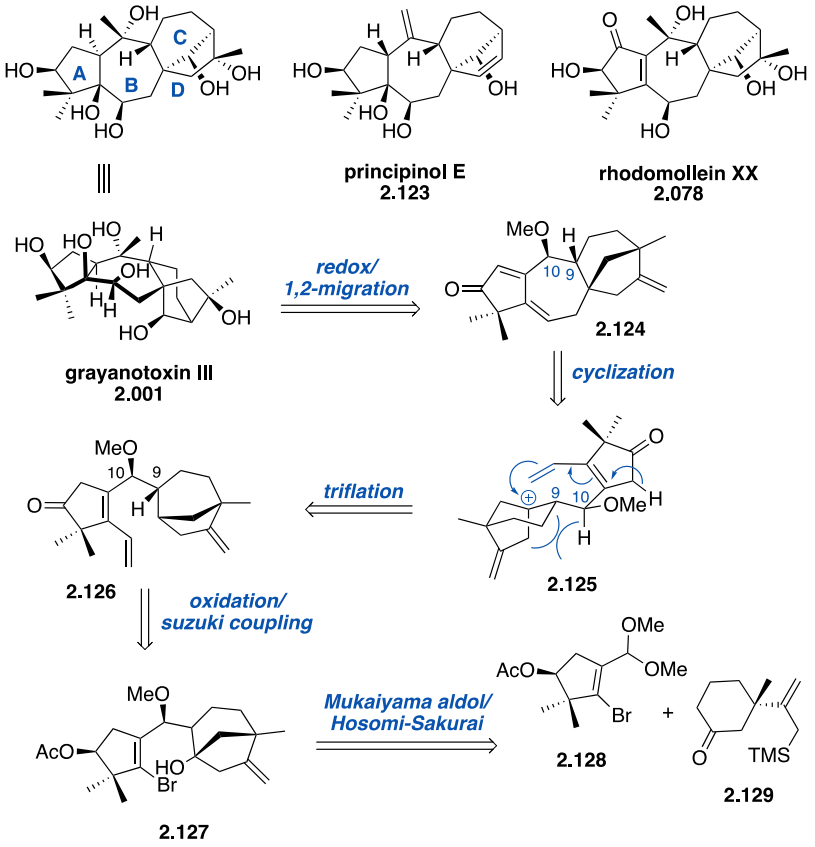

Scheme 14. Luo's retrosynthetic analysis of grayanane diterpenoids

In 2022, Luo and co-workers presented a synthetic strategy that allowed for late-stage manipulation of an advanced intermediate (**2.124**) to access three grayanane-diterpenoids, grayanotoxin III, principipinol E and rhodomollein XX. It was proposed that advanced intermediate **2.124** could be accessed by intramolecular cyclization of the bridgehead tertiary carbocation of **2.125**. Precursor **2.126** prepared by oxidation and Suzuki coupling of **2.127**, which is accessed from starting ketal **2.128** and ketone **2.129** via a Mukaiyama aldol reaction followed by intramolecular Hosomi–Sakurai reaction.

Indeed, following this approach Luo and co-workers completed the total synthesis of grayanotoxin III, principinol E and rhodomollein XX, outlined in Scheme 15, 16 and 17.[27]

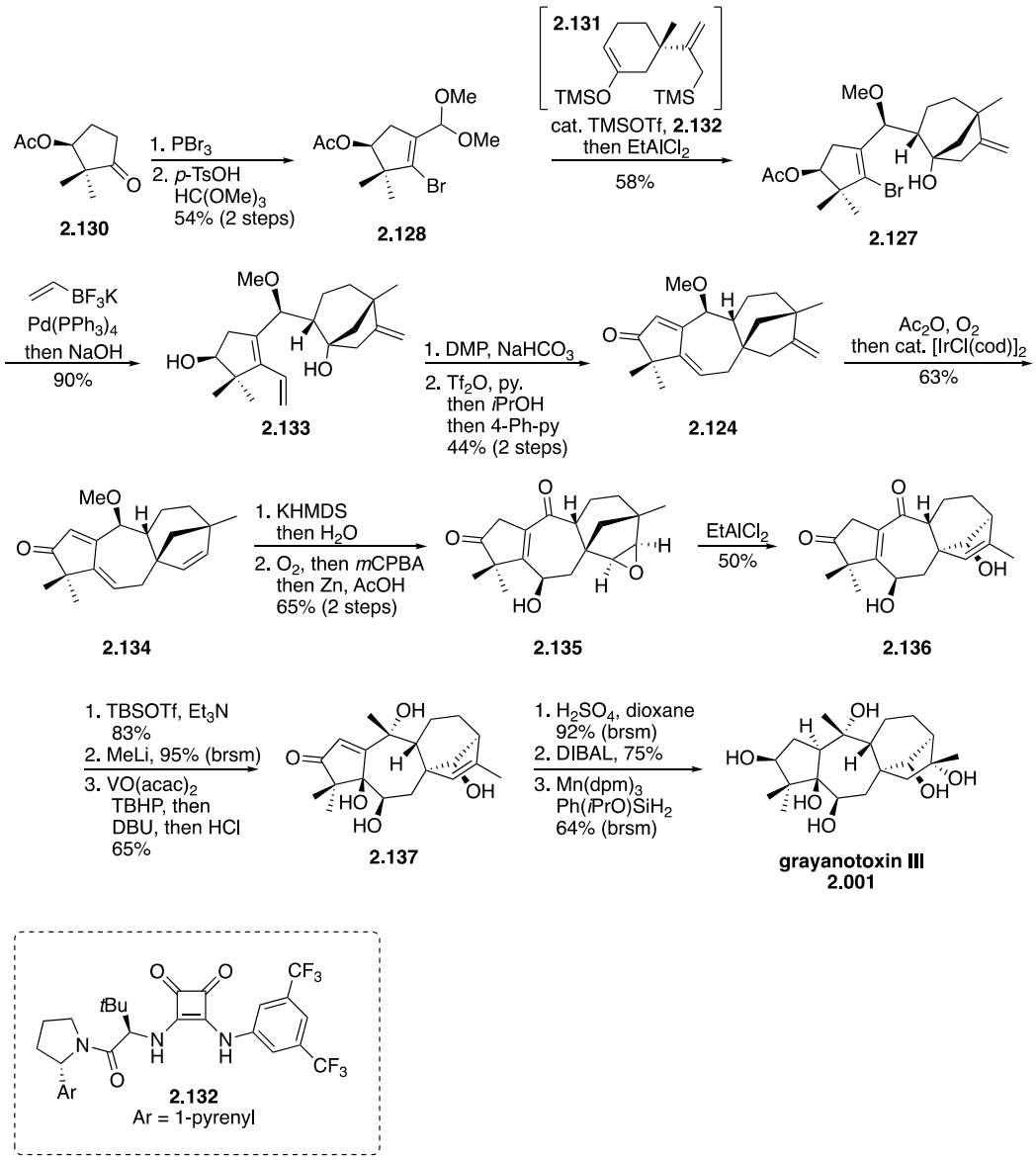

Scheme 15. Luo's synthesis of grayanotoxin III

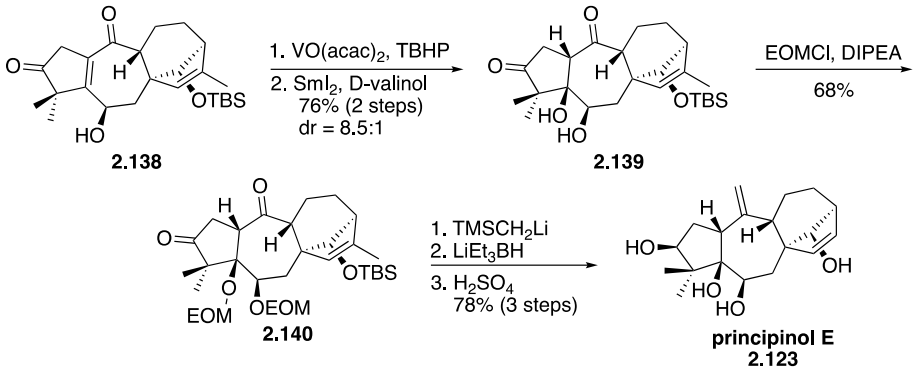

Scheme 16. Luo's synthesis of principinol E

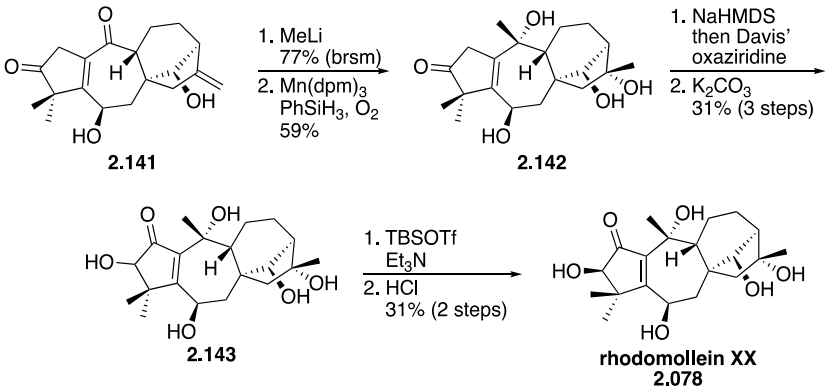

Scheme 17. Luo's synthesis of rhodomollein XX

2.2 Results and Discussion

2.2.1 Retrosynthetic Analysis

Motivated by the evident need for novel non-opioid analgesics and the promising antinociceptive activity of rhodojaponin III, we sought to establish a convenient route to access rhodojaponin III to further assess its potential as an analgesic therapeutic as well as for the development of a chemical probe to investigate the mechanism of action of this natural product.

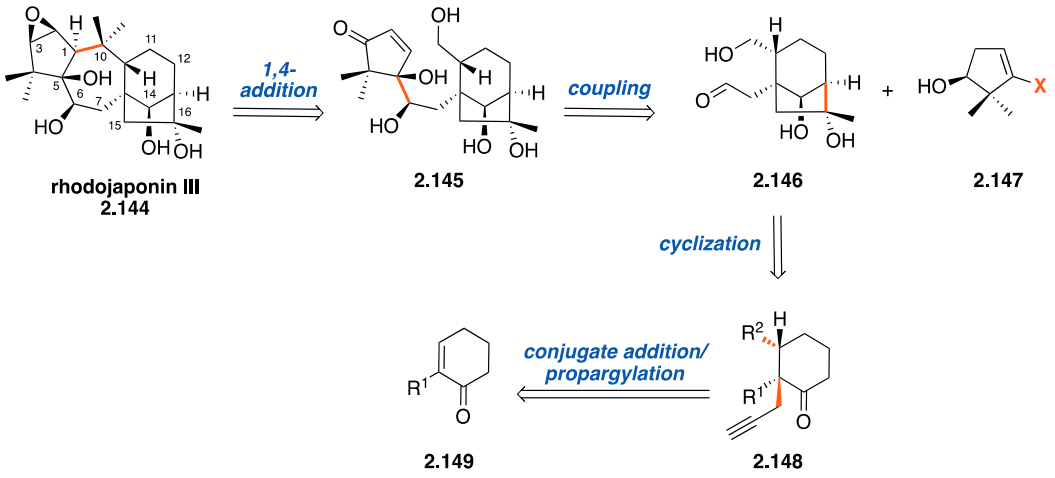

Scheme 18. Retrosynthetic analysis of rhodojaponin III

To accomplish the total synthesis of rhodojaponin III, a convergent approach was devised, in which two major fragments are synthesized separately and coupled together to give the 5/7/6/5 ring system of grayanane-type natural products. This strategy relies on the construction of the bicyclo[3.2.1]octane fragment (**2.146**) via conjugate addition and subsequent propargylation of a simple cyclic enone (**2.149**). Cyclization of the resulting alkynyl ketone (**2.148**) will provide the desired 5/6 bridged system, which can be coupled to the vinyl moiety of the 5-membered ring fragment (**2.147**). The goal of this chapter is to develop a synthetic strategy to access the two coupling fragments, with an emphasis on the enantioselective synthesis of the key bicyclo[3.2.1]octane fragment (**2.146**). The work presented in this chapter was achieved in collaboration with Dr. Hyeri Park, a former member of the Hong Lab.

2.2.2 Synthesis of the 5-membered Ring Fragment

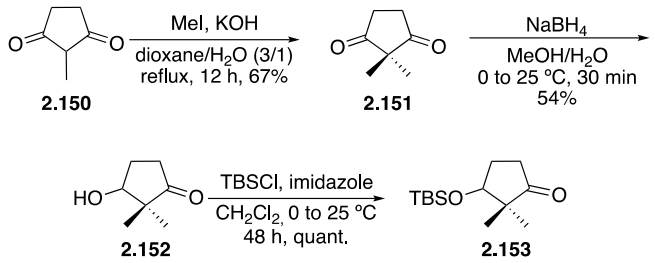

Scheme 19. Synthesis of the 5-membered ring fragment

The racemic synthesis of the 5-membered ring fragment began with the methylation of commercially available 2-methylcyclopentadione, followed by sodium borohydride reduction and subsequent protection of the newly formed secondary alcohol with TBS, quantitatively (Scheme 19).[28, 29] [29]For the enantioselective synthesis we plan to utilize the Corey-Bakshi-Shibata catalyst (CBS) for the reduction of **2.151**, which has been previously reported.[30]

Next, we turned towards the formation of a vinyl species. Initially, we attempted the formation of a vinyl bromide (Scheme 20) from **2.153** using triphenyl phosphite, bromine and triethylamine in hopes to couple to the bicyclo[3.2.1]octane fragment via lithium halogen exchange.[31] Unfortunately, this reaction only produced an unidentifiable product.

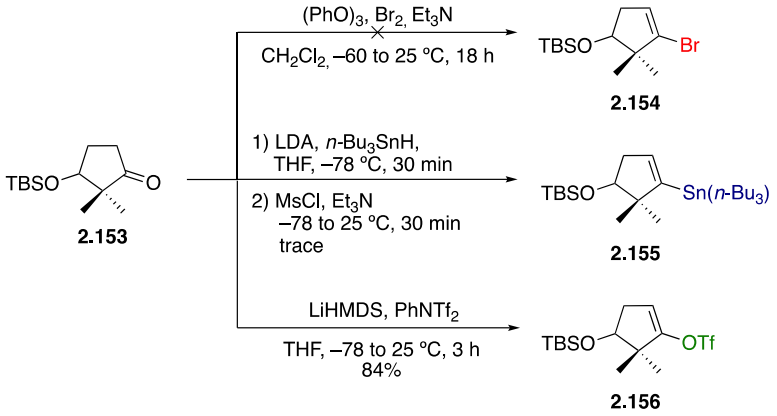

Scheme 20. Formation of vinyl triflate 2.151

Next, we focused our attention on the formation of a vinyl tin species, in which a lithium-metalloid or a Stille-type reaction could be attempted. The formation of the vinyl tin species began with *in situ* generation of LDA, followed by addition of tributyltin to the ketone of **2.153**. MsCl is then added to form a mesylate intermediate that is eliminated by Et_3N to provide the desired vinyl tin species.[32] Although the desired vinyl tin **2.155**, was obtainable by this route, poor yields and the generation of tetrabutyltin as a side product, which was extremely difficult to remove, pushed us to seek out another route. Finally, vinyl triflate **2.156** was generated in 84% yield upon treatment with LiHMDS and PhNTf.[33] We envision a Nozaki-Hiyama-Kishi type coupling reaction will allow us to couple our vinyl triflate to the aldehyde of our bicyclo[3.2.1]octane fragment.

2.2.3 Formation of the Bicyclo[3.2.1]octane Fragment

2.2.3.1 Formation of the Alkynyl Ketone Substrate

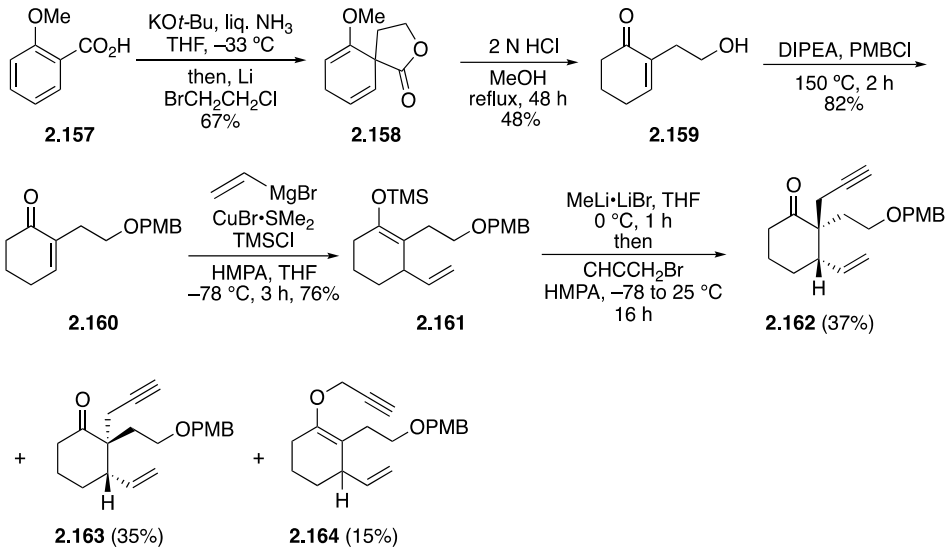

Scheme 21. Synthesis of alkynyl ketone 2.157

The synthesis of the bicyclo[3.2.1]octane fragment began with the preparation of alkynyl ketone **2.162**, as outlined in Scheme 21. Starting from commercially available 2-methyoxybenzoic acid, Birch reduction with liquid ammonia followed by alkylation of the resulting anion provided spirolactone **2.158**.[34] Hydrolysis of the spirolactone with 2 N HCl provided primary alcohol **2.159**, which was protected with PMBCl under basic conditions. Copper-catalyzed 1,4-addition of vinylmagnesium bromide with subsequent enolate trapping with TMSCl provided intermediate **2.161**, poised for alkylation. With the addition of MeLi·LiBr and propargyl bromide, we obtained a 1:1 diastereomeric mixture of the alkynyl ketone. Additionally, we observed the formation of the O-alkylation product **2.164** (15%). As the stereochemistry of diastereomers **2.162** and **2.163** could not be distinguished by ^{1}H NMR, one attempt at crystallization via liquid-liquid

diffusion was made. Gratifyingly, the crystal of the desired diastereomer **2.162** was obtained and x-ray crystallography confirmed the structure (Figure 10).

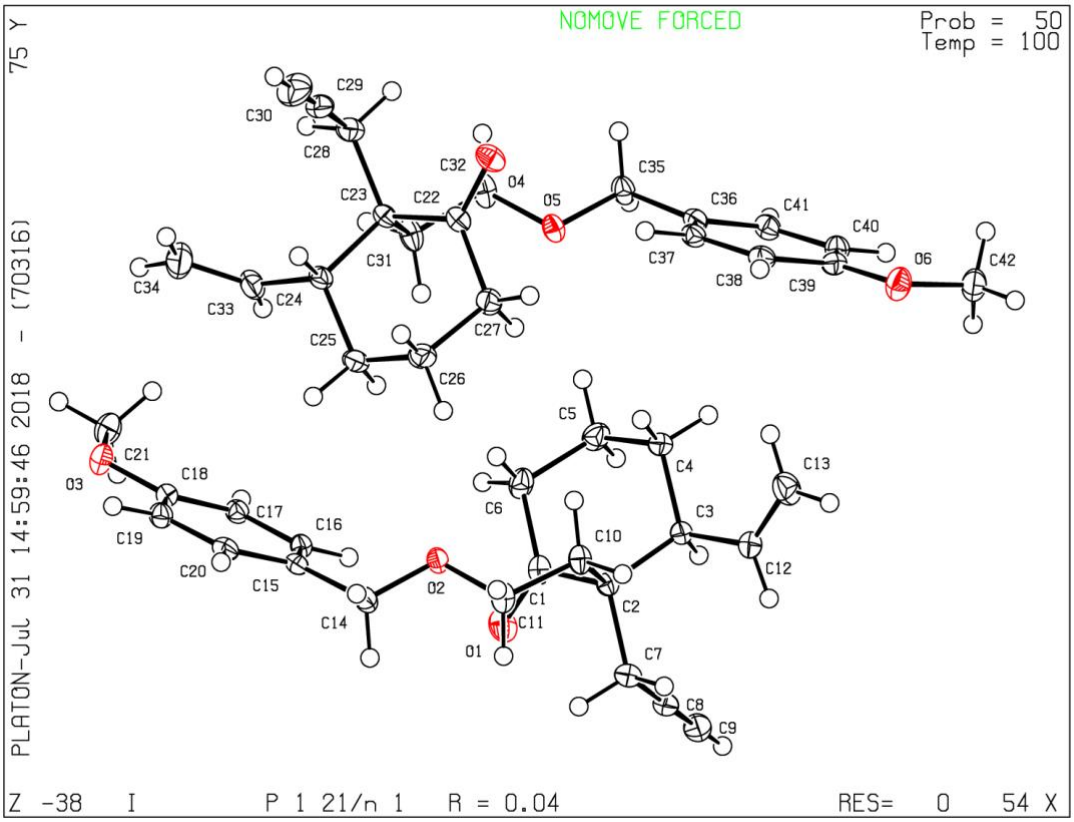

Figure 10. X-ray crystallographic data of 2.162

2.2.3.2 Conia-ene Type Cyclizations

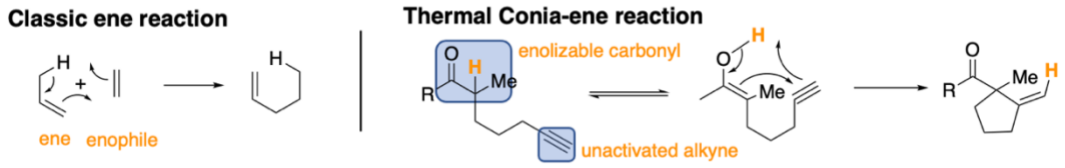

Figure 11. Conia-ene cyclization

With alkynyl ketone **2.162** in hand, we began our investigation of cyclization conditions to form the 5/6 bridged system of the bicyclo[3.2.1]octane fragment. One of the most powerful tools to accomplish the intramolecular addition of enols to alkynes for the formation of carbon-carbon bonds is the Conia-ene reaction. Conia-ene reactions were first reported in 1975 by Conia and Le Perche, in which, they described the thermal cyclization of enolizable carbonyl compounds with a tethered alkyne or alkene moiety, leading to valuable 5 or 6 membered carbocycles.[35] Mechanistically, the Conia-ene proceeds similarly to that of the classic ene reaction but an enolizable carbonyl replaces the ene component (Figure 11). Traditionally, the necessity of high temperatures (due to a relatively low population of the enol tautomer) restricted the use of many functional groups but recent reports on transition-metal catalyzed cyclizations of β-keto esters or silyl enol ethers, as well as base-mediated conditions has widened the scope for Conia-ene type reactions.[36]

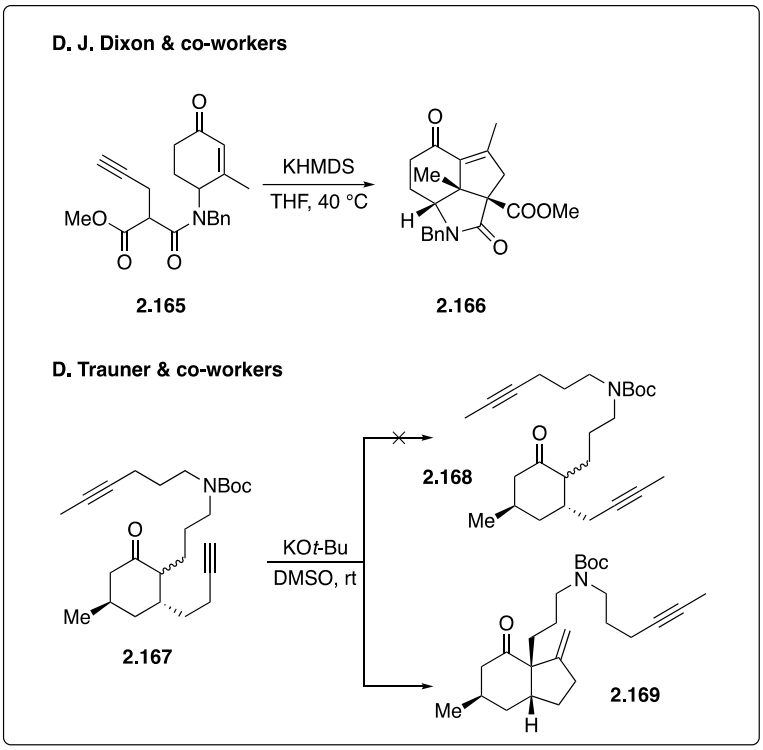

Although base-mediated Conia-ene reactions are less common compared to transition-metal catalyzed, several examples have been reported in the literature. For example, in the synthesis of *Daphniphyllum* alkaloids, Dixon and co-workers treated terminal alkyne **2.165** with KHMDS to form cyclized product **2.166**.[37] Additionally, Trauner and co-workers reported the use of a base-mediated Conia-ene reaction in the total synthesis of (–)-lycoposerramine R. Initially, they intended to convert terminal alkyne **2.167** to the rearranged internal alkyne **2.168** under basic conditions but instead obtained the *cis*-hydrindane product (**2.169**).[38]

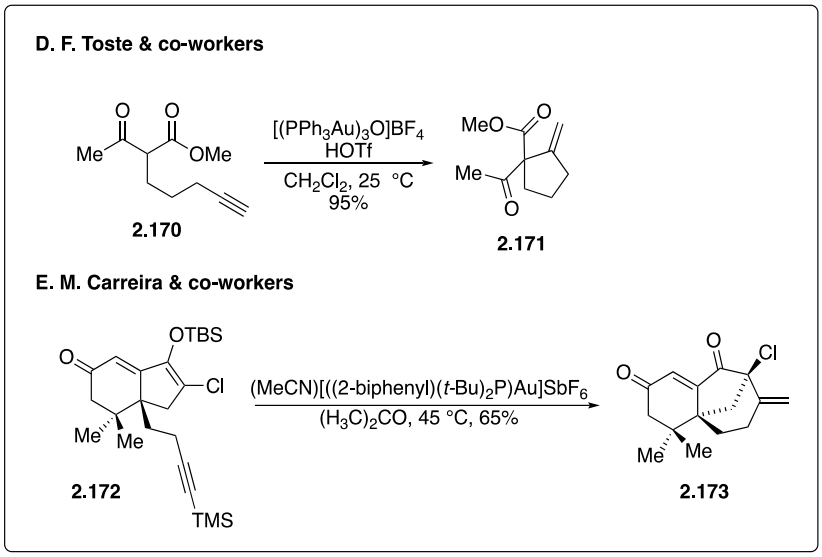

First reported by Toste and co-workers, cationic gold complexes have become one of the most influential catalysts for transition-metal catalyzed Conia-ene cyclizations and have been readily utilized in natural product synthesis.[39] In 2012, Carreira and co-workers reported the first and only total synthesis of gomerone C, a chlorinated sesquiterpene that possesses a bicyclo[3.2.1]octane moiety, analogous to rhodojaponin III. Utilizing a Johnphos gold complex, TBS-enol ether **2.172** was cyclized to form the desired 6-*exo* product (**2.173**).[40]

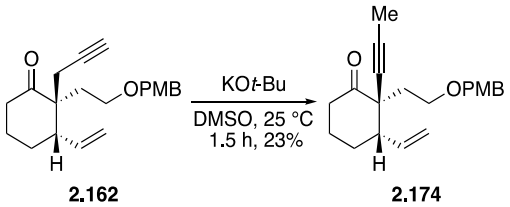

Scheme 22. Attempt at base-mediated Conia-ene cyclization

Excited about the applicability of the Conia-ene reaction to our system, we started with the simpler base-mediated approach. Applying Trauner's methodology to

our substrate, we treated alkynyl ketone **2.162** with KO*t*-Bu in DMSO for 1.5 h but rather than obtaining the cyclized product, we observed isomerization to form the internal alkyne **2.174**. This result is not altogether that surprising as terminal alkynes are known to isomerize under basic conditions and similar reports have been made, such as the example below by Jamison and co-workers.[41]

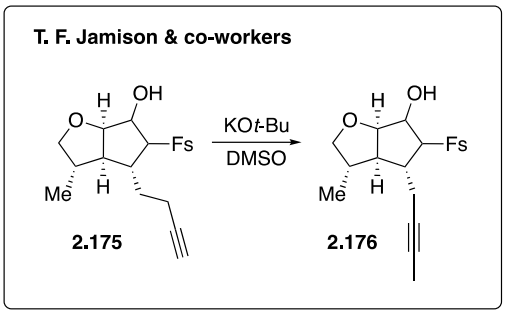

Table 1. Gold-catalyzed Conia-ene cyclization

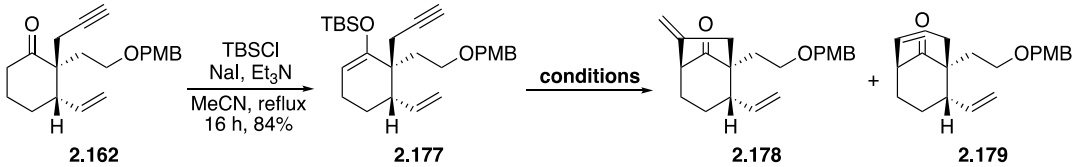

entry	catalyst	conditions	result
1	[(CyJohnphos)Au(MeCN)]SbF_6	acetone, 45 °C, 5 h	**2.179**
2	[(CyJohnphos)Au(MeCN)]SbF_6	CH_2Cl_2, 25 °C, 5 h	**2.179**

As base-mediated Conia-ene simply gave us undesired by-product **2.174**, we synthesized the silyl enolate **2.177** to attempt the gold-catalyzed version. Therefore, upon treatment of our alkynyl ketone **2.162** with TBSCl, NaI and Et_3N under refluxing conditions we formed silyl enolate **2.177**. We then subjected **2.177** to the gold-catalyzed

Conia-ene cyclization with the [(CyJohnphos)Au(MeCN)]SbF_6 ligand (Table 1) but regrettably, the undesired 6-*endo-dig* product (**2.179**) was obtained. The structural determination was made by ^{1}H NMR, as we see a multiplet at ~5.6 ppm corresponding to the two methine protons of the 6-*endo-dig* product as they are split by additional vicinal protons, whereas we would expect to see two doublets for the exo-methylene protons of the 5-*endo-dig* product (Figure 12).

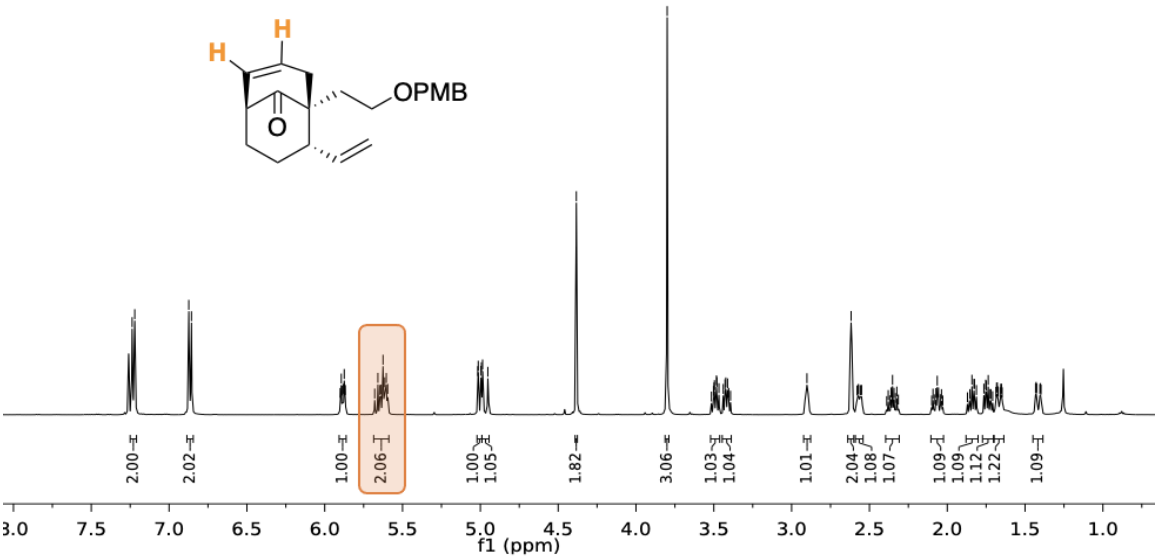

Figure 12. ^{1}HNMR ($CDCl_3$, 500 MHz) of 6-*endo-dig* product 2.179

As initial attempts at the gold-catalyzed Conia-ene reaction with terminal alkyne **2.162** afforded the undesired 6-*endo-dig* cyclized product, we synthesized the TMS-protected alkyne **2.181** (Scheme 23) to block the free terminal alkyne and attempted

cyclization with the [(*t*-BuJohnPhos)Au(MeCN)]SbF_6 ligand (Table 2). Similar to previous attempts, byproduct **2.179** was obtained or unidentifiable products. Although frustrating, obtaining the 6-*endo-dig* cyclized product was corroborated by work published by Barriault and co-workers and may proceed in a similar manner to their transition state depicted below.[42]

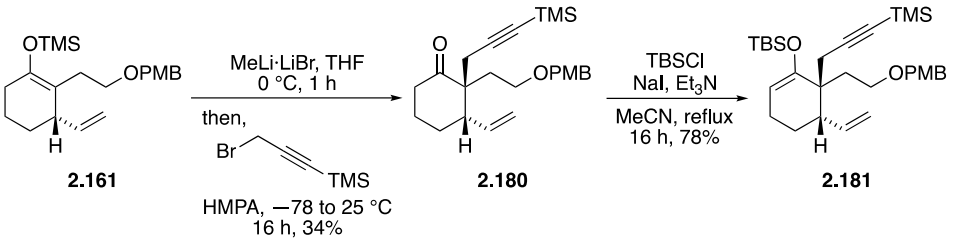

Scheme 23. Formation of TMS-protected Conia-ene substrate 2.181

Table 2. Gold-catalyzed conia-ene cyclization of TMS-protected alkyne

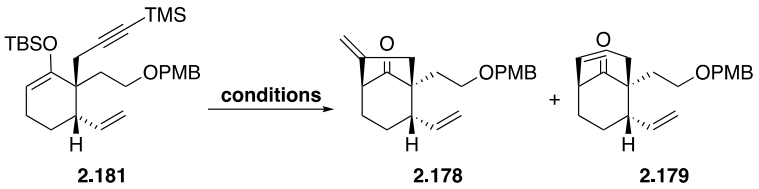

entry	catalyst	conditions	result
1	[(*t*-BuJohnPhos)Au(MeCN)]SbF_6	acetone, 45 °C, 5 h	**2.179**
2	[(*t*-BuJohnPhos)Au(MeCN)]SbF_6	CH_2Cl_2, 25 °C, 5 h	unidentified

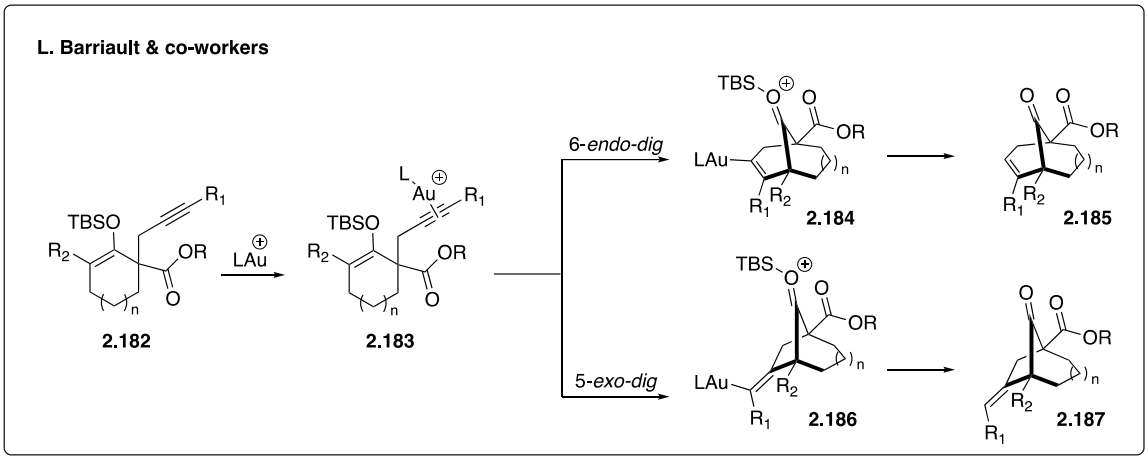

2.2.3.3 Mn(III)-mediated Radical Cyclization

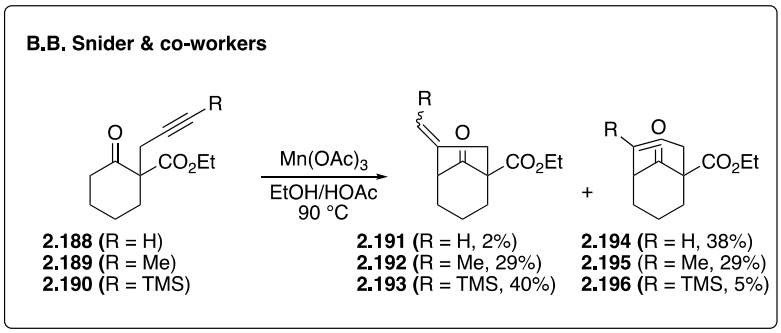

As Conia-ene type cyclizations failed to provide our desired 5-*exo-dig* product, we explored other types of cyclization reactions and came across work published by Snider and co-workers, in which they reported the Mn(III)-mediated radical cyclization of alkynyl ketones. In their studies they explored the effect substituents on the alkyne have on the formation of the 5-*exo*-cyclization product versus the 6-*endo*. They observed an increase in yield and regioselectivity for the 5-*exo*-cyclization product with the addition of a terminal trimethylsilyl group compared to a proton or methyl group. They postulated that the trimethylsilyl may make the alkyne more electron rich to react faster

with the deficient α-keto radical, stabilize the intermediate cyclic vinyl radical, facilitate hydrogen abstraction and/or stabilize the final product.[43]

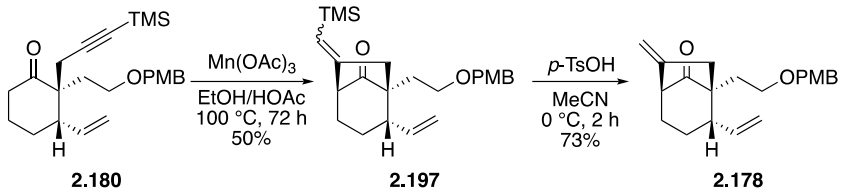

Scheme 24. Mn(III)-mediated radical cyclization

Inspired by Snider's work, we subjected our TMS-protected alkynyl ketone **2.180** to $Mn(OAc)_3$ in ethanol and acetic acid at 100 °C for 72 hours. Satisfyingly, we obtained the desired 5-*exo* cyclized product in 50% yield. As shown in Figure 13, the ^{1}H NMR now shows a broad singlet at ~5.5 ppm coming from the exo-methylene proton of the desired product. The TMS group can be removed under acidic conditions with *p*-toluenesulfonic acid in 73% yield (Scheme 24). In congruence with our findings, Jia and co-workers reported a Mn(III)-mediated radical cyclization for the preparation of a bicyclo[3.2.1]octane fragment in their synthesis of glaucocalyxin A (described in section 2.1.3.6).[26]

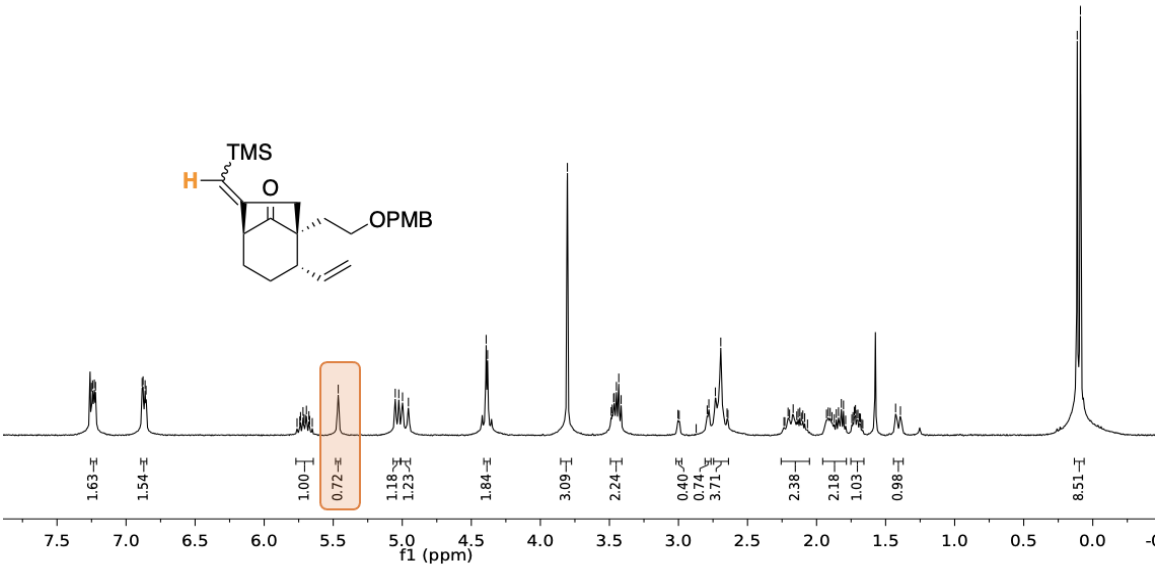

Figure 13. ^{1}H NMR ($CDCl_3$, 500 MHz) of 5-*exo-dig* product 2.197

2.2.4 Formation of the Equatorial Alcohol

2.2.4.1 PMB Protected γ-hydroxyl Ketone

Table 3. Direct reduction of PMB protected γ-hydroxyl ketone

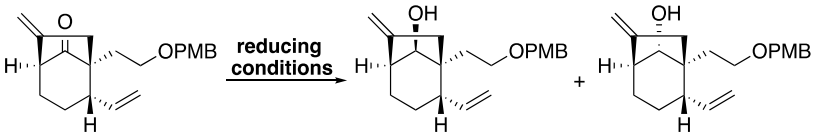

2.178 ***equatorial* (2.198)** ***axial* (2.199)**

entry	reagents	result
1	$NaBH_4$	**2.199**
2	DIBAL-H	**2.199**
3	L-Selectride	**2.199**
4	(R)-Me-CBS	**2.199**
5	(S)-Me-CBS	**2.199**

Having achieved the cyclization of alkynyl ketone **2.180** to form the desired 5/6 bridged ring system, we turned our attention to the stereoselective reduction of the C14 ketone. We began with the direct reduction of **2.178** with sodium borohydride.

Unfortunately, under these conditions we obtained a single product, the undesired axial alcohol **2.199**. Further attempts at direct reduction with various reducing reagents such as DIBAL-H, L-Selectride, (R)-Me-CBS and (S)-Me-CBS (Table 3) only provided undesired axial alcohol **2.199**. At this stage, we believed the nucleophile could not readily approach the more hindered *Si* face and inversion of the axial alcohol may be a more practical approach.

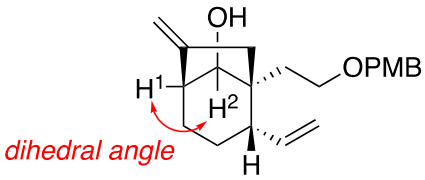

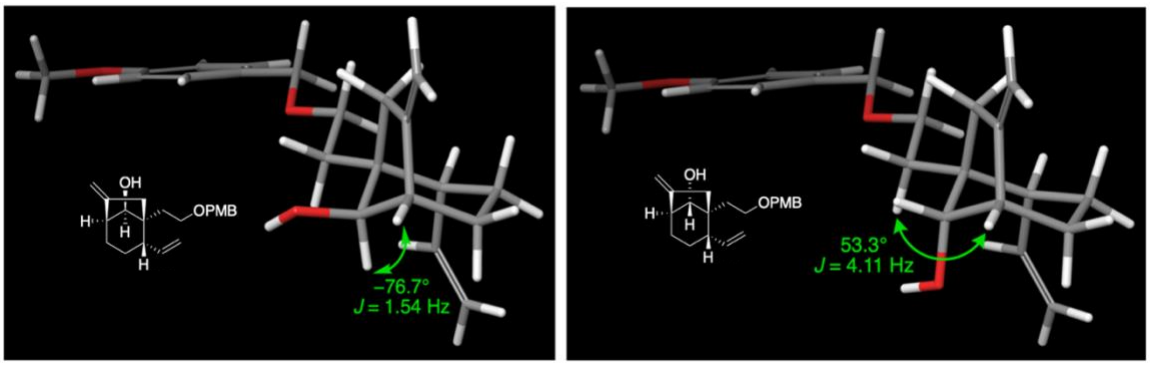

Figure 14. Stereochemical model of 2.198 and 2.199

The stereochemical assignment of the newly formed C14 hydroxyl was determined via ^{1}H-NMR. First, the theoretical coupling constants between protons labeled H^1 and H^2 (Figure 14) for each stereoisomer were calculated from their dihedral angles using Maestro (12.6.144, Schrödinger). Equatorial alcohol **2.198** has a dihedral angle of −76.7 °, therefore we would expect to see a small coupling constant around 1.54 Hz. In contrast, the axial alcohol **2.199** has a dihedral angle of 53.3 ° with a calculated

coupling constant of 4.11 Hz. Looking at the ^{1}H NMR spectral data for **2.199** (Figure 15), we see H^1 appears as a triplet with a coupling constant of 4.4 Hz, as it is coupled to H^2 and another vicinal proton. Likewise, H^2 is a triplet with a coupling constant of 4.4 Hz, as it is coupled with H^1 and the hydroxyl proton. Taken together, we determined the single isomer obtained was the undesired axial alcohol.

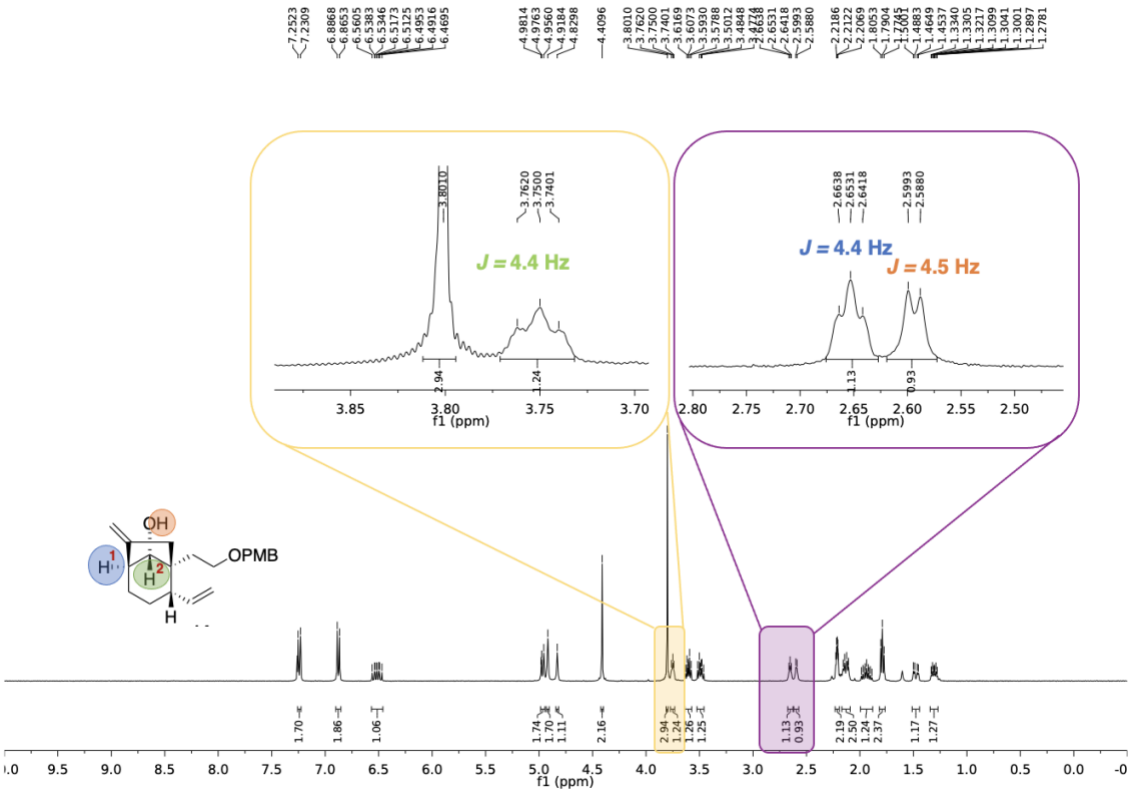

Figure 15. ^{1}H-NMR ($CDCl_3$, 500 MHz) spectrum of axial alcohol 2.199

As direct nucleophilic attack only provided the undesired axial alcohol, the inversion of axial alcohol **2.199** under Mitsunobu-type conditions was attempted. Unfortunately, this only resulted in the recovery of axial alcohol or decomposition (Scheme 25).

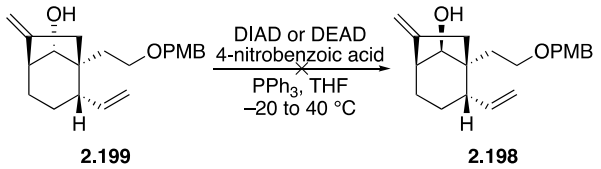

Scheme 25. Attempt at the inversion of axial alcohol 2.199

2.2.4.2 *β*-keto Ester Substrate

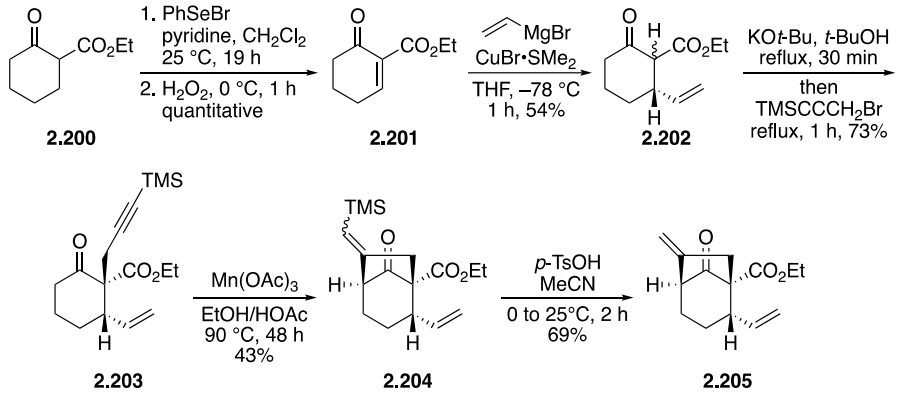

Scheme 26. Preparation of the *β*-keto ester substrate

Having had no success with obtaining the C14 equatorial alcohol from the PMB-protected γ-hydroxyl ketone, we synthesized *β*-keto ester **2.205**, as several reports have utilized esters as chelation control for the stereoselective reduction of ketones with SmI_2. The preparation of the *β*-keto ester substrate began with phenylselenylation and elimination of **2.200** to provide enone **2.201**.[44] Cu(I)-mediated conjugate addition of vinylmagnesium bromide provided **2.202** in 54% yield. Treatment of **2.202** with KO*t*-Bu followed by TMS-protected propargyl bromide provided intermediate **2.203** in 73% yield, poised for cyclization with $Mn(OAc)_3$. Lastly, the TMS group was removed with *p*-toluenesulfonic acid in 69% yield.

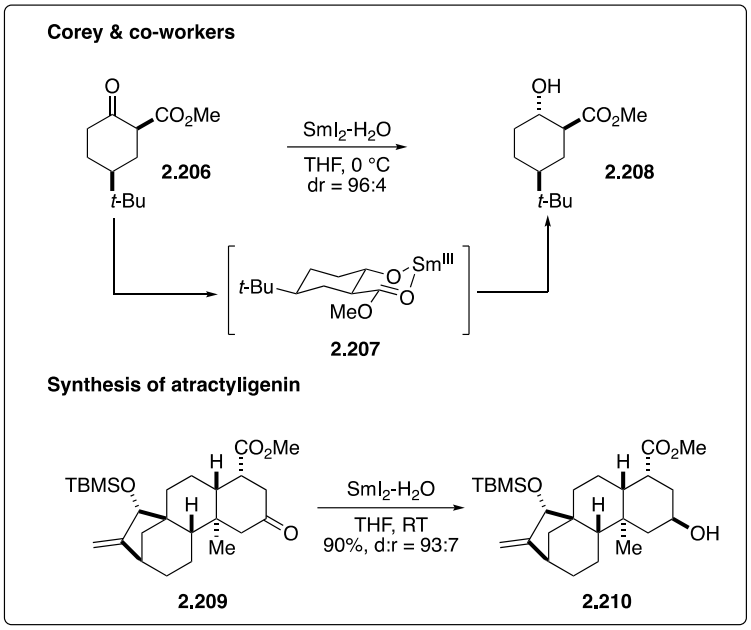

Inspiration for the chelation-controlled reduction of *β*-keto ester **2.205** came from work reported by Corey and co-workers in their synthesis of atractyligenin, in which they utilized an ester directed SmI_2 reduction in a 90% yield and d:r = 93:7.[45] Therefore, varying conditions for the SmI_2 reduction of our *β*-keto ester were attempted (Table 4). Excitingly, SmI_2 reduction in the presence of PhSH and HMPA in THF gave a 1:3 mixture (**2.211**: **2.212**) of products but unfortunately this ratio could not be improved under several different conditions for the SmI_2 reduction (entry 2-4).[46]

Table 4. SmI_2 reduction of β-keto ester substrate

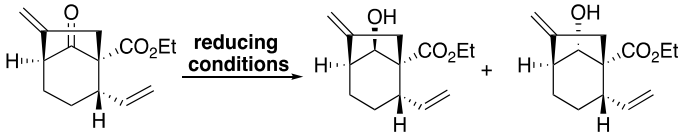

2.205 *equatorial* **(2.211)** *axial* **(2.212)**

entry	reagents	result
1	PhSH, HMPA, SmI_2, THF	1:3 mixture (**2.211**: **2.212**)
2	MeOH, HMPA, SmI_2, THF	unidentifiable
3	SmI_2, THF/MeOH	**2.212**
4	SmI_2, THF/H_2O	**2.212**

As shown in Figure 16, the stereochemistry of the β-keto ester substrate was also determined via ^{1}H-NMR. For the axial alcohol (**2.212**), H^1 appears as a triplet with a coupling constant of 4.7 Hz, and H^2 as a doublet of doublets with coupling constants 5.2 and 1.8 Hz. Conversely, H^2 of the equatorial alcohol (**2.211**) is a broad singlet.

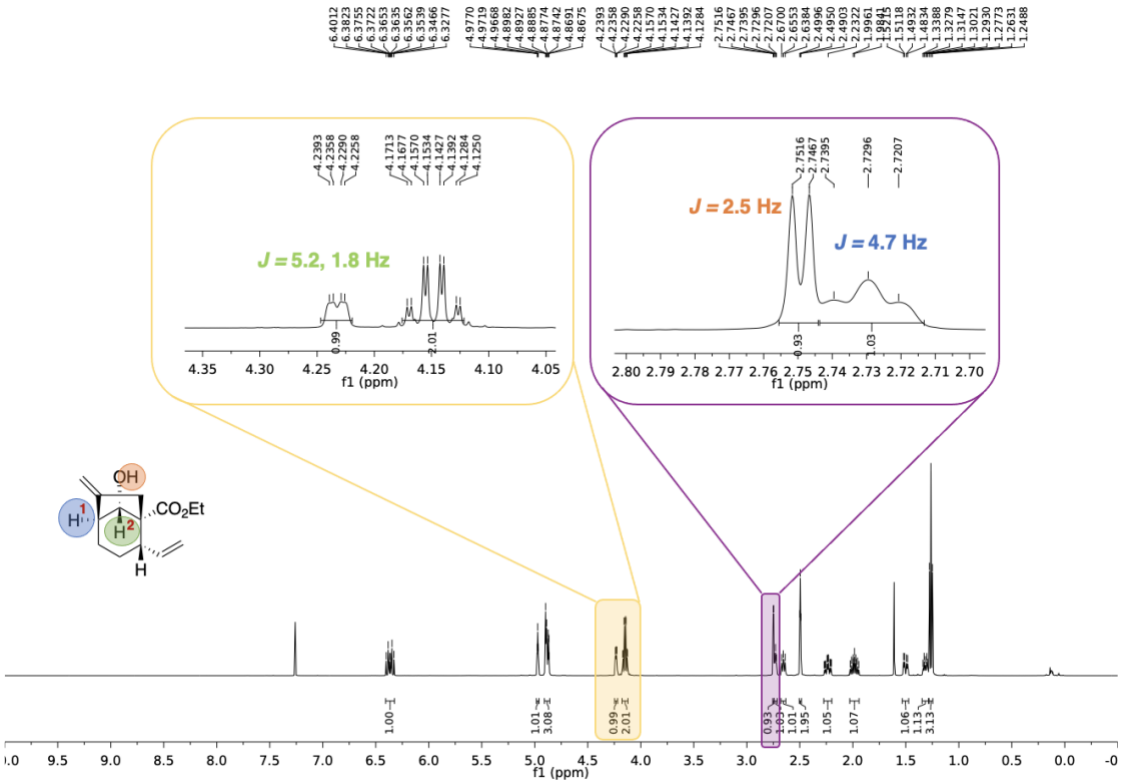

Figure 16. ^{1}H-NMR ($CDCl_3$, 500 MHz) spectrum of axial alcohol 2.212

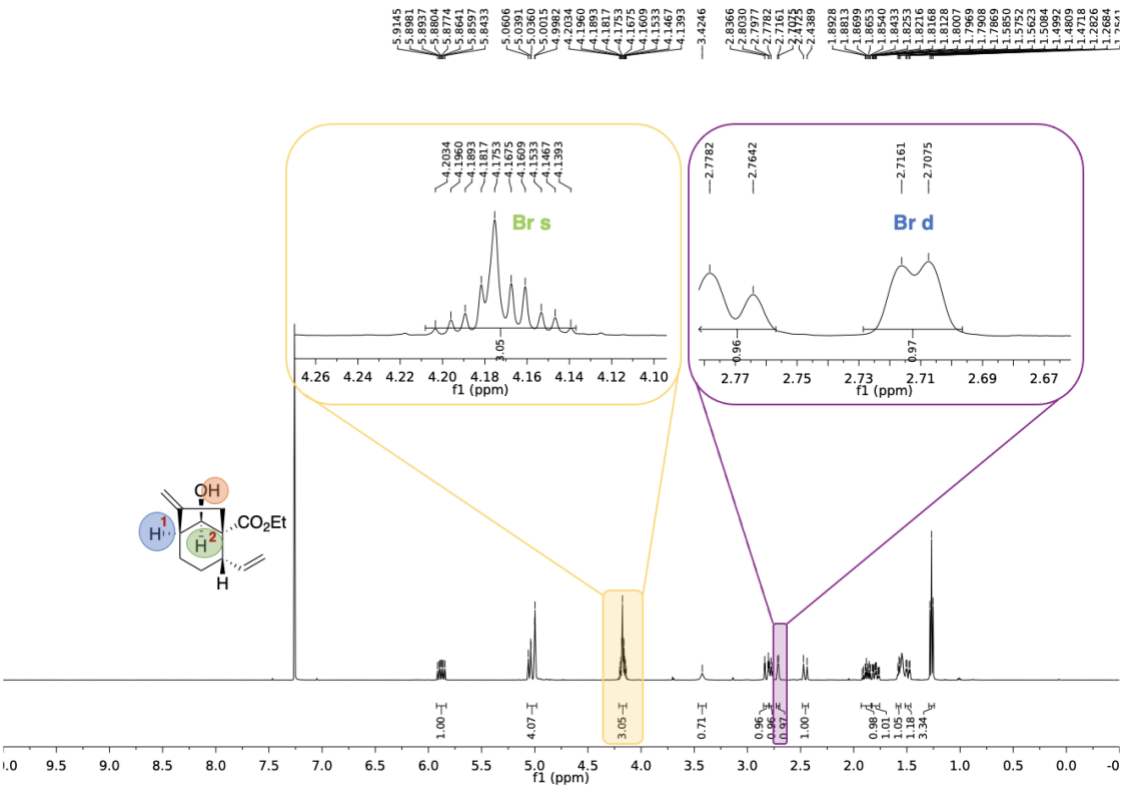

Figure 17. ^{1}H-NMR ($CDCl_3$, 500 MHz) spectrum of equatorial alcohol 2.211

With very limited success with SmI_2, we screened a very wide range of reducing conditions including $NaBH_4$, ruthenium catalyzed reductions with chiral ligands **2.214** and **2.215**, and an enzymatic reduction with Baker's yeast but frustratingly we could not obtain the desired equatorial alcohol **2.211** (Table 5).[47]

Table 5. Direct reduction of *β*-keto ester substrate

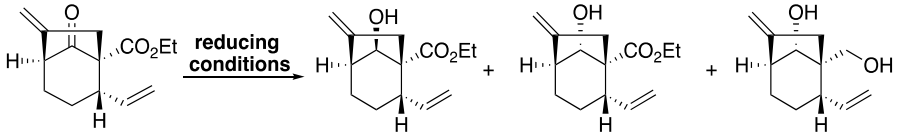

2.205 ***equatorial* (2.211)** ***axial* (2.212)** **2.213**

entry	condition	result
1	$NaBH_4$	**2.212**
2	$Zn(BH_4)_2$, THF, 0 °C, 1 h	**2.212**
3	$Me_4NBH(OAc)_3$, MeCN/AcOH, 10 °C, 5.5 h	**2.212**
4	(**L**$_{2.214}$, $[RuCl_2(p\text{-cymene})]_2$, sodium formate, H_2O, 30 °C, 3 d	**2.212**
5	(**L**$_{2.215}$, $[RuCl_2(p\text{-cymene})]_2$, sodium formate, H_2O, 30 °C, 3 d	**2.212**
6	Baker's yeast, sucrose, H_2O, 25 to 40 °C, 48 h	no reaction
7	H_2, PtO_2, EtOH, 25 °C, 1 h	olefin reduction
8	$MnCl_2$, $NaBH_4$, MeOH, 0 °C, 15 min	**2.212**
10	$H_3N\text{-}BH_3$, isopropanol, 25 °C, 3 h	**2.212**
11	$Zn(tmp)_2$, $LiBH_3NMe_2$, THF, 0 °C	**2.213**

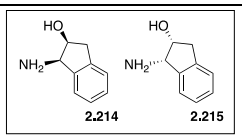

After thoroughly screening reducing conditions, we studied the inversion of axial alcohol **2.212** through activation by assorted activating reagents and inversion with KO_2 (Table 6). Firstly, activation of **2.212** with chloromethanesulfonyl chloride followed by inversion with KO_2 provided the desired equatorial alcohol **2.211** in 5% yield as well as undesired axial alcohol **2.212** in 14% yield. Although activation of **2.212** with methanesulfonyl chloride (entry 2) was successful, inversion with KO_2 provided undesired by-product **2.217**. We also attempted the inversion of the triflate (entry 3) but an unidentifiable mixture was obtained. Lastly, activation of **2.212** with *p*-toluenesulfonyl chloride was unsuccessful and only starting material was recovered.

Table 6. Inversion of β-keto ester substrate

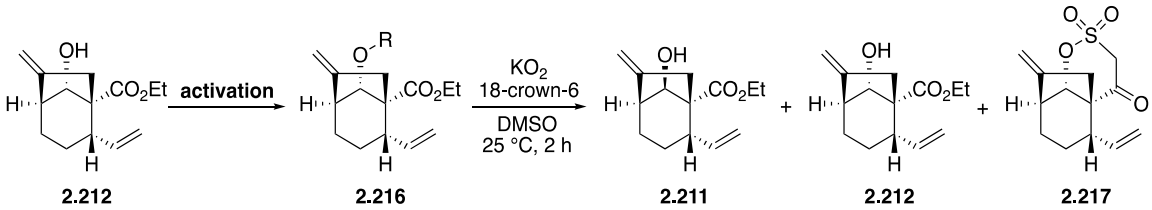

entry	activating reagent	result
1	chloromethanesulfonyl chloride	5% (**2.211**), 14% (**2.212**)
2	methanesulfonyl chloride	**2.217**
3	triflic anhydride	unidentified
4	*p*-toluenesulfonyl chloride	no reaction

2.2.4.3 β-hydroxy Ketone

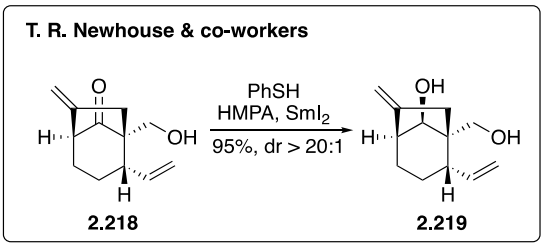

As previously discussed (section 2.1.3.4), Newhouse and co-workers published the total synthesis of principinol D, a grayanane-type diterpenoid in 2019.[24] In their synthetic approach, they utilized a SmI_2 reduction of a β-hydroxy ketone substrate to stereoselectively reduce the C14 ketone to provide equatorial alcohol **2.219**. Therefore, we decided to adopt their substrate to our synthetic approach and convert our β-keto ester substrate to the β-hydroxy ketone.

The formation of the β-hydroxy ketone started with $LiAlH_4$ reduction of our β-keto ester **2.205**, to form a diol. Following TBS protection of the primary alcohol, PCC oxidization reforms the ketone in a 79% yield and the TBS protecting group is removed

under acidic conditions to provide Newhouse's β-hydroxy ketone substrate. In congruence with Newhouse's findings, SmI_2 reduction with PhSH and HMPA resulted in the desired equatorial alcohol **2.219** in 78% yield.

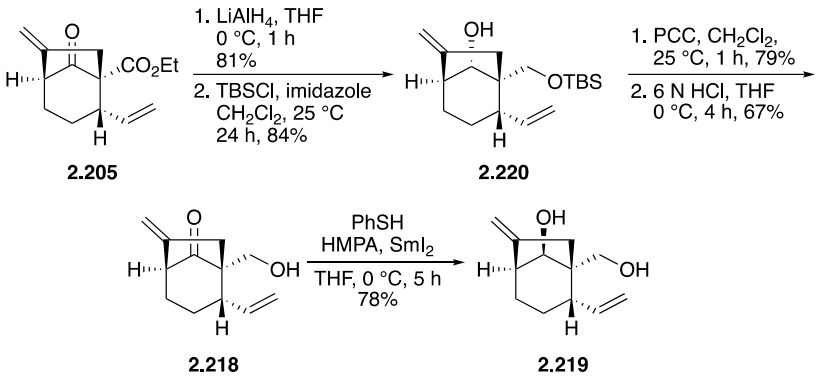

Scheme 27. SmI_2 reduction of the β-hydroxy ketone

In addition to the direct reduction of the β-hydroxy ketone, we also attempted the inversion of TBS-protected substrate **2.220** (Table 7). Activation using chloromethanesulfonyl chloride was achieved quantitatively but attempts to invert the stereochemistry with KO_2 or $Cs(OAc)_2$ were unsuccessful, resulting in the recovery of the axial alcohol **2.220** or in the case of $Cs(OAc)_2$ as the nucleophile, the activated substrate **2.221** was obtained.

Table 7. Attempts to invert *β*-hydroxy ketone

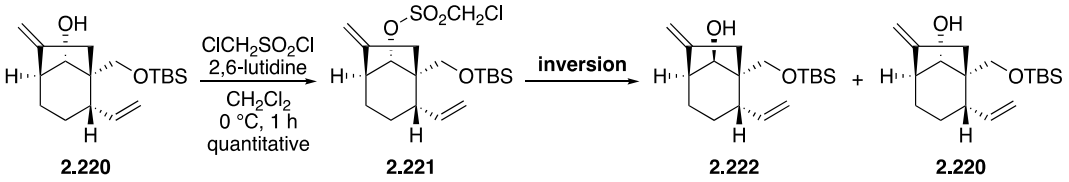

entry	nucleophile	result
1	KO_2	2.220
2	$Cs(OAc)_2$	2.221

2.2.5 Enantioselective Synthesis of the Bicyclo[3.2.1]octane Fragment

2.2.5.1 Asymmetric Conjugate Addition with Maduit-type Ligand

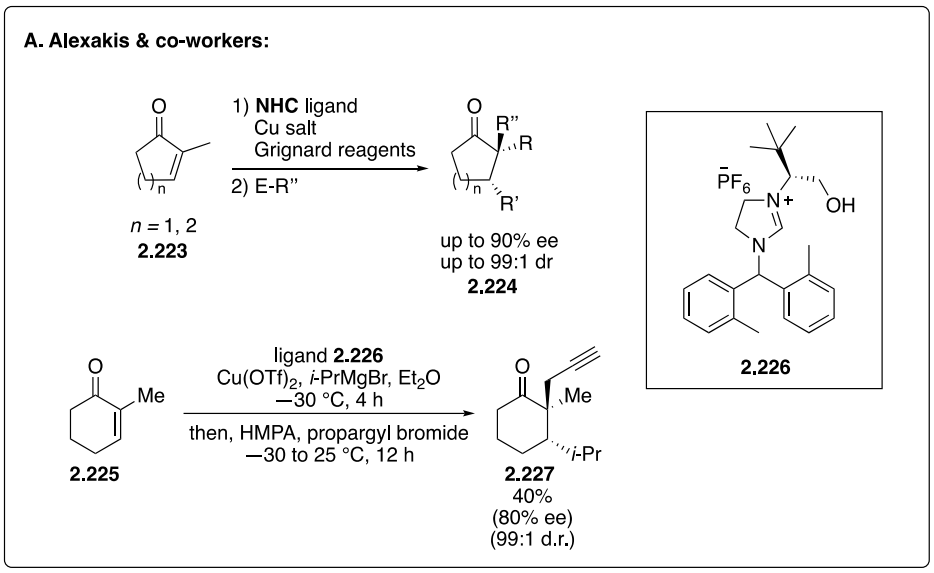

During our efforts to reduce the C14 ketone stereoselectively, we simultaneously worked on the development of an enantioselective route towards our key bicyclo[3.2.1]octane fragment. Our focus was on methodology to asymmetrically introduce substituents to the *β*-position of cyclic enones. In 2015, Alexakis *et al.* reported the use of a Maduit-type N-heterocyclic carbene (NHC) ligand in the copper-catalyzed

conjugate addition of Grignard reagents to α-substituted cyclic enones. Specifically, copper(I)-mediated addition of *i*-PrMgBr to 2-methylcyclohexanone (**2.225**) provided the magnesium enolate intermediate and subsequent addition of propargyl bromide afforded **2.227** in 40% yield and 80% ee.[48]

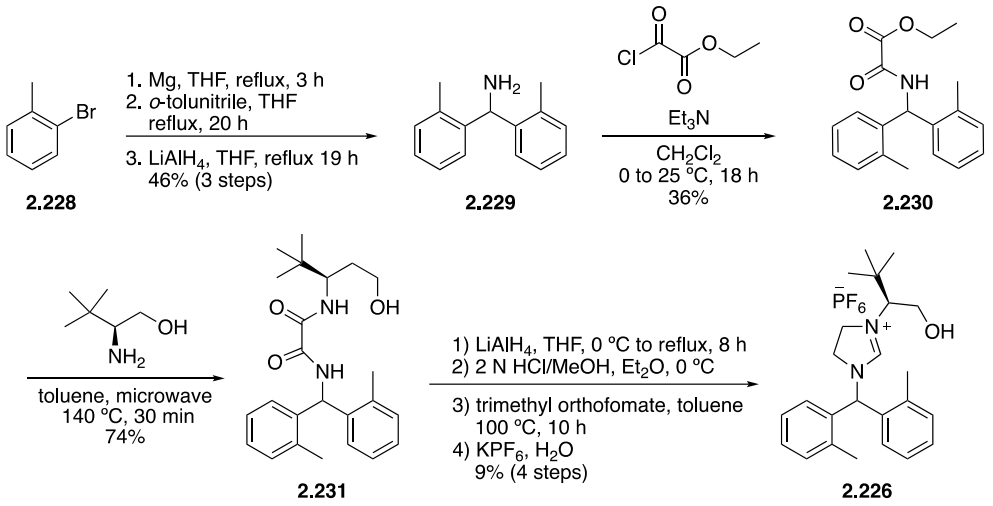

Scheme 28. Preparation of Maduit-type ligand

To apply this methodology to our system we first began by synthesizing ligand **2.226** in 9 steps following previously reported procedures, outlined in Scheme 28.[49] We then subjected our PMB-protected γ-hydroxyl ketone (**2.160**) to Cu(I)-mediated conjugate addition of vinylmagnesium bromide in the presence our newly synthesized ligand (Table 8). Initially, 1 mol% of ligand **2.26.**, 0.75 mol% of $Cu(OTf)_2$ and 1.2 equiv. of vinylmagnesium bromide provided our desired product **2.232** as a racemic mixture, determined by chiral HPLC (Figure 18). As shown in entry 2 of Table 8, we then increased ligand **2.226** to 20 mol%, while keeping the Cu mol% and Grignard the same,

this reaction did not provide any desired product but recovery of the starting material. Lastly, we attempted to increase not only the ligand mol% but the $Cu(OTf)_2$ and vinylmagnesium bromide proportionally and unfortunately a racemic mixture of **2.232** was obtained.

Table 8. Asymmetric conjugate addition attempts

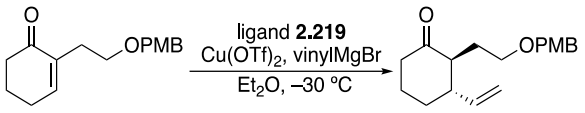

2.160 **2.232**

entry	Ligand (mol%)	$Cu(OTf)_2$ (mol%)	vinylMgBr (equiv)	result
1	1	0.75	1.2	racemic
2	20	0.75	1.2	no reaction
3	15	11.25	5.0	racemic

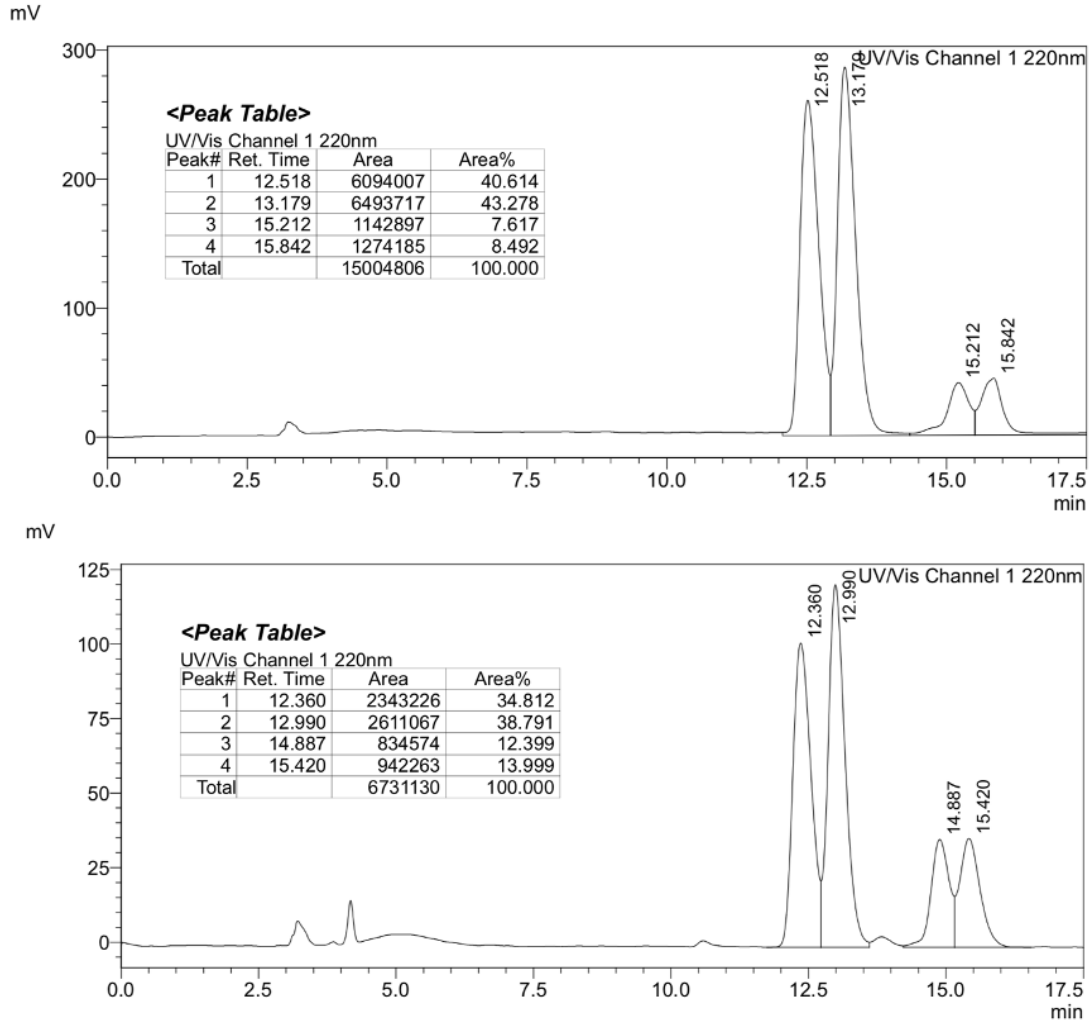

<Peak Table>

UV/Vis Channel 1 220nm

Peak#	Ret. Time	Area	Area%
1	12.518	6094007	40.614
2	13.179	6493717	43.278
3	15.212	1142897	7.617
4	15.842	1274185	8.492
Total		15004806	100.000

<Peak Table>

UV/Vis Channel 1 220nm

Peak#	Ret. Time	Area	Area%
1	12.360	2343226	34.812
2	12.990	2611067	38.791
3	14.887	834574	12.399
4	15.420	942263	13.999
Total		6731130	100.000

Figure 18. HPLC data for ACA reaction. (Top) racemic (bottom) attempt with maduit-type ligand

2.2.5.2 Rhodium Catalyzed Conjugate Addition

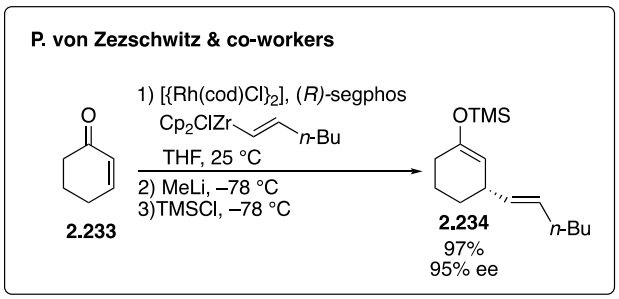

As the Maduit-type NHC ligand failed to provide any enantioselectivity in our copper(I)-mediated conjugate addition, we explored alternative ligands to accomplish this task. In 2013, Zezschwitz *et al*. reported the $[(Rh(cod)Cl)]_2$ and (*R*)-segphos catalyzed addition of an alkenylzirconocene to the *β*-position of cyclohexanone, followed by enolate trapping with TMSCl. They reported an excellent yield of 97% and 95% ee.[50]

Inspired by their work, we attempted the first step, introduction of the alkenylzirconocene. Initially, 2.5 mol% of $[(Rh(cod)Cl)]_2$, racemic BINAP (6 mol%), 1.3 equiv. of Schwartz' reagent ($Cp_2Zr(H)Cl$) and 1.2 equiv. of hexyne was used. Under these conditions, no reaction was observed (Table 9). Next, chiral (*R*)-Segphos was used but again no reaction. Therefore, we increased the equiv. of $[(Rh(cod)Cl)]_2$ and (*R*)-Segphos but the results remained the same. Lastly, to no avail we increased the equiv. of Schwartz reagent and hexyne but could not obtain our desired product.

Table 9. Attempts at rhodium catalyzed conjugate addition

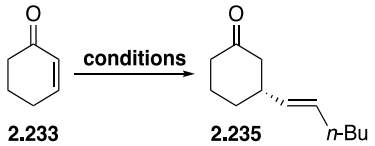

Entry	$Rh(cod)Cl_2$ (mol%)	Ligand	$Cp_2Zr(H)Cl$ (equiv)	Hexyne	result
1	2.5	(±)- BINAP (6 mol%)	1.3	1.2	no reaction
2	2.5	(*R*)-Segphos (6 mol%)	1.3	1.2	no reaction
3	5.0	(*R*)-Segphos (18 mol%)	1.3	1.2	no reaction
4	2.5	(*R*)-Segphos (6 mol%)	5.5	5.0	no reaction

2.2.5.3 ACA with Helmchen's Auxiliary

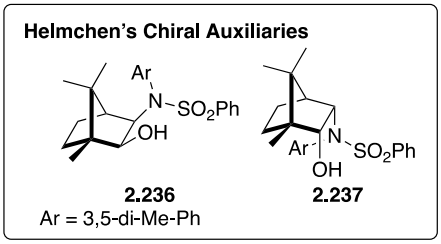

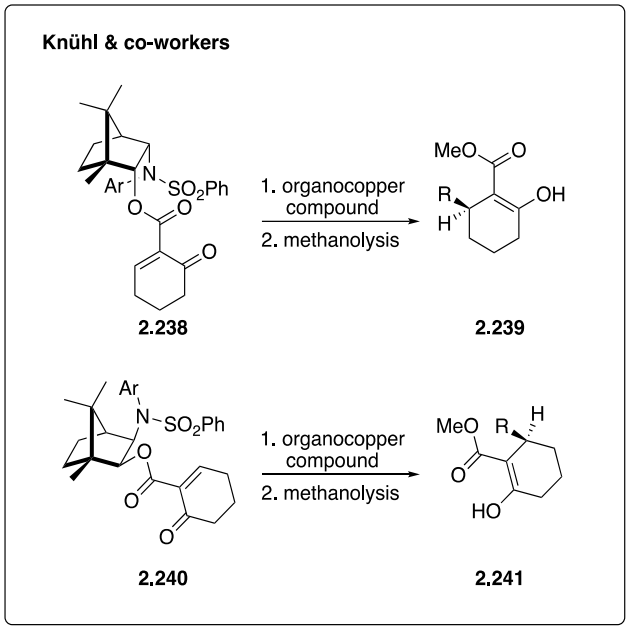

In 1981, Helmchen and co-workers introduced the sulfonamide-shielded alcohols **2.236** and **2.237** as valuable chiral auxiliaries for asymmetric synthesis with esters.[51] Methodology that was exploited by Knühl and co-workers during their synthesis of (–)-chokol A and (+)-heptelidic acid. Utilizing Helmchen's auxiliary, various cuprates were added to asymmetric protected 2-oxo-cyclohexenecarboxylates to prepare enantiomerically pure 5-substituted 2-oxo-cyclopentane-carboxylates and 6-substituted 2-oxo-cyclohexanecarboxylates.[52]

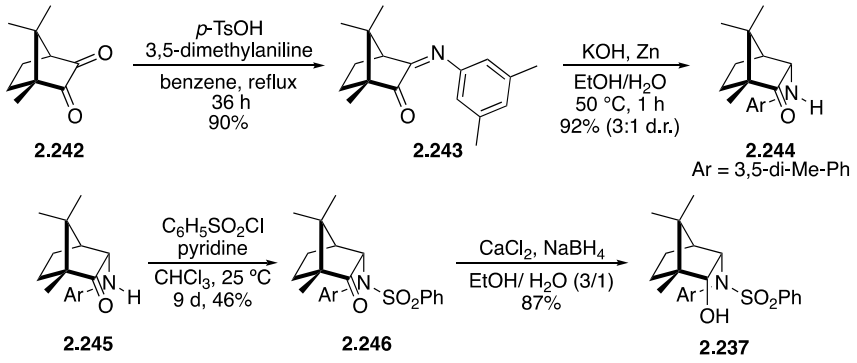

Scheme 29. Synthesis of Helmchen's Chiral Auxiliary

Following Knühl and co-workers lead, Helmchen's auxiliary was synthesized in 4 steps from previously reported procedures (Scheme 29).[53] The auxiliary was then coupled to ethyl 2-oxocyclohexanecarboxylate by refluxing in toluene in the presence of DMAP (Scheme 30). Phenylselenylation and elimination with *m*CPBA provided shielded enoate **2.238**. Finally, vinyl cuprate addition provided **2.249** in 68% yield.

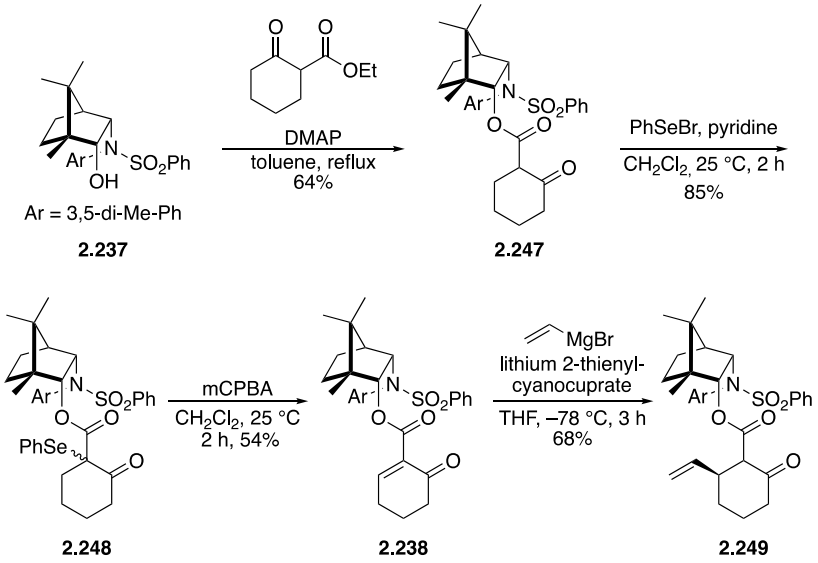

Scheme 30. ACA with Helmchen's chiral auxiliary

The removal of Helmchen's auxiliary was first attempted via methanolysis in the microwave at 135 °C for 3.5 h. Although the chiral auxiliary was recycled, product **2.250** was decomposed (Table 10). We then attempted hydrolysis with LiOH, H_2O_2 in THF/MeOH but even after 48 h, no reaction occurred. Returning to methanolysis, we attempted the reaction under milder conditions with a sealed tube rather than the microwave. When the reaction was warmed to 135 °C for 4 h there was no reaction but by increasing the temperature to 150 °C for 8 h, the desired methyl ester (**2.250**) was obtained in 52% yield. Additionally, the ethyl ester was prepared by treating **2.249** with ethanol at 150 °C for 48 h in a 41% yield.

Table 10. Removal of Helmchen's chiral auxiliary

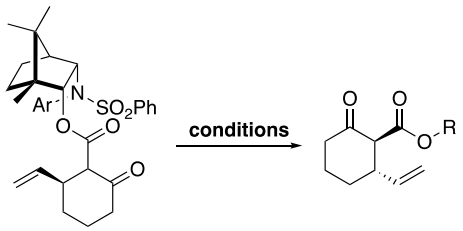

2.249 **2.250**

entry	conditions	temp. (°C)	time (h)	R	result
1	microwave, MeOH	135	3.5	Me	recovery of auxiliary
2	LiOH, H_2O_2, THF/MeOH	25	48	Me	no reaction
3	sealed tube, MeOH	135	4	Me	no reaction
4	sealed tube, MeOH	150	8	Me	52%
5	sealed tube, EtOH	150	48	Et	41%

2.3 Conclusion

Throughout history natural products have provided a rich source of therapeutic compounds for treating a wide variety of ailments and may provide an excellent platform for the development of non-opioid analgesics. Rhodojaponin III is a grayanane-type natural product that is extracted from the roots of *Rhododendron molle* and possesses potent analgesic properties. In a mouse model, it was even more potent than morphine in acute and inflammatory derived pain and 100-fold more potent than gabapentin in a diabetic neuropathic pain model. Notably, rhodojaponin III does not affect the endogenous opioid peptidergic system but the mechanism of action has yet to be established. Therefore, for further assessment of its analgesic properties and for the development of a chemical probe to study its mechanism of action we sought to establish an efficient route to complete the total synthesis of rhodojaponin III.

Our synthetic strategy relies on a convergent approach in which two major fragments are synthesized separately and coupled together to give the 5/7/6/5 ring system of grayanane-type natural products. The simpler 5-membered ring fragment was obtained in 4 steps from commercially available 2-methylcyclopentadione to provide a vinyl triflate primed for coupling to the 5/6 bicycle.

The construction of the key bicyclo[3.2.1]octane fragment was accomplished via a copper(I)-mediated conjugate addition to a simple cyclic enone, followed by propargylation to form an alkynyl intermediate poised for cyclization. Mn(III)-mediated radical cyclization of a TMS-protected alkynyl ketone then provided the 5/6 bridged

system. Finally, stereoselective reduction of a β-hydroxy ketone substrate with SmI_2 provided the coveted equatorial alcohol. The enantioselective synthesis was achieved utilizing Helmchen's chiral auxiliary to direct the copper(I)-mediated conjugate addition to a shielded enoate. These efforts will aid in the total synthesis of rhodojaponin III for the development of novel non-opioid analgesic therapeutics.

2.4 Experimental

General Methods

All reactions were conducted in oven-dried glassware under nitrogen or argon. Unless otherwise stated all reagents were purchased from commercial suppliers and used without further purification. All solvents were American Chemical Society (ACS) grade or better and used without further purification except tetrahydrofuran (THF), which was freshly distilled from sodium/benzophenone each time before use. Analytical thin layer chromatography (TLC) was performed with glass backed silica gel (60 Å) plates with fluorescent indication (Whatman). Visualization was accomplished by UV irradiation at 254 nm, or by staining with *p*-anisaldehyde solution or potassium permanganate solution followed by heating. Flash column chromatography was performed by using silica gel (particle size 230–400 mesh, 60 Å). All ^{1}H NMR and ^{13}C NMR spectra were recorded with a Varian 400 (400 MHz) and a Bruker 500 (500 MHz) spectrometer. All NMR δ values are given in parts per million (ppm) and are referenced to the residual isotopomer solvent signals ($CDCl_3$: δ = 7.26 ppm) for ^{1}H NMR spectra, or the solvent signals for ^{13}C spectra. Coupling constants (*J*) are given in Hertz (Hz) and

multiplicities are indicated using the conventional abbreviation (s = singlet, d = doublet, t = triplet, q = quartet, m = multiplet or overlap of non-equivalent resonances, br = broad). Electrospray ionization (ESI) mass spectrometry (MS) was recorded with an Agilent 6224 LC/MS-TOF (high resolution) spectrometer and performed to obtain the molecular masses of the compounds. Infrared (IR) absorption spectra were determined with a Thermo-Fisher (Nicolet iS50) spectrometer.

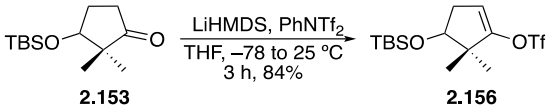

2.153 (100 mg, 0.41 mmol) in (2.0 mL) THF was cooled to –78 °C and LiHMDS (0.82 mmol) was added dropwise. The reaction was allowed to stir for 1 h. $PhNTf_2$ (206 mg, 0.58 mmol) in 2.5 mL THF was added dropwise and the reaction was allowed to warm to 25 °C over 3 h. The reaction was quenched with an addition of saturated NH_4Cl, and the resulting mixture was diluted with EtOAc. The layers were separated, and the aqueous layer was extracted with EtOAc. The combined organic layers were dried over anhydrous Na_2SO_4, filtered, and concentrated *in vacuo.* The residue was purified by column chromatography (hexanes) to afford **2.156** (130 mg, 84%). NMR data is in accordance with previously recorded data.[30]

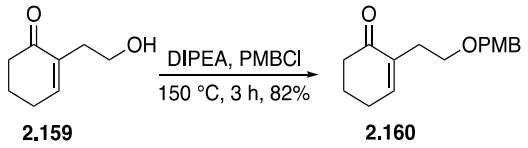

A mixture of PMBCl (0.11 mL, 0.79 mmol), DIPEA (0.15 mL, 0.87 mmol), and **2.159** (101 mg, 0.72 mmol) in a sealed tube was stirred at 150 °C for 3 h. After cooling down to 25 °C, the reaction was quenched with an addition of saturated aqueous $NaHCO_3$, and the resulting mixture was diluted with EtOAc. The layers were separated, and the aqueous layer was extracted with EtOAc. The combined organic layers were dried over anhydrous Na_2SO_4, filtered, and concentrated *in vacuo*. The residue was purified by column chromatography (silica gel, hexanes/EtOAc, 5/1) to afford **2.160** as a pale yellow oil (154 mg, 82%): ^{1}H NMR (400 MHz, $CDCl_3$) δ 7.22 (d, *J* = 7.5 Hz, 2H), 6.85 (d, *J* = 7.2 Hz, 2H), 6.80 (t, *J* = 4.5 Hz, 1H), 4.41 (s, 2H), 3.78 (s, 3H), 3.50 (t, *J* = 6.6 Hz, 2H), 2.48 (t, *J* = 6.5 Hz, 2H), 2.40 (t, *J* = 6.2 Hz, 2H), 2.36–2.31 (m, 2H), 1.99–1.93 (m, 2H); IR (neat, cm^{-1}) 2929, 2863, 1663, 1611, 1510, 1245, 1173, 1081, 1024, 819; HRMS (ESI) *m*/*z* 283.1313 [(M+Na)$^+$ calcd for $C_{16}H_{20}O_3$ 283.1305].

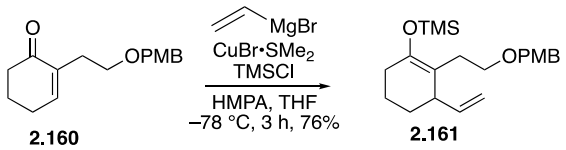

To a cooled solution (–78 °C) of CuBr·SMe_2 (26 mg, 0.13 mmol) in THF (2 mL) was added vinylmagnesium bromide (0.7 M in THF, 2.80 mmol) dropwise. After stirring for 15 min, HMPA (0.19 mL, 1.11 mmol) was added at –78 °C. After 20 min, the solution

of **2.160** (145 mg, 0.56 mmol) and TMSCl (0.14 mL, 1.11 mmol) in THF (0.2 mL) was added dropwise over 10 min at –78 °C. The stirring was continued for 3 h at –78 °C. Et_3N (0.16 mL, 1.69 mmol) was added and after 10 min, *n*-pentane was added. The mixture was poured into H_2O, the layers were separated while each phase was still cold, and the aqueous layer was extracted with EtOAc. The combined organic layers were dried over anhydrous Na_2SO_4, filtered, and concentrated *in vacuo*. The residue was purified by column chromatography (silica gel, hexanes/EtOAc, 8/1) to afford **2.161** as a colorless oil (153 mg, 76%): ^{1}H NMR (500 MHz, $CDCl_3$) δ 7.25 (d, *J* = 8.1 Hz, 2H), 6.86 (d, *J* = 8.6 Hz, 2H), 5.69 (ddd, *J* = 17.0, 10.2, 8.0 Hz, 1H), 4.98 (d, *J* = 9.9 Hz, 1H), 4.96 (d, *J* = 16.9 Hz, 1H), 4.42 (d, *J* = 1.9 Hz, 2H), 3.80 (s, 3H), 3.44–3.41 (m, 2H), 2.78–2.75 (m, 1H), 2.59–2.53 (m, 1H), 2.12–1.96 (m, 3H), 1.72–1.53 (m, 3H), 1.48–1.43 (m, 1H), 0.17 (s, 9H); IR ($CHCl_3$, cm^{-1}) 2935, 2864, 1708, 1610, 1512, 1247, 1214, 1171, 1097, 1032, 822.

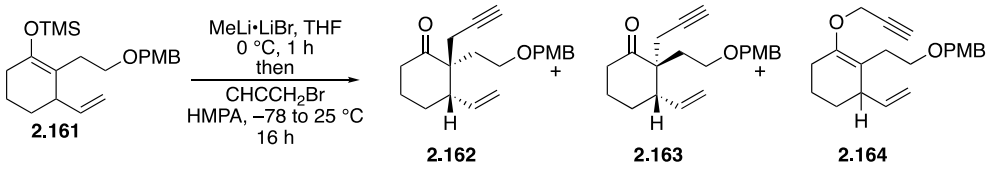

To a cooled solution (0 °C) of **2.161** (265 mg, 0.73 mmol) in THF (6.5 mL) was added MeLi·LiBr (1.5 M in Et_2O, 0.81 mmol) dropwise. The resulting mixture was stirred for 1 h and then cooled to –78 °C. Propargyl bromide (80% in toluene, 1.84 mmol) in HMPA (1.8 mL) was added dropwise at –78 °C. The resulting solution was allowed to stir for 16 h with gradual warming to 25 °C. The reaction was quenched with an addition

of H_2O, and the resulting mixture was diluted with EtOAc. The layers were separated, and the aqueous layer was extracted with EtOAc. The combined organic layers were dried over anhydrous Na_2SO_4, filtered, and concentrated *in vacuo*. The residue was purified by column chromatography (silica gel, hexanes/EtOAc, 15/1) to afford **2.162**, **2.163**, and **2.164**. For **2.162** (colorless oil, 88 mg, 37%): ^{1}H NMR (500 MHz, $CDCl_3$) δ 7.20 (d, *J* = 8.5 Hz, 2H), 6.85 (d, *J* = 8.5 Hz, 2H), 5.79 (ddd, *J* = 18.4, 10.3, 8.4 Hz, 1H), 5.21 (d, *J* = 17.1 Hz, 1H), 5.11 (d, *J* = 10.4 Hz, 1H), 4.31–4.26 (m, 2H), 3.79 (s, 3H), 3.42–3.37 (m, 1H), 3.21 (ddd, *J* = 9.4, 7.2, 7.2 Hz, 1H), 2.91–2.83 (m, 2H), 2.56 (ddd, *J* = 14.1, 14.1, 6.3 Hz, 1H), 2.34 (d, *J* = 14.2 Hz, 1H), 2.23 (ddd, *J* = 14.5, 7.3, 7.3 Hz, 1H), 2.11 (dd, *J* = 16.5, 2.6 Hz, 1H), 2.00 (t, *J* = 2.6 Hz, 1H), 2.02–1.97 (m, 1H), 1.92–1.83 (m, 1H), 1.73–1.60 (m, 3H); ^{13}C NMR (125 MHz, $CDCl_3$) δ 211.4, 159.3, 137.0, 130.2, 129.6 (2C), 117.4, 113.9 (2C), 82.0, 73.1, 71.0, 65.7, 55.4, 53.8, 48.8, 39.2, 32.2, 26.6, 25.1, 23.3; IR (neat, cm^{-1}) 3306, 3273, 2943, 2859, 2112, 1704, 1611, 1513, 1245, 1174, 1103, 1082, 1032, 918, 814; HRMS (ESI) *m*/*z* 327.1946 [$(M+H)^+$ calcd for $C_{21}H_{26}O_3$ 327.1955]; For **2.163** (colorless oil, 35%): ^{1}H NMR (400 MHz, $CDCl_3$) δ 7.20 (d, *J* = 8.6 Hz, 2H), 6.85 (d, *J* = 8.6 Hz, 2H), 5.67 (ddd, *J* = 16.9, 10.1, 10.1 Hz, 1H), 5.16 (dd, *J* = 16.9, 1.9 Hz, 1H), 5.07 (dd, *J* = 10.2, 1.9 Hz, 1H), 4.32 (s, 2H), 3.78 (s, 3H), 3.55–3.50 (m, 1H), 3.35–3.30 (m, 1H), 2.79–2.71 (m, 2H), 2.56 (dd, *J* = 17.6, 2.7 Hz, 1H), 2.44–2.37 (m, 1H), 2.32–2.11 (m, 4H), 1.93 (t, *J* = 2.7 Hz, 1H), 1.91–1.85 (m, 2H), 1.64–1.58 (m, 1H); IR (neat, cm^{-1}) 3288, 2935, 2869, 2116, 1701, 1612, 1512, 1244, 1173, 1093, 1033, 920, 819; HRMS (ESI) *m*/*z* 349.1780 [$(M+Na)^+$ calcd for $C_{21}H_{26}O_3$ 349.1774]; For **2.164** (A colorless oil, 15%): ^{1}H NMR (400 MHz, $CDCl_3$) δ 7.26 (d, *J* = 8.6 Hz, 2H), 6.87 (d, *J* = 8.6 Hz, 2H),

5.69 (ddd, *J* = 16.2, 10.9, 8.1 Hz, 1H), 5.02 (s, 1H), 4.99 (d, *J* = 5.5 Hz, 1H), 4.44 (s, 2H), 4.37 (d, *J* = 2.4 Hz, 2H), 3.80 (s, 3H), 3.52–3.43 (m, 2H), 2.83–2.78 (m, 1H), 2.74–2.65 (m, 1H), 2.39 (t, *J* = 2.4 Hz, 1H), 2.15–2.08 (m, 2H), 1.75–1.58 (m, 4H), 1.51–1.45 (m, 1H); IR (neat, cm^{-1}) 3290, 2932, 2859, 2117, 1612, 1511, 1244, 1142, 1085, 1032, 917, 819; HRMS (ESI) *m*/*z* 349.1779 [$(M+Na)^+$ calcd for $C_{21}H_{26}O_3$ 349.1774].

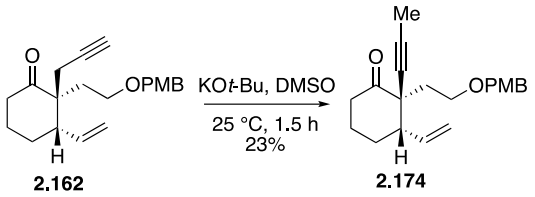

To a solution of **2.162** (22 mg, 0.07 mmol) in degassed DMSO (0.05 mL) was added KO*t*-Bu (8 mg, 0.07 mmol) in degassed DMSO (1.0 mL) at 25 °C. After stirring for 1.5 h, the reaction was quenched with an addition of H_2O and saturated aqueous NH_4Cl, and the resulting mixture was diluted with EtOAc. The layers were separated, and the aqueous layer was extracted with EtOAc. The combined organic layers dried over anhydrous Na_2SO_4, filtered and concentrated *in vacuo*. The residue was purified by column chromatography (silica gel, hexanes/EtOAc, 10/1) to afford **2.174** as a colorless oil (5 mg, 23%). ^{1}H NMR (500 MHz, $CDCl_3$) δ 7.24 (d, *J* = 8.6 Hz, 2H), 6.86 (d, *J* = 8.6 Hz, 2H), 5.79 (ddd, *J* = 17.1, 10.5, 8.2 Hz, 1H), 5.11 (d, *J* = 10.9 Hz, 1H), 5.08 (d, *J* = 17.2 Hz, 1H), 4.40 (d, *J* = 11.3 Hz, 1H), 4.34 (d, *J* = 11.3 Hz, 1H), 3.79 (s, 3H), 3.65–3.54 (m, 2H), 2.76 (ddd, *J* = 13.8, 8.5, 5.7 Hz, 1H), 2.67 (ddd, *J* = 7.6, 7.6, 4.0 Hz, 1H), 2.43 (ddd, *J* = 13.3, 7.8, 5.5 Hz, 1H), 2.24–2.12 (m, 2H), 1.98–1.90 (m, 1H), 1.86 (s, 3H), 1.82–1.75 (m, 1H), 1.73–

1.64 (m, 2H); IR ($CHCl_3$, cm^{-1}) 2937, 2865, 1716, 1612, 1513, 1247, 1214, 1098, 1035, 743; HRMS (ESI) *m/z* 327.1958 [$(M+H)^+$ calcd for $C_{21}H_{26}O_3$ 327.1955].

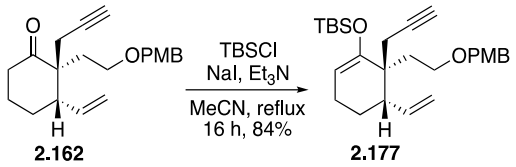

To a solution of **2.162** (50 mg, 0.15 mmol) in MeCN (2 mL) was added Et_3N (0.09 mL, 0.61 mmol), and then flame dried NaI (69 mg, 0.46 mmol) and TBSCl (69 mg, 0.46 mmol) were added. The mixture was allowed to reflux for 16 h. After cooling down to 25 °C, the reaction was quenched with an addition of saturated aqueous $NaHCO_3$, and the resulting mixture was diluted with EtOAc. The layers were separated, and the aqueous layer was extracted with EtOAc. The combined organic layers were dried over anhydrous Na_2SO_4, filtered, and concentrated *in vacuo*. The residue was purified by column chromatography (silica gel, hexanes/EtOAc, 10/1) to afford **2.177** as a colorless oil (57 mg, 84%): ^1H NMR (400 MHz, $CDCl_3$) δ 7.24 (d, *J* = 8.5 Hz, 2H), 6.87 (d, *J* = 8.6 Hz, 2H), 5.78 (ddd, *J* = 17.1, 10.3, 8.8 Hz, 1H), 5.14 (d, *J* = 17.1 Hz, 1H), 5.06 (dd, *J* = 10.2, 1.9 Hz, 1H), 4.82 (dd, *J* = 5.2, 2.3 Hz, 1H), 4.40 (s, 2H), 3.80 (s, 3H), 3.60–3.47 (m, 2H), 2.77–2.67 (m, 1H), 2.60 (dd, *J* = 16.3, 2.5 Hz, 1H), 2.18–2.09 (m, 2H), 2.04–1.97 (m, 1H), 1.92–1.91 (m, 1H), 1.83–1.75 (m, 1H), 1.62–1.55 (m, 3H), 0.93 (s, 9H), 0.20 (s, 3H), 0.16 (s, 3H); IR (neat, cm^{-1}) 3307, 2928, 2855, 1661, 1612, 1512, 1246, 1194, 1093, 1037, 836; HRMS (ESI) *m/z* 441.2818 [$(M+H)^+$ calcd for $C_{27}H_{40}O_3Si$ 441.2820].

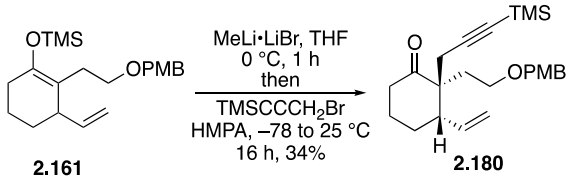

To a cooled solution (0 °C) of **2.161** (516 mg, 1.43 mmol) in THF (10 mL) was added dropwise MeLi·LiBr (1.5 M in Et_2O, 1.50 mmol). The resulting mixture was stirred for 1 h and then cooled to –78 °C. (3-Bromoprop-1-yn-1-yl)trimethylsilane (0.6 mL, 3.58 mmol) in HMPA (2.5 mL) was added dropwise at –78 °C. The resulting solution was allowed to stir for 16 h with gradual warming to 25 °C. The reaction was quenched with an addition of H_2O, and the resulting mixture was diluted with EtOAc. The layers were separated, and the aqueous layer was extracted with EtOAc. The combined organic layers were dried over anhydrous Na_2SO_4, filtered, and concentrated *in vacuo*. The residue was purified by column chromatography (silica gel, hexanes/EtOAc, 20/1) to afford **2.180** as a colorless oil (194 mg, 34%, d.r. = 1:1): ^{1}H NMR (400 MHz, $CDCl_3$) δ 7.20 (d, *J* = 8.6 Hz, 2H), 6.85 (d, *J* = 8.6 Hz, 2H), 5.81 (ddd, *J* = 17.2, 10.3, 8.4 Hz, 1H), 5.19 (d, *J* = 17.1 Hz, 1H), 5.09 (dd, *J* = 10.3, 1.8 Hz, 1H), 4.28 (d, *J* = 4.8 Hz, 2H), 3.79 (s, 3H), 3.43–3.38 (m, 1H), 3.23–3.17 (m, 1H), 2.87–2.79 (m, 2H), 2.56 (ddd, *J* = 14.0, 14.0, 6.2 Hz, 1H), 2.32 (d, *J* = 14.4 Hz, 1H), 2.26–2.19 (m, 2H), 2.03–1.98 (m, 1H), 1.92–1.82 (m, 1H), 1.73–1.64 (m, 3H), 0.13 (s, 9H); ^{13}C NMR (125 MHz, $CDCl_3$) δ 211.2, 159.3, 137.2, 130.3, 129.6 (2C), 117.1, 113.9 (2C), 104.9, 87.6, 73.1, 65.8, 55.4, 53.9, 49.4, 39.2, 32.2, 26.8, 25.3, 24.7, 0.2 (3C); IR ($CHCl_3$, cm^{-1}) 2956, 2864, 2174, 1705, 1612, 1513, 1246, 1173, 1109, 1035, 911, 839; HRMS (ESI) *m/z* 399.2346 [$(M+H)^+$ calcd for $C_{24}H_{34}O_3Si$ 399.2350].

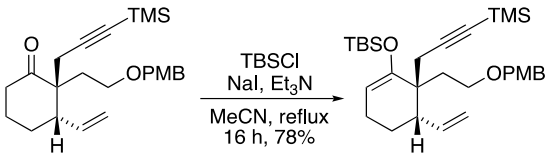

2.180 **2.181**

To a solution of **2.180** (16 mg, 0.04 mmol) in acetonitrile (0.5 mL) was added Et_3N (0.02 mL, 0.16 mmol), and then flame dried NaI (18 mg, 0.12 mmol) and TBSCl (18 mg, 0.12 mmol) were added. The mixture was allowed to reflux for 16 h. After cooling down to room temperature, the reaction mixture was quenched with saturated aqueous $NaHCO_3$ and diluted with EtOAc. The layers were separated, and the aqueous layer was extracted with EtOAc. The combined organic layers were dried over anhydrous Na_2SO_4, filtered, and concentrated *in vacuo*. The residue was purified by column chromatography (silica gel, hexane/EtOAc, 20/1) to afford **2.181** as a colorless oil (55 mg, 78%): ^{1}H NMR (400 MHz, $CDCl_3$) δ 7.23 (d, *J* = 8.6 Hz, 2H), 6.86 (d, *J* = 8.6 Hz, 2H), 5.79 (ddd, *J* = 16.9, 10.2, 8.8 Hz, 1H), 5.12 (dd, *J* = 17.0, 2.2 Hz, 1H), 5.05 (dd, *J* = 10.2, 2.3 Hz, 1H), 4.80 (dd, *J* = 5.3, 2.6 Hz, 1H), 4.39 (s, 2H), 3.80 (s, 3H), 3.57–3.45 (m, 2H), 2.74 (td, *J* = 9.0, 5.5 Hz, 1H), 2.59 (d, *J* = 16.4 Hz, 1H), 2.16 (d, *J* = 16.5 Hz, 1H), 2.14–1.94 (m, 2H), 1.80–1.73 (m, 1H), 1.64–1.47 (m, 3H), 0.92 (s, 9H), 0.19 (s, 3H), 0.15 (s, 3H), 0.12 (s, 9H).

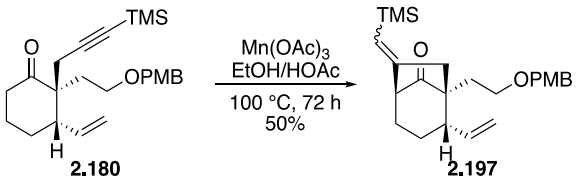

2.180 **2.197**

A solution of **2.180** (180 mg, 0.45 mmol) in EtOH (7.2 mL) and HOAc (0.8 mL) was degassed with argon at –78 °C for 25 min. After warming to 25 °C, $Mn(OAc)_3$ (1.05

g, 4.52 mmol) was added and the reaction mixture was warmed to 100 °C for 36 h. The reaction mixture was then cooled to 25 °C and additional $Mn(OAc)_3$ (1.05 g, 4.52 mmol) was added. The reaction mixture was then heated to 100 °C for 36 h. Upon cooling to 25 °C, the reaction was diluted with EtOAc, washed with 10 % $NaHSO_3$ and saturated aqueous $NaHCO_3$. The organic layer was dried with anhydrous Na_2SO_4, filtered and concentrated *in vacuo*. The residue was purified by column chromatography (silica gel, hexanes/EtOAc, 10/1) to afford **2.197** as a mixture of *E*/*Z* isomers (colorless oil, 90 mg, 50%): ^{1}H NMR (400 MHz, $CDCl_3$) δ 7.24 (dd, *J* = 8.5, 3.4 Hz, 2H), 6.87 (dd, *J* = 8.6, 2.8 Hz, 2H), 5.71 (dddd, *J* = 16.9, 10.0, 9.7, 7.7 Hz, 1H), 5.46 (s, 1H), 5.04 (d, *J* = 10.2 Hz, 1H), 4.98 (d, *J* = 17.1 Hz, 1H), 4.39 (d, *J* = 4.1 Hz, 2H), 3.80 (s, 3H), 3.49–3.42 (m, 2H), 3.00 (d, *J* = 3.4 Hz, 1H, minor), 2.79 (d, *J* = 4.7 Hz, 1H, major) 2.73–2.64 (m, 3H), 2.24–2.06 (m, 2H), 1.93–1.79 (m, 2H), 1.74–1.67 (m, 1H), 1.41 (d, *J* = 14.0 Hz, 1H), 0.11 (s, 9H, minor), 0.09 (s, 9H, major); IR ($CHCl_3$, cm^{-1}) 2951, 1746, 1608, 1513, 1248, 1214, 1117, 1100, 1034, 838; HRMS (ESI) *m*/*z* 399.2355 [$(M+H)^+$ calcd for $C_{24}H_{34}O_3Si$ 399.2350].

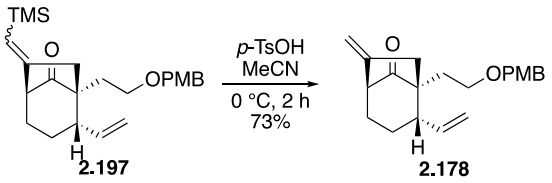

To a cooled solution (0 °C) of **2.197** (25 mg, 0.06 mmol) in MeCN (1.0 mL) was added *p*-TsOH (24 mg, 0.12 mmol). After stirring for 2 h at 0 °C, the reaction was quenched with an addition of saturated aqueous $NaHCO_3$, and the resulting mixture

was diluted with CH_2Cl_2. The layers were separated, and the aqueous layer was extracted with CH_2Cl_2. The combined organic layers were dried over anhydrous Na_2SO_4, filtered, and concentrated *in vacuo*. The residue was purified by column chromatography (silica gel, hexanes/EtOAc, 10/1) to afford **2.178** as a colorless oil (15 mg, 73%): ^{1}H NMR (400 MHz, $CDCl_3$) δ 7.23 (d, *J* = 8.5 Hz, 2H), 6.87 (d, *J* = 8.5 Hz, 2H), 5.70 (ddd, *J* = 16.8, 10.1, 10.1 Hz, 1H), 5.03 (dd, *J* = 10.3, 1.6 Hz, 1H), 4.99–4.95 (m, 3H), 4.39 (d, *J* = 4.5 Hz, 2H), 3.81 (s, 3H), 3.44 (t, *J* = 6.8 Hz, 2H), 2.87 (d, *J* = 4.7 Hz, 1H), 2.74–2.62 (m, 3H), 2.25–2.09 (m, 2H), 1.93–1.87 (m, 1H), 1.83 (ddd, *J* = 14.1, 6.3, 6.3 Hz, 1H), 1.70 (ddd, *J* = 14.5, 7.1, 7.1 Hz, 1H), 1.41 (d, *J* = 12.1 Hz, 1H); ^{13}C NMR (125 MHz, $CDCl_3$) δ 218.0, 159.3, 144.7, 137.5, 130.7, 129.3 (2C), 117.0, 113.9 (2C), 107.8, 72.6, 66.1, 55.4, 54.80, 54.79, 53.3, 39.4, 36.2, 30.3, 25.2; IR ($CHCl_3$, cm^{-1}) 2937, 2859, 1746, 1612, 1513, 1247, 1214, 1096, 1034; HRMS (ESI) *m/z* 327.1955 [$(M+H)^+$ calcd for $C_{21}H_{26}O_3$ 327.1955].

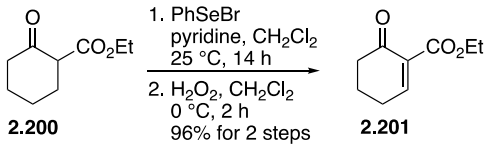

Compound **2.201** was prepared according to a previously reported procedure.[44] To a solution of PhSeBr (7.6 g, 32.31 mmol) in CH_2Cl_2 (345 mL) was added pyridine (2.6 mL) dropwise. After stirring for 25 min, ethyl 2-oxocyclohexanecarboxylate (4.7 mL, 29.38 mmol) in CH_2Cl_2 (155 mL) was slowly added. After stirring for 14 h, the reaction was quenched with 1 N HCl and the layers were separated. The organic layer was dried over anhydrous Na_2SO_4, filtered and concentrated *in vacuo*. The residue was purified by

column chromatography (silica gel, hexanes/EtOAc, 10/1) to afford the phenyl selenide (9.8 g, quantitative). The phenyl selenide (9.8 g, 30.13 mmol) was dissolved in CH_2Cl_2 (550 mL) and the resulting solution was cooled to 0 °C. H_2O_2 (7.5 mL) was then added dropwise over 2 h. The reaction mixture was quenched with an addition of H_2O and the layers were separated. The organic layer was washed with saturated aqueous $NaHCO_3$, dried over anhydrous Na_2SO_4, filtered, and concentrated *in vacuo*. The residue was purified by column chromatography (silica gel, hexane/EtOAc, 5/1) to afford **2.201** as a yellow oil (4.7g, 96%) in about a 1:0.6 mixture of keto and enol tautomers, respectively. ^{1}H NMR (400 MHz, $CDCl_3$) δ 12.49 (s, 0.3H, enol), 7.65 (t, *J* = 4.2 Hz, 0.5H, keto) 6.24–6.20 (m, 0.3H, enol), 5.44–5.40 (m, 0.3H, enol), 4.27–4.20 (m, 2H), 2.52–2.42 (m, 3.5H), 2.31–2.24 (m, 1H), 2.04 (ddd, *J* = 12.8, 6.4, 6.4 Hz, 1H), 1.30 (t, *J* = 7.1 Hz, 3H); IR (neat, cm^{-1}) 2940, 1733, 1682, 1643, 1370, 1263, 1217, 1058, 1046, 860; HRMS (ESI) *m/z* 169.0863 [(M+H)$^+$ calcd for $C_9H_{12}O_3$ 169.0863].

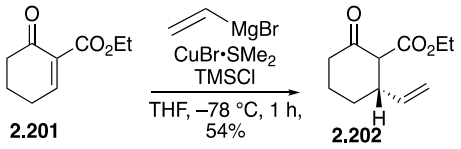

To a cooled solution (–78 °C) of $CuBr{\cdot}SMe_2$ (1.8 g, 8.92 mmol) in THF (150 mL) was added vinylmagnesium bromide (1.0 M in THF, 59.60 mmol) dropwise. After stirring for 30 min, **2.201** (2.5 g, 14.86 mmol) in THF (10 mL) was added dropwise at –78 °C. After stirring for 1 h at the same temperature, the reaction was quenched with an addition of saturated aqueous NH_4Cl, and the resulting mixture was diluted with EtOAc. The layers were separated, and the aqueous layer was extracted with EtOAc. The combined organic layers were dried over anhydrous

Na_2SO_4, filtered, and concentrated *in vacuo*. The residue was purified by column chromatography (silica gel, hexanes/EtOAc, 10/1) to afford **2.202** as a colorless oil (1.36 g, 54%) in about a 5:1 mixture of enol and keto tautomers: ^{1}H NMR (500 MHz, $CDCl_3$) δ 12.52 (s, 1H, enol), 5.81 (ddd, *J* = 16.9, 10.2, 6.1 Hz, 1H, enol), 5.72 (ddd, *J* = 17.4, 10.4, 7.3 Hz, 0.2H, keto), 5.10 (d, *J* = 17.2 Hz, 0.2H, keto), 5.04 (d, *J* = 10.4 Hz, 0.2H, keto), 5.00 (ddd, *J* = 10.2, 1.4, 1.4 Hz, 1H, enol), 4.89 (ddd, *J* = 17.1, 1.6, 1.6 Hz, 1H, enol), 4.22–4.14 (m, 2.4H keto/enol), 3.29–3.26 (m, 1H, enol), 3.24–3.22 (m, 0.2H, keto), 2.89 (dddd, *J* = 11.3, 11.3, 7.3, 3.9 Hz, 0.2H, keto) 2.51–2.46 (m, 0.2H, keto), 2.34–2.29 (m, 0.2H, keto), 2.29–2.24 (m, 2H, enol), 2.23–2.20 (m, 0.2H, keto), 2.10–2.05 (m, 0.2H, keto), 2.00–1.95 (m, 0.2H, keto), 1.80–1.73 (m, 0.2H, keto), 1.70–1.59 (m, 4H, enol), 1.25 (t, *J* = 7.12 Hz, 3.6H, keto/enol); IR (neat, cm^{-1}) 2938, 1744, 1714, 1643, 1611, 1298, 1264, 1215, 1175, 1086, 913, 832; HRMS (ESI) *m/z* 197.1178 [$(M+H)^+$ calcd for $C_{11}H_{16}O_3$ 197.1172].

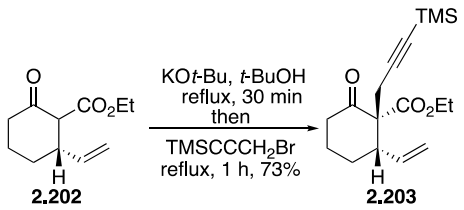

To a solution of **2.202** (600 mg, 3.06 mmol) in *t*-BuOH (14 mL) was added KO*t*-Bu (343 mg, 3.06 mmol) at 25 °C. The reaction mixture was heated to reflux for 30 min and a solution of (3-bromoprop-1-yn-1-yl)trimethylsilane (585 mg, 3.06 mmol) in *t*-BuOH (1.0 mL) was added. After refluxing for 1 h, the reaction was quenched with an addition of H_2O, and the resulting mixture was diluted with CH_2Cl_2. The layers were separated, and the aqueous layer was extracted with CH_2Cl_2. The combined organic layers were dried over anhydrous Na_2SO_4, filtered, and concentrated *in vacuo.* The residue was purified by

column chromatography (silica gel, hexanes/EtOAc, 20/1) to afford **2.203** as a colorless oil (686 mg, 73%, d.r.>10:1): ^{1}H NMR (500 MHz, $CDCl_3$) δ 5.82 (ddd, *J* = 18.0, 9.4, 9.4 Hz, 1H), 5.18 (d, *J* = 17.0 Hz, 1H), 5.09 (d, *J* = 10.3 Hz, 1H), 4.18–4.09 (m, 2H), 2.98 (d, *J* = 16.8 Hz, 1H), 2.89 (t, *J* = 10.3 Hz, 1H), 2.71–2.54 (m, 1H), 2.60 (d, *J* = 16.8 Hz, 1H), 2.50 (d, *J* = 15.2 Hz, 1H), 2.13–2.04 (m, 2H), 1.79–1.69 (m, 2H), 1.24 (t, *J* = 7.0 Hz, 3H) 0.11 (s, 9H); ^{13}C NMR (125 MHz, $CDCl_3$) δ 205.2, 169.3, 137.2, 117.4, 103.6, 87.8, 63.4, 61.6, 48.6, 39.9, 27.7, 23.9, 23.6, 14.2, 0.2 (3C); IR (neat, cm^{-1}) 2957, 2177, 1738, 1711, 1249, 1222, 1201, 1030, 838; HRMS (ESI) *m*/*z* 307.1729 [(M+H)$^+$ calcd for $C_{17}H_{26}O_3Si$ 307.1724].

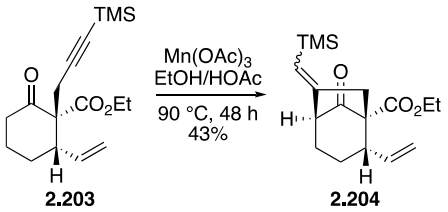

A solution of **2.203** (400 mg, 1.31 mmol) in EtOH (23.6 mL) and HOAc (2.62 mL) was degassed by bubbling argon through the mixture at –78 °C for 25 min. After warming to 25 °C, $Mn(OAc)_3$ (2.28 g, 9.83 mmol) was added and the reaction mixture was warmed to 90 °C for 24 h. The reaction mixture was then cooled to 25 °C and additional $Mn(OAc)_3$ (1.52 g, 6.55 mmol) was added. The reaction mixture was then heated to 90 °C for 24 h. After cooling down to 25 °C, the reaction was diluted with EtOAc, washed with 10 % $NaHSO_3$ and saturated aqueous $NaHCO_3$. The organic layer was dried with anhydrous Na_2SO_4, filtered, and concentrated *in vacuo*. The residue was purified by column chromatography (silica gel, hexanes/EtOAc, 20/1) to afford **2.204** as a mixture of *E*/*Z* isomers (colorless oil, 175 mg, 43%): ^{1}H NMR (400 MHz, $CDCl_3$) δ 5.90–

5.79 (m, 1H), 5.54–5.52 (m, 1H), 5.15–5.07 (m, 2H), 4.26–4.10 (m, 2H), 3.25 (br s, 1H), 3.09–2.87 (m, 3H), 2.38–2.22 (m, 1H), 2.17–2.05 (m, 1H), 1.93–1.89 (m, 1H), 1.62–1.57 (m, 1H), 1.27–1.22 (m, 3H), 0.11 (d, *J* = 17.3 Hz, 9H); IR (neat, cm^{-1}) 2952, 1757, 1730, 1629, 1445, 1247, 1233, 1201, 1109, 1094, 1019, 834; HRMS (ESI) *m/z* 307.1725 [$(M+H)^+$ calcd for $C_{17}H_{26}O_3Si$ 307.1724].

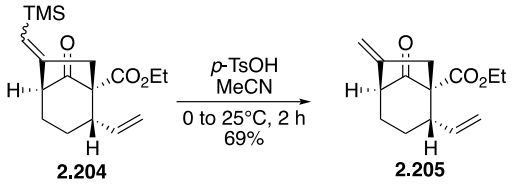

To a cooled (0 °C) solution of **2.204** (175 mg, 0.57 mmol) in MeCN (5.7 mL) was added *p*-TsOH (217 mg, 1.14 mmol). The reaction mixture was warmed to 25 °C and stirred for 2 h. The reaction was quenched with an addition of saturated aqueous $NaHCO_3$, and the resulting mixture was diluted with CH_2Cl_2. The layers were separated, and the aqueous layer was extracted with CH_2Cl_2. The combined organic layers were dried over anhydrous Na_2SO_4, filtered, and concentrated *in vacuo*. The residue was purified by column chromatography (silica gel, hexanes/EtOAc, 10/1) to afford **2.205** as a colorless oil (92 mg, 69%): ^{1}H NMR (500 MHz, $CDCl_3$) δ 5.85 (ddd, *J* = 17.3, 10.5, 7.7 Hz, 1H), 5.12 (d, *J* = 17.3 Hz, 1H), 5.09 (d, *J* = 10.7 Hz, 1H), 5.06–5.04 (m, 2H), 4.23–4.12 (m, 2H), 3.24 (t, *J* = 6.8 Hz, 1H), 3.06 (ddd, *J* = 17.4, 2.6, 2.6 Hz, 1H), 2.96 (br s, 1H), 2.90 (d, *J* = 17.4 Hz, 1H), 2.28 (dddd, *J* = 13.2, 13.2, 4.8, 2.2 Hz, 1H), 2.15 (dddd, *J* = 13.7, 13.7, 5.5, 5.5 Hz, 1H), 1.93–1.89 (m, 1H), 1.63–1.59 (m, 1H), 1.24 (t, *J* = 7.1 Hz, 3H); ^{13}C NMR (125 MHz, $CDCl_3$) δ 210.1, 170.5, 142.5, 136.8, 116.8, 108.6, 61.3, 61.1, 55.3, 51.9, 39.7, 36.3, 24.0, 14.2;

IR ($CHCl_3$, cm^{-1}) 2945, 1757, 1728, 1661, 1446, 1259, 1229, 1096, 1024, 911; HRMS (ESI) *m/z* 235.1336 [$(M+H)^+$ calcd for $C_{14}H_{18}O_3$ 235.1329].

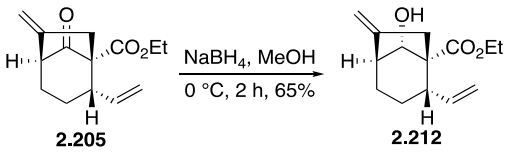

To a cooled solution (0 °C) of **2.205** (124 mg, 0.53 mmol) in MeOH (10.5 mL) was added $NaBH_4$ (60 mg, 1.59 mmol). After stirring for 30 min at the same temperature, the mixture was quenched with an addition of saturated aqueous $NaHCO_3$, and the resulting mixture was diluted with EtOAc. The layers were separated, and the aqueous layer was extracted with EtOAc. The combined organic layers were dried over anhydrous Na_2SO_4, filtered and concentrated. The residue was purified by column chromatography (silica gel, hexanes/EtOAc, 20/1) to afford **2.212** as a colorless oil (80 mg, 65%): ^{1}H NMR (500 MHz, $CDCl_3$) δ 6.40–6.33 (m, 1H), 4.97 (t, *J* = 2.6 Hz, 1H), 4.90–4.86 (m, 3H), 4.23 (dd, *J* = 5.2, 1.8 Hz, 1H), 4.17–4.13 (m, 2H), 2.75 (d, *J* = 2.5 Hz, 1H), 2.73 (t, *J* = 4.7 Hz, 1H), 2.67–2.64 (m, 1H), 2.50 (t, *J* = 2.3 Hz, 2H), 2.24 (dddd, *J* = 13.4, 13.4, 5.2, 1.8 Hz, 1H), 1.98 (dddd, *J* = 13.9, 13.9, 6.0, 6.0 Hz, 1H), 1.50 (dd, *J* = 14.2, 4.9 Hz, 1H), 1.34–1.29 (m, 1H), 1.26 (t, *J* = 7.1 Hz, 3H); ^{13}C NMR (125 MHz, $CDCl_3$) δ 176.1, 147.5, 141.2, 114.1, 107.6, 74.4, 60.7, 54.5, 46.8, 45.6, 39.4, 22.9, 22.4, 14.4; IR ($CHCl_3$, cm^{-1}) 3527, 3072, 2979, 2939, 2870, 1717, 1662, 1633, 1301, 1226, 1087, 1036, 914, 883; HRMS (ESI) *m/z* 237.1492 [$(M+H)^+$ calcd for $C_{14}H_{20}O_3$ 237.1485].

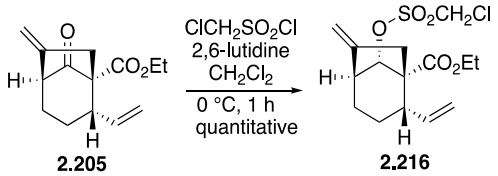

To a cooled (0 °C) solution of **2.205** (40 mg, 0.17 mmol) in CH_2Cl_2 (3.4 mL) was added chloromethanesulfonyl chloride (0.23 mL, 2.54 mmol) and 2,6-lutidine (0.39 mL, 3.4 mmol). After stirring for 1 h at the same temperature, the reaction was quenched with an addition of saturated aqueous NH_4Cl, and the resulting mixture was diluted with CH_2Cl_2. The layers were separated, and the aqueous layer was extracted with CH_2Cl_2. The combined organic layers were dried over anhydrous Na_2SO_4, filtered, and concentrated *in vacuo*. The residue was purified by column chromatography (silica gel, hexanes/EtOAc, 20/1) to afford **2.216** as a yellow oil (59 mg, quantitative): ^{1}H NMR (500 MHz, $CDCl_3$) δ 6.11 (ddd, *J* = 17.0, 10.2, 9.3 Hz, 1H), 5.11 (d, *J* = 5.4 Hz, 1H), 5.05 (t, *J* = 2.4 Hz, 1H), 4.99–4.94 (m, 3H), 4.87 (d, *J* = 12.3 Hz, 1H), 4.73 (d, *J* = 12.3 Hz, 1H), 4.22–4.12 (m, 2H), 3.00 (t, *J* = 3.9 Hz, 1H), 2.89–2.86 (m, 1H), 2.58 (d, *J* = 17.4 Hz, 1H), 2.49 (ddd, *J* = 17.4, 2.6, 2.6 Hz, 1H), 2.22 (dddd, *J* = 13.5, 13.5, 5.2, 1.9 Hz, 1H), 2.00 (ddd, *J* = 20.2, 13.8, 6.0 Hz, 1H), 1.58 (dd, *J* = 14.3, 5.0 Hz, 1H), 1.48–1.43 (m, 1H), 1.27 (t, *J* = 7.1 Hz, 3H); IR ($CHCl_3$, cm^{-1}) 3020, 2946, 1723, 1635, 1368, 1309, 1262, 1214, 1180, 1095, 1046, 985, 890; HRMS (ESI) *m/z* 349.0876 [$(M+H)^+$ calcd for $C_{15}H_{21}ClO_5S$ 349.0871].

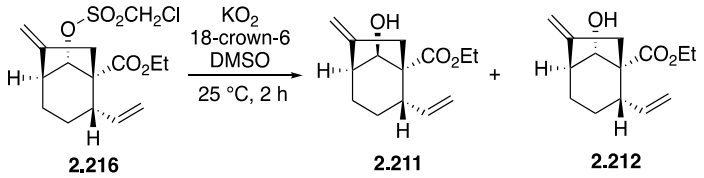

To a stirring solution of KO_2 (52 mg, 0.73 mmol) in DMSO (2.5 mL) was added 18-crown-6 (95 mg, 0.36 mmol) at 25 °C. After 30 min, **2.216** (32 mg, 0.09 mmol) in DMSO (0.5 mL) was added dropwise. After stirring for 2 h, the reaction was quenched with an addition of H_2O, and the resulting mixture was diluted with CH_2Cl_2. The layers were separated, and the aqueous layer was extracted with CH_2Cl_2. The combined organic layers were dried over anhydrous Na_2SO_4, filtered and concentrated. The residue was purified by column chromatography (silica gel, hexanes/EtOAc, 20/1) to afford **2.211** (1 mg, 5%) and **2.212** (3 mg, 14%); For **2.211**: ^{1}H NMR (500 MHz, $CDCl_3$) δ 5.88 (ddd, *J* = 17.0, 10.4, 8.2 Hz, 1H), 5.05 (d, *J* = 10.8 Hz, 1H), 5.02 (d, *J* = 17.3 Hz, 1H), 5.00 (br s, 2H), 4.20–4.14 (m, 3H), 3.42 (br s, 1H), 2.82 (ddd, *J* = 17.0, 2.6, 2.6 Hz, 1H), 2.79–2.76 (m, 1H), 2.71 (d, *J* = 4.3 Hz, 1H), 2.46 (d, *J* = 16.8 Hz, 1H), 1.88 (dddd, *J* = 13.3, 13.3, 5.6, 5.6 Hz, 1H), 1.79 (dddd, *J* = 13.4, 13.4, 4.5, 1.9 Hz, 1H), 1.59–1.56 (m, 1H), 1.49 (dd, *J* = 13.8, 4.6 Hz, 1H), 1.27 (t, *J* = 7.1 Hz, 3H); IR ($CHCl_3$, cm^{-1}) 3533, 2938, 1710, 1662, 1447, 1294, 1213, 1066, 920, 889; HRMS (ESI) *m*/*z* 237.1483 [$(M+H)^+$ calcd for $C_{14}H_{20}O_3$ 237.1485].

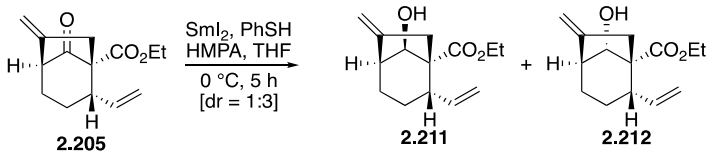

To a cooled (0 °C) solution of **2.205** (20 mg, 0.09 mmol) in THF (0.85 mL) was added PhSH (0.05 mL, 0.51 mmol), HMPA (0.15 mL, 0.85 mmol), and SmI_2 (0.1 M in THF, 2.55 mL) dropwise. After stirring for 5 h at the same temperature, the reaction was quenched with an addition of saturated aqueous $Na_2S_2O_3$, and the resulting mixture was diluted with EtOAc. The layers were separated and the aqueous layer was extracted with EtOAc. The combined organic layers were dried over anhydrous Na_2SO_4, filtered and concentrated *in vacuo.* The crude material showed a 1:3 mixture of **2.211** and **2.212** determined by ^{1}H NMR.

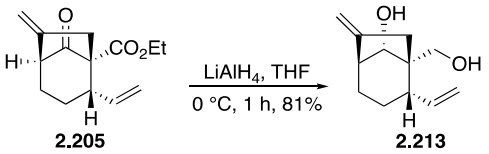

To a cooled solution (0 °C) of **2.205** (50 mg, 0.21 mmol) in THF (5.3 mL) was added $LiAlH_4$ (2.0 M in THF, 0.84 mmol). After stirring for 1 h at the same temperature, the reaction was quenched with an addition of Rochelle salt, and the resulting mixture was diluted with CH_2Cl_2. The layers were separated, and the aqueous layer was extracted with CH_2Cl_2. The combined organic layers were dried over anhydrous Na_2SO_4, filtered, and concentrated *in vacuo.* The residue was purified by column chromatography (silica gel, hexanes/EtOAc, 5/1) to afford **2.213** as a colorless oil (33 mg, 81%): ^{1}H NMR (500 MHz, $CDCl_3$) δ 6.66 (ddd, *J* = 17.3, 9.8, 9.8 Hz, 1H), 5.11–5.07 (m, 1H), 4.99 (dd, *J* =

10.1, 2.0 Hz, 1H), 4.95 (t, *J* = 2.5 Hz, 1H), 4.85 (br s, 1H), 4.00 (d, *J* = 5.3 Hz, 1H), 3.82 (d, *J* = 11.4 Hz, 1H), 3.66 (d, *J* = 11.4 Hz, 1H), 2.70 (t, *J* = 4.1 Hz, 1H), 2.33–2.30 (m, 1H), 2.25–2.19 (m, 2H), 2.16–2.14 (m, 2H), 1.98 (dddd, *J* = 13.9, 13.9, 6.0, 6.0 Hz, 1H), 1.46 (dd, *J* = 14.2, 4.9 Hz, 1H), 1.37–1.32 (m, 1H); IR ($CHCl_3$, cm^{-1}) 3356, 3068, 2932, 2869, 1658, 1632, 1420, 1151, 1088, 1068, 1001, 910, 879; HRMS (ESI) *m*/*z* 201.1456 [$(M+Li)^+$ calcd for $C_{12}H_{18}O_2$ 201.1461].

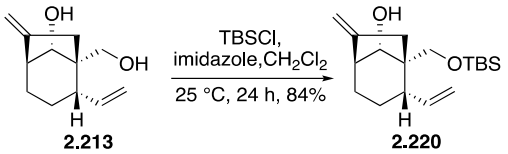

To a cooled solution (0 °C) of **2.213** (33 mg, 0.17 mmol) in CH_2Cl_2 (1.7 mL) were added imidazole (35 mg, 0.51 mmol) and TBSCl (51 mg, 0.34 mmol). The reaction mixture was allowed to warm to 25 °C and stirred for 24 h. The reaction was quenched with an addition of saturated aqueous NH_4Cl, and the resulting mixture was diluted with CH_2Cl_2. The layers were separated, and the aqueous layer was extracted with CH_2Cl_2. The combined organic layers were dried over anhydrous Na_2SO_4, filtered, and concentrated *in vacuo*. The residue was purified by column chromatography (silica gel, hexanes/EtOAc, 20/1) to afford **2.220** as a colorless oil (44 mg, 84%): ^{1}H NMR (500 MHz, $CDCl_3$) δ 6.42 (ddd, *J* = 17.4, 10.3, 8.2 Hz, 1H), 5.02 (ddd, *J* = 17.3, 1.7, 1.7 Hz, 1H), 4.97 (ddd, *J* = 10.4, 2.0, 1.0 Hz, 1H), 4.92 (t, *J* = 2.4 Hz, 1H), 4.84 (br s, 1H), 3.89 (d, *J* = 5.3 Hz, 1H), 3.66 (d, *J* = 10.0 Hz, 1H), 3.58 (d, *J* = 10.0 Hz, 1H), 2.65 (t, *J* = 4.0 Hz, 1H), 2.34–2.31 (m, 1H), 2.29 (t, *J* = 2.6 Hz, 1H), 2.22–2.15 (m, 2H), 1.94 (dddd, *J* = 13.9, 13.9, 6.0, 6.0 Hz, 1H), 1.55 (dd, *J* = 14.2, 4.8 Hz, 1H), 1.37–1.33 (m, 1H), 0.89 (s, 9H), 0.05 (s, 3H), 0.04 (s,

3H); IR ($CHCl_3$, cm^{-1}) 3444, 3069, 2928, 2856, 1659, 1633, 1471, 1253, 1214, 1087, 1005, 834; HRMS (ESI) *m/z* 309.2245 [$(M+H)^+$ calcd for $C_{18}H_{32}O_2Si$ 309.2244].

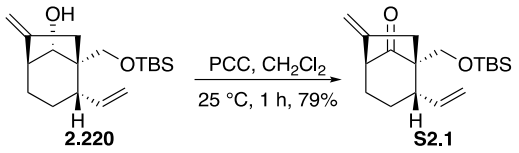

To a solution of **2.220** (44 mg, 0.14 mmol) in CH_2Cl_2 (1.4 mL) was added PCC (37 mg, 0.17 mmol). After stirring for 1 h, the reaction was diluted with Et_2O and washed with H_2O. The organic layer was dried over anhydrous Na_2SO_4, filtered, and concentrated *in vacuo*. The residue was purified by column chromatography (silica gel, hexanes/EtOAc, 20/1) to afford **S2.1** as a colorless oil (34 mg, 79%): ^1H NMR (500 MHz, $CDCl_3$) δ 5.72 (ddd, *J* = 16.6, 10.2, 10.2 Hz, 1H), 5.07–5.06 (m, 1H), 5.04 (dd, *J* = 10.0, 1.8 Hz, 1H), 5.01–5.00 (m, 2H), 3.62 (d, *J* = 10.2 Hz, 1H), 3.55 (d, *J* = 10.2 Hz, 1H), 2.92–2.89 (m, 1H), 2.86 (d, *J* = 4.2 Hz, 1H), 2.75 (ddd, *J* = 17.6, 2.6, 2.6 Hz, 1H), 2.68 (d, *J* = 17.7 Hz, 1H), 2.27–2.20 (m, 1H), 2.16 (dddd, *J* = 13.8, 13.8, 5.2, 5.2 Hz, 1H), 1.95–1.90 (m, 1H), 1.44 (dd, *J* = 13.8, 4.4 Hz, 1H), 0.87 (s, 9H), 0.01 (s, 3H), 0.00 (s, 3H); IR ($CHCl_3$, cm^{-1}) 3075, 2928, 2856, 1748, 1658, 1471, 1252, 1214, 1094, 834; HRMS (ESI) *m/z* 307.2090 [$(M+H)^+$ calcd for $C_{18}H_{30}O_2Si$ 307.2088].

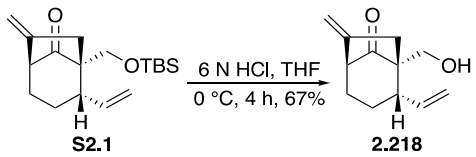

To a cooled solution (0 °C) of **S2.1** (34 mg, 0.11 mmol) in THF (0.85 mL) was added 6 N HCl (1.8 mL) and the reaction mixture was allowed to warm to 25 °C. After

stirring for 4 h, the reaction mixture was diluted with the addition of H_2O and Et_2O. The layers were separated, and the aqueous layer was extracted with Et_2O. The combined organic layers were dried over anhydrous Na_2SO_4, filtered and concentrated *in vacuo*. The residue was purified by column chromatography (silica gel, hexanes/EtOAc, 5/1) to afford **2.218** as a colorless oil (14 mg, 67%): ^{1}H NMR (500 MHz, $CDCl_3$) δ 5.74 (ddd, *J* = 16.8, 10.1, 10.1 Hz, 1H), 5.07–5.02 (m, 4H), 3.90 (d, *J* = 11.8 Hz, 1H), 3.34 (d, *J* = 11.8 Hz, 1H), 3.01 (ddd, *J* = 17.4, 2.5, 2.5 Hz, 1H), 2.89 (d, *J* = 4.8 Hz, 1H), 2.68 (dd, *J* = 9.9, 4.9 Hz, 1H), 2.60 (d, *J* = 17.5 Hz, 1H), 2.27–2.18 (m, 2H), 1.96–1.93 (m, 1H), 1.55 (s, 1H), 1.49–1.41 (m, 1H); IR ($CHCl_3$, cm^{-1}) 3432, 3074, 2939, 1742, 1657, 1638, 1214, 1050, 1016, 920, 883; HRMS (ESI) *m*/*z* 193.1225 [$(M+H)^+$ calcd for $C_{12}H_{16}O_2$ 193.1223]. Data collected is consistent with those previously reported in literature.[24]

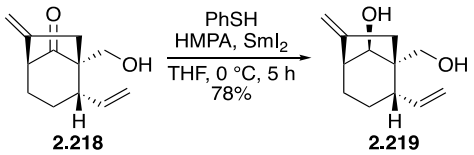

Compound **2.219** was prepared according to the previously reported procedure.[24] To a cooled (0 °C) solution of **2.218** (14 mg, 0.06 mmol) in THF (0.6 mL) was added PhSH (0.04 mL, 0.36 mmol), HMPA (0.1 mL, 0.60 mmol), and SmI_2 (0.1 M in THF, 3.6 mmol) dropwise. After stirring for 5 h at the same temperature, the reaction was quenched with an addition of saturated aqueous $Na_2S_2O_3$, and the resulting mixture was diluted with EtOAc. The layers were separated, and the aqueous layer was extracted with EtOAc. The combined organic layers were dried over anhydrous Na_2SO_4, filtered,

and concentrated *in vacuo.* The residue was purified by column chromatography (silica gel, hexanes/EtOAc, 5/1) to afford **2.219** as a colorless oil (11 mg, 78%): ^{1}H NMR (500 MHz, $CDCl_3$) δ 6.00 (m, 1H), 5.06–5.06 (m, 1H), 5.03 (br s, 1H), 5.01–5.00 (m, 2H), 4.06 (s, 1H), 3.98 (d, *J* = 11.6 Hz, 1H), 3.56 (d, *J* = 11.6 Hz, 1H), 2.82 (ddd, *J* = 17.1, 2.5, 2.5 Hz, 1H), 2.62 (d, *J* = 4.3 Hz, 1H), 2.39 (br s, 2H), 2.26 (dd, *J* = 9.3, 6.0 Hz, 1H), 2.07 (d, *J* = 17.1 Hz, 1H), 1.90–1.82 (m, 1H), 1.81–1.74 (m, 1H), 1.59–1.55 (m, 1H), 1.35–1.30 (m, 1H); IR ($CHCl_3$, cm^{-1}) 3342, 3070, 2934, 1660, 1635, 1446, 1214, 1064, 1023, 914, 889; HRMS (ESI) *m*/*z* 201.1463 [$(M+Li)^+$ calcd for $C_{12}H_{18}O_2$ 201.1461]. Data collected is consistent with those previously reported in literature.[24]

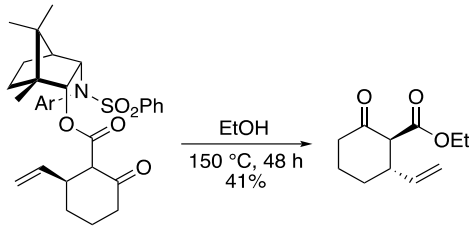

2.249 **2.250**

EtOH (2.0 mL) was added to **2.249** (50 mg, 0.09 mmol) in a sealed tube, and the resulting solution was warmed to 150 °C for 48 h. After cooling down to 25 °C, the solvent was evaporated under reduced pressure and the residue was purified by column chromatography (silica gel, hexanes/EtOAc, 30/1) to afford **2.250** as a colorless oil (17 mg, ~41%) in about a 1:0.8 mixture of enol and keto tautomers, respectively.

3. Design and Synthesis of Novel ENT Inhibitors

3.1 Introduction

3.1.1 Equilibrative Nucleoside Transporters

Nucleosides are vital components of human physiology as they are important building blocks in RNA, DNA and ATP synthesis and function as signaling molecules in a broad range of cellular events. Composed of a purine or pyrimidine nucleobase and a 5-carbon sugar (Figure 19), they are hydrophilic in nature and are unable to diffuse across cell membranes without the aid of specialized Nucleoside Transporters (NTs).[54] NTs belong to two different Solute Carrier (SLC) families, genetically encoded *SLC28* and *SLC29.* Classically, the transporters were characterized by their dependence on extracellular sodium, substrate preference and sensitivity to the inhibitor *S*-(4-nitrobenzyl)-6-thioinosine (NBMPR). Therefore, NTs are classified as ***c***oncentrative/NBMPR-***i***nsensitive/transports-***t***hymidine (*cit*), ***c***oncentrative/NBMPR-***i***nsensitive/transports-***f***ormycin (*cif*), *concentrative*/NBMPR-***i***nsensitive/transports-***b***oth-purines-and-pyrimidines (*cib*), ***e***quilibrium/NBMPR-***s***ensitive (*es*) or ***e***quilibrium/NBMPR-***i***nsensitive (*ei*).[55]

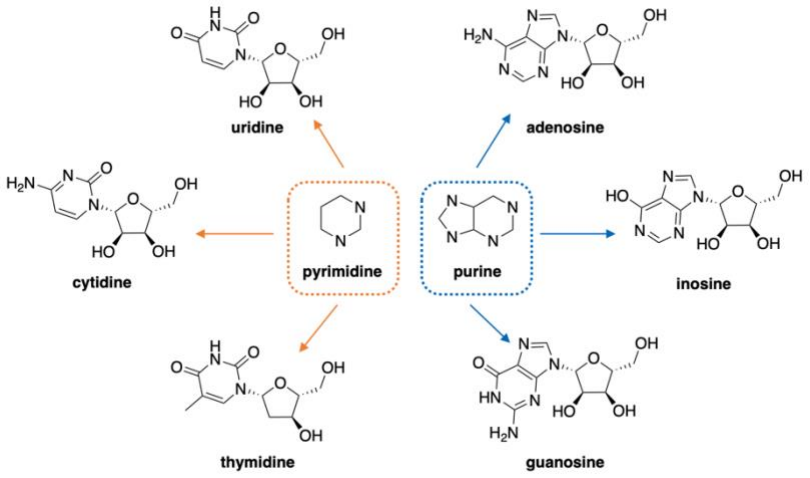

Figure 19. Examples of purine and pyrimidine-based nucleosides

The concentrative nucleoside transporters (hCNT1, 2 and 3, (*cit*, *cif* and *cib)*), encoded by *SLC28*, mediate the uptake of nucleosides unidirectionally by coupling to the influx of sodium ions. Although all CNTs transport uridine, hCNT1 preferentially transports pyrimidines, hCNT2 purines and hCNT3 exhibits broad selectivities.[56] The equilibrative nucleoside transporters (hENT1, 2, 3 and 4), encoded by *SLC29*, passively transport nucleoside and nucleoside drug analogs. hENT1 (*es*), is potently inhibited by NBMPR, whereas hENT2–4 (*ei)*, show little to no sensitivity to NBMPR. While hENT1–3 exhibit broad tissue distributions and substrate preference (Table 11), hENT4, also known as ***p***lasma membrane ***m***ono***a***mine ***t***ransporter (PMAT), specifically transports adenosine and monoamines, such as serotonin and dopamine, and is highly expressed in the heart and brain.[54] In addition to nucleosides and nucleobases, hENTs are critical in delivering >30 FDA/EMA approved nucleoside analog therapeutics to their intracellular targets (examples shown in Figure 20).[57] [58]

Table 11. Equilibrative Nucleoside Transporter Family. Adapted from ref 54

ENT Isoform	Tissue Expression	Subcellular Localization	Permeant Selectivities	Transport Inhibitors
hENT1	Ubiquitous	Plasma membrane	Purine, pyrimidine nucleosides, their analogs	NBMPR, dilazep, dipyridamole, rapadocin
hENT2	Ubiquitous	Plasma membrane Nuclear membrane	Purine, pyrimidine nucleosides, their analogs	dilazep, dipyridamole
hENT3	Kidney, lungs, liver	Lysosomal membrane	Purine, pyrimidine nucleosides, their analogs, ATP	NBMPR, dilazep, dipyridamole
hENT4	Brain and heart	Plasma membrane	Adenosine, dopamine, serotonin	dilazep, dipyridamole

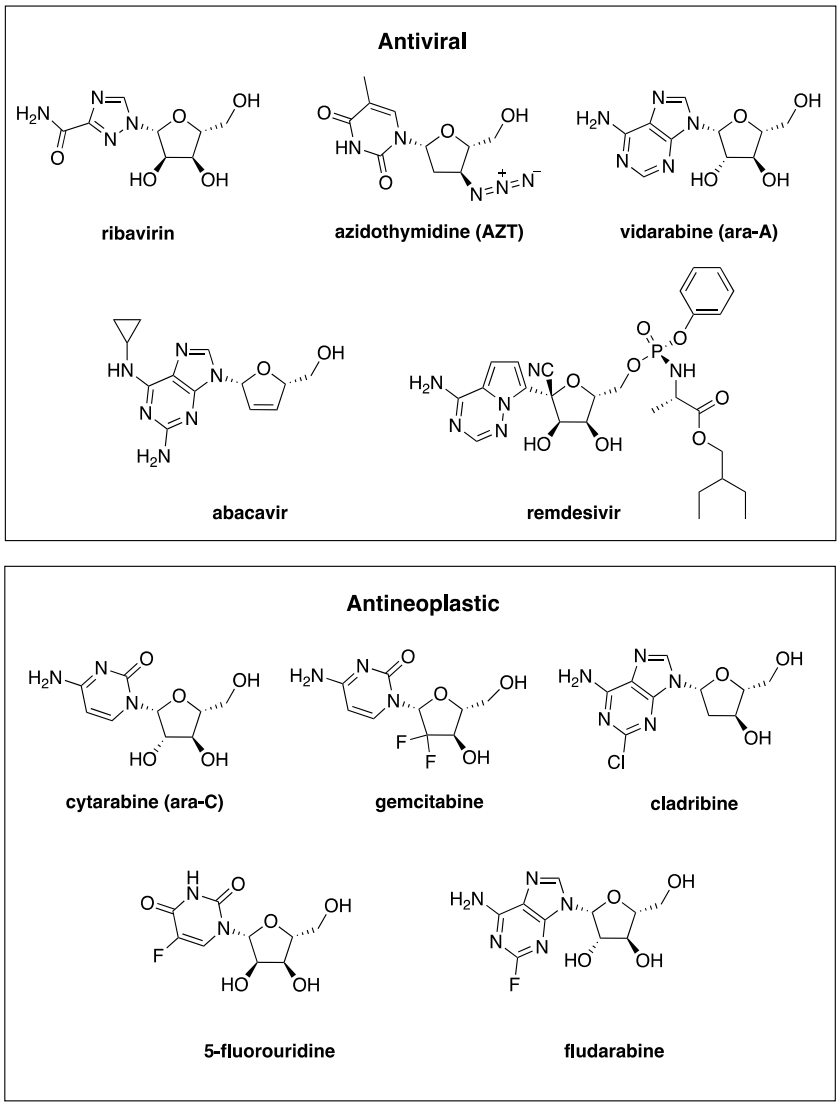

Figure 20. Antiviral and antineoplastic nucleoside analog therapeutics. Figure adapted from ref 58

In addition to the transport of nucleoside analog drugs, inhibitors of hENT (Figure 21), also known as adenosine reuptake inhibitors (AdoRIs), have shown significant clinical relevance due to their ability to regulate metabolic functions and cell signaling cascades via increasing extracellular adenosine concentrations. Increased adenosine concentrations in-turn activates four G-protein coupled receptors (GPCRs)

(A_1R, $A_{2A}R$, $A_{2B}R$ and A_3R) which mediates many physiological responses including, vasodilation, coronary blood flow, inflammation, neurotransmission, hypoxia, trauma, ischemia, and analgesia.[59] [57] While AdoRIs are traditionally used for their antiarrhythmic and cardioprotective effects, their ability to mediate pain holds great potential for the development of novel non-opioid pain-relieving therapeutics.

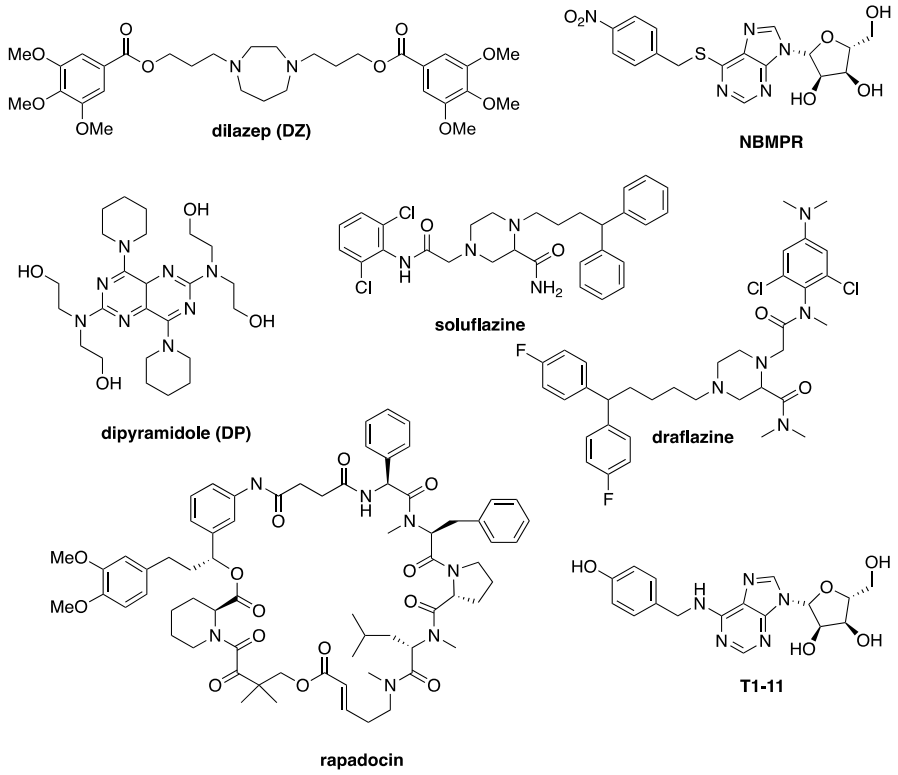

Figure 21. Selected ENT1 Inhibitors

As shown in Figure 22, extracellular adenosine levels are maintained by the dephosphorylation of ATP by ectonuleosidase triphosphate diphosphohydrolase (CD39) and dephosphorylation of ADP and AMP by ecto-5′-nucleotidase (CD73). Adenosine then mediates analgesia in a variety of ways by binding to adenosine receptors (ARs).[59] Consequently, there has been significant interest in the development of therapeutic

agents that target the AR for the treatment of pain. Although several AR agonists have made it to clinical trials, success in targeting the AR receptor has proven limited due to unacceptable side effects (mainly cardiovascular). Additionally, intravenous infusion of adenosine has been effective in relieving neuropathic, experimental, and perioperative pain but due to adenosine's short half-life a continuous infusion is necessary.[60 61]

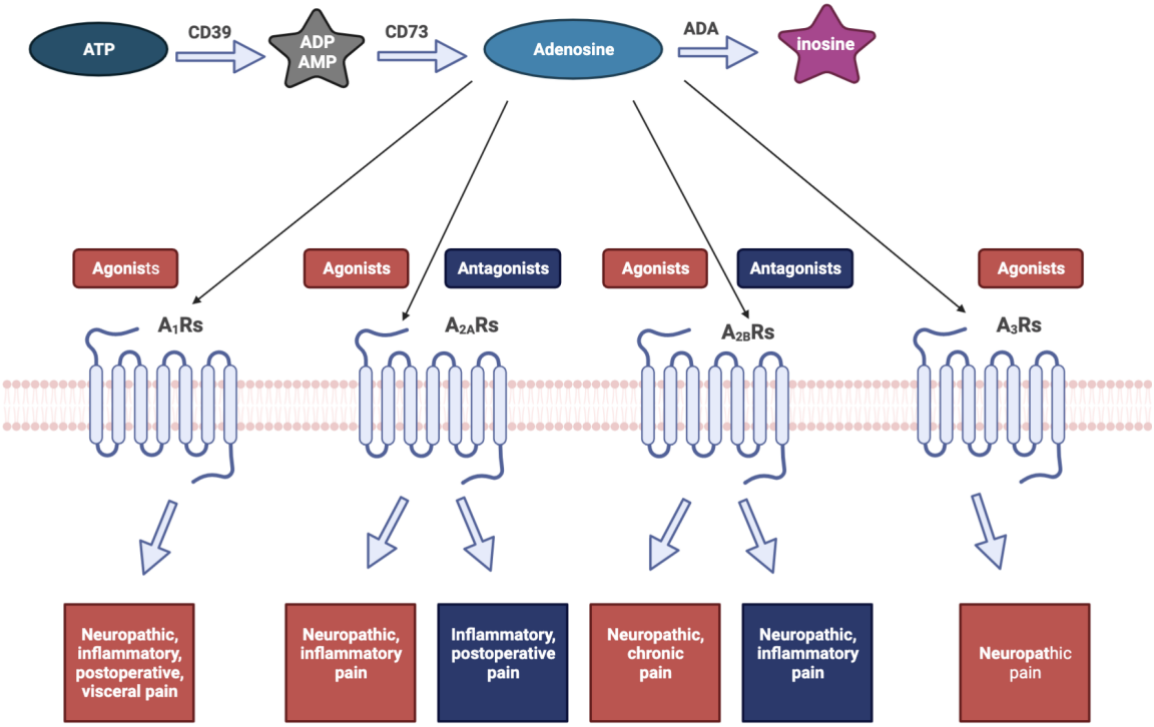

Figure 22. Analgesic effect of AR receptor activation. Figure adapted from ref. 59

Another tactic for eliciting the analgesic effect of AR activation, without the use of an AR agonist, is inhibiting the intracellular transport of adenosine by hENT, thereby increasing extracellular pools of adenosine (Figure 23).[62] Notably, ENT1 is colocalized with the A_1R and highly expressed in the superficial dorsal horn laminae, substantia

gelatinosa and the dorsal root ganglia, all of which are highly involved in the modulation of pain transmission.[63 64 65]

The analgesic effect of ENT inhibition has been shown experimentally and clinically. Firstly, Keil *et al.* showed intrathecal administration of dilazep could induce antinociception by altering adenosine levels in a mouse tail flick assay.[66] Additionally, Maes *et al*. demonstrated the antihyperalgesic effect of ENT inhibitors on guinea pigs in two inflammatory pain models (Freund's adjuvant (CFA)-induced and carrageenan-induced) by inhibiting the A_1R and A_2R subtypes.[61] Clinically, the ENT inhibitor dipyridamole had beneficial effects in chronic pain patients and showed improvement in osteoarthritis patients' pain and functionality when combined with a low dose of prednisolone.[67 68]

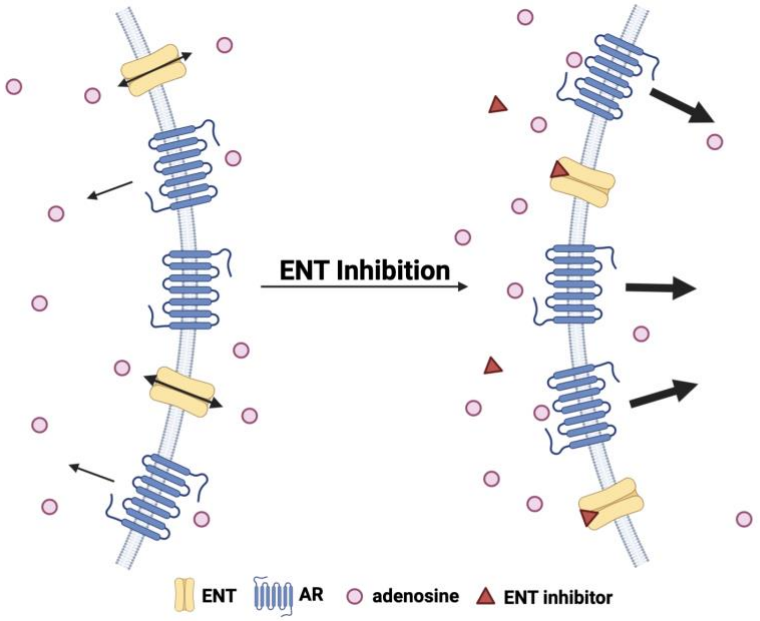

Figure 23. AR activation by ENT inhibition. Figure adapted from ref 62.

Although physiologically and clinically important, the development of novel inhibitors of ENT has been limited due to a lack of structural and functional data of hENT. The first experimentally determined crystal structures of hENT were published by Prof. Seok-Yong Lee and Dr. Nicholas J. Wright in 2019.[69] In which they published the co-crystal structure of hENT1 in complex with inhibitors dilazep and NBMPR. Their studies shed light on both the molecular basis for hENT1-mediated adenosine transport, as well as its inhibition by AdoRI's. For the crystallization of hENT1, three-point mutations (L168F, P175A and N288K) and a disordered-loop truncation (ΔPro243–Gln247) were found to enhance transporter detergent solution behavior while maintaining a functionally competent construct, labeled $hENT1_{cryst}$. Crystallization of $hENT1_{cryst}$ in complex with dilazep and NBMPR was then carried out to 2.3 Å and 2.9 Å resolution, respectively (Figure 24A), providing key insights into transporter architecture. $hENT1_{cryst}$, composed of 11 transmembrane helices, exhibits a pseudo-symmetric 6 + 5 topology, shown in Figure 24B. Similar to the major facilitator superfamily (MFS) transporters which exhibit a pseudo-symmetric 6 + 6 topology.

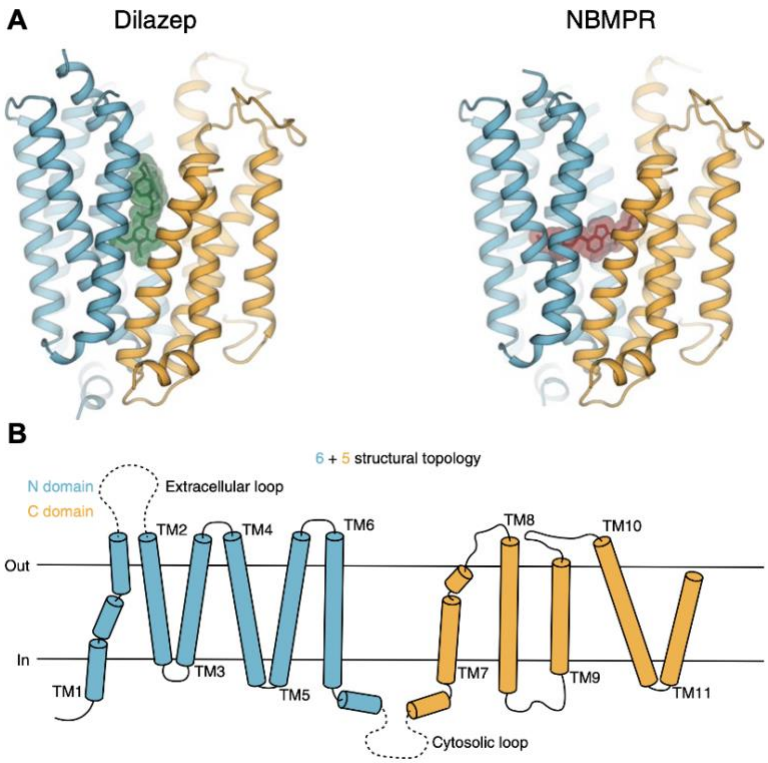

Figure 24. A) Co-crystal structure of hENT1 in complex with dilazep and NBMPR. B) 6 + 5 structural topology of hENT1. Figure reprinted with permission from ref 69.

Taking a closer look at dilazep-bound hENT1$_{cryst}$, the inhibitor adopts a crescent conformation with two distinct binding sites within the central cavity (Figure 25A). One of the two trimethoxyphenyl rings interacts with Trp29 and Gln158 deep within the central cavity. As this site was previously indicated as important for nucleoside recognition, it was termed the 'orthosteric site' (Figure 25A). The second binding site, occupied by the other trimethoxyphenyl ring and the central diazepane ring, is consequently termed 'opportunistic site 1'. In the 'opportunistic site 1', the diazepane

ring is cradled by a hydrophobic contact with Met33 and the trimethoxyphenyl ring forms π–π stacking with Phe307 and Phe334 and hydrogen bonding with Asn338.

Similar to dilazep, NBMPR also exhibits two distinct binding sites. The adenosine-like thioinosine moiety occupying the 'orthosteric site' via interactions with Arg345 and Asp341 by the 2′-OH and 3′-OH, N-1 and N-3 amino groups coordinating to Gln158 and several hydrophobic residues (Leu26, Met89, Leu92 and Leu442) surrounding the purine moiety. The second binding-site, termed 'opportunistic site 2', is occupied by the *p*-nitrobenzyl ring and is buried deep within a hydrophobic cavity.

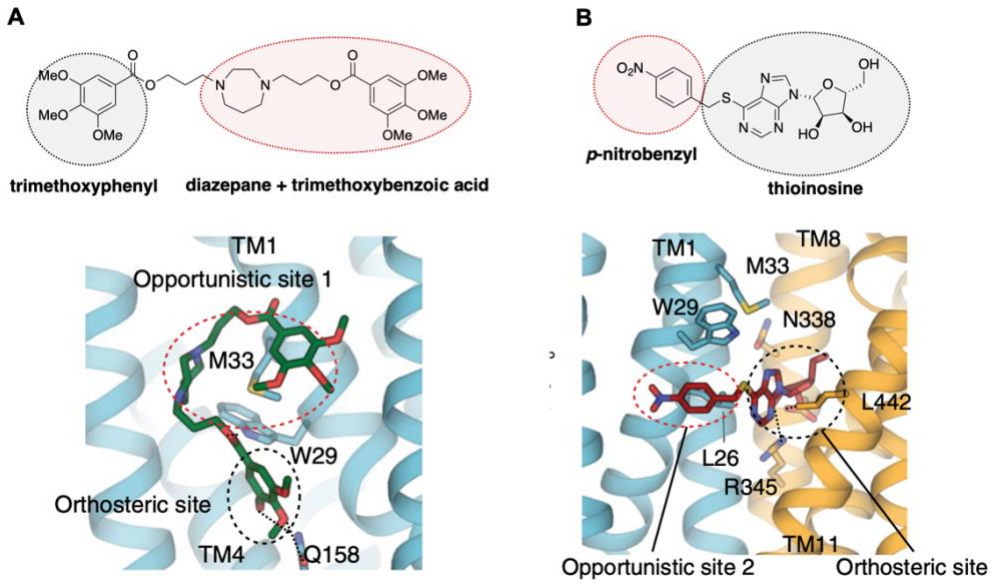

Figure 25. Dilazep and NBMPR binding sites within ENT1 binding pocket. Figure reprinted with permission from ref 69.

The two inhibitor bound states of hENT1 provides valuable insight into the mechanism for nucleoside transport and inhibition. Based on the two-domain architecture, it was posited that hENT1 utilizes a global rocker-switch-like reorientation

of the N and C domains for an alternating-access mechanism for nucleoside and nucleoside-analog drug transport. As shown in Figure 26, both inhibitors lock hENT1 in the outward-facing state. For the transporter to transition to the inward-facing state, substrate binding closes the extracellular thin gate and upon N- and C-domain reorientation the extracellular thick gate is formed to transform the transporter to the outward-facing state. As dilazep occupies 'opportunistic site 1' within the extracellular thin gate, it sterically prevents thin gate formation. Contrastingly, NBMPR does not occlude thin gate formation but prevents reorientation of the N-domain by binding to 'opportunistic site 2' with the *p*-nitrobenzyl moiety (Figure 26). Taken together, the structural and mechanistic information provided by these studies offers an excellent starting point for the rational design of novel ENT inhibitors.

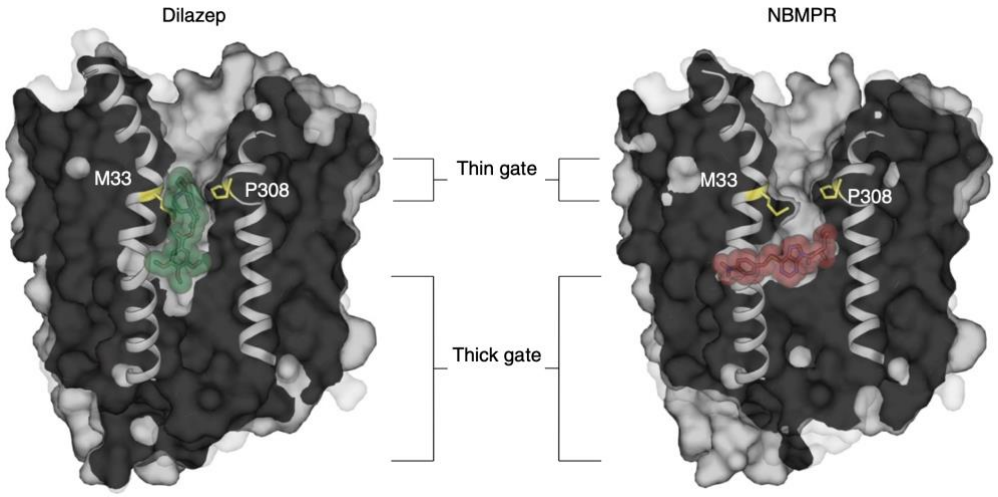

Figure 26. Dilazep and NBMPR bound hENT1. Figure reprinted with permission from ref 69.

3.2 Results and Discussion

Although the inhibition of hENT by AdoRIs has had long standing interest within the scientific community, the lack of crystallographic data has made the rational design of novel compounds challenging. As classic AdoRIs lack selectivity, isoform specificity, toxicity, and poor bioavailability, there is an urgent need for the development of novel ENT inhibitors.

Therefore, the goal of this chapter is to take advantage of the structural data provided by the co-crystal structure of hENT1 in complex with dilazep and NBMPR to rationally design inhibitors with improved target potency, pharmacological properties, and subtype specificity, for the development of non-opioid analgesic compounds. Our efforts towards each of these aims will be addressed in the following sections. The work accomplished in this chapter was done in collaboration with Dr. Pyeongwha Jeong and Yiquan Zhao, members of the Hong Lab.

3.2.1 Development of Novel ENT1 Inhibitors

3.2.1.1 Hybrid Analog Design

To improve the target potency of ENT inhibitors, we postulated that we could design a hybrid analog of dilazep and NBMPR that takes advantage of both their shared and distinct binding sites to provide an inhibitor with increased binding affinity for ENT1. Therefore, for the design of our first hybrid analog, we utilized dilazep as the core to occupy the 'orthosteric site' and 'opportunistic site 1' and introduced the *p*-

nitrobenzyl moiety to occupy 'opportunistic site 2' (Figure 27). With our first target compound in mind, we began the synthesis of our first hybrid analog.

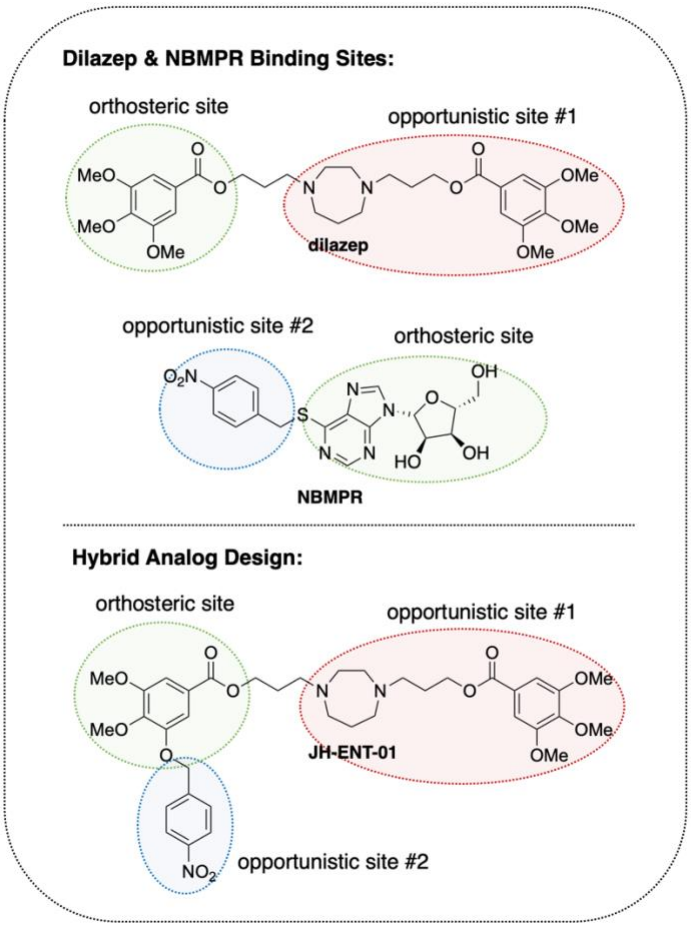

Figure 27. Hybrid analog design for ENT1 inhibitors

3.2.1.2 JH-ENT-01 Synthesis and Bioactivity

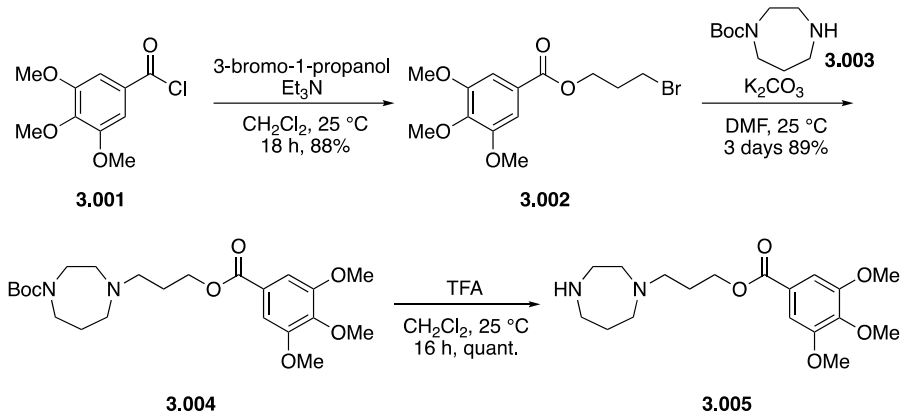

Scheme 31. Synthesis of 3.005

The synthesis began with the right-hand portion of our hybrid analogs, homopiperazine **3.005** (Scheme 31). First 3-bromo-1-propanol was coupled to acyl chloride **3.001** to provide bromide **3.002**, which was then coupled to 1-Boc-homopiperzine in the presence of K_2CO_3. Finally, TFA deprotection provided homopiperazine **3.005**, quantitatively. Next, to build up the left-hand side, phenol **3.006** was coupled to 4-nitrobenzylbromide with the addition of K_2CO_3 under refluxing conditions. The resulting ester (**3.007**) was hydrolyzed with 1 N LiOH and converted to an acyl chloride intermediate upon treatment with $SOCl_2$. The acyl chloride was then coupled to 3-bromo-1-propanol under basic conditions to provide bromide **3.009**. Finally, bromide **3.009** was coupled to homopiperazine **3.005**, in the presence of K_2CO_3 to provide JH-ENT-01.

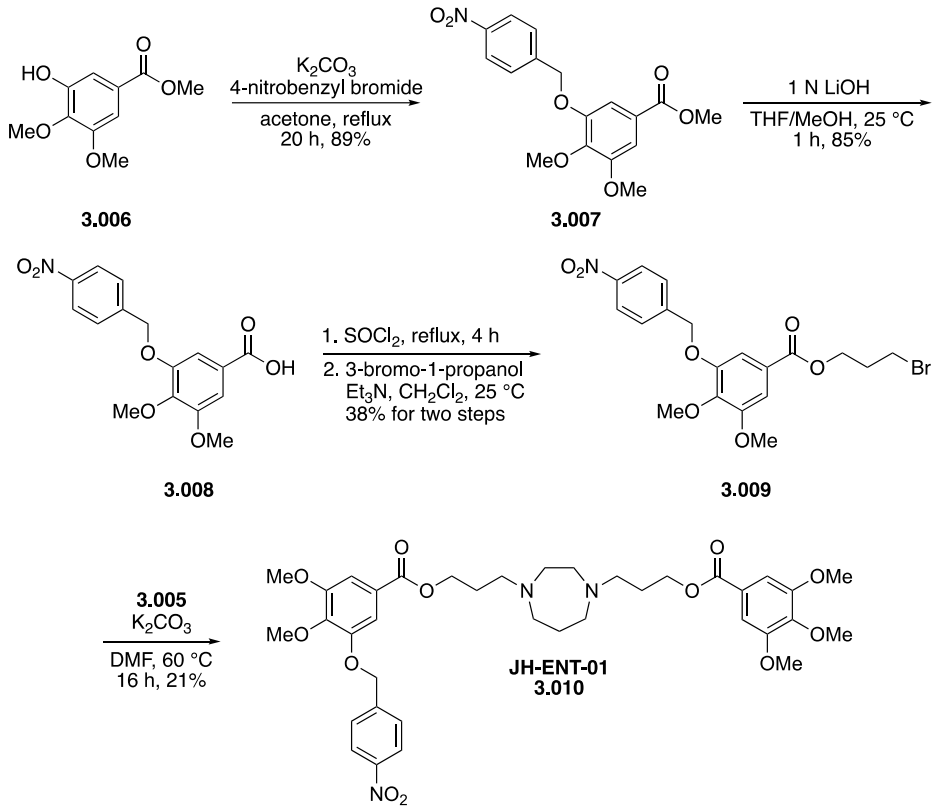

Scheme 32. Synthesis of JH-ENT-01

Following the synthesis of JH-ENT-01, our collaborators in Prof. Seok-Yong Lee's lab tested our hybrid design by comparing the binding affinity of JH-ENT-01 (**3.010**) to ENT1 compared to dilazep in a cold-competition scintillation proximity assay (SPA). SPA measures the fraction of ^{3}H-NBMPR bound to ENT1 upon treatment with JH-ENT-01 or dilazep. Excitingly, JH-ENT-01 showed a 2-fold increase in binding affinity (Figure 28) compared to dilazep. Encouraged by these results, Prof. Lee's group obtained the crystal structure of JH-ENT-01 bound to ENT1. From this data we compared the binding mode of JH-ENT-01 to that of dilazep and NBMPR. Shown in Figure 29, our hybrid analog exactly mimics the binding mode of dilazep, taking advantage of 'opportunistic

site 1′ and the ‘orthosteric site’. In comparison to NBMPR, the *p*-nitrobenzyl moiety does occupy the same hydrophobic pocket (‘opportunistic site 2′) but at a slight rotation of ~12.5 °. Additionally, JH-ENT-01 fails to take advantage of the part of the binding pocket that interacts with the ribose unit of NBMPR.

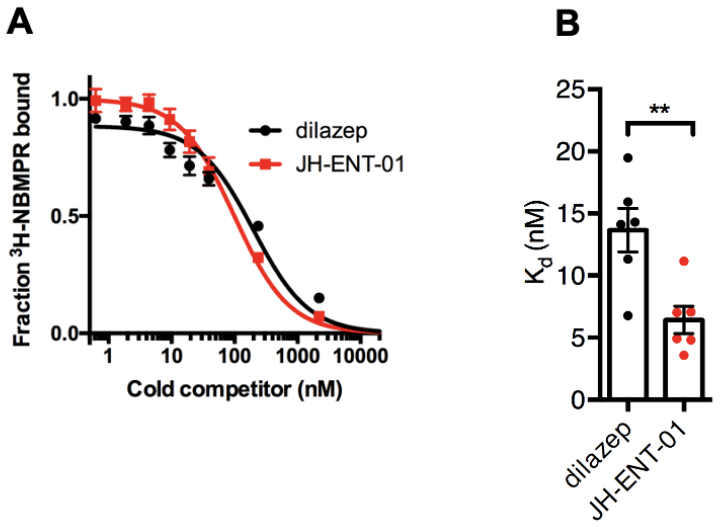

Figure 28. Cold-competition Scintillation Proximity Assay (SPA)

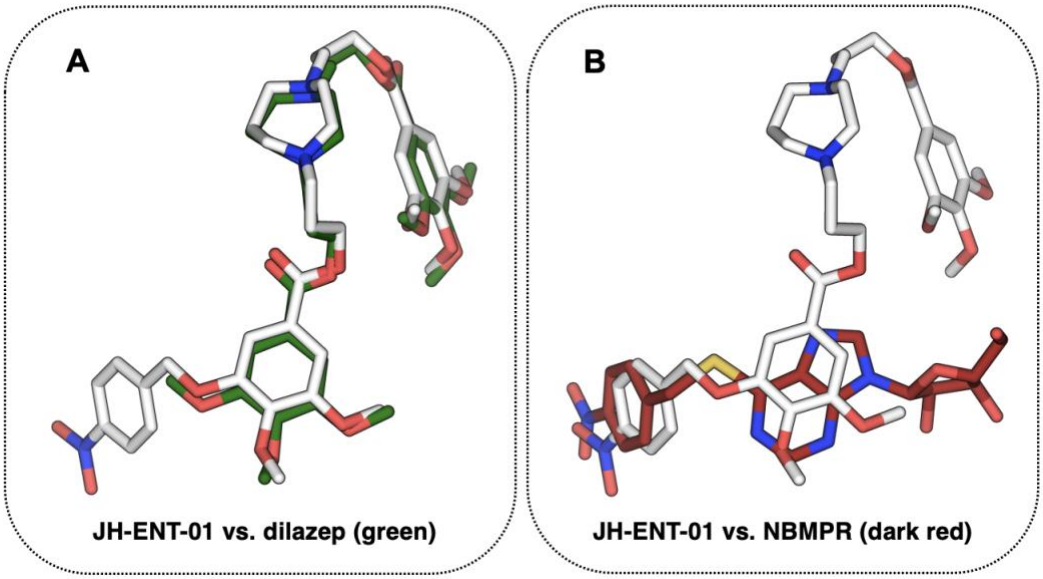

Figure 29. Overlay of JH-ENT-01's (white) binding pose with dilazep (left) and NBMPR (right)

3.2.1.3 Design and Synthesis of ENT1 Inhibitor Library

Based on our analysis of JH-ENT-01's binding mode, we designed a small library of inhibitors to develop preliminary structure-activity relationships (SAR). For our inhibitor library, we focused on three aspects of our hybrid analog. Firstly, driven by the slight rotation of the *p*-nitrobenzyl moiety, we designed analogs JH-ENT-02, 03, & 04 (Figure 30) in hopes to adjust the angle to mimic NBMPR. Secondly, the truncated analog JH-ENT-05 was devised to determine if we could take advantage of 'opportunistic site 1', while making our inhibitors smaller, simpler to synthesize. Lastly, an additional ribose unit was introduced to analogs JH-ENT-06 & 07 to take advantage of the additional interactions observed with the ribose unit of NBMPR. The synthesis of each of these inhibitors we will now be briefly discussed.

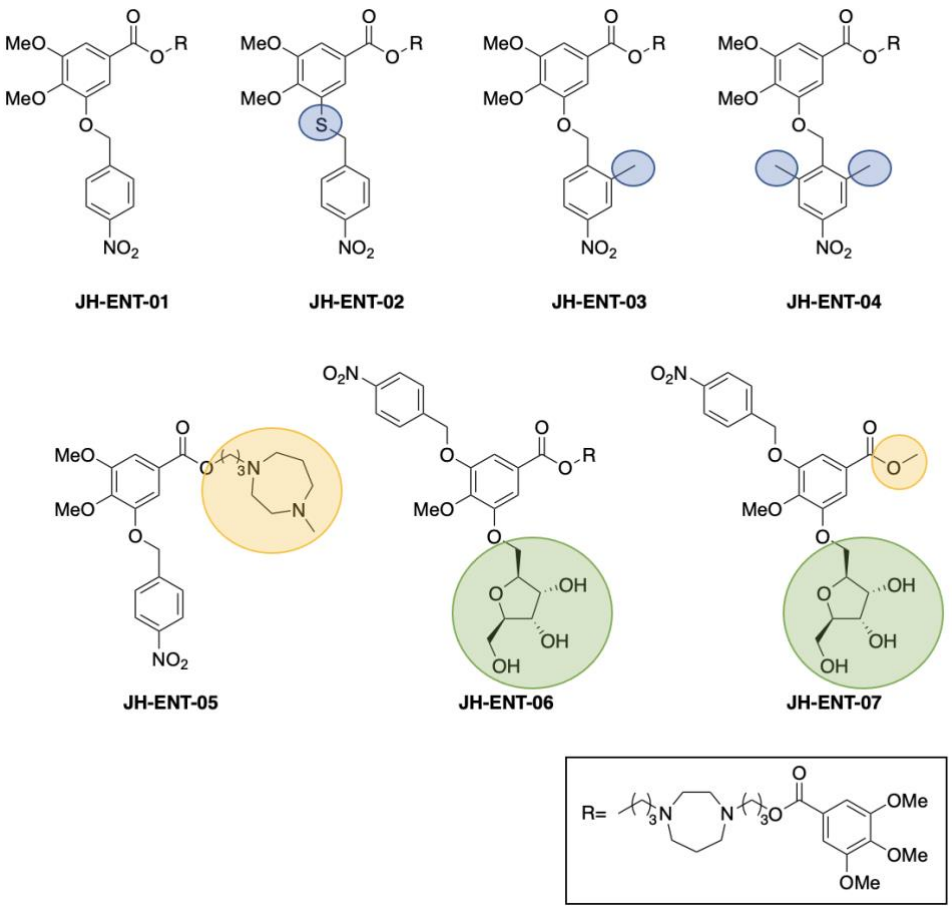

Figure 30. ENT1 inhibitor library

To synthesize JH-ENT-02 we first needed to replace the phenol of ester **3.006** of JH-ENT-01 (**3.010**) with a thiol. This was accomplished by coupling dimethylthiocarbamoyl chloride (**3.011**) with 3,4-dimethoxy-5-hydroxybenzoic acid methyl ester (**3.006**) with the addition of NaH, followed by reflux in phenyl ether to provide the rearranged product **3.013**. Finally, transesterification with NaOMe provides thiol **3.014** in 82% yield (Scheme 33).

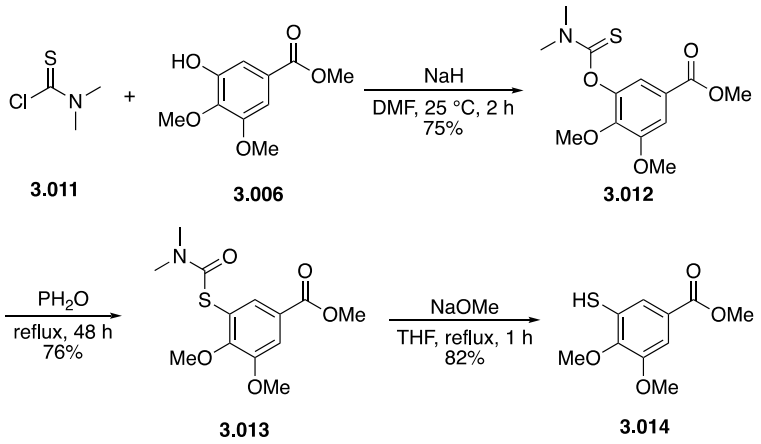

Scheme 33. Synthesis of 3.014

With the thiol (**3.014**) in hand, we proceeded with the same synthetic approach as JH-ENT-01. The *p*-nitrobenzyl moiety was introduced via reflux with thiol (**3.014**) under basic conditions and the resulting ester was hydrolyzed with 1 N LiOH to provide carboxylic acid **3.016**. Next to introduce the alkyl chain, we treated **3.016** with thionyl chloride to form the acyl intermediate and then 3-bromo-1-propanol but unfortunately the conditions were too harsh and the *p*-nitrobenzyl group was removed and resulted in alkylation of the thiol (Scheme 34). As *N, N'*-dicyclohexylcarbodiimide (DCC) is a commonly used reagent for the formation of amide, peptide, or ester bonds, we treated **3.016** with DCC, 3-bromo-1-propanol in CH_2Cl_2 and successfully introduced the alkyl chain to form intermediate **3.017**. Finally, **3.017** was coupled to homopiperazine **3.005** to provide JH-ENT-02 in a 44% yield.

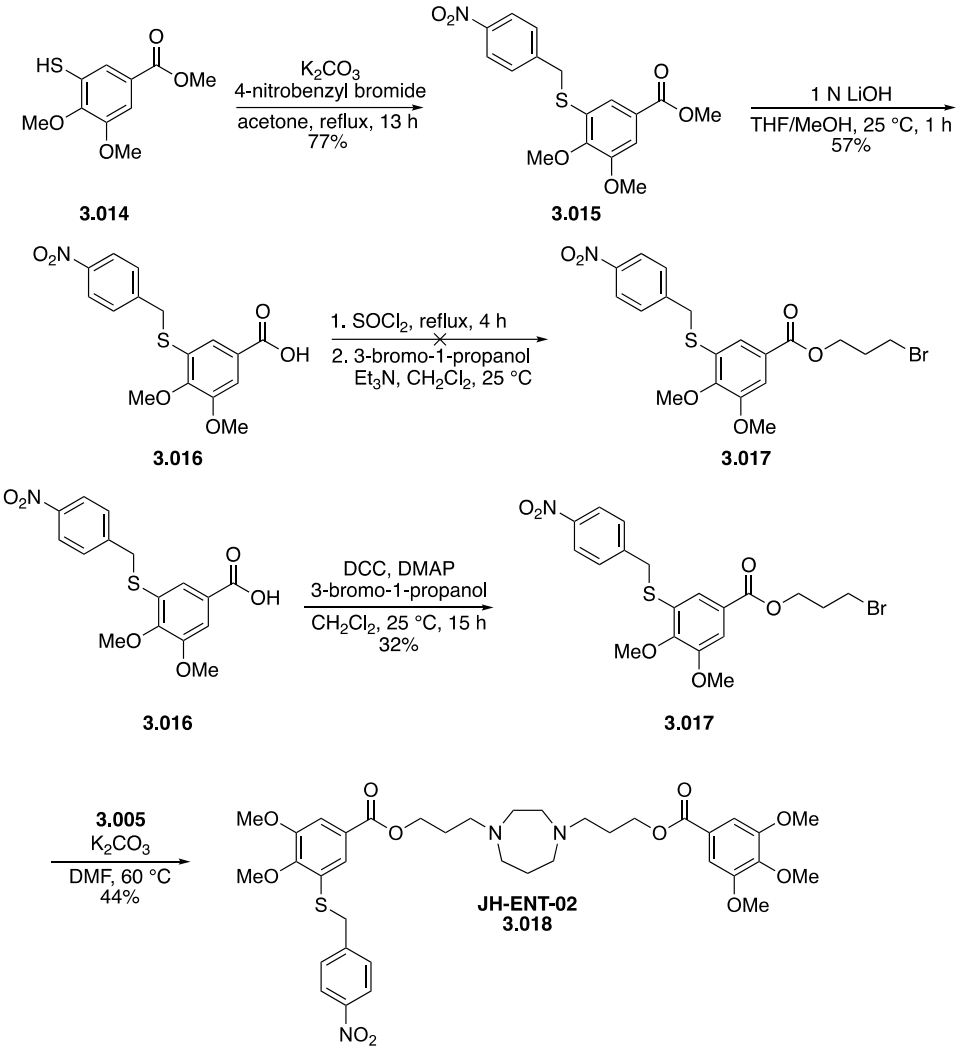

Scheme 34. Synthesis of JH-ENT-02

We next turned our attention to the monomethyl analog JH-ENT-03. We began with the reduction of carboxylic acid **3.019** to the primary alcohol with BH_3·DMS and $B(OCH_3)_3$, which was then converted to bromide **3.020** upon treatment with PBr_3 (Scheme 35). The remainder of the synthesis is carried out analogously to JH-ENT-02. Coupling to methyl ester **3.006**, hydrolysis with 1 N LiOH, DCC coupling to 3-bromo-1-

propanol and finally coupling to homopiperazine **3.005** to complete the synthesis of JH-ENT-03 (Scheme 35).

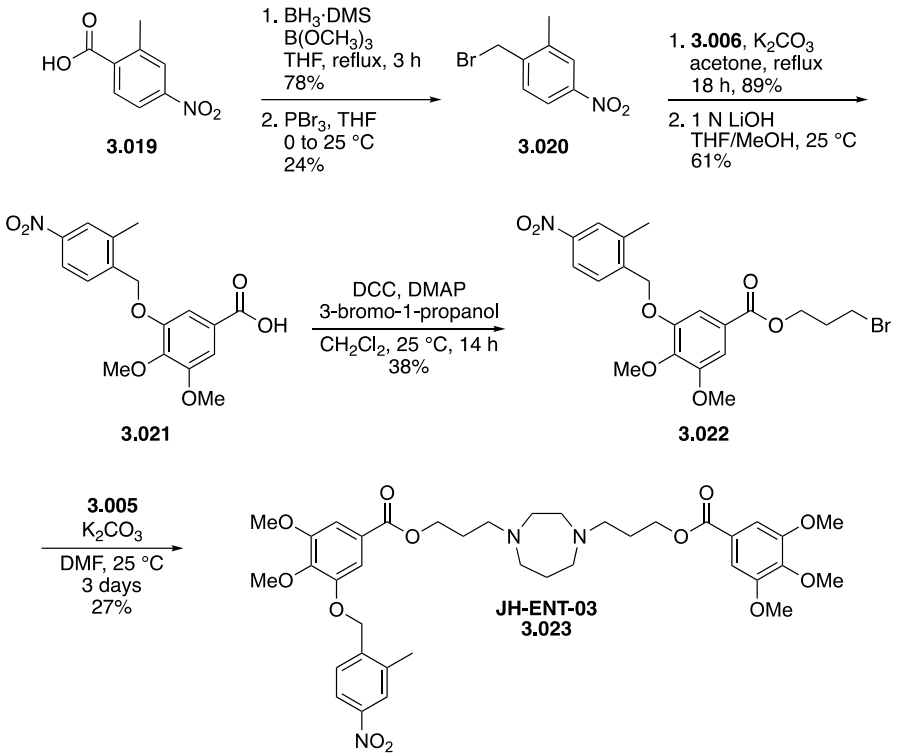

Scheme 35. Synthesis of JH-ENT-03

The introduction of the dimethyl nitrobenzyl moiety of JH-ENT-04 was slightly more complicated than the monomethyl analog. To construct the dimethyl nitrobenzyl bromide **3.030**, we began by protecting 2,6-dimethylaniline with *p*-TsCl and then successively introduced the nitro moiety by treating **3.025** with $NaNO_2$ under reflux in AcOH, H_2O, and HNO_3 (Scheme 36). The tosyl protecting group was removed with concentrated sulfuric acid and the resulting free aniline was converted to nitrile **3.028** via a Sandmeyer reaction. **3.028** was then treated with DIBALH and 1 N HCl to form an aldehyde intermediate that was reduced by $NaBH_4$ to provide primary alcohol **3.029**.[70]

Finally, **3.029** was treated with PBr_3 to obtain bromide **3.030.** Following the same synthetic approach as JH-ENT-02 & 03, the dimethyl analog JH-ENT-04 is obtained (Scheme 36).

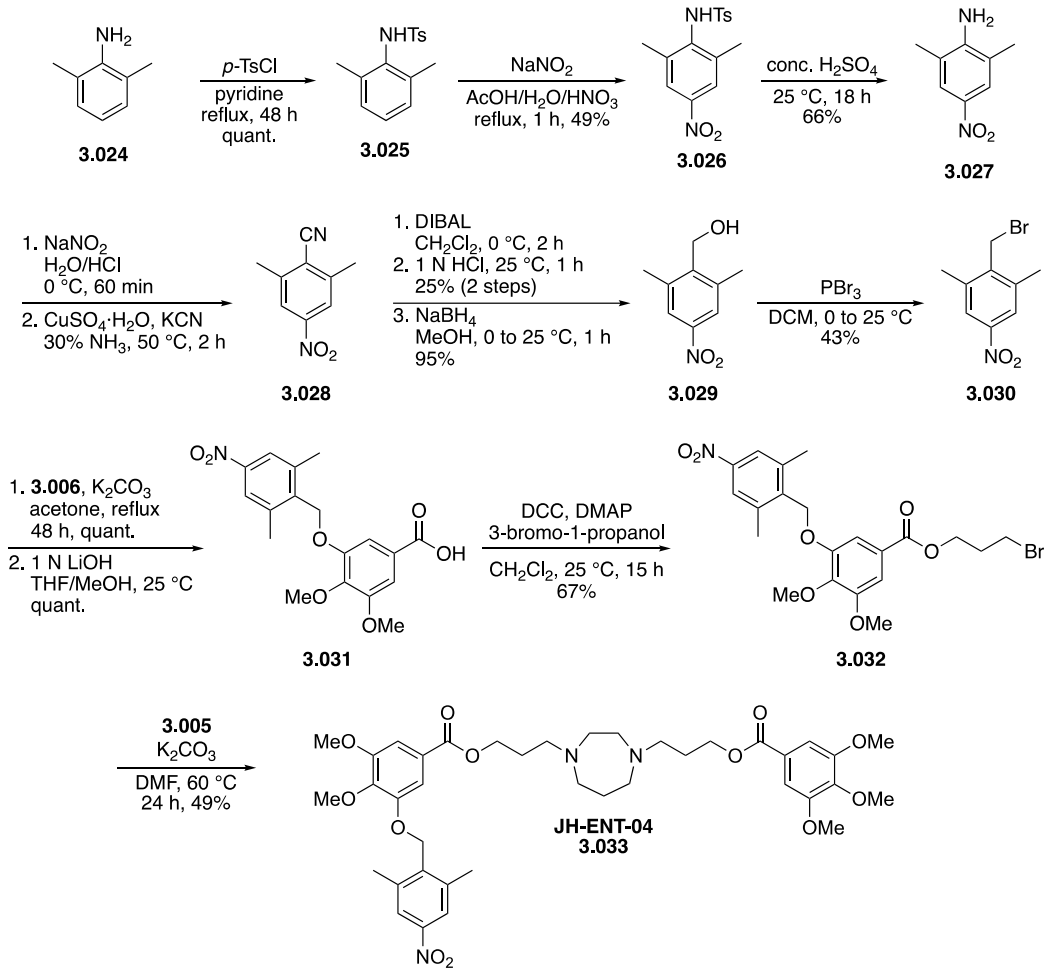

Scheme 36. Synthesis of JH-ENT-04

Our simplest analog, JH-ENT-05, was attained by coupling intermediate **3.009** of JH-ENT-01 with 1-methylhomopiperazine under basic conditions in acetone in a 64% yield (Scheme 37).

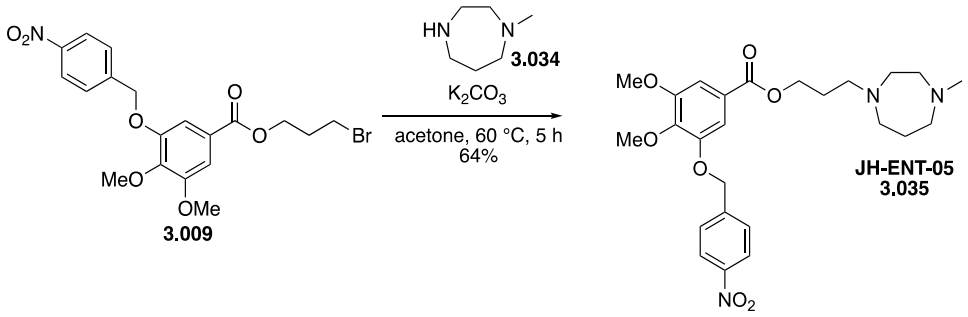

Scheme 37. Synthesis of JH-ENT-05

For the synthesis of JH-ENT-06 & 07, we began with the ribose moiety **3.039** (Scheme 38). Firstly, commercially available acetate **3.036** was converted to methyl ester **3.037** in 69% yield for 3 steps. **3.036** was treated with TMSCN and $BF_3{\cdot}OEt_2$ to form a nitrile intermediate which was subsequently treated with NaOMe to form the methyl ester and simultaneously remove the benzoyl protecting groups.[71 72] The resulting *syn*-diol was then protected with 2,2-dimethoxypropane in the presence of *p*-TsOH. Next, the primary alcohol was protected with TBDPSCl to provide **3.038**. Finally, ester reduction with $NaBH_4$ and tosylation provides the ribose moiety **3.039** (Scheme 38).

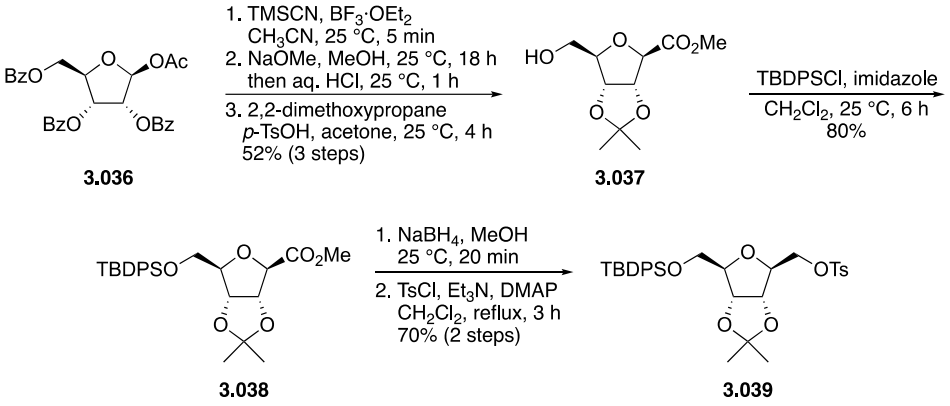

Scheme 38. Synthesis of 3.039

To introduce the ribose moiety to our substrate, methyl 3,4,5-trihydroxybenzoate **3.040** was treated with MeI and K_2CO_3 to give the *para*-methylated phenol in a 60% yield (Scheme 39). From there, ribose moiety **3.039** was introduced under basic conditions in DMF warmed to 40 °C over 3 days. Next, *p*-nitrobenzyl bromide was coupled to phenol **3.042** to provide **3.043**. The synthesis was completed as our other inhibitors, hydrolysis with 1 N LiOH, DCC coupling of 3-bromo-1-propanol and coupling to homopiperazine **3.005** but an additional deprotection step with TFA provides JH-ENT-06. For our final inhibitor, JH-ENT-07 was obtained by treating intermediate **3.043** with TFA (Scheme 40).

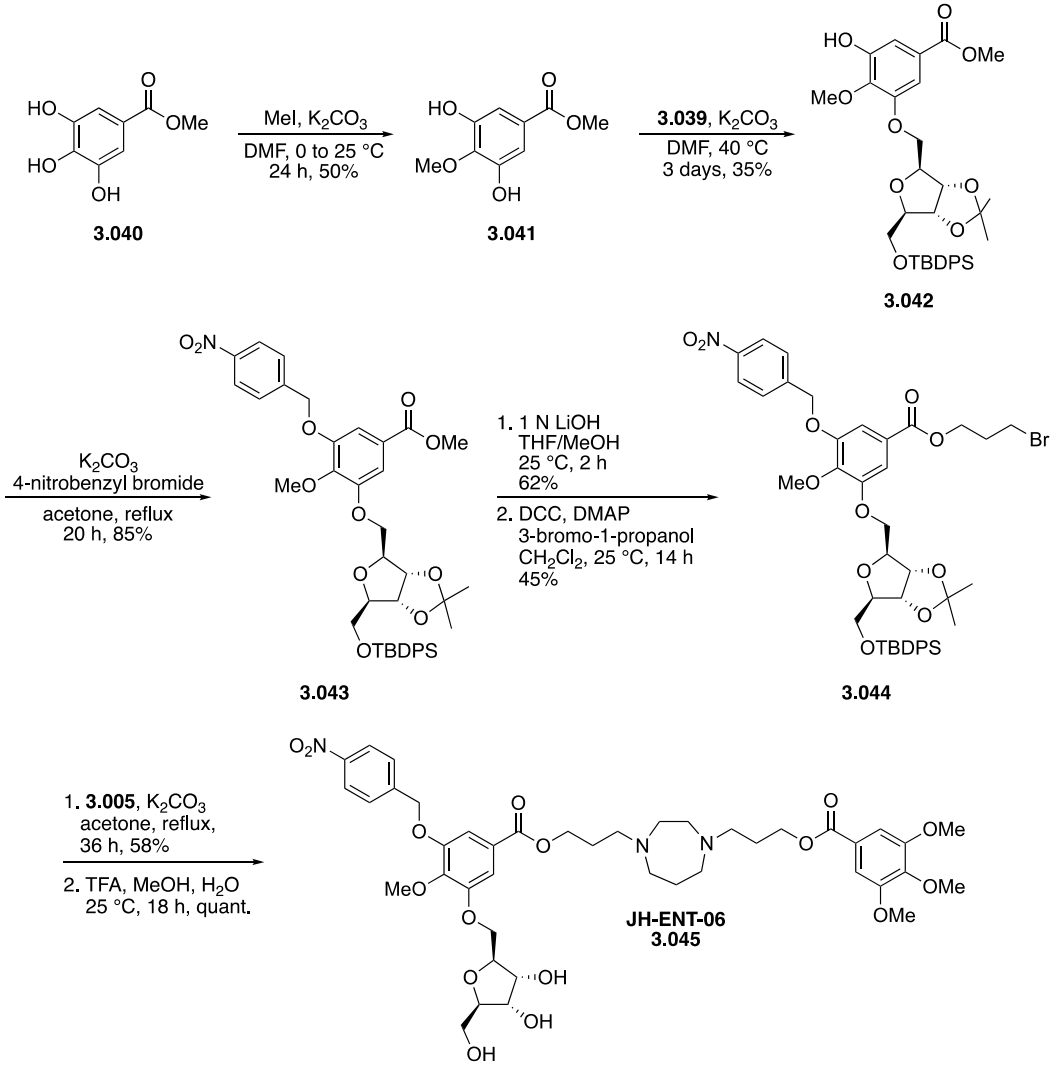

Scheme 39. Synthesis of JH-ENT-06

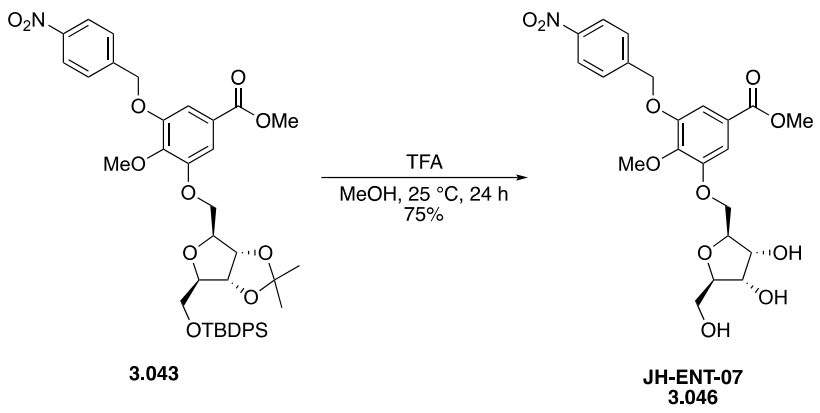

Scheme 40. Synthesis of JH-ENT-07

3.2.1.4 Bioactivity of ENT1 Inhibitor Library

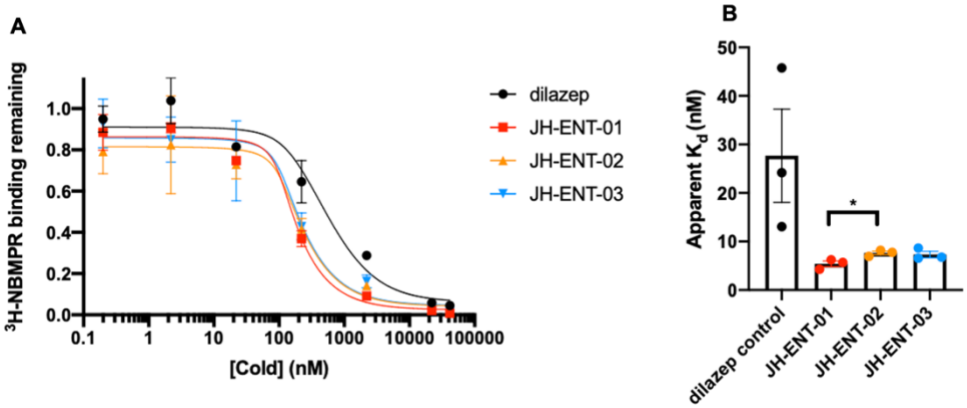

Figure 31. Cold-competition SPA for JH-ENT-01, 02 & 03

Following the synthesis of our ENT1 inhibitor library, our collaborators in Prof. Seok-Yong Lee and Prof. Ru-Rong Ji's groups began their evaluation of our inhibitors with respect to their binding affinity to ENT1 and their analgesic activity in a streptozotocin (STZ) induced diabetic neuropathic pain model. Currently, from our library, Prof. Lee's group has determined the binding affinity of JH-ENT-01, 02 and 03. Although we saw an initial 2-fold increase in binding of our original hybrid analog JH-ENT-01 compared to dilazep, our rationally designed analogs JH-ENT-02 and 03 did not

show an improvement in affinities compared to JH-ENT-01 (Figure 31). The remainder of the library will be investigated shortly.

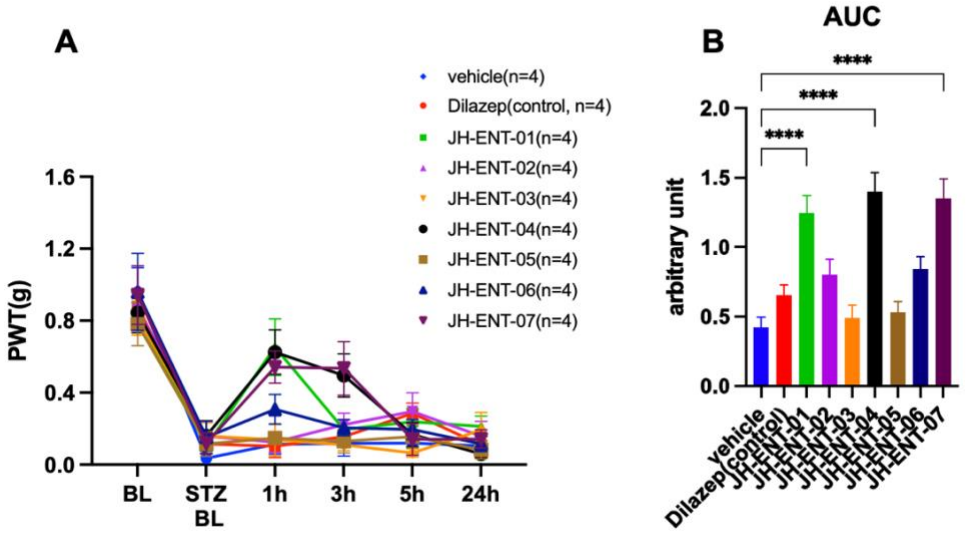

Figure 32. Analgesic activity of JH-ENT-01 to 07

In addition to the binding affinity data, Prof. Ji's group has provided promising data for the analgesic activity of our ENT1 inhibitor library. As shown in Figure 32, STZ-induced diabetic mice were treated with 10 nmol of inhibitor, or dilazep as a control through intrathecal injection and their paw withdraw threshold was measured over the course of 24 hours. Three of our designed inhibitors (JH-ENT-01, JH-ENT-04 and JH-ENT-07) showed significant reduction in mechanical pain compared to vehicle or dilazep (control) treated mice (Figure 32).

Encouraged by these results, Prof. Ji's group further evaluated JH-ENT-01 and JH-ENT-07 using repeated intravenous injections of 30 mg/kg every other day. The experimental design is shown in Figure 33A. Excitingly, both JH-ENT-01 and JH-ENT-07

significantly reduced mechanical pain with accumulating effects that are enhanced after the 3rd injection, lasting for 24-48 h (Figure 33B). Additionally, both compounds significantly reduced mechanical allodynia, another method for measuring mechanical pain, as shown in Figure 33C. Lastly, JH-ENT-01 and JH-ENT-07 did not show any effect on cold related pain (Figure 33D). Importantly, the motor function of the mice treated with novel inhibitors was assessed using a rotarod test and no significant effects were observed (Figure 34).

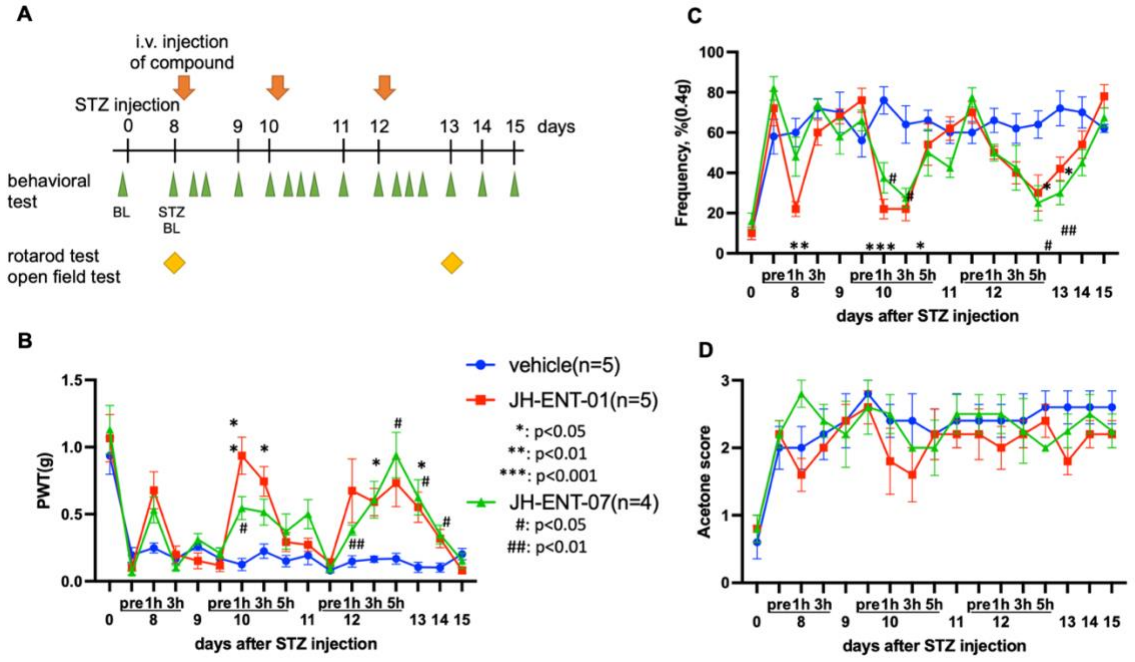

Figure 33. Further analysis of JH-ENT-01 & 07. A) experimental design B) mechanical pain C) mechanical allodynia D) cold related pain

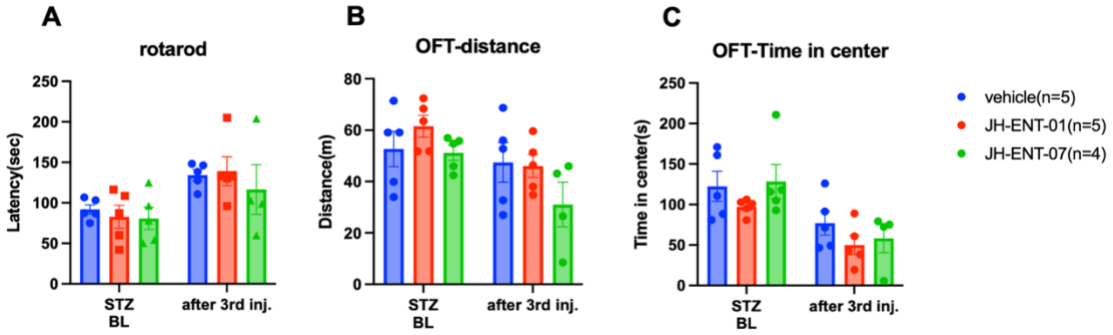

Figure 34. Rotarod test for motor function assessment

3.2.1.3 Rational Design for Second Generation ENT1 Inhibitors

Motivated by the promising activity of our JH-ENT-07 inhibitor, we sought to expand on this novel chemotype for the development of more potent ENT1 inhibitors. To design novel compounds, the co-crystal structure of NBMPR in complex with hENT1 was utilized to study the binding pose of JH-ENT-07. Shown in Figure 35, additional space at the top of the binding pocket is available for expansion off of the methyl ester of JH-ENT-07, as well as the potential for additional interactions with Gln158 at the bottom. Therefore, ~150 compounds were rationally designed and evaluated using Maestro's Glide (Schrödinger). The top two hit compounds that exhibited excellent docking scores, maintained key interactions with Gln158 and Trp29 but additionally showed hydrogen bonding with Thr85 have been synthesized and are currently being evaluated for their bioactivity.

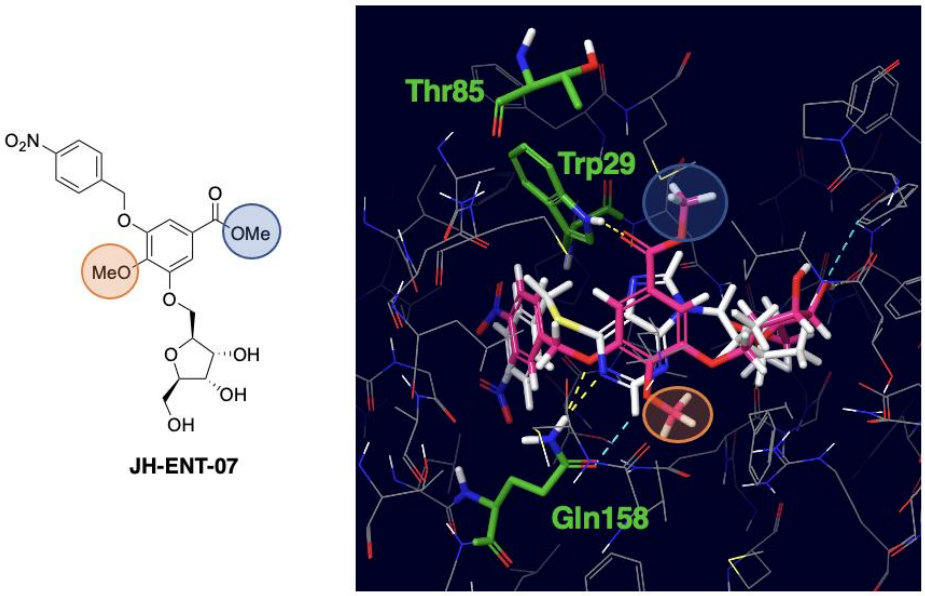

Figure 35. Evaluation of JH-ENT-07 binding pose. NBMPR (white)/JH-ENT-07 (pink)

3.2.2 Efforts Towards a Macrocyclic ENT Inhibitor

3.2.2.1 Macrocyclic Design

Regarding our second aim, improving the pharmacological properties of ENT inhibitors, we hypothesized that a macrocyclic version of dilazep would help us achieve this goal by decreasing conformational flexibility, which will reduce entropy on binding, and increase selectivity and permeability of the inhibitor. Therefore, to best determine the optimal linker length and stereochemistry of our macrocycle, we performed a docking study (Maestro's Glide, Schrödinger) utilizing the crystal structure of ENT1 in complex with dilazep. This study demonstrated that a 3-carbon linker (highlighted in

red, Figure 36) and *R* stereochemistry (highlighted in blue) were necessary to mimic the binding pose of dilazep (Figure 36).

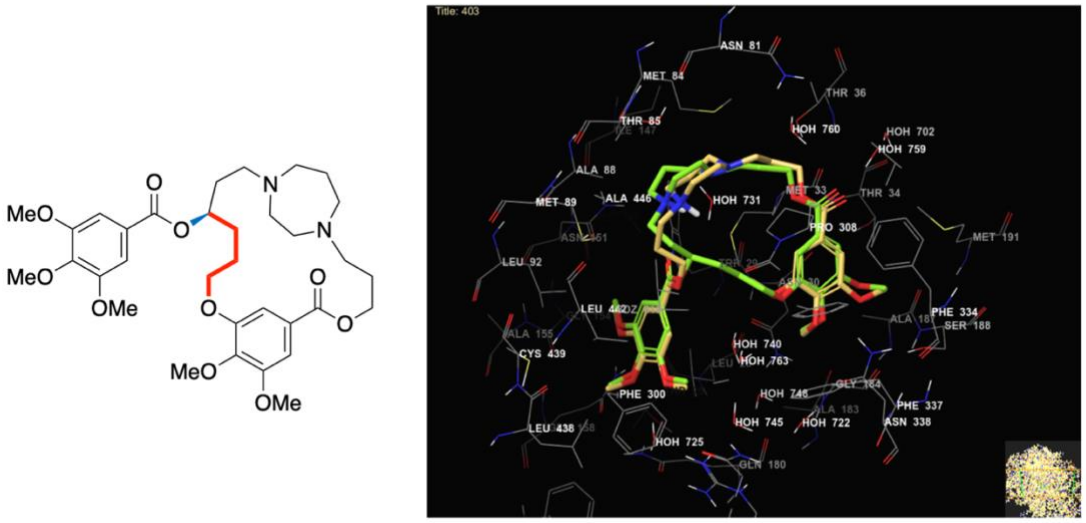

Figure 36. Docking result for the macrocyclic design. dilazep (yellow) macrocycle (green)

When designing the synthesis of our macrocyclic inhibitor, we envisioned several different approaches towards macrocyclization. As shown in Scheme 41, advanced intermediate **3.048** could be obtained through ring-closing metathesis (RCM) of **3.049** with Grubbs 2nd generation catalyst, an S_N2-type reaction involving the homopiperazine of **3.050** under basic conditions or a base-mediated alkyne/aldehyde coupling reaction with **3.051.** Our efforts towards each of these three approaches will be discussed in the next several sections.

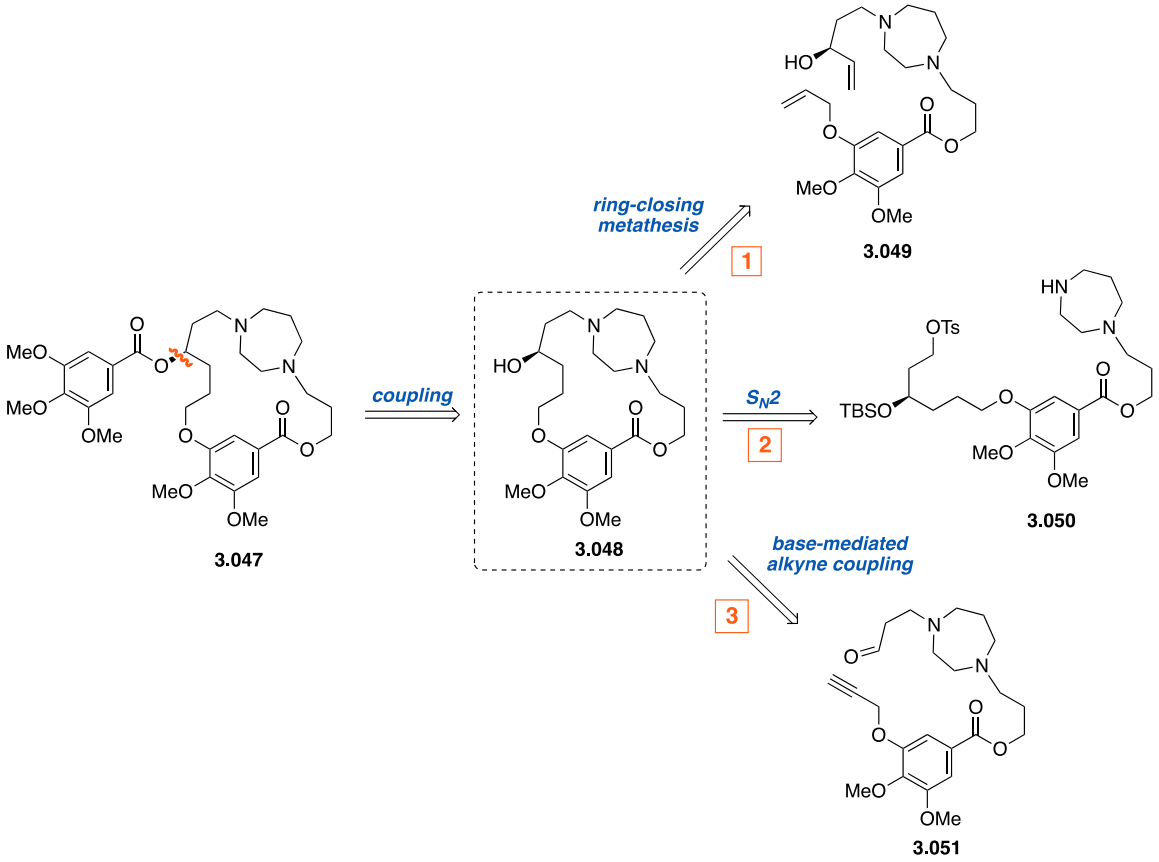

Scheme 41. Approaches towards macrocyclization

3.2.2.2 First Approach Towards Macrocyclization

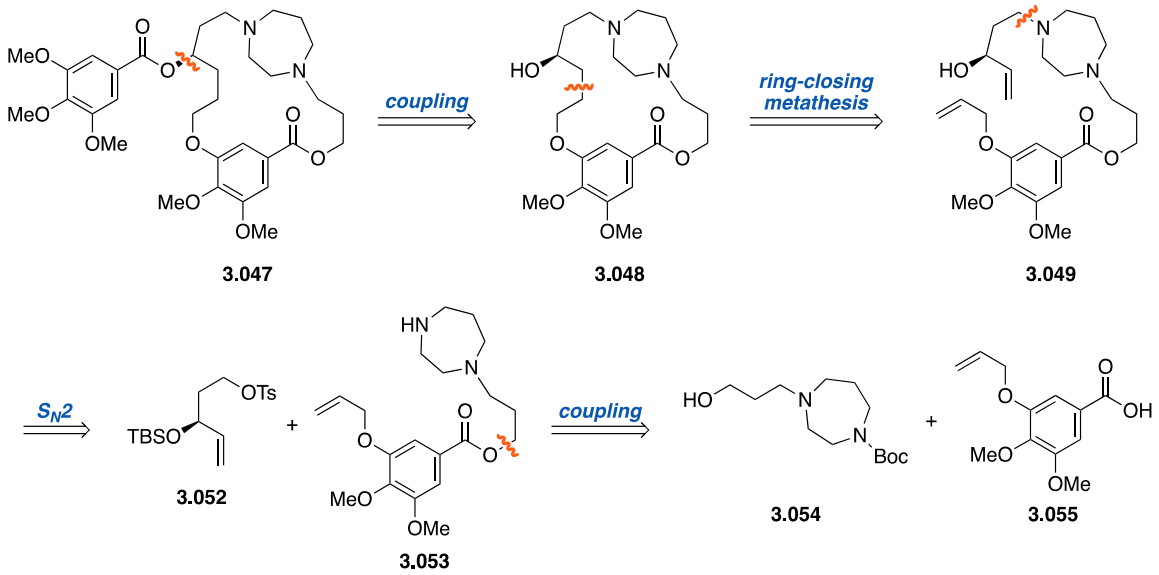

Scheme 42. Retrosynthetic analysis of first approach

Our initial efforts began with the RCM approach (Scheme 42). We anticipated that our substrate for RCM could be obtained by coupling easily synthesizable building blocks **3.054** and **3.055** to provide homopiperazine **3.053**, which can be further coupled to tosylate **3.052** through an S_N2-type reaction. Therefore, **3.055** was synthesized via coupling of phenol **3.006** with allyl bromide, followed by hydrolysis of the methyl ester with 1 N LiOH (Scheme 43). Next, homopiperazine **3.053** was obtained by coupling 1-Boc-homopiperazine with 3-bromo-1-propanol. The resulting primary alcohol was coupled to the carboxylic acid of **3.055** via DCC coupling in the presence of DMAP. Finally, the Boc protecting group was removed quantitatively upon treatment with TFA.

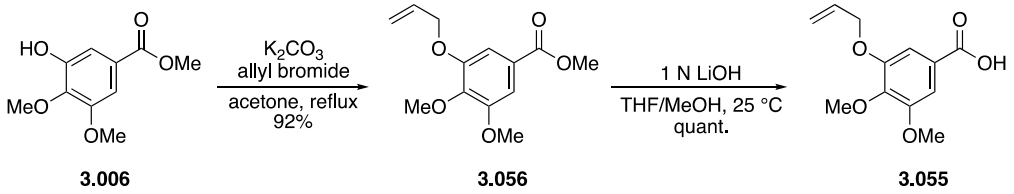

Scheme 43. Synthesis of 3.055

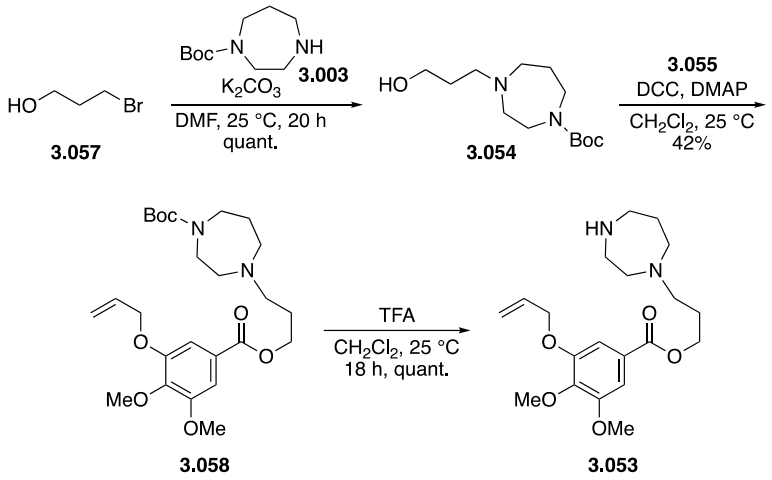

Scheme 44. Synthesis of 3.053

For the synthesis of **3.052**, we began by coupling *t*-butylacetate to ethyl 3-chloropropionate via *in situ* generation of LDA, followed by elimination of the resulting chloride with Et_3N to provide **3.060**. Next, the ketone was reduced with $NaBH_4$ to provide an enantiomeric mixture of **3.061** in 25% yield over three steps. The enantiomers were then separated using enzymatic resolution with vinyl acetate and amano lipase to provide the desired *S* acetate in 40% yield. The acetate was then removed with K_2CO_3, and the resulting secondary alcohol was protected with TBSCl to provide **3.064**.

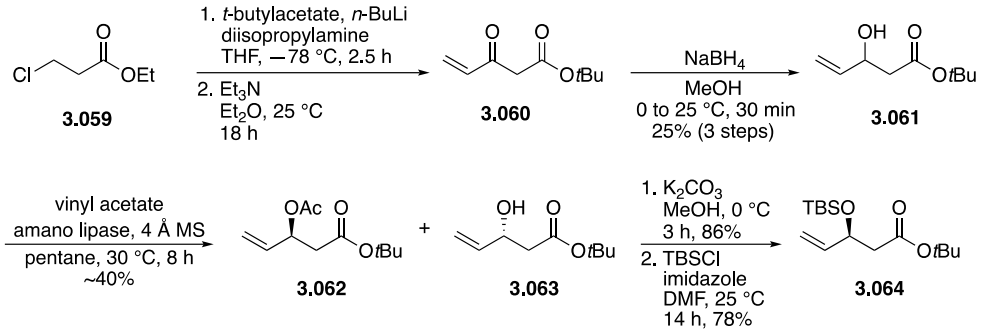

Scheme 45. Synthesis of 3.064

To determine the stereoselectivity of our enzymatic resolution with amano lipase, we utilized Mosher's acid chloride (**3.067**) to generate diastereomers **3.068** and **3.069** (Scheme 46). We compared the ^{1}H NMR spectrum (Figure 38) to racemic Mosher ester **3.070** (Figure 37). Looking at the racemic mixture, we clearly see two sets of methoxy peaks around 3.5 ppm and alkyl peaks further shifted upfield from 2.5 ppm. For our enantio-enriched material we do not see peaks upfield of 2.5 ppm and see a ratio of 30:1 for the methoxy peaks. Therefore, we concluded our enzymatic resolution provided $\geq$ 95% e.e. for our desired secondary alcohol.

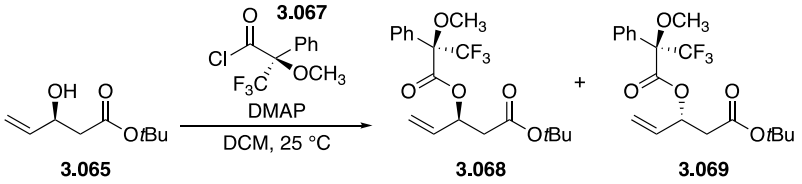

Scheme 46. Mosher ester synthesis

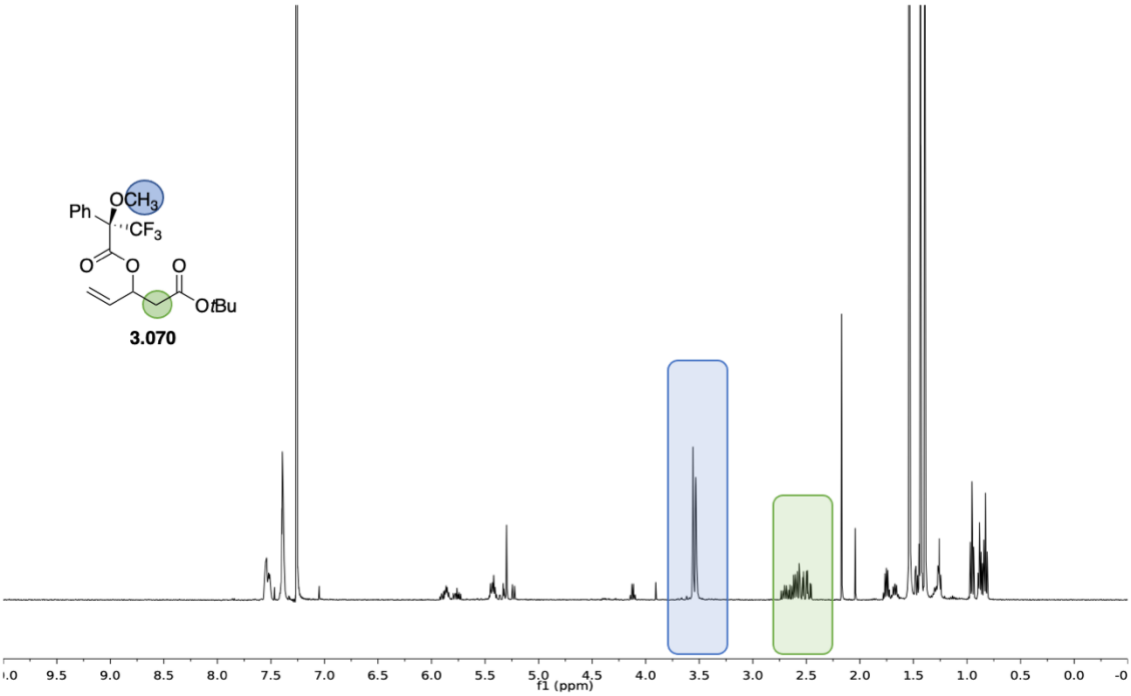

Figure 37. ^{1}H NMR ($CDCl_3$, 500 MHz) of racemic Mosher ester

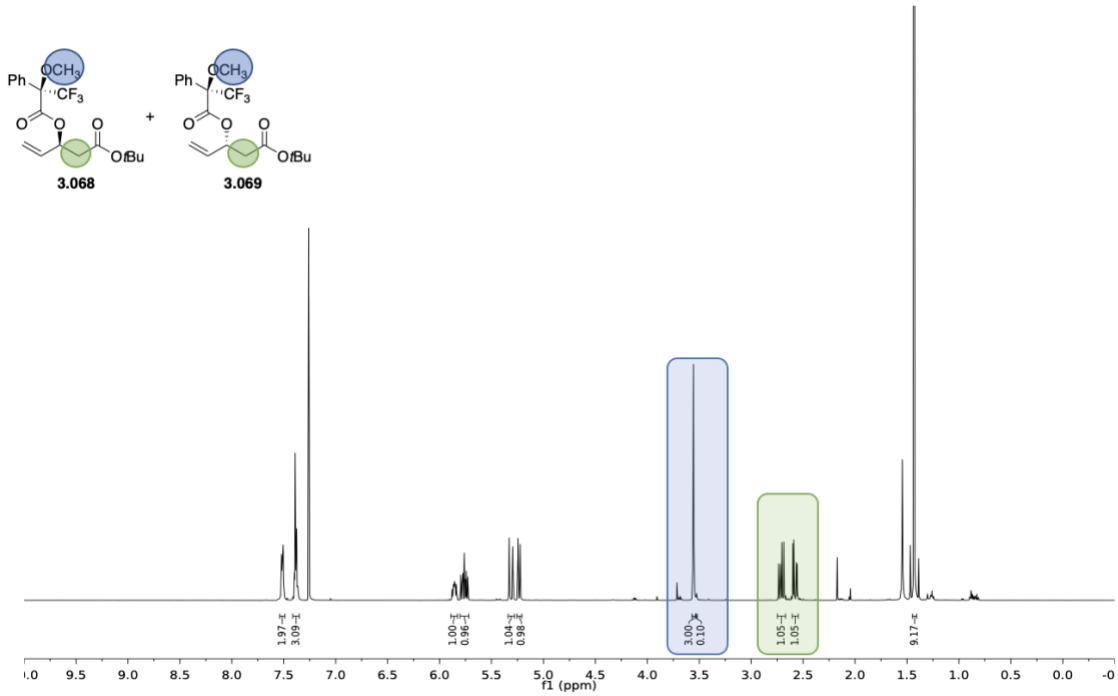

Figure 38. ^{1}H NMR ($CDCl_3$, 500 MHz) of Mosher esters 3.068 & 3.069

To conserve material, the racemic form of our ester was utilized for our attempts at the RCM reaction. Moving forward, ester **3.071** was reduced with DIBAL to the primary alcohol, which was then converted to tosylate **3.072** by treatment with *p*-TsCl in the presence of Et_3N. Tosylate **3.072** was then coupled to homopiperazine **3.053** under refluxing conditions with K_2CO_3 to provide **3.073**, our substrate for RCM. Subsequently, **3.073** was treated with Grubbs II (20 mol%) in very dilute CH_2Cl_2 (1 mM) under reflux. After 14 h, several new spots on TLC were observed in addition to the starting material but due to limited material and tight separation, instead of purification, the crude material was treated with TBAF to remove the TBS protecting group to provide **3.075**.

Although the small scale prevented purification and isolation, HRMS confirmed the formation of **3.075**.

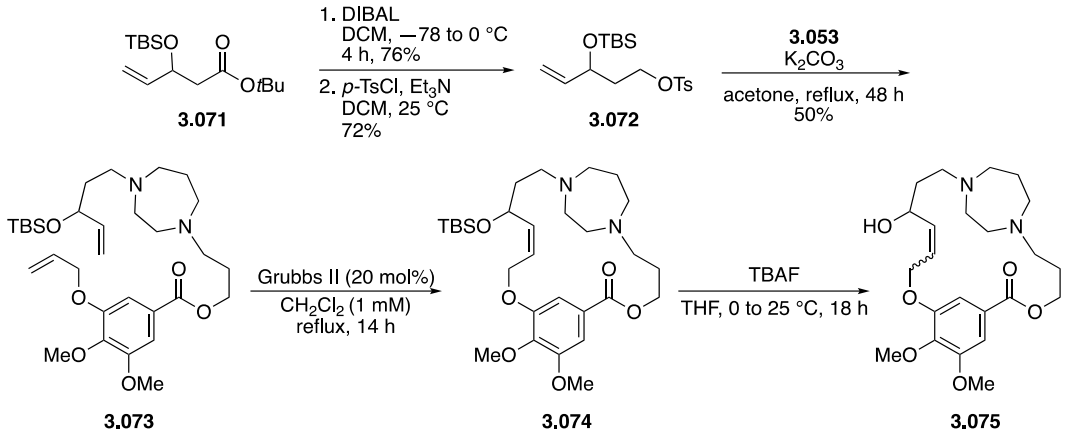

Scheme 47. Attempt towards RCM with Grubbs' II

Encouraged by these results, additional attempts for the RCM reaction were attempted in CH_2Cl_2 and benzene (Table 12). Unfortunately, we were not able to reproduce our initial attempt and mostly starting material was obtained from these trials. To determine if this approach is applicable for the formation of our macrocycle several modifications should be attempted. Including, exploring other variations of the Grubb's catalyst as well as varying the concentration of the reaction. Very dilute (1 mM) concentrations were used to promote intramolecular olefin metathesis but by increasing the concentration we may be able to push the reaction forward and consume the starting material.

Table 12. Attempts towards cyclization with Grubbs II

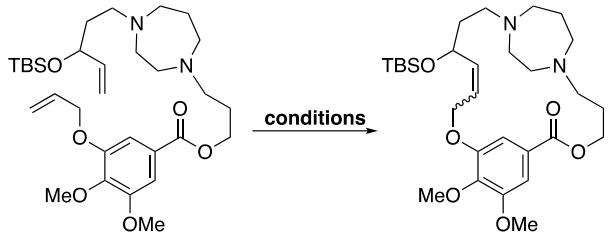

3.073 **3.074**

Entry	Conditions	result
1	Grubbs II (25 mol%), CH_2Cl_2, reflux, 48 h	**3.073**
2	Grubbs II (25 mol%), benzene, reflux, 48 h	**3.073**

3.2.2.3 Second Approach Towards Macrocyclization

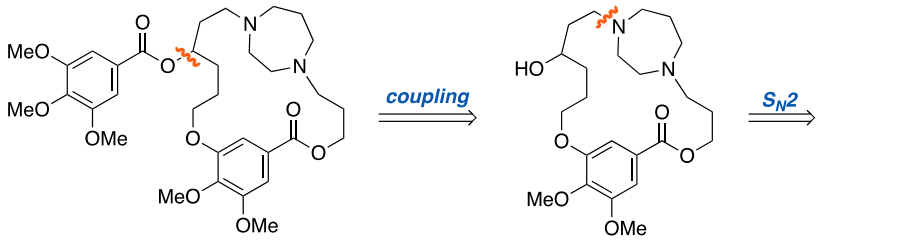

3.047 **3.048**

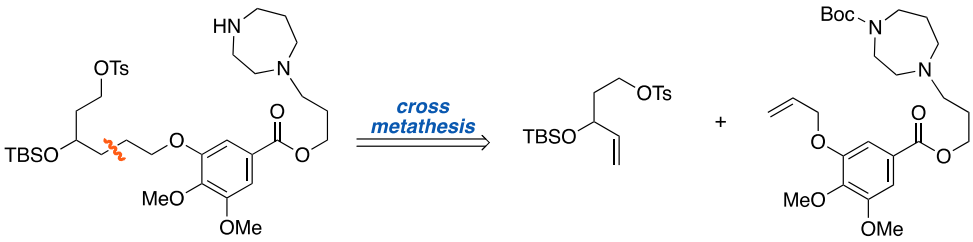

3.050 **3.072** **3.058**

Scheme 48. Retrosynthetic analysis of second approach

With very limited success with RCM, we got to work on the second approach that relied on macrocyclization via S_N2 with homopiperazine **3.050**. We postulated that we could attain the macrocyclization substrate **3.050** by cross-metathesis (CM) of our

previously synthesized intermediates **3.072** and **3.058**. Therefore, we subjected **3.072** and **3.058** to CM conditions with Grubbs II (Table 13) but unfortunately, we simply isomerized the terminal olefin of **3.058** to produce a mixture of *cis* and *trans* alkene in a 1:2.5 ratio, respectively**.** No CM product was observed.

Table 13. CM attempts with 3.072 and 3.058

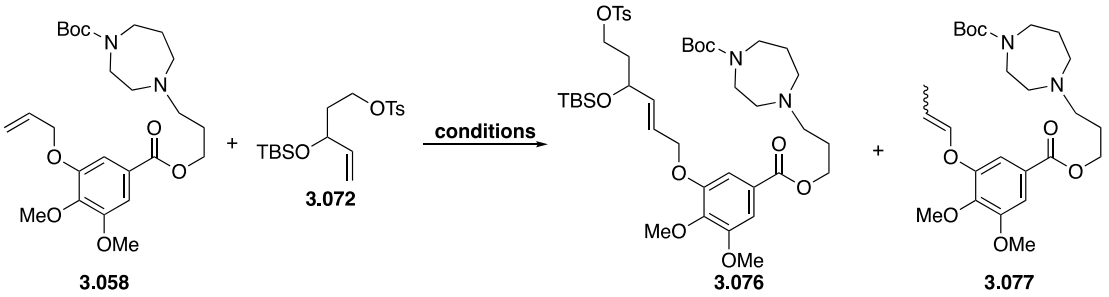

Entry	Conditions	result
1	Grubbs II (25 mol%), CH_2Cl_2, reflux, 48 h	**3.077**
2	Grubbs II (20 mol%), benzene, reflux, 48 h	**3.077**

At this stage we revised our approach towards intermediate **3.050** with the intention to extend **3.072** first and then couple to phenol to provide the macrocyclization substrate **3.050**. Initially, we sought to build the alkyl chain through CM with *cis*-1,4-diacetoxy-2-butene (**3.078**) and substrates (**3.072** and **3.071**), but the coupling reactions were unsuccessful and the only newly formed product we obtained in addition to starting material was *trans*-1,4-diacetoxy-2-butene (**3.080**) (Scheme 49).

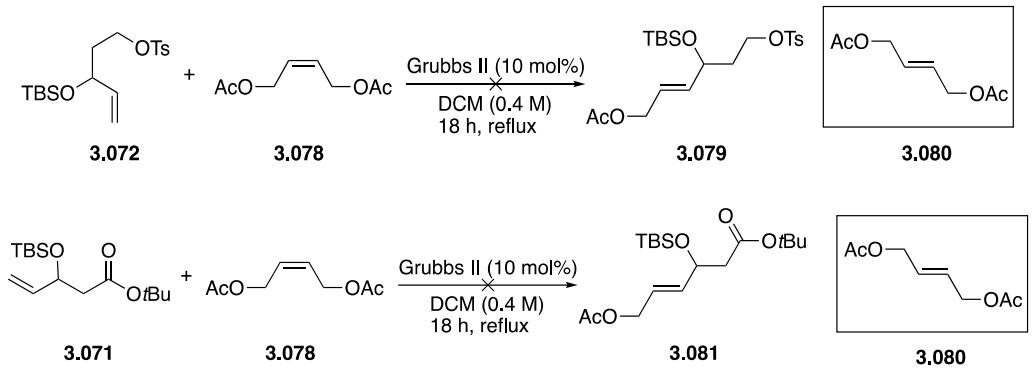

Scheme 49. Attempts at CM with 3.078

As CM had proven very difficult with our substrate, we began to explore other options for extending the alkyl chain and started with a Horner–Wadsworth–Emmons (HWE) reaction. First, *t*-butyl ester **3.071** was reduced with DIBAL to provide a primary alcohol which was subsequently protected with BnBr. Next, alkene **3.082** was oxidized to an aldehyde via ozonolysis in the presence of PPh_3 and immediately reacted with Ph_3PCHCO_2Et to provide the HWE product **3.083** in 10% for two steps.

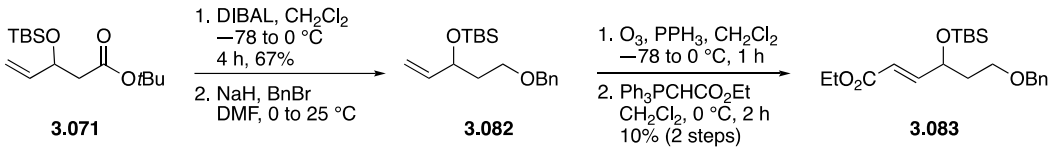

Scheme 50. Synthesis of 3.083

Although we were able to obtain the HWE product via ozonolysis, unacceptably low yields pushed us to seek out another route for oxidation. Consequently, we decided to synthesize our aldehyde necessary for the HWE reaction via oxidative cleavage with OsO_4, NMO and $NaIO_4$. To apply this approach, we reduced *t*-butyl ester **3.061** with LAH and selectively protected the primary alcohol with TrCl and subsequent benzyl protection of the secondary alcohol (Scheme 51). We then treated **3.085** with OsO_4 and

NMO, followed by $NaIO_4$ to form an aldehyde intermediate which was immediately subjected to HWE with Ph_3PCHCO_2Et to provide **3.086** in 49% for three steps. Content with the yield, we proceeded by reducing the ethyl ester with DIBAL and activating the newly formed alcohol with MsCl to provide substrate **3.087** primed for coupling with the phenol.

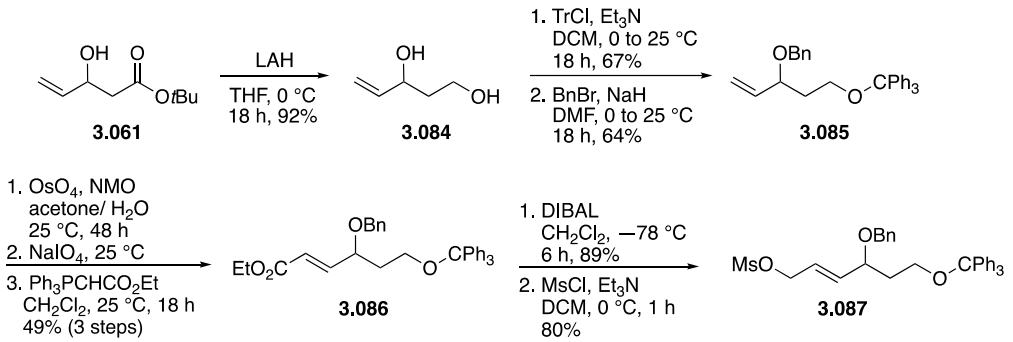

Scheme 51. Synthesis of mesylate 3.087

Allyl deprotection of **3.058** with $Pd(Ph_3P)_4$ and dimedone in THF provided phenol **3.088,** which was then coupled to mesylate **3.087** upon treatment with K_2CO_3 in acetone. The trityl protecting group was selectively removed in the presence of Boc utilizing dichloroacetic acid. The primary alcohol was then converted to mesylate **3.090** and the Boc group was removed with TFA. Crude homopiperazine was subjected to K_2CO_3 in acetone or DMF but regrettably, no cyclized product was obtained. Instead, starting material was recovered or the material decomposed. Like the first approach, additional efforts would be required to determine the applicability of this approach towards macrocyclization. Many different changes could be made to optimize this reaction, such as, varying the base, solvent, and reaction temperature.

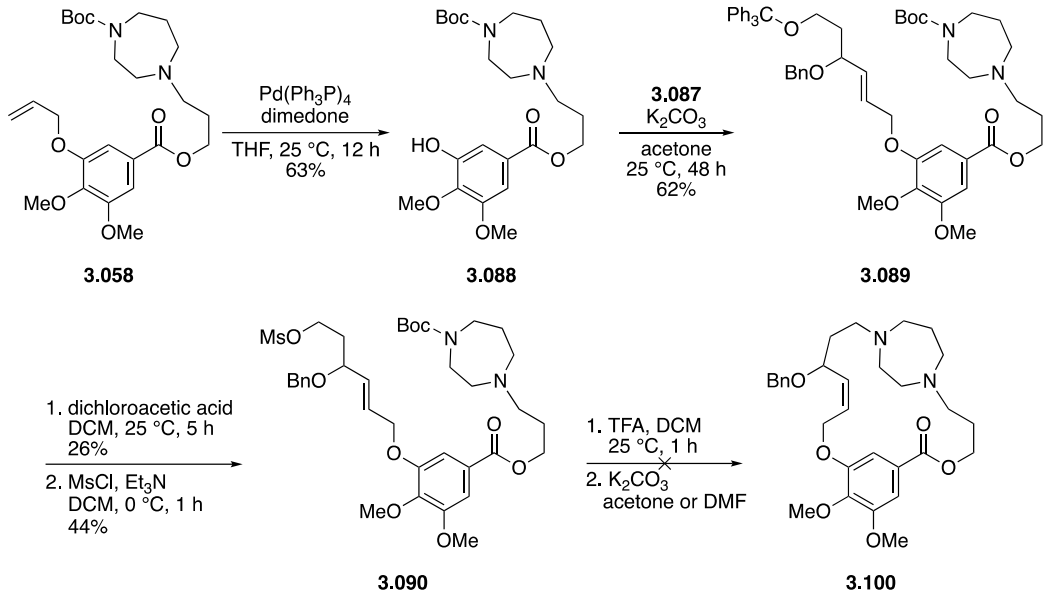

Scheme 52. Attempt at cyclization with SN2

3.2.2.4 Third Approach Towards Macrocyclization

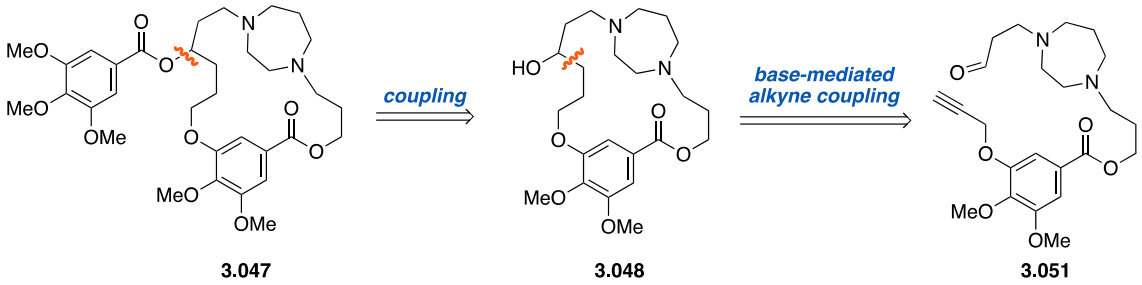

Scheme 53. Retrosynthetic analysis for the third approach

Although additional work needs to be done to determine the viability of our SN2 reaction, we embarked on our third approach. We anticipated that alkyne intermediate **3.051** may be more reactive and therefore more conducive towards cyclization. To obtain alkynyl intermediate **3.051**, we began by propargylation of phenol **3.006**, followed by hydrolysis and DCC coupling of the resulting carboxylic acid. Following deprotection

with TFA, the homopiperazine was coupled to 3-bromo-1-propanol to provide intermediate **3.103**.

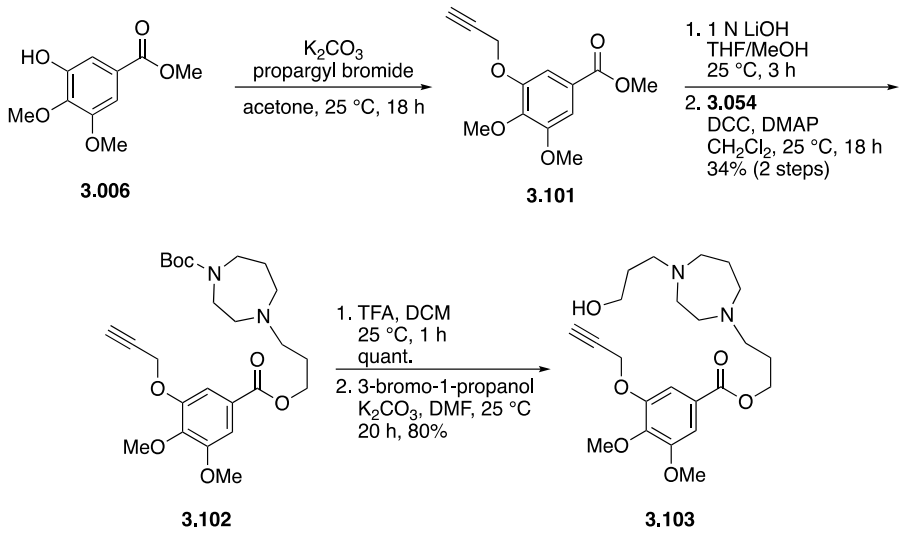

Scheme 54. Synthesis of 3.103

With the primary alcohol in hand, oxidation was first attempted with PCC. (Table 14). Regrettably, these conditions were too harsh and the material decomposed. Next, we tried oxidation with Dess–Martin periodinane (DMP) but unfortunately, this also resulted in decomposition. Finally, Swern oxidation was attempted but starting material was recovered. While additional efforts can be made for the oxidation of **3.103**, we envision the use of a Weinreb amide will provide a more stable intermediate and allow us to attempt the macrocyclization under basic conditions (Scheme 55).

Table 14. Attempts for oxidation of 3.103

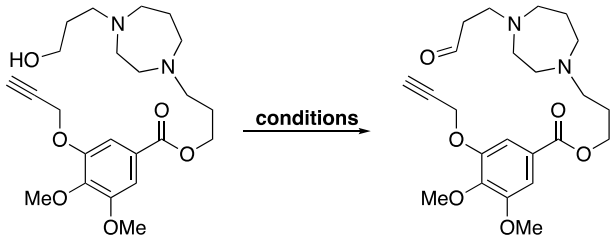

3.103 **3.051**

Entry	Conditions	result
1	PCC, CH_2Cl_2, 25 °C, 1 h	decomposed
2	DMP, CH_2Cl_2, 25 °C, 1 h	decomposed
3	oxalyl chloride, DMSO, Et_3N, CH_2Cl_2, −78 °C, 2 h	**3.103**

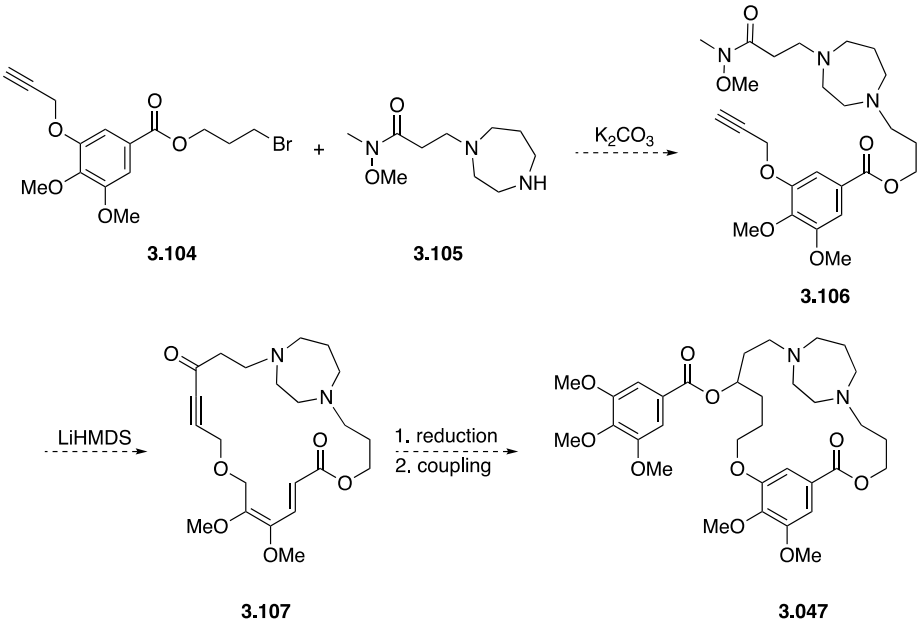

3.104 **3.105** **3.106**

3.107 **3.047**

Scheme 55. Future plan for the macrocycle

3.2.3 Design and Synthesis of ENT3 Selective Inhibitors

3.2.3.1 Design of ENT3 Selective Inhibitors

While hENT1 and hENT2 are primarily found in the plasma membrane, hENT3 is unique in that it is located in the intracellular membranes of lysosomes and mitochondria. Expressed highly in peripheral T cells, hENT3 plays a key role in immunity by maintaining the availability of nucleosides necessary for proliferation and survival of T cells.[73] Dysregulation of hENT3 is linked to multiple diseases, including H syndrome, pigmented hypertrichosis with insulin-dependent diabetes (PHID) syndrome, Faisalabad histiocytosis and sinus histiocytosis with massive lymphadenopathy.[57] To better understand the role hENT3 plays within these disease states, we aim to develop an hENT3 selective inhibitor.

To develop an hENT3 selective inhibitor, we first needed to determined key differences between amino acid composition within the binding pocket of ENT1 compared to ENT3. As there are no experimentally determined crystal structures of hENT3, Dr. Pyeonghwa Jeong built a homology model of hENT3 using the biologics homology modeling protocol accessible through Maestro 13.0 (Schrödinger, Inc). Dr. Jeong used the crystal structure of ENT1 in complex with JH-ENT-01 as the structural template. The protein sequence of hENT3 was obtained from the Uniprot database (Entry Q9BZD2). The target and template sequence alignment exhibited conserved secondary structural elements but showed several differences in amino acid composition within the tri-methoxy phenyl binding site (Figure 39).

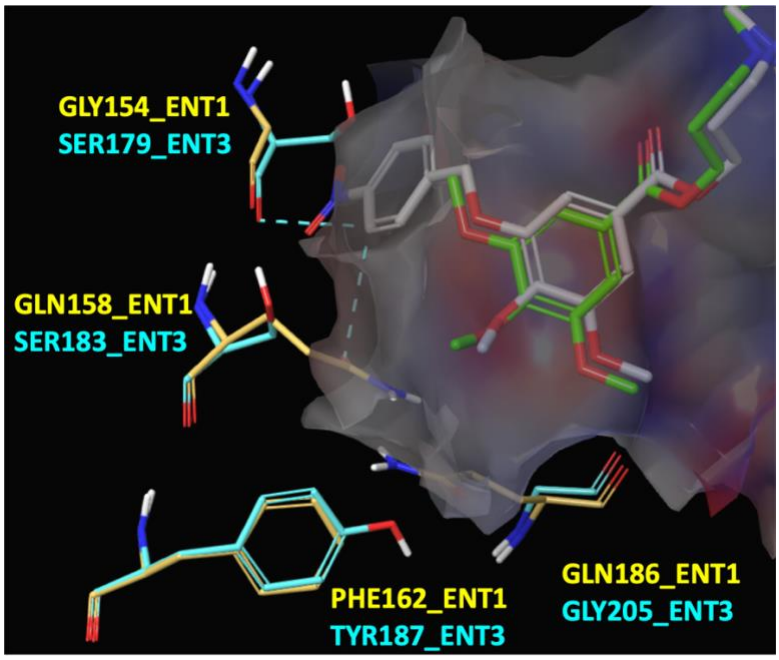

Figure 39. Overlay of ENT1 and ENT3 binding pockets

Also shown in Figure 39, when we docked JH-ENT-01 in the binding pocket of ENT3, there was steric hindrance of the *p*-nitrobenzyl moiety with SER179. Therefore, the first design rationale for novel ENT3 inhibitors was to apply a smaller functional group at the R^1 position (Figure 40). Secondly, the larger cavity of ENT3 as a result of GLN158$_{ENT1}$/SER183$_{ENT3}$ and potential hydrogen bonding with TYR187 was taken into consideration and various heterocycles placed at the R^2 position were docked. Lastly, only methoxy or hydrogen was docked at the R^3 position. Of 5,460 compounds docked, two top candidates that exhibited promising docking scores compared to ENT1 binding, candidate 1 and candidate 2 were chosen for further investigation. Shown in Figure 40, candidate 1 takes advantage of aromatic hydrogen bonding with SER176 and hydrogen

bonding with TYR187. Candidate 2, with a slightly different binding pose, exhibits hydrogen bonding with Ser183.

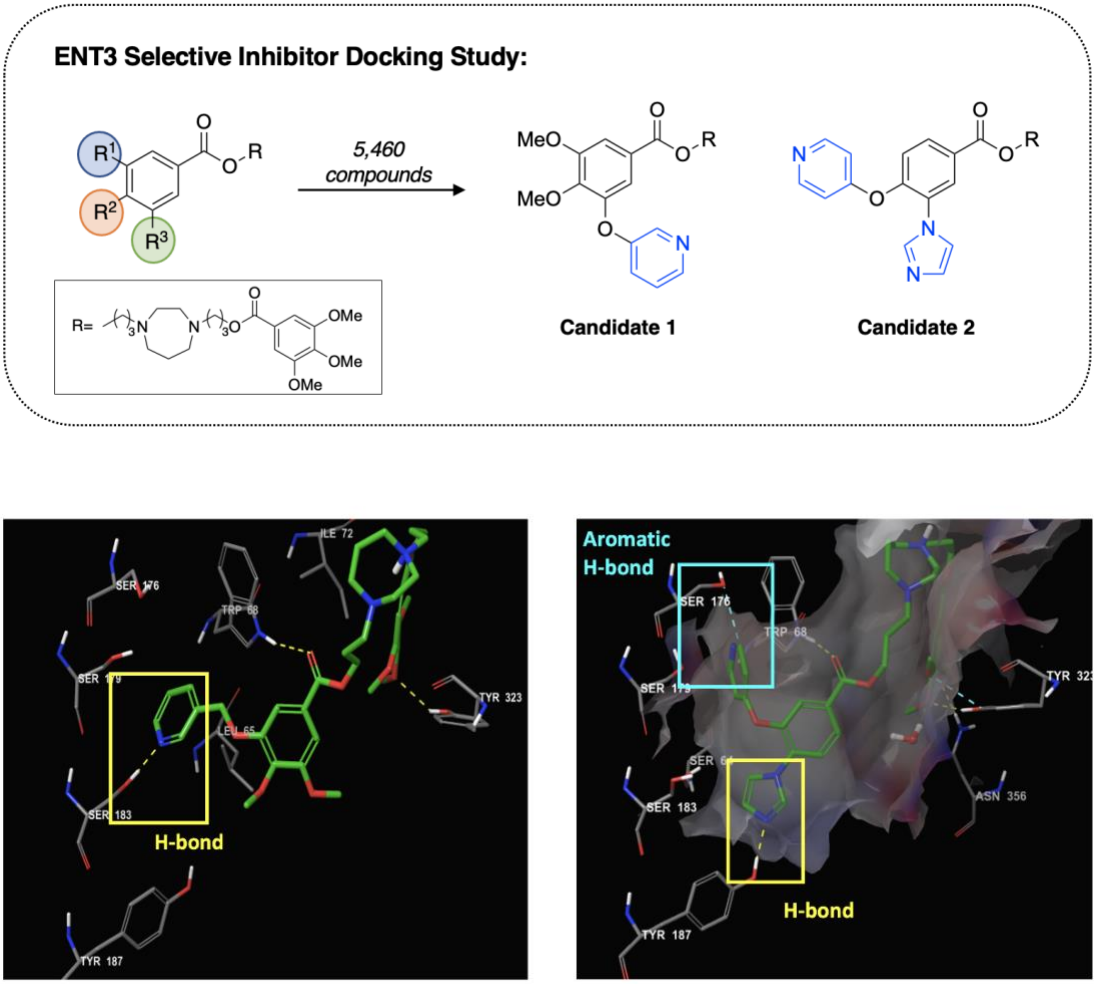

Figure 40. Key binding interactions of candidate 1 and 2

3.2.3.2 Synthesis of ENT3 Selective Inhibitors

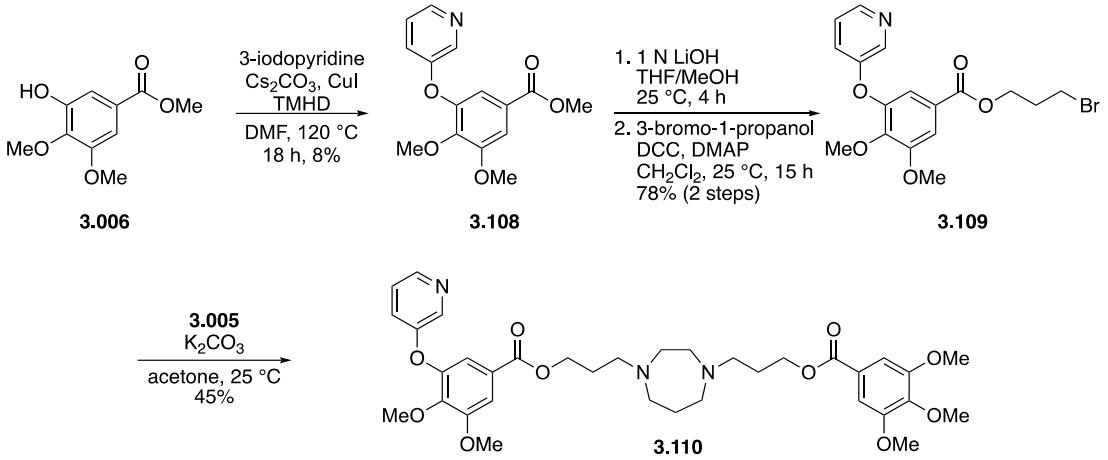

Scheme 56. Synthesis of candidate 1 (3.120)

Excited by the docking results, the synthesis of candidate 1 commenced with the coupling of phenol **3.006** with 3-iodopyridine with Cs_2CO_3, CuI and TMHD in DMF at 120 °C. From intermediate **3.108**, **3.110** was synthesized analogously to the other ENT inhibitors. Methyl ester **3.108** was hydrolyzed with 1 N LiOH, the resulting carboxylic acid was coupled to 3-bromo-1-propanol with DCC and finally, homopiperazine **3.005** was coupled under basic conditions to complete the synthesis of **3.110**.

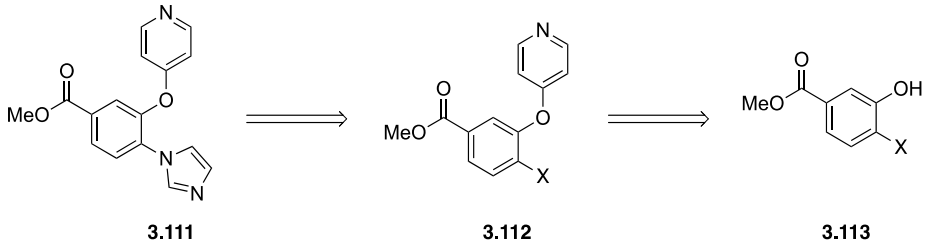

Scheme 57. Retrosynthetic analysis of 3.111

As candidate 2 deviates more significantly than candidate 1 to our typical ENT inhibitor, a novel route was devised. We envisioned intermediate methyl ester **3.111**

could be obtained via iodopyridine coupling to phenol **3.113** followed by imidazole coupling to the halide of **3.112** (Scheme 57). Consequently, we treated **3.114** with 4-iodopyridine, CS_2CO_3, CuI and THMD in DMF at 60 °C (Table 15) but unfortunately did not obtain any coupled product. Instead, several new spots were observed on TLC that were more polar than the starting material, but none contained peaks coming from the pyridine moiety in ^{1}H NMR. Additionally, we tried coupling in the presence of K_2CO_3 under reflux in DMAc. Under these conditions, we simply lost a methyl peak in ^{1}H NMR, which we presume corresponds to undesired product **3.117**.

Table 15. Iodopyridine coupling conditions

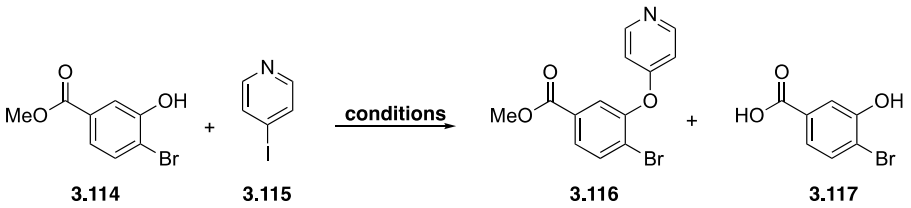

entry	conditions	result
1	Cs_2CO_3, CuI, TMHD, DMF, 60 °C	undesired
2	K_2CO_3, DMAc, reflux	**3.117**

As our original route towards candidate 2 did not provide coupled product **3.116,** we decided to invert the order of our coupling reactions. The imidazole coupling would be carried out first, followed by iodopyridine coupling. As shown in Table 16, the first set of conditions we tried were with Cs_2CO_3 and CuI in DMF at 120 °C. The major product obtained under this set of conditions was the hydrolyzed product **3.121**. As we

thought the conditions may have been too harsh, we reduced the temperature to 60 °C but after 48 h only hydrolyzed product was obtained.

Table 16. Imidazole coupling conditions

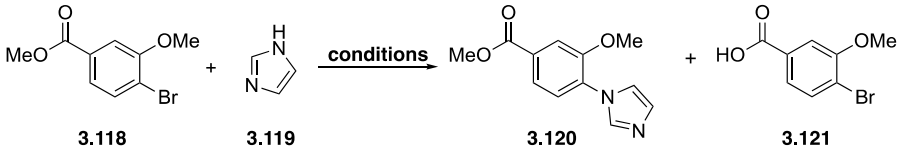

Entry	Conditions	result
1	Cs_2CO_3 (4.0 equiv), CuI (20 mol%), DMF, 120 °C, 24 h	**3.121**
2	Cs_2CO_3 (4.0 equiv), CuI (20 mol%), DMF, 60 °C, 48 h	**3.121**
3	CuI (10 mol%), proline (20 mol%), K_3PO_4 (2.0 equiv), DMF, 110 °C, 18 h	13% (**3.120**)
4	CuI (20 mol%), proline (25 mol%), K_3PO_4 (2.0 equiv), DMF, 110 °C, 18 h	7% (**3.120**)
5	CuI (20 mol%), proline (25 mol%), K_3PO_4 (2.0 equiv), DMF, 110 °C, 6 h	18% (**3.120**)
6	CuI (20 mol%), proline (25 mol%), K_3PO_4 (2.0 equiv), toluene, 110 °C, 48 h	**3.118**
7	CuI (20 mol%), **3.122** (25 mol%), K_3PO_4 (2.0 equiv), DMF, 110 °C, 18 h	unidentified
8	CuI (20 mol%), **3.122** (25 mol%), K_3PO_4 (2.0 equiv), toluene, 110 °C, 18 h	**3.118**

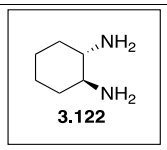

Therefore, as shown in entry 3 (Table 16) we attempted the coupling reaction with the addition of a chiral ligand (proline). Initially, 10 mol% CuI, 20 mol% proline, 2.0 equiv. K_3PO_4 in DMF at 110 °C for 18 h was used and pleasingly, we obtained the desired coupled product **3.120** in 13% yield. In an attempt to increase the yield, CuI was increased to 20 mol% and proline to 25 mol% but the yield decreased to 7%. As we were seeing the formation of many by-products after 18 h, we shortened the reaction time to 6

h. This improved the yield slightly to 18%. Additionally, the reaction was run in toluene but after 48 h mostly starting material remained.

In addition to proline, other chiral diamino compounds such as (1S,2S)-(+)-1,2-diaminocyclohexane (**3.122**) are commonly utilized for the Ullman-type reaction.[74 75] Therefore, we attempted our coupling reaction with **3.122** in DMF (entry 7) but only an unidentifiable product was obtained. Finally, we tried the same conditions in toluene, but no reaction was observed.

Although the yield of our imidazole coupling reaction could be further improved, we moved on to the methoxy deprotection (Table 17). Initial attempts with BBr_3 were too harsh and we observed decomposition of our starting material. Next, reflux in 48% HBr provided hydrolyzed product **3.124**. Future attempts for the methoxy deprotection will include trimethylsilyl iodide or EtSNa. If the methoxy group proves to be too difficult to remove, we will replace it with another protecting group, such as MOM, that can be removed under milder conditions.

Table 17. Methoxy deprotection attempts

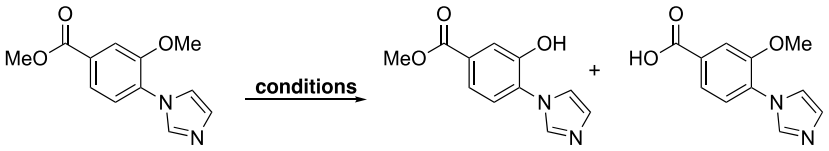

3.120 **3.123** **3.124**

Entry	Conditions	result
1	BBr_3 (6.0 equiv), DCM 0 to 50 °C, 18 h	decomposed
2	48% HBr, reflux 18 h	**3.124**

3.3 Conclusion

Equilibrative nucleoside transporters (ENT) play a critical role in human physiology by maintaining nucleoside homeostasis and delivering nucleoside analog therapeutics to their intracellular targets. Inhibition of ENTs by AdoRIs produces an analgesic effect by increasing extracellular adenosine that in turn activates the AR and holds promise as a non-opioid therapeutic modality for pain relief. As current AdoRIs lack selectivity, isoform specificity, toxicity, and poor bioavailability, the development of novel ENT inhibitors is imperative. By utilizing the co-crystal structure of ENT1 in complex with dilazep and NBMPR novel inhibitors have been rationally designed to overcome these limitations.

Firstly, the co-crystal structure of ENT1 in complex with dilazep and NBMPR identified shared and distinct binding sites that guided the design of a hybrid analog (JH-ENT-01) that had a two-fold increase in binding affinity compared to dilazep. Expanding the hybrid design, 6 additional ENT1 inhibitors were synthesized and evaluated for their analgesic properties in a streptozotocin (STZ) induced diabetic neuropathic pain model. Excitingly, two compounds (JH-ENT-01, and JH-ENT-07) significantly reduced mechanical pain with accumulating effects that are enhanced after multiple treatments and lasted for 24-48 h. Importantly, treatment with JH-ENT-01 and JH-ENT-07 did not appear to affect the motor function of the mice. As JH-ENT-07 provided a novel scaffold for further elaboration, additional inhibitors were designed, synthesized and are currently being evaluated for the bioactivity.

Next, a macrocyclic version of dilazep was designed to decrease conformational flexibility, which will reduce entropy on binding, and increase selectivity and permeability of the inhibitor. When planning the synthesis of the macrocycle, we envisioned several different approaches for macrocyclization that included RCM with Grubb's catalyst, an S_N2-type reaction with the homopiperazine ring or an alkyne/aldehyde coupling reaction. Efforts towards each of these approaches has laid the groundwork for completing the macrocyclic inhibitor.

Finally, by examining the differences of amino acid composition within the binding pocket of ENT1 compared to ENT3, two ENT3 selective inhibitors were designed. The first ENT3 selective inhibitor has been synthesized and awaits evaluation. Headway has been made towards the second inhibitor but requires additional work to complete the synthesis. Taken together, the rational design and synthesis of novel ENT inhibitors has made progress towards inhibitors with improved potency, selectivity, and pharmacological properties for the development of non-opioid analgesics.

3.4 Experimental

General Methods

All reactions were conducted in oven-dried glassware under nitrogen or argon. Unless otherwise stated all reagents were purchased from commercial suppliers and used without further purification. All solvents were American Chemical Society (ACS) grade or better and used without further purification except tetrahydrofuran (THF), which was freshly distilled from sodium/benzophenone each time before use. Analytical

thin layer chromatography (TLC) was performed with glass backed silica gel (60 Å) plates with fluorescent indication (Whatman). Visualization was accomplished by UV irradiation at 254 nm, or by staining with *p*-anisaldehyde solution or potassium permanganate solution followed by heating. Flash column chromatography was performed by using silica gel (particle size 230–400 mesh, 60 Å). All ^{1}H NMR and ^{13}C NMR spectra were recorded with a Varian 400 (400 MHz) and a Bruker 500 (500 MHz) spectrometer. All NMR δ values are given in parts per million (ppm) and are referenced to the residual isotopomer solvent signals ($CDCl_3$: δ = 7.26 ppm, CD_3OD: δ = 3.31 ppm) for ^{1}H NMR spectra, or the solvent signals for ^{13}C spectra. Coupling constants (*J*) are given in Hertz (Hz) and multiplicities are indicated using the conventional abbreviation (s = singlet, d = doublet, t = triplet, q = quartet, m = multiplet or overlap of non-equivalent resonances, br = broad). Electrospray ionization (ESI) mass spectrometry (MS) was recorded with an Agilent 6224 LC/MS-TOF (high resolution) spectrometer and performed to obtain the molecular masses of the compounds.

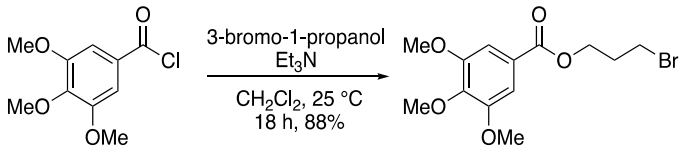

3.001 **3.002**

To a solution of 3,4,5-trimethoxybenzoyl chloride (350 mg, 1.52 mmol) in CH_2Cl_2 (2.5 mL) was added 3-bromo-1-propanol (0.15 mL, 1.67 mmol) and Et_3N (0.5 mL) at 25 °C. After stirring for 18 h, the reaction was quenched with H_2O and the resulting mixture was diluted with CH_2Cl_2. The layers were separated, and the aqueous layer was

extracted with CH_2Cl_2. The combined organic layers were dried over anhydrous Na_2SO_4, filtered and concentrated *in vacuo*. The residue was purified by column chromatography (silica gel, hexanes/EtOAc, 4/1) to afford **3.002** (432 mg, 88%). ^{1}H NMR (500 MHz, $CDCl_3$) δ 7.29 (s, 2H), 4.47 (t, *J* = 6.1 Hz, 2H), 3.91 (s, 9H), 3.54 (t, *J* = 6.5 Hz, 2H), 2.34 (dt, *J* = 6.3, 6.3 Hz, 2H).

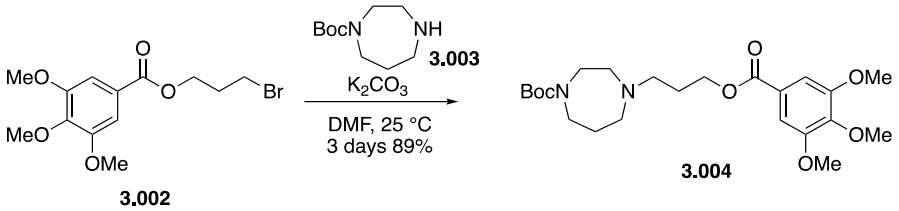

To a solution of **3.002** (136 mg, 0.42 mmol) in DMF (1.5 mL) was added 1-Boc-homopiperazine (0.11 mL, 0.84 mmol) and K_2CO_3 (582 mg, 4.21 mmol) at 0 °C. After stirring for 3 days at 25 °C, the reaction was quenched with the addition of H_2O and the resulting mixture was diluted with EtOAc. The layers were separated, and the aqueous layer was extracted with EtOAc. The combined organic layers dried over anhydrous Na_2SO_4, filtered and concentrated *in vacuo*. The residue was purified by column chromatography (silica gel, CH_2Cl_2/MeOH, 50/1) to afford **3.004** (169 mg, 89%). ^{1}H NMR (500 MHz, $CDCl_3$) δ 7.28 (s, 2H), 4.40 (t, *J* = 6.4 Hz, 2H), 4.27–4.23 (m, 2H), 3.90 (s, 6H), 3.90 (s, 3H), 3.52–3.32 (m, 8H), 2.13 (dt, *J* = 6.3, 6.2 Hz, 2H), 1.86–1.82 (m, 2H), 1.44 (s, 9H).

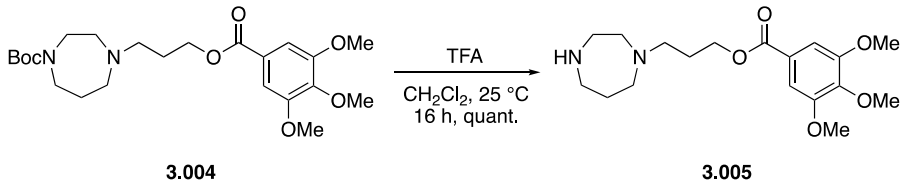

To a solution of **3.004** (72 mg, 0.16 mmol) in CH_2Cl_2 (1 mL) was added TFA (1 mL) at 25 °C. After stirring for 16 h, the reaction was concentrated *in vacuo* and the crude material was used without further purification.

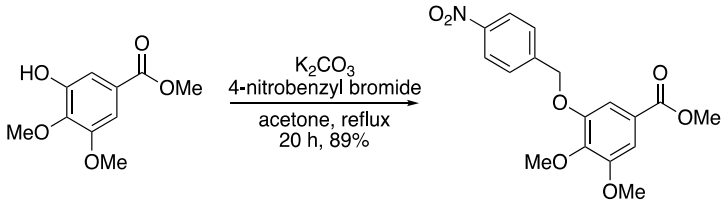

3.006 **3.007**

To a solution of 3,4-dimethoxy-5-hydroxybenzoic acid methyl ester (50 mg, 0.24 mmol) in acetone (1 mL) was added 4-nitrobenzylbromide (76 mg, 0.35 mmol) and K_2CO_3 (52 mg, 0.38 mmol) at 25 °C. The reaction mixture was then heated to reflux for 20 h. Upon cooling to 0 °C, the reaction was quenched with an addition of saturated aqueous NH_4Cl and the resulting mixture was diluted with EtOAc. The layers were separated, and the aqueous layer was extracted with EtOAc. The combined organic layers were dried over anhydrous Na_2SO_4, filtered, and concentrated *in vacuo*. The residue was purified by column chromatography (silica gel, hexanes/CH_2Cl_2/EtOAc, 5/1/1) to afford **3.007** (73 mg, 89%). ^{1}H NMR (400 MHz, $CDCl_3$) δ 8.24 (d, *J* = 8.6 Hz, 2H), 7.63 (d, *J* = 8.5 Hz, 2H), 7.33 (d, *J* = 1.5 Hz, 1H), 7.30 (d, *J* = 1.7 Hz, 1H), 3.93 (s, 3H), 3.91 (s, 3H), 3.89 (s, 3H).

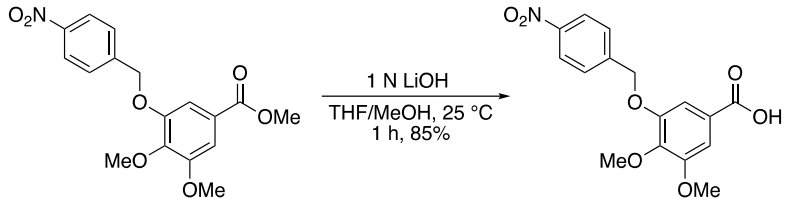

3.007 **3.008**

To a solution of **3.007** (42 mg, 0.12 mmol), in THF/MeOH (3/1) (4 mL) was added 1 N LiOH (1 mL) at 25 °C. After stirring for 1 h, 1 M HCl was added until the solution became acidic and the resulting mixture was diluted with EtOAc. The layers were separated, and the aqueous layer was extracted with EtOAc. The combined organic layers were dried over anhydrous Na_2SO_4, filtered, and concentrated *in vacuo*. The residue was purified by column chromatography (silica gel, CH_2Cl_2/MeOH, 10/1) to afford **3.008** (34 mg, 85%). ^{1}H NMR (400 MHz, $CDCl_3$) δ 8.26 (d, *J* = 7.3 Hz, 2H), 7.64 (d, *J* = 7.7 Hz, 2H), 7.40 (s, 1H), 7.36 (s, 1H), 3.96 (s, 3H), 3.94 (s, 3H).

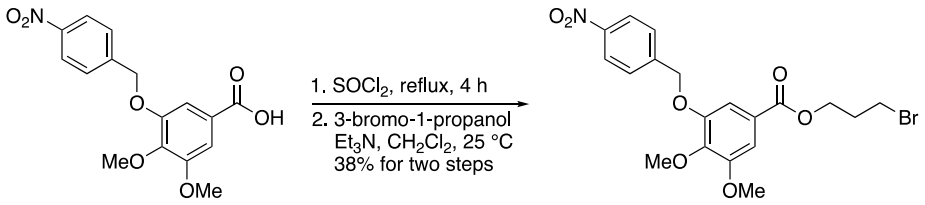

3.008 **3.009**

To a solution of **3.008** (34 mg, 0.10 mmol) was added $SOCl_2$ (0.5 mL) at 25 °C. The reaction mixture was then heated to reflux for 4 h. Upon cooling to 25 °C, the reaction mixture was concentrated *in vacuo.* To the crude mixture in CH_2Cl_2 (0.25 mL) was added 3-bromo-1-propanol (0.01 mL, 0.11 mmol) and Et_3N (0.05 mL) at 25 °C. After stirring 18 h, the reaction was quenched with the addition of H_2O and the resulting mixture was diluted with CH_2Cl_2. The layers were separated, and the aqueous layer was extracted

with CH_2Cl_2. The combined organic layers were dried over anhydrous Na_2SO_4, filtered and concentrated *in vacuo*. The residue was purified by column chromatography (silica gel, hexanes/EtOAc, 3/1) to afford **3.009** (17 mg, 38% for 2 steps). ^{1}H NMR (500 MHz, $CDCl_3$) δ 8.26 (d, *J* = 8.8 Hz, 2H), 7.64 (d, *J* = 8.8 Hz, 2H), 7.32 (d, *J* = 1.8 Hz, 1H), 7.29 (d, *J* = 1.8 Hz, 1H), 5.26 (s, 2H), 4.44 (t, *J* = 6.1 Hz, 2H), 3.94 (s, 3H), 3.92 (s, 3H), 3.50 (t, *J* = 6.5 Hz, 2H), 2.31 (dt, *J* = 6.3, 6.3 Hz, 2H).

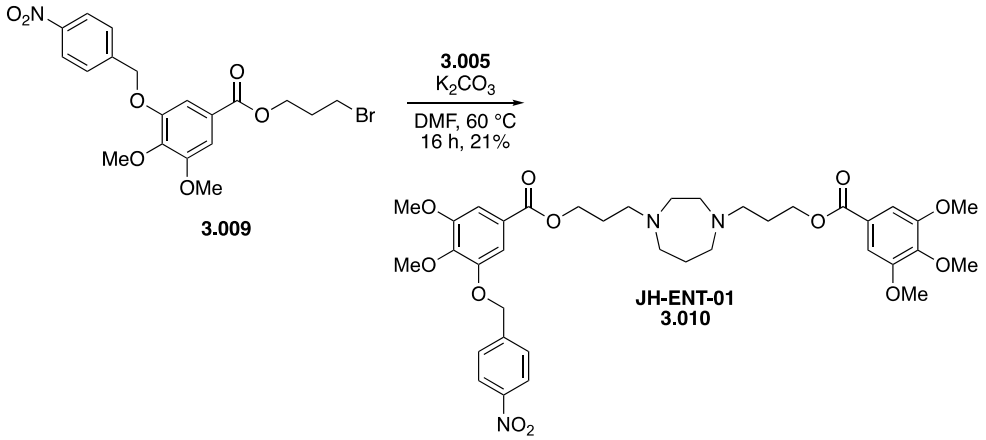

To a solution of **3.009** (17 mg, 0.04 mmol) and **3.005** (30 mg, 0.07 mmol) in DMF (0.14 mL) was added K_2CO_3 at 25 °C. The reaction mixture was then heated to 60 °C for 16 h. Upon cooling to 25 °C, the reaction was quenched with the addition of H_2O and the resulting mixture was diluted with EtOAc. The layers were separated, and the aqueous layer was extracted with EtOAc. The combined organic layers dried over anhydrous Na_2SO_4, filtered and concentrated *in vacuo*. The residue was purified by column chromatography (silica gel, CH_2Cl_2/MeOH, 10/1) to afford **3.010** (6 mg, 21%). ^{1}H NMR (500 MHz, CD_3OD) δ 8.27–8.25 (m, 2H), 7.72 (s, 1H), 7.71 (s, 1H), 7.34 (s, 2H), 7.31 (s, 1H),

7.30 (s, 1H), 5.31 (s, 2H), 4.39–4.35 (m, 4H), 3.89 (s, 6H), 3.86 (s, 6H), 3.82 (s, 3H), 2.96–2.91 (m, 8H), 2.87–2.79 (m, 4H), 2.06–1.92 (m, 6H).

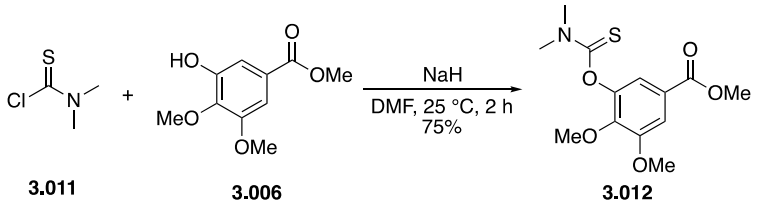

To a solution of NaH (60% in mineral oil) (112 mg, 2.84 mmol) in DMF (6 mL) was added 3,4-dimethoxy-5-hydroxybenzoic acid methyl ester (136 mg, 0.64 mmol) and dimethylthiocarbamoyl chloride (439 mg, 3.55 mmol) at 25 °C. After stirring for 2 h, the reaction was diluted with EtOAc and filtered through celite. The filtrate was then washed with H_2O and the organic layer dried over anhydrous Na_2SO_4, filtered and concentrated *in vacuo*. The residue was purified by column chromatography (silica gel, hexanes/EtOAc, 20/1 to 5/1) to afford **3.012** as a white solid (144 mg, 75%). ^{1}H NMR (500 MHz, $CDCl_3$) δ 7.52 (d, *J* = 1.8 Hz, 1H), 7.40 (d, *J* = 1.9 Hz, 1H), 3.94 (s, 3H), 3.93 (s, 3H), 3.88 (s, 3H), 3.46 (s, 3H), 3.37 (s, 3H).

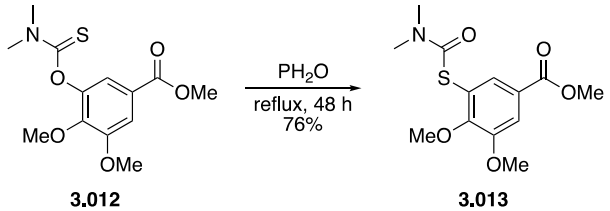

A solution of **3.012** (144 mg, 0.48 mmol) in Ph_2O (0.72 mL) was warmed to reflux for 48 h. After cooling to 25 °C, the crude material was purified by column chromatography (silica gel, hexanes/EtOAc, 20/1 to 5/1) to afford **3.013** (110 mg, 76%). ^{1}H

NMR (500 MHz, $CDCl_3$) δ 7.83 (br s, 1H), 7.66 (br s, 1H), 3.93 (s, 6H), 3.90 (s, 3H), 3.15 (br s, 3H), 3.04 (br s, 3H).

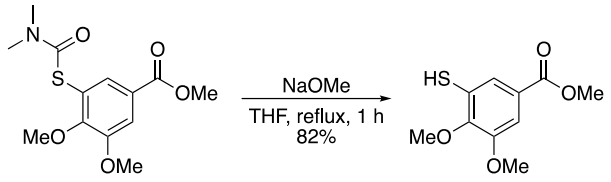

3.013 **3.014**

To a solution of **3.013** (203 mg, 0.68 mmol) in THF (6.0 mL) was added MeONa (0.5 M in methanol, 0.68 mmol) at 25 °C. The reaction mixture was then heated to reflux for 1 h. Upon cooling to 25 °C, the reaction mixture was quenched with 1 M HCl and diluted with EtOAc. The layers were separated, and the aqueous layer was extracted with EtOAc. The combined organic layers were washed with brine and dried over anhydrous Na_2SO_4, filtered and concentrated *in vacuo*. The residue was purified by column chromatography (silica gel, hexanes/EtOAc, 5/1) to afford **3.014** (127 mg, 82%). ^{1}H NMR (400 MHz, $CDCl_3$) δ 7.57 (d, *J* = 1.7 Hz, 1H), 7.35 (d, *J* = 1.7 Hz, 1H), 3.90 (s, 3H), 3.89 (s, 3H), 3.88 (s, 3H).

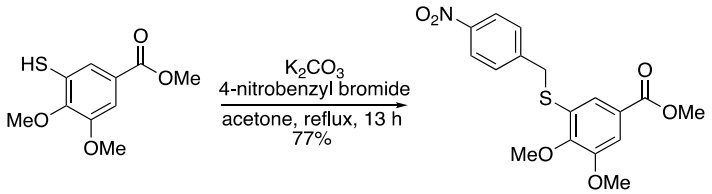

3.014 **3.015**

To a solution of **3.014** (127 mg, 0.56 mmol) in acetone (2.2 mL) was added 4-nitrobenzyl bromide (179 mg, 0.83 mmol) and K_2CO_3 (123 mg, 0.89 mmol) at 25 °C. The reaction mixture was then heated to reflux for 20 h. Upon cooling to 0 °C, the reaction

was quenched with an addition of saturated aqueous NH_4Cl and the resulting mixture was diluted with EtOAc. The layers were separated, and the aqueous layer was extracted with EtOAc. The combined organic layers were dried over anhydrous Na_2SO_4, filtered, and concentrated *in vacuo*. The residue was purified by column chromatography (silica gel, hexanes/EtOAc, 5/1) to afford **3.015** (157 mg, 77%). ^{1}H NMR (400 MHz, $CDCl_3$) δ 8.12 (d, *J* = 8.3 Hz, 2H), 7.50 (br s, 1H), 7.47 (d, *J* = 8.4 Hz, 2H), 7.45 (br s, 1H), 4.20 (s, 2H), 3.90 (s, 6H), 3.87 (s, 3H).

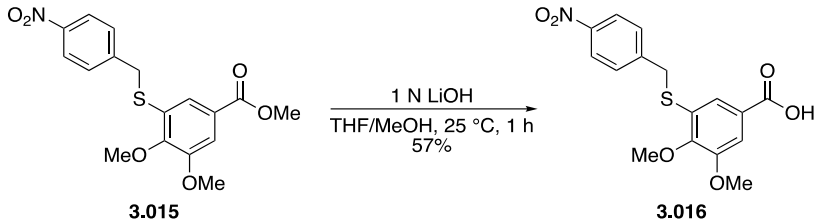

To a solution of **3.015** (157 mg, 0.43 mmol), in THF/MeOH (3/1) (14 mL) was added 1 N LiOH (2.6 mL) at 25 °C. After stirring for 1 h, 1 M HCl was added until the solution became acidic and the resulting mixture was diluted with CH_2Cl_2. The layers were separated, and the aqueous layer was extracted with CH_2Cl_2. The combined organic layers were dried over anhydrous Na_2SO_4, filtered, and concentrated *in vacuo*. The residue was purified by column chromatography (silica gel, CH_2Cl_2/MeOH, 10/1) to afford **3.016** (80 mg, 53%). ^{1}H NMR (400 MHz, $CDCl_3$) δ 8.11 (d, *J* = 8.4 Hz, 2H), 7.57 (s, 1H), 7.50 (s, 1H), 7.47 (d, *J* = 8.2 Hz, 2H), 4.19 (s, 2H), 3.90 (s, 3H), 3.89 (s, 3H).

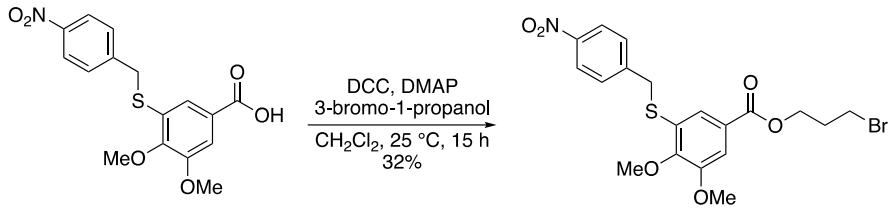

3.016 **3.017**

To a solution of **3.016** (7 mg, 0.02 mmol) in CH_2Cl_2 (0.4 mL) was added 3-bromo-1-propanol (3 mg, 0.022 mmol), DCC (5 mg, 0.024 mmol), and DMAP (0.002 mmol) at 25 °C. After stirring for 15 h, the reaction was concentrated *in vacuo*. The residue was purified by column chromatography (silica gel, hexanes/EtOAc, 5/1) to afford **3.017** (3 mg, 32%). ^{1}H NMR (500 MHz, $CDCl_3$) δ 8.13 (d, *J* = 8.7 Hz, 2H), 7.49 (d, *J* = 8.7 Hz, 2H), 7.47 (d, *J* = 1.9 Hz, 1H), 7.45 (d, *J* = 1.8 Hz, 1H), 4.43 (t, *J* = 6.1 Hz, 2H), 4.21 (s, 2H), 3.91 (s, 3H), 3.90 (s, 3H), 3.49 (t, *J* = 6.5 Hz, 2H), 2.29 (dt, *J* = 6.3, 6.3 Hz, 2H).

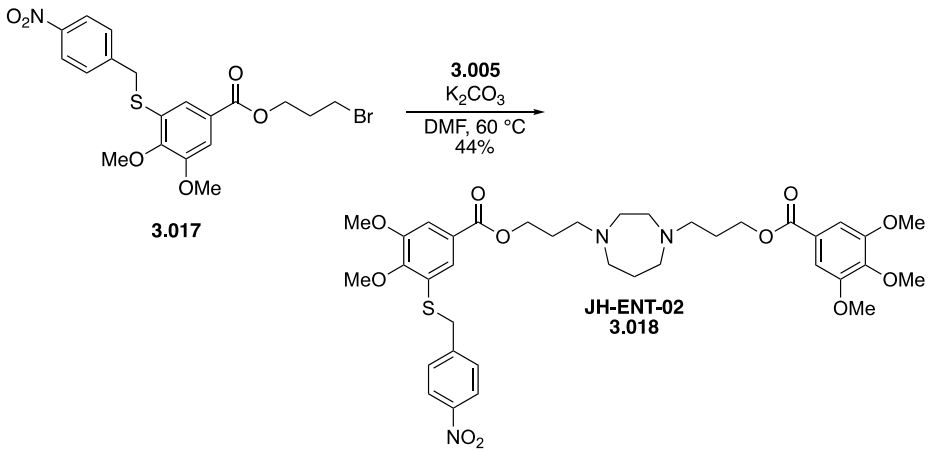

3.017

To a solution of **3.017** (3 mg, 0.006 mmol) and **3.005** (4 mg, 0.012 mmol) in DMF (0.05 mL) was added K_2CO_3 (8 mg, 0.06 mmol) at 25 °C. The reaction was then heated to 60 °C for 3 days. Upon cooling to 25 °C, the reaction was quenched with the addition of

H_2O and the resulting mixture was diluted with EtOAc. The layers were separated, and the aqueous layer was extracted with EtOAc. The combined organic layers dried over anhydrous Na_2SO_4, filtered and concentrated *in vacuo*. The residue was purified by column chromatography (silica gel, CH_2Cl_2/MeOH, 10/1) to afford **3.018** (2 mg, 44%). ^{1}H NMR (500 MHz, CD_3OD) δ 8.13 (d, *J* = 8.3 Hz, 2H), 7.56 (d, *J* = 8.2 Hz, 2H), 7.47 (s, 1H), 7.44 (s, 1H), 7.31 (s, 2H), 4.36 (t, *J* = 6.3 Hz, 2H), 4.31 (t, *J* = 6.3 Hz, 2H), 3.88 (s, 3H), 3.87 (s, 9H), 3.82 (s, 3H), 2.80–2.75 (m, 8H), 2.69 (dd, *J* = 7.3, 7.4 Hz, 2H), 2.63 (dd, *J* = 7.3, 7.2 Hz, 2H), 2.00–1.90 (m, 4H), 1.84 (dt, *J* = 10.1, 5.3 Hz, 2H); HRMS (ESI) *m/z* 742.3012 [$(M+H)^+$ calcd for $C_{37}H_{47}N_3O_{11}S$ 742.3004].

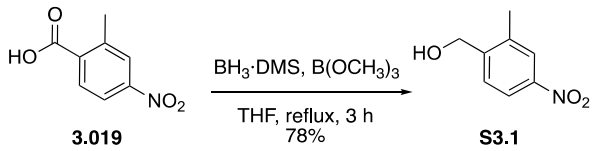

To a solution of 2-methyl-4-nitrobenzoic acid (200 mg, 1.1 mmol) in THF (11 mL) was added BH_3·DMS (0.2 mL, 3.3 mmol) and $B(OCH_3)_3$ (0.48 mL, 5.0 mmol) at 25 °C. The reaction was then warmed to reflux for 3 h. Upon cooling to 25 °C, the reaction was quenched with an addition of methanol and 1 M HCl the resulting mixture was diluted with EtOAc and H_2O. The layers were separated, and the aqueous layer was extracted with EtOAc. The combined organic layers were washed with brine and dried over anhydrous Na_2SO_4, filtered and concentrated *in vacuo*. The residue was purified by column chromatography (silica gel, hexanes/EtOAc, 2/1) to afford **S3.1** (143 mg, 78%). ^{1}H

NMR (500 MHz, $CDCl_3$) δ 8.08 (dd, *J* = 8.4, 2.2 Hz, 1H), 8.03 (d, *J* = 2.0 Hz, 1H), 7.62 (d, *J* = 8.4 Hz, 1H), 4.80 (s, 2H), 2.40 (s, 3H).

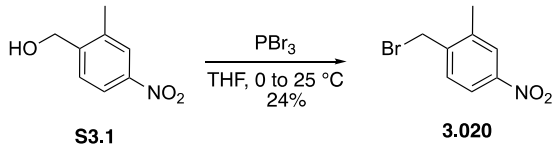

To a cooled (0 °C) solution of **S3.1** (70 mg, 0.42 mmol) in CH_2Cl_2 (8.4 mL) was added PBr_3 (0.04 mL, 0.84 mmol). The reaction was then allowed to slowly warm to 25 °C. After stirring for 4 h, the reaction was quenched with an addition of H_2O. The layers were separated, and the aqueous layer was extracted with CH_2Cl_2. The combined organic layers were dried over anhydrous Na_2SO_4, filtered, and concentrated *in vacuo*. The residue was purified by column chromatography (silica gel, hexanes/EtOAc, 10/1) to afford **3.020** (23 mg, 24%). ^{1}H NMR (500 MHz, $CDCl_3$) δ 8.06 (d, *J* = 2.0 Hz, 1H), 8.02 (dd, *J* = 8.4, 2.3 Hz, 1H), 7.47 (d, *J* = 8.4 Hz, 1H), 4.51 (s, 2H), 2.51 (s, 3H).

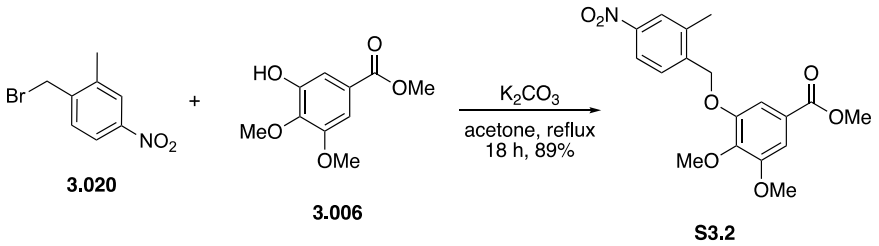

To a solution of **3.020** (94 mg, 0.41 mmol) in acetone (1 mL) was added 3,4-dimethoxy-5-hydroxybenzoic acid methyl ester (58 mg, 0.27 mmol) and K_2CO_3 (59 mg, 0.43 mmol) at 25 °C. The reaction mixture was then heated to reflux for 18 h. Upon cooling to 0 °C, the reaction was quenched with an addition of saturated aqueous NH_4Cl and the resulting mixture was diluted with EtOAc. The layers were separated, and the

aqueous layer was extracted with EtOAc. The combined organic layers were dried over anhydrous Na_2SO_4, filtered, and concentrated *in vacuo*. The residue was purified by column chromatography (silica gel, hexanes/EtOAc, 5/1) to afford **S3.2** (88 mg, 89%). ^{1}H NMR (400 MHz, $CDCl_3$) δ 8.10–8.06 (m, 2H), 7.68 (d, *J* = 9.0 Hz, 1H), 7.34 (s, 2H), 5.18 (s, 2H), 3.92 (s, 3H), 3.91 (s, 3H), 3.90 (s, 3H), 2.48 (s, 3H).

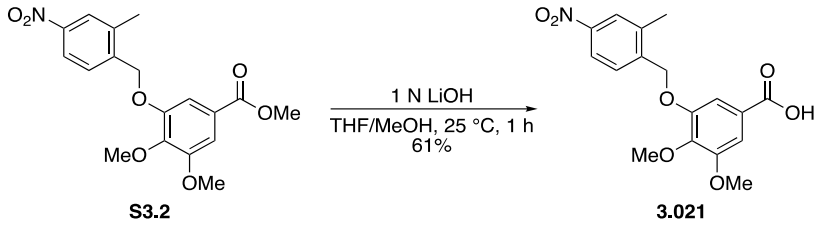

To a solution of **S3.2** (53 mg, 0.15 mmol), in THF/MeOH (3/1) (5 mL) was added 1 N LiOH (0.88 mL) at 25 °C. After stirring for 1 h, 1 M HCl was added until the solution became acidic and the resulting mixture was diluted with CH_2Cl_2. The layers were separated, and the aqueous layer was extracted with CH_2Cl_2. The combined organic layers were dried over anhydrous Na_2SO_4, filtered, and concentrated *in vacuo*. The residue was purified by column chromatography (silica gel, CH_2Cl_2/MeOH, 10/1) to afford **3.021** (31 mg, 61%). ^{1}H NMR (500 MHz, $CDCl_3$) δ 8.11–8.06 (m, 2H), 7.68 (d, *J* = 9.0 Hz, 1H), 7.41 (s, 1H), 7.40 (s, 1H), 5.20 (s, 2H), 3.94 (s, 6H), 2.49 (s, 3H).

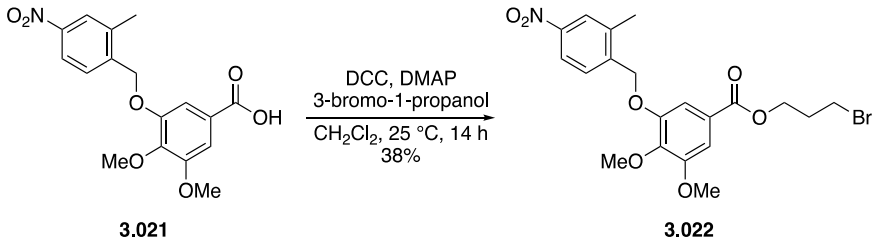

To a solution of **3.021** (31 mg, 0.09 mmol) in CH_2Cl_2 (2 mL) was added 3-bromo-1-propanol (14 mg, 0.98 mmol), DCC (23 mg, 0.11 mmol), and DMAP (0.009 mmol) at 25 °C. After stirring for 14 h, the reaction was concentrated *in vacuo*. The residue was purified by column chromatography (silica gel, hexanes/EtOAc, 5/1) to afford **3.022** (16 mg, 38%). ^{1}H NMR (500 MHz, $CDCl_3$) δ 8.10–8.06 (m, 2H), 7.67 (d, *J* = 9.1 Hz, 1H), 7.33 (s, 1H), 7.32 (s, 1H), 5.19 (s, 2H), 4.46 (t, *J* = 6.1 Hz, 2H), 3.92 (s, 3H), 3.91 (s, 3H), 3.51 (t, *J* = 6.5 Hz, 2H), 2.49 (s, 3H), 2.32 (dt, *J* = 6.3, 6.3 Hz, 2H).

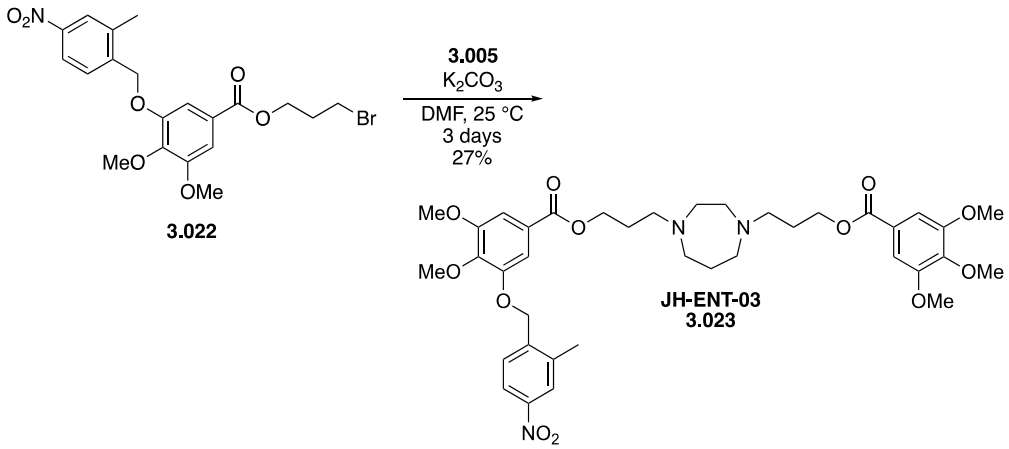

To a solution of **3.022** (8 mg, 0.017 mmol) and **3.005** (11 mg, 0.03 mmol) in DMF (0.14 mL) was added K_2CO_3 (24 mg, 0.17 mmol) at 25 °C. After stirring for 3 days, the reaction was quenched with the addition of H_2O and the resulting mixture was diluted

with EtOAc. The layers were separated, and the aqueous layer was extracted with EtOAc. The combined organic layers dried over anhydrous Na_2SO_4, filtered and concentrated *in vacuo*. The residue was purified by column chromatography (silica gel, CH_2Cl_2/MeOH, 10/1) to afford **3.023** (3.4 mg, 27%). ^{1}H NMR (500 MHz, CD_3OD) δ 8.11 (br s, 1H), 8.07 (d, *J* = 8.5 Hz, 1H), 7.70 (d, *J* = 8.5 Hz, 1H), 7.36 (br s, 2H), 7.31 (br s, 2H), 5.27 (s, 2H), 4.41–4.36 (m, 4H), 3.89 (s, 3H), 3.86 (s, 9H), 3.82 (s, 3H), 3.03–2.93 (m, 8H), 2.90–2.83 (m, 4H), 2.51 (s, 3H), 2.07–2.01 (m, 4H), 1.99–1.93 (m, 2H).

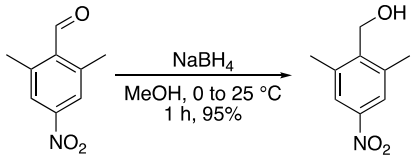

S3.3 **3.029**

Compound **S3.3** was prepared according to the previously reported procedure.[70] To a cooled solution (0 °C) of **S3.3** (373 mg, 2.08 mmol) in MeOH (40 mL) was added $NaBH_4$ (157 mg, 4.16 mmol). After slowly warming to 25 °C for 1 h, the reaction was quenched with an addition of saturated aqueous $NaHCO_3$ and the resulting mixture was diluted with EtOAc. The layers were separated, and the aqueous layer was extracted with EtOAc. The combined organic layers were dried over anhydrous Na_2SO_4, filtered, and concentrated *in vacuo*. The residue was purified by column chromatography (silica gel, hexanes/EtOAc, 2/1) to afford **3.029** (355 mg, 95%). ^{1}H NMR (400 MHz, $CDCl_3$) δ 7.90 (s, 2H), 4.79 (s, 2H), 2.53 (s, 6H).

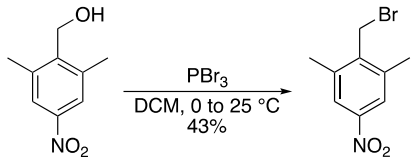

To a cooled (0 °C) solution of **3.029** (275 mg, 1.52 mmol) in CH_2Cl_2 (3 mL) was added PBr_3 (0.36 mL, 3.8 mmol). The reaction was then allowed to slowly warm to 25 °C. After stirring for 4 h, the reaction was quenched with an addition of H_2O. The layers were separated, and the aqueous layer was extracted with CH_2Cl_2. The combined organic layers were dried over anhydrous Na_2SO_4, filtered, and concentrated *in vacuo*. The residue was purified by column chromatography (silica gel, hexanes/EtOAc, 10/1) to afford **3.030** (160 mg, 43%). ^{1}H NMR (500 MHz, $CDCl_3$) δ 7.90 (s, 2H), 4.52 (s, 2H), 2.51 (s, 6H).

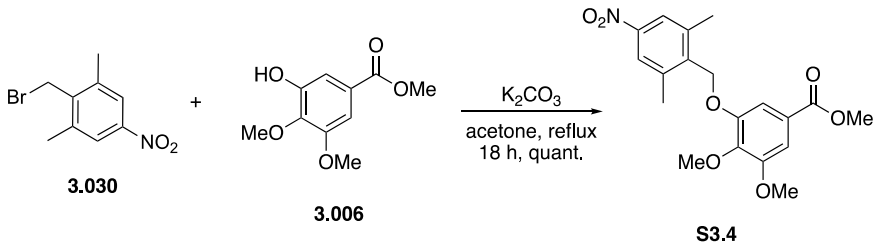

To a solution of **3.030** (150 mg, 0.61 mmol) in acetone (2 mL) was added 3,4-dimethoxy-5-hydroxybenzoic acid methyl ester (155 mg, 0.73 mmol) and K_2CO_3 (126 mg, 0.92 mmol) at 25 °C. The reaction mixture was then heated to reflux for 18 h. Upon cooling to 0 °C, the reaction was quenched with an addition of saturated aqueous NH_4Cl and the resulting mixture was diluted with EtOAc. The layers were separated, and the aqueous layer was extracted with EtOAc. The combined organic layers were dried over

anhydrous Na_2SO_4, filtered, and concentrated *in vacuo*. The residue was purified by column chromatography (silica gel, hexanes/EtOAc, 5/1) to afford **S3.4** (229 mg, quantitative). ^{1}H NMR (500 MHz, $CDCl_3$) δ 7.93 (s, 2H), 7.44 (d, *J* = 1.7 Hz, 1H), 7.36 (d, *J* = 1.6 Hz, 1H), 5.14 (s, 2H), 3.93 (s, 3H), 3.92 (s, 3H), 3.82 (s, 3H), 2.53 (s, 6H).

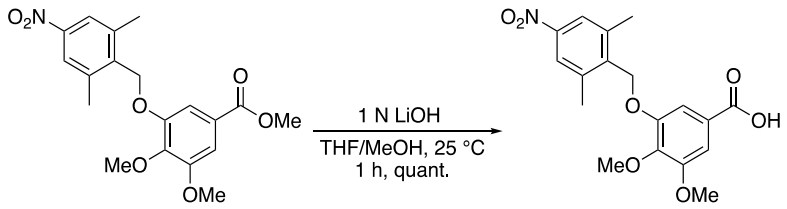

S3.4 **3.031**

To a solution of **S3.4** (200 mg, 0.53 mmol), in THF/MeOH (3/1) (18 mL) was added 1 N LiOH (3.2 mL) at 25 °C. After stirring for 1 h, 1 M HCl was added until the solution became acidic and the resulting mixture was diluted with CH_2Cl_2. The layers were separated, and the aqueous layer was extracted with CH_2Cl_2. The combined organic layers were dried over anhydrous Na_2SO_4, filtered, and concentrated *in vacuo*. The residue was purified by column chromatography (silica gel, CH_2Cl_2/MeOH, 10/1) to afford **3.031 (**192 mg, quantitative). ^{1}H NMR (500 MHz, $CDCl_3$) δ 7.94 (s, 2H), 7.51 (d, *J* = 1.6 Hz, 1H), 7.43 (d, *J* = 1.6 Hz, 1H), 5.16 (s, 2H), 3.94 (s, 3H), 3.85 (s, 3H), 2.54 (s, 6H).

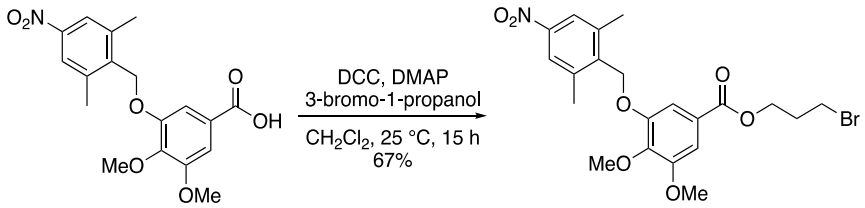

3.031 **3.032**

To a solution of **3.031** (155 mg, 0.43 mmol) in CH_2Cl_2 (9 mL) was added 3-bromo-1-propanol (65 mg, 0.47 mmol), DCC (107 mg, 0.52 mmol), and DMAP (0.043 mmol) at 25 °C. After stirring for 15 h, the reaction was concentrated *in vacuo*. The residue was purified by column chromatography (silica gel, hexanes/EtOAc, 5/1) to afford **3.032** (140 mg, 67%). ^{1}H NMR (500 MHz, $CDCl_3$) δ 7.94 (s, 2H), 7.42 (d, *J* = 1.6 Hz, 1H), 7.35 (d, *J* = 1.6 Hz, 1H), 5.14 (s, 2H), 4.49 (t, *J* = 6.1 Hz, 2H), 3.92 (s, 3H), 3.83 (s, 3H), 3.54 (t, *J* = 6.5 Hz, 2H), 2.53 (s, 6H), 2.35 (dt, *J* = 6.3, 6.3 Hz, 2H).

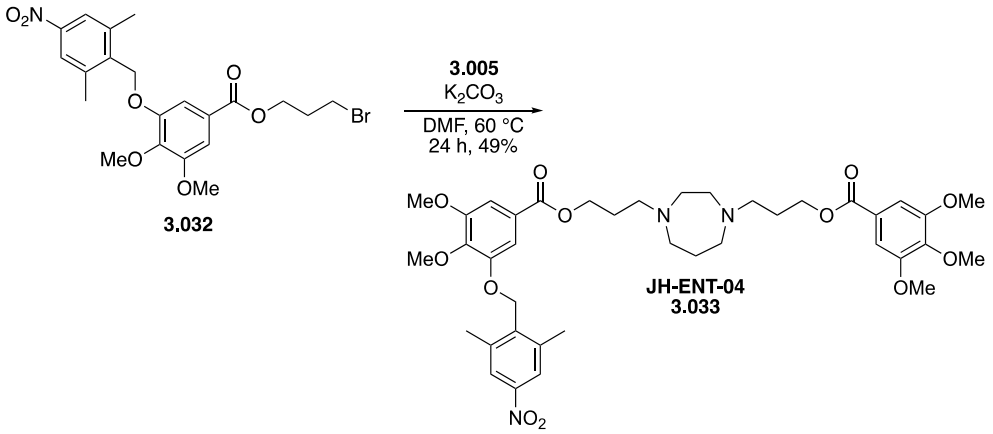

To a solution of **3.032** (45 mg, 0.09 mmol) and **3.005** (63 mg, 0.18 mmol) in DMF (0.75 mL) was added K_2CO_3 (124 mg, 0.9 mmol) at 25 °C. After stirring for 3 days, the reaction was quenched with the addition of H_2O and the resulting mixture was diluted with EtOAc. The layers were separated, and the aqueous layer was extracted with EtOAc. The combined organic layers dried over anhydrous Na_2SO_4, filtered and concentrated *in vacuo*. The residue was purified by column chromatography (silica gel, CH_2Cl_2/MeOH, 10/1) to afford **3.033** (33 mg, 49%). ^{1}H NMR (500 MHz, $CDCl_3$) δ 7.92 (s,

2H), 7.41 (d, J = 1.8 Hz, 1H), 7.33 (d, J = 1.8 Hz, 1H), 7.27 (s, 2H), 5.14 (s, 2H), 4.39–4.35 (m, 4H), 3.91 (s, 3H), 3.90 (s, 9H), 3.82 (s, 3H), 2.95–2.83 (m, 8H), 2.78–2.74 (m, 4H), 2.52 (s, 6H), 2.05–1.92 (m, 6H); HRMS (ESI) m/z 740.3385 [$(M+H)^+$ calcd for $C_{38}H_{49}N_3O_{12}$ 740.3316]; HRMS (ESI) m/z 754.3546 [$(M+H)^+$ calcd for $C_{39}H_{51}N_3O_{12}$ 754.3557].

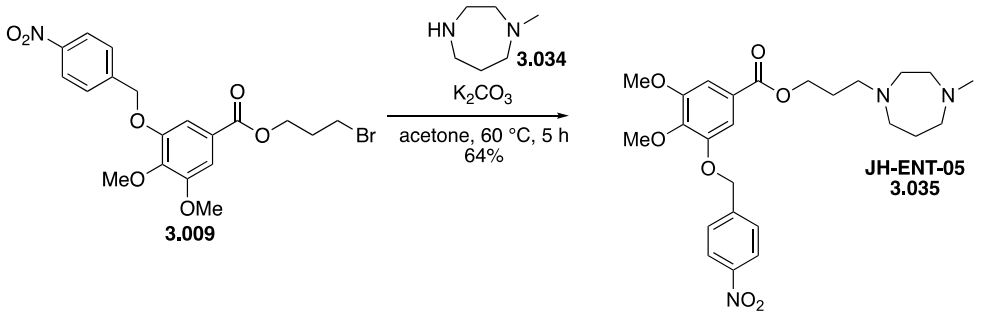

To a solution of **3.009** (34 mg, 0.08 mmol) in acetone (0.25 mL) was added 1-methylhomopiperazine (17 mg, 0.15 mmol) and K_2CO_3 (104 mg, 0.75 mmol) at 25 °C. The reaction mixture was then warmed to 60 °C for 5 h. Upon cooling to 25 °C, the reaction was quenched with the addition of saturated aqueous NH_4Cl and the resulting mixture was diluted with CH_2Cl_2. The layers were separated, and the aqueous layer was extracted with CH_2Cl_2. The combined organic layers dried over anhydrous Na_2SO_4, filtered, and concentrated *in vacuo*. The residue was purified by column chromatography (silica gel, CH_2Cl_2/MeOH, 10/1) to afford **3.035** (23 mg, 64%). ^{1}H NMR (500 MHz, $CDCl_3$) δ 8.25 (d, J = 8.8 Hz, 2H), 7.63 (d, J = 8.8 Hz, 2H), 7.32 (d, J = 1.8 Hz, 1H), 7.29 (d, J = 1.8 Hz, 1H), 5.26 (s, 2H), 4.34 (t, J = 6.6 Hz, 2H), 3.93 (s, 3H), 3.91 (s, 3H), 2.73–2.70 (m, 4H), 2.63–2.59 (m, 6H), 2.35 (s, 3H), 1.91 (dt, J = 13.7, 6.7 Hz, 2H), 1.81 (dt, J = 5.9, 5.9 Hz, 2H).

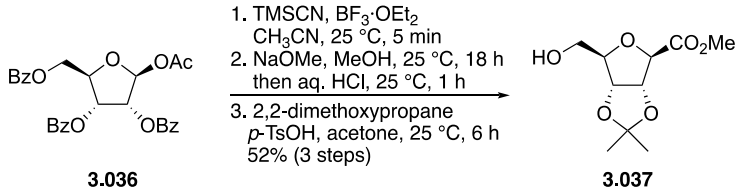

To a solution of β-D-ribofuranose-1-acetate 2,3,5-tribenzoate (10.1 g, 20.0 mmol) in CH_3CN (120 mL) was added TMSCN (10 mg, 80.0 mmol) and a few drops of $BF_3{\cdot}OEt_2$ at 25 °C. After stirring for 5 min, the reaction was quenched with an addition of saturated aqueous $NaHCO_3$ and diluted with Et_2O. The layers were separated, and the aqueous layer was extracted with Et_2O. The combined organic layers were dried over anhydrous Na_2SO_4, filtered, and concentrated *in vacuo*. The crude residue was dissolved in MeOH (200 mL) and NaOMe (0.5 M in MeOH, 40 mL) was added at 25 °C. After stirring for 18 h, 1 M HCl was added until the solution became acidic. After stirring 1 h, the reaction was concentrated *in vacuo*. The crude residue was dissolved in acetone (100 mL) and 2,2-dimethoxypropane (7.4 mL, 60.0 mmol) and *p*-TsOH (1.9 g, 10.0 mmol) were added at 25 °C. After stirring for 6 h, the reaction was quenched with the addition of H_2O and the resulting mixture was diluted with EtOAc. The layers were separated, and the aqueous layer was extracted with EtOAc. The combined organic layers dried over anhydrous Na_2SO_4, filtered, and concentrated *in vacuo*. The residue was purified by column chromatography (silica gel, hexane/EtOAc, 2/3) to afford **3.037** (2.4 g, 52% for 3 steps). ^{1}H NMR (400 MHz, $CDCl_3$) δ 4.85 (dd, *J* = 6.0, 3.1 Hz, 1H), 4.75 (dd, *J* = 6.1, 1.7 Hz, 1H), 4.59 (d, *J* = 3.1 Hz, 1H), 4.40 (br s, 1H), 3.85 (dd, *J* = 12.5, 2.8 Hz, 1H), 3.81 (s, 3H), 3.54 (dd, *J* = 12.5, 3.7 Hz, 1H), 1.55 (s, 3H), 1.35 (s, 3H).

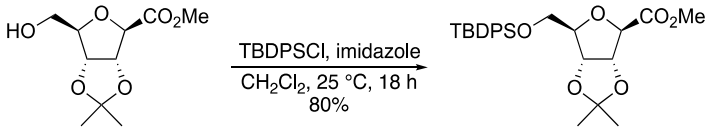

3.037 **3.038**

To a solution of **3.037** (1.21 g, 5.2 mmol) in CH_2Cl_2 (60 mL) was added TBDPSCl (2.57 mg, 10.4 mmol) and imidazole (1.07 g, 15.6 mmol) at 25 °C. After stirring for 18 h, the reaction was quenched with the addition of H_2O and the resulting mixture was diluted with CH_2Cl_2. The layers were separated, and the aqueous layer was extracted with CH_2Cl_2. The combined organic layers dried over anhydrous Na_2SO_4, filtered, and concentrated *in vacuo*. The residue was purified by column chromatography (silica gel, hexane/EtOAc, 13/1) to afford **3.038** (1.95 g, 80%). ^{1}H NMR (400 MHz, $CDCl_3$) δ 7.67–7.63 (m, 4H), 7.44–7.35 (m, 6H), 4.91 (dd, *J* = 6.2, 3.8 Hz, 1H), 4.73 (dd, *J* = 6.2, 2.0 Hz, 1H), 4.49 (d, *J* = 3.9 Hz, 1H), 4.26 (td, *J* = 4.4, 2.1 Hz, 1H), 3.73 (d, *J* = 4.4 Hz, 2H), 3.68 (s, 3H), 1.54 (s, 3H), 1.35 (s, 3H), 1.03 (s, 3H).

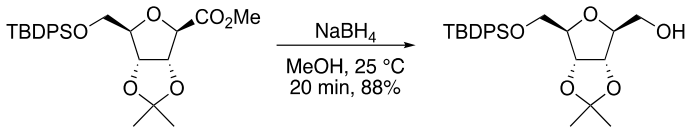

3.038 **S3.5**

To a solution of **3.038** (1.95 g, 4.1 mmol) in MeOH (45 mL) was added $NaBH_4$ (784 mg, 20.7 mmol) at 25 °C. After stirring for 20 min, the reaction was quenched with the addition of a saturated aqueous solution of NH_4Cl and the resulting mixture was diluted with EtOAc. The layers were separated, and the aqueous layer was extracted with EtOAc. The combined organic layers dried over anhydrous Na_2SO_4, filtered, and concentrated *in vacuo*. The residue was purified by column chromatography (silica gel,

hexane/EtOAc, 4/1) to afford **S3.5** (1.62 g, 88%). ^{1}H NMR (500 MHz, $CDCl_3$) δ 7.69–7.66 (m, 4H), 7.47–7.37 (m, 6H), 4.79 (dd, *J* = 6.4, 4.5 Hz, 1H), 4.70 (dd, *J* = 6.4, 3.3 Hz, 1H), 4.17 (ddd, *J* = 3.2, 3.2, 3.2 Hz, 1H), 4.05 (ddd, *J* = 4.4, 3.0, 3.0 Hz, 1H), 3.90 (dd, *J* = 11.4, 3.1 Hz, 1H), 3.84 (dd, *J* = 11.9, 2.9, Hz, 1H), 3.75 (dd, 11.4, 3.0 Hz, 1H), 3.65 (dd, *J* = 11.9, 3.4 Hz, 1H), 1.53 (s, 3H), 1.36 (s, 3H), 1.07 (s, 9H).

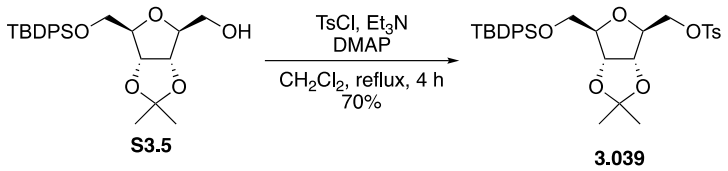

To a solution of **S3.5** (670 mg, 1.52 mmol) in CH_2Cl_2 (8 mL) was added TsCl (317 mg, 1.66 mmol), Et_3N (0.25 mL, 1.82 mmol), and DMAP (18 mg, 0.15 mmol) at 25 °C. After warming to reflux, the reaction was stirred for 4 h. After cooling to 25 °C, the reaction was diluted with CH_2Cl_2 and washed with 0.5 M HCl. The combined organic layers dried over anhydrous Na_2SO_4, filtered, and concentrated *in vacuo*. The residue was purified by column chromatography (silica gel, hexane/EtOAc, 9/2) to afford **3.039** (640 mg, 70%). ^{1}H NMR (500 MHz, $CDCl_3$) δ 7.73 (d, *J* = 8.3 Hz, 2H), 7.65–7.64 (m, 4H), 4.66 (dd, *J* = 6.5, 3.4 Hz, 1H), 4.5 (dd, *J* = 6.4, 3.9 Hz, 1H), 4.12–4.09 (m, 3H), 4.07 (dt *J* = 7.5, 3.6 Hz, 1H), 3.72–3.65 (m, 2H), 2.40 (s, 3H), 1.50 (s, 3H), 1.32 (s, 3H).

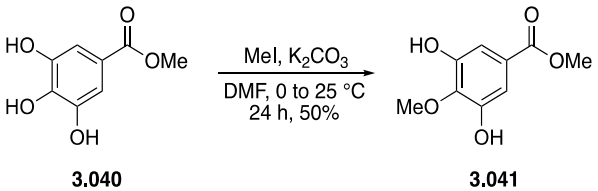

To a solution of methyl gallate (2.0 g, 16.3 mmol) in DMF (20 mL) was added K_2CO_3 (1.8 g, 19.5 mmol) at 25 °C. After stirring for 1 h, the solution was cooled to 0 °C and MeI (1.05 mL, 16.9 mmol) was added. After stirring 30 min, the reaction was warmed to 25 °C. After 24 h, the reaction was filtered and diluted with brine and EtOAc. The layers were separated, and the aqueous layer was extracted with EtOAc. The combined organic layers dried over anhydrous Na_2SO_4, filtered, and concentrated *in vacuo*. The residue was purified by column chromatography (silica gel, $CHCl_3$/MeOH 50/1) to afford **3.041** (1.6 g, 50%). ^{1}H NMR (500 MHz, $CDCl_3$) δ 9.54 (s, 2H), 7.00 (s, 2H), 3.83 (s, 3H), 3.79 (s, 3H).

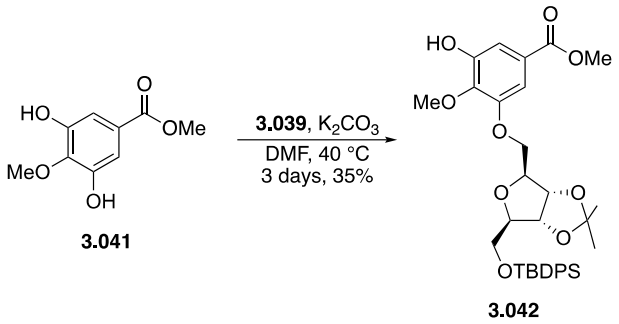

To a solution of **3.041** (425 mg, 2.14 mmol) in DMF (12 mL) was added K_2CO_3 (296 g, 2.14 mmol) and **3.039** (640 mg, 1.07 mmol) at 25 °C. The reaction mixture was then heated to 40 °C for 3 days. Upon cooling to 0 °C, the reaction was quenched with an addition of saturated aqueous NH_4Cl and the resulting mixture was diluted with EtOAc. The layers were separated, and the aqueous layer was extracted with EtOAc. The combined organic layers were dried over anhydrous Na_2SO_4, filtered, and concentrated *in vacuo*. The residue was purified by column chromatography (silica gel,

hexanes/EtOAc, 4/1) to afford **3.042** (466 mg, 35%). ^{1}H NMR (400 MHz, $CDCl_3$) δ 7.66–7.64 (m, 4H), 7.42–7.30 (m, 7H), 7.14 (d, *J* = 1.7 Hz, 1H), 4.73 (dd, *J* = 6.4, 3.3 Hz, 1H), 4.65–4.63 (m, 1H), 4.35 (ddd, *J* = 4.9, 4.9, 4.8 Hz, 1H), 4.20–4.10 (m, 3H), 3.92 (s, 3H), 3.85 (s, 3H), 3.78 (t, *J* = 4.0 Hz, 2H), 1.56 (s, 3H), 1.37 (s, 3H), 1.05 (s, 9H).

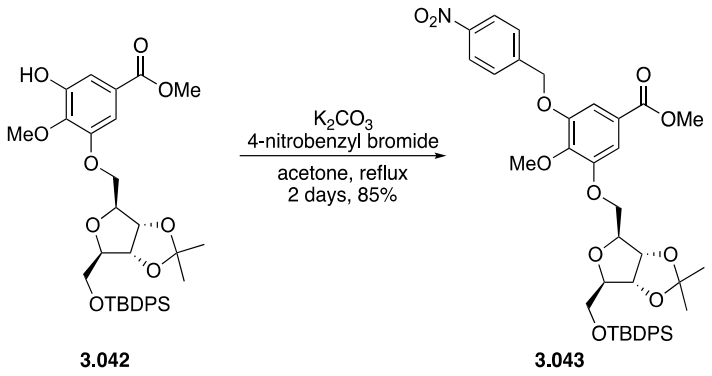

To a solution of **3.042** (140 mg, 0.23 mmol) in acetone (10 mL) was added 4-nitrobenzyl bromide (100 mg, 0.46 mmol) and K_2CO_3 (310 mg, 2.24 mmol) at 25 °C. The reaction mixture was then heated to reflux for 2 days. Upon cooling to 25 °C, the reaction was quenched with an addition of saturated aqueous NH_4Cl and the resulting mixture was diluted with EtOAc. The layers were separated, and the aqueous layer was extracted with EtOAc. The combined organic layers were dried over anhydrous Na_2SO_4, filtered, and concentrated *in vacuo*. The residue was purified by column chromatography (silica gel, hexanes/EtOAc, 7/2) to afford **3.043** (148 mg, 85%). ^{1}H NMR (400 MHz, $CDCl_3$) δ 8.25 (d, *J* = 8.6 Hz, 2H), 7.66–7.61 (m, 6H), 7.38–7.29 (m, 8H), 5.24 (s, 2H), 4.74 (dd, *J* = 6.4, 3.4 Hz, 1H), 4.68 (dd, *J* = 6.2, 4.2 Hz, 1H), 4.39 (ddd, *J* = 4.6, 4.6, 4.4 Hz, 1H), 4.20

(ddd, J = 4.2, 4.0, 4.0 Hz, 1H), 4.16–4.09 (m, 2H), 3.86 (s, 3H), 3.85 (s, 3H), 3.80 (t, J = 4.4 Hz, 2H), 1.57 (s, 6H), 1.26 (s, 3H), 1.05 (s, 9H).

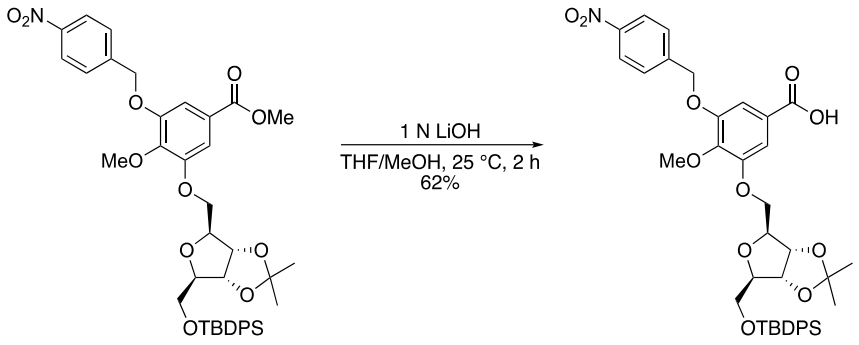

3.043 **S3.6**

To a solution of **3.043** (60 mg, 0.08 mmol), in THF/MeOH (3/1) (3 mL) was added 1 N LiOH (0.6 mL) at 25 °C. After stirring for 2 h, 1 M HCl was added until the solution became acidic and the resulting mixture was diluted with EtOAc. The layers were separated, and the aqueous layer was extracted with EtOAc. The combined organic layers were dried over anhydrous Na_2SO_4, filtered, and concentrated *in vacuo*. The residue was purified by column chromatography (silica gel, hexane/EtOAc, 1/4) to afford **S3.6 (**36 mg, 62%). ^{1}H NMR (500 MHz, $CDCl_3$) δ 8.26 (d, J = 8.6 Hz, 2H), 7.67–7.62 (m, 6H), 7.39–7.31 (m, 8H), 5.25 (s, 2H), 4.74 (dd, J = 6.4, 3.4 Hz, 1H), 4.68 (dd, J = 6.4, 4.2 Hz, 1H), 4.39 (ddd, J = 4.7, 4.7, 4.6 Hz, 1H), 4.22–4.19 (m, 1H), 4.18–4.10 (m, 2H), 3.88 (s, 3H), 3.81 (t, J = 4.7 Hz, 2H), 1.57 (s, 3H), 1.37 (s, 3H), 1.05 (s, 9H).

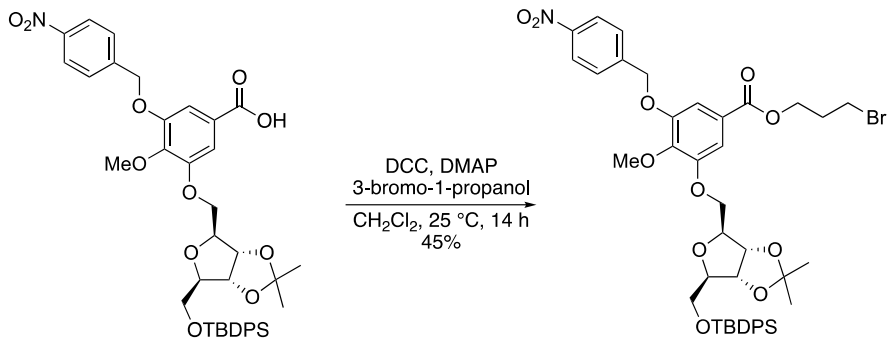

S3.6 **3.044**

To a solution of **S3.6** (30 mg, 0.04 mmol) in CH_2Cl_2 (1 mL) was added 3-bromo-1-propanol (4 μL, 0.044 mmol), DCC (10 mg, 0.048 mmol), and DMAP (0.6 mg) at 25 °C. After stirring for 14 h, the reaction was concentrated *in vacuo*. The residue was purified by column chromatography (silica gel, hexanes/EtOAc, 6/1) to afford **3.044** (15 mg, 45%). ^{1}H NMR (500 MHz, $CDCl_3$) δ 8.26 (d, *J* = 8.6 Hz, 2H), 7.67–7.62 (m, 6H), 7.40–7.28 (m, 8H), 5.25 (s, 2H), 4.74 (dd, *J* = 6.5, 3.5 Hz, 1H), 4.68 (dd, *J* = 6.5, 4.2 Hz, 1H), 4.41 (t, *J* = 6.1 Hz, 2H), 4.39–4.37 (m, 1H), 4.20 (ddd, *J* = 4.2, 4.1, 4.1 Hz, 1H), 4.18–4.12 (m, 2H), 3.87 (s, 3H), 3.83–3.79 (m, 2H), 3.46 (t, *J* = 6.5 Hz, 2H), 2.27 (dddd, *J* = 6.3, 6.3, 6.3, 6.3 Hz, 2H), 1.57 (s, 3H), 1.25 (s, 3H), 1.05 (s, 9H).

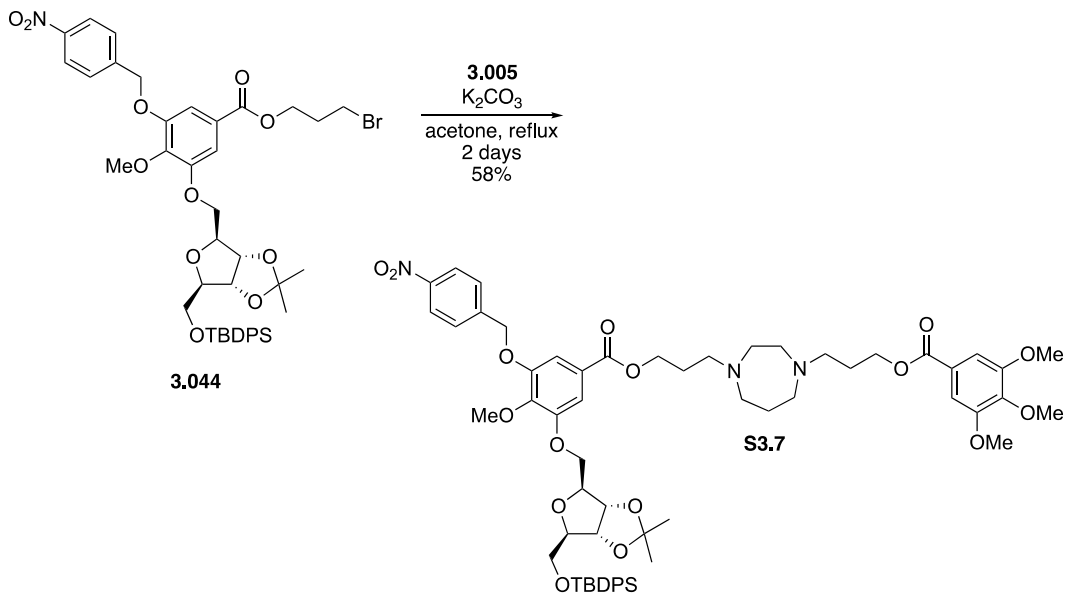

To a solution of **3.044** (9 mg, 0.01 mmol) in acetone (0.5 mL) was added **3.005** (10 mg, 0.03 mmol) and K_2CO_3 (20 mg, 0.1 mmol) at 25 °C. The reaction mixture was then warmed to reflux for 2 days. Upon cooling to 25 °C, the reaction was quenched with the addition of saturated aqueous NH_4Cl and the resulting mixture was diluted with EtOAc. The layers were separated, and the aqueous layer was extracted with EtOAc. The combined organic layers dried over anhydrous Na_2SO_4, filtered, and concentrated *in vacuo*. The residue was purified by column chromatography (silica gel, CH_2Cl_2/MeOH, 30/1 to 20/1) to afford **S3.7** (7 mg, 58%). ^{1}H NMR (500 MHz, $CDCl_3$) δ 8.25 (d, *J* = 8.7 Hz, 2H), 7.66–7.63 (m, 6H), 7.39–7.28 (m, 10H), 5.25 (s, 2H), 4.73 (dd, *J* = 6.4, 3.5 Hz, 1H), 4.68 (dd, *J* = 6.3, 4.3 Hz, 1H), 4.38–4.26 (m, 3H), 4.32 (t, *J* = 6.5 Hz, 2H), 4.20–4.12 (m, 3H), 3.90 (s, 9H), 3.85 (s, 3H), 3.79 (t, *J* = 4.1 Hz, 2H), 2.96–2.59 (m, 12H), 2.08–1.85 (m, 6H), 1.56 (s, 3H), 1.37 (s, 3H), 1.04 (s, 9H).

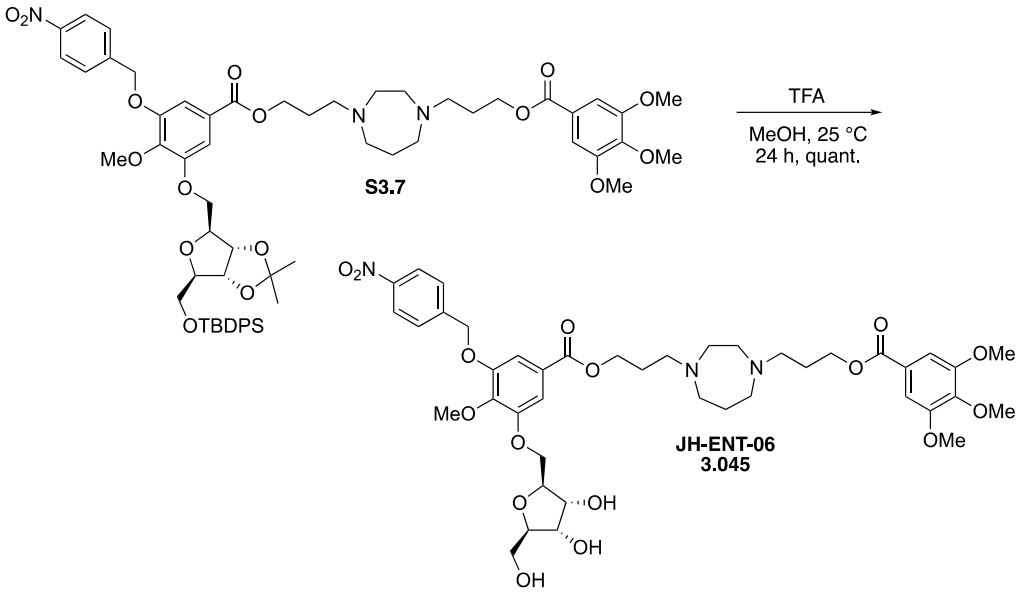

To a solution of **S3.7** (7 mg, 0.006 mmol) in MeOH (1 mL) was added TFA (0.2 mL) at 25 °C. After stirring for 24 h, the reaction was concentrated *in vacuo* to provide **3.045** (5 mg, quantitative). ^{1}H NMR (500 MHz, $CDCl_3$) δ 8.26 (d, *J* = 8.7 Hz, 2H), 8.65 (d, *J* = 8.7 Hz, 2H), 7.35 (br s, 1H), 7.31 (br s, 1H), 7.26 (s, 2H), 5.25 (s, 2H), 4.41 (t, *J* = 5.9 Hz, 2H), 4.38–4.29 (m, 5H), 4.22–4.20 (m, 1H), 4.18–4.16 (m, 1H), 4.03 (br s, 1H), 3.94 (s, 3H), 3.91 (s, 3H), 3.91 (s, 6H), 3.85–3.82 (m, 4H), 3.63 (dd, *J* = 12.4, 3.2 Hz, 1H), 3.60–3.52 (m, 3H), 3.33–3.29 (m, 2H), 3.28–3.24 (m, 2H), 2.51–2.49 (m, 2H), 2.29–2.22 (m, 6H).

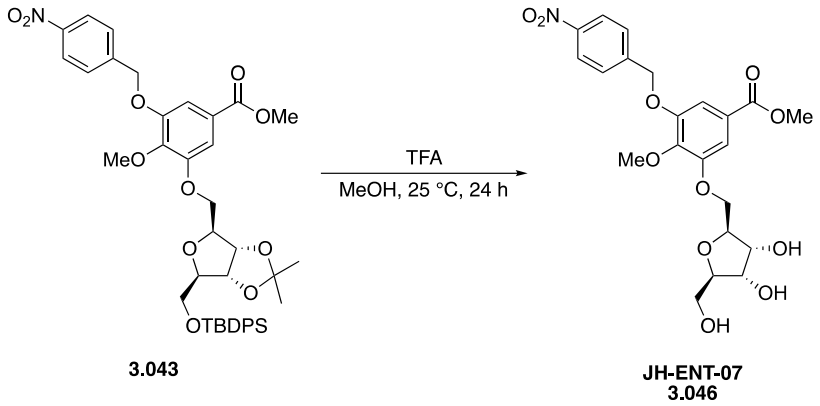

To a solution of **3.043** (50 mg, 0.066 mmol) in MeOH (4 mL) was added TFA (1 mL) at 25 °C. After stirring for 24 h, the reaction was concentrated *in vacuo* to provide **3.046** (31 mg, quantitative). ^{1}H NMR (500 MHz, $CDCl_3$) δ 8.26 (d, *J* = 8.6 Hz, 2H), 7.63 (d, *J* = 8.4 Hz, 2H), 7.36 (d, *J* = 1.8 Hz, 1H), 7.34 (d, *J* = 1.8 Hz, 1H), 5.25 (s, 2H), 4.48 (t, *J* = 6.1 Hz, 1H), 4.32 (dd, *J* = 5.5, 3.2 Hz, 1H), 4.28 (d, *J* = 2.9 Hz, 2H), 4.19 (ddd, *J* = 6.2, 2.9, 2.9, 1H), 4.09 (ddd, *J* = 2.9, 2.9, 2.8, 1H), 3.92 (s, 3H), 3.90 (s, 3H), 3.89–3.86 (m, 1H), 3.69 (dd, *J* = 12.4, 2.8 Hz, 1H).

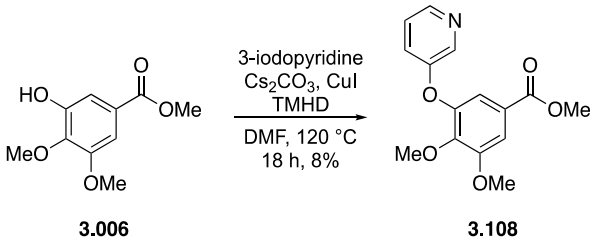

To a solution of **3.006** (438 mg, 2.05 mmol) in DMF (2 mL) was added 3-iodopyridine (840 mg, 4.1 mmol), Cs_2CO_3 (2.67 g, 8.2 mmol), CuI (20 mg, 0.10 mmol) and TMHD (0.04 mL, 0.21 mmol) at 25 °C. The reaction mixture was then warmed to 120 °C for 18 h. Upon cooling to 25 °C, the reaction was quenched with the addition of saturated aqueous NH_4Cl and the resulting mixture was diluted with EtOAc. The layers

were separated, and the aqueous layer was extracted with EtOAc. The combined organic layers dried over anhydrous Na_2SO_4, filtered, and concentrated *in vacuo*. The residue was purified by column chromatography (silica gel, CH_2Cl_2/MeOH, 10/1) to afford **3.108** (46 mg, 8%). ^{1}H NMR (500 MHz, $CDCl_3$) 8.38 (s, 1H), 8.33 (br s, 1H), 7.47 (d, *J* = 1.8 Hz, 1H), 7.34 (d, *J* = 1.9 Hz, 1H), 7.24 (dd, *J* = 8.3, 4.5 Hz, 1H), 7.20 (ddd, *J* = 8.4, 2.5, 1.3 Hz, 1H), 3.94 (s, 3H), 3.86 (s, 3H), 3.86 (s, 3H).

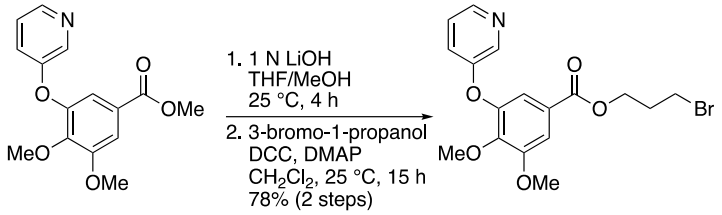

3.108 **3.109**

To a solution of **3.108** (46 mg, 0.16 mmol), in THF/MeOH (3/1) (5 mL) was added 1 N LiOH (0.95 mL) at 25 °C. After stirring for 4 h, 1 M HCl was added until the solution became acidic and the resulting mixture was diluted with EtOAc. The layers were separated, and the aqueous layer was extracted with EtOAc. The combined organic layers were dried over anhydrous Na_2SO_4, filtered, and concentrated *in vacuo*. The crude residue was dissolved in CH_2Cl_2 (3 mL) and 3-bromo-1-propanol (0.015 mL, 0.17 mmol), DCC (43 mg, 0.21 mmol) and DMAP (2 mg, 0.014 mmol) was added at 25 °C. After stirring for 15 h, the reaction was concentrated *in vacuo*. The residue was purified by column chromatography (silica gel, hexanes/EtOAc, 5/1) to afford **3.109** (43 mg, 78%). ^{1}H NMR (500 MHz, $CDCl_3$) δ 8.38 (s, 1H), 8.34 (d, *J* = 3.9 Hz, 1H), 7.47 (d, *J* = 1.9 Hz, 1H),

7.34 (d, *J* = 1.9 Hz, 1H), 7.27–7.24 (m, 1H), 7.21 (ddd, *J* = 8.4, 2.7, 1.3 Hz, 1H), 4.43 (t, *J* = 6.1 Hz, 2H), 3.94 (s, 3H), 3.85 (s, 3H), 3.49 (t, *J* = 6.5 Hz, 2H), 2.29 (dt, *J* = 6.3, 6.3 Hz, 2H).

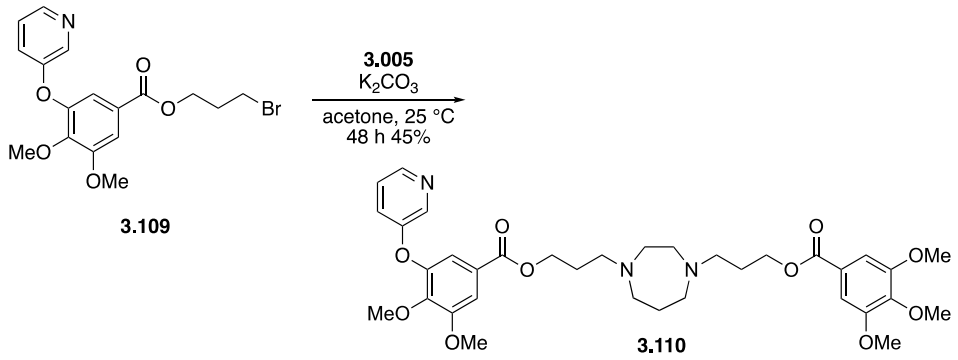

To a solution of **3.109** (43 mg, 0.11 mmol) in acetone (0.4 mL) was added **3.005** (58 mg, 0.17 mmol) and K_2CO_3 (152 mg, 1.1 mmol) at 25 °C. After stirring for 48 h, the reaction was quenched with the addition of saturated aqueous NH_4Cl and the resulting mixture was diluted with EtOAc. The layers were separated, and the aqueous layer was extracted with EtOAc. The combined organic layers dried over anhydrous Na_2SO_4, filtered, and concentrated *in vacuo*. The residue was purified by column chromatography (silica gel, CH_2Cl_2/MeOH, 10/1) to afford **3.110** (32 mg, 45%). ^{1}H NMR (500 MHz,CD_3OD) δ 8.27–8.25 (m, 2H), 7.54 (d, *J* = 1.9 Hz, 1H), 7.40 (dd, *J* = 8.4, 4.7 Hz, 1H), 7.36–7.33 (m, 2H), 7.30 (s, 2H), 4.34 (dt, *J* = 6.4, 6.4 Hz, 4H), 3.93 (s, 3H), 3.87 (s, 6H), 3.82 (s, 3H), 3.78 (s, 3H), 2.80–2.76 (m, 8H), 2.68 (dt, *J* = 14.4, 7.5 Hz, 4H), 1.99–1.91 (m, 4H), 1.84 (dddd, *J* = 6.0, 6.0, 5.9, 5.9 Hz, 2H).

4. Conclusion

Daily chronic pain has become the most common reason individuals seek out medical care and affects roughly 1 in 5 Americans.[4] Current pain management relies heavily on NSAIDs and opioid analgesics but these options only provide relief for ~25% of patients.[5] Additionally, opioids are associated with very serious side effects such as addiction, dependence and tolerance. Due to these addictive properties, the United States now faces an epidemic of opioid overdose which resulted in ~70,000 deaths in 2020.[9] Therefore, it is imperative to discover novel analgesics that are safe, effective and non-addictive.

Throughout history, drug discovery has drawn inspiration from natural products as they are a rich source of scaffold diversity, structural complexity and are 'optimized' to serve a biological function.[15] Natural products belonging to the grayanane family possess a unique 5/7/6/5 ring system and exhibit a plethora of biological activities including, analgesic, PTP1B inhibition, antitumor, antiviral and many more.[17] Specifically, rhodojaponin III demonstrates potent analgesic activity in mice for acute, inflammatory and diabetic neuropathic pain. Importantly, rhodojaponin III does not affect the endogenous opioid system but the mechanism of action has yet to be established.[19]

As rhodojaponin III is an excellent starting point for the development of a non-opioid analgesic therapeutic and a chemical probe, we devised an enantioselective route to access this compound. Our strategy relies on a convergent approach in which two

fragments, a 5-membered ring fragment and the key bicyclo[3.2.1]octane fragment, are synthesized separately and then coupled together to provide the core of grayanane-type natural products.

The synthesis of the simpler 5-membered ring fragment was accomplished in 4 steps from commercially available 2-methylcyclopentadione to provide a vinyl triflate primed for coupling to the bicyclo[3.2.1]octane fragment. Construction of the key bicycle was carried out via a copper(I)-mediated conjugate addition to a simple cyclic enone, followed by propargylation to form an alkynyl intermediate that was cyclized via a Mn(III)-mediated radical cyclization to provide the 5/6 bridged system. Lastly, SmI_2 was utilized in the stereoselective reduction of a β-hydroxy ketone substrate to provide the desired equatorial alcohol. The enantioselective synthesis of the bicyclo[3.2.1]octane fragment was achieved using Helmchen's chiral auxiliary to direct the copper(I)-mediated conjugate addition to a shielded enoate.

Alongside natural product synthesis, our efforts towards novel non-opioid analgesics includes the structure-guided design of adenosine reuptake inhibitors (AdoRIs). By increasing extracellular adenosine, the inhibition of hENT provides an analgesic effect and a promising approach for pain-relief. Consequently, the co-crystal structures of hENT1 in complex with two known inhibitors, dilazep and NBMPR, were utilized to rationally design novel ENT inhibitors with improved potency, selectivity and pharmacological properties.

Analysis of the co-crystal structure of ENT1 in complex with dilazep and NBMPR identified shared and distinct binding sites that were taken advantage of in the design of our first hybrid analog JH-ENT-01. As JH-ENT-01 exhibited a two-fold increase in binding affinity for ENT1 compared to dilazep, we expanded the hybrid design with 6 additional ENT1 inhibitors. The hybrid library was evaluated for their analgesic properties in an STZ-induced diabetic neuropathic pain model. Excitingly, two compounds (JH-ENT-01 and JH-ENT-07) significantly reduced mechanical pain with accumulating effects. Excited by JH-ENT-07 as a novel scaffold, additional inhibitors were designed, synthesized and are currently being tested for their bioactivity.

To improve the pharmacological properties of dilazep, a macrocyclic inhibitor was designed. Synthetically, we envisioned several routes to achieve macrocyclization, including RCM with Grubb's catalyst, an S_N2-type reaction with the homopiperazine ring or an alkyne/aldehyde coupling reaction. Synthetic efforts towards each of these approaches has been made and provides the groundwork for completing the macrocyclic inhibitor.

Finally, two ENT3 selective compounds were designed by examining the differences in amino acid composition within the binding pocket of ENT1 compared to ENT3. One of the ENT3 selective inhibitors has been synthesized and will be tested for bioactivity and selectivity. Altogether, novel ENT inhibitors with improved potency, selectivity and pharmacological properties were rationally designed for the development of novel non-opioid analgesics.

Appendix A. Spectral Data for Chapter 2

2.160

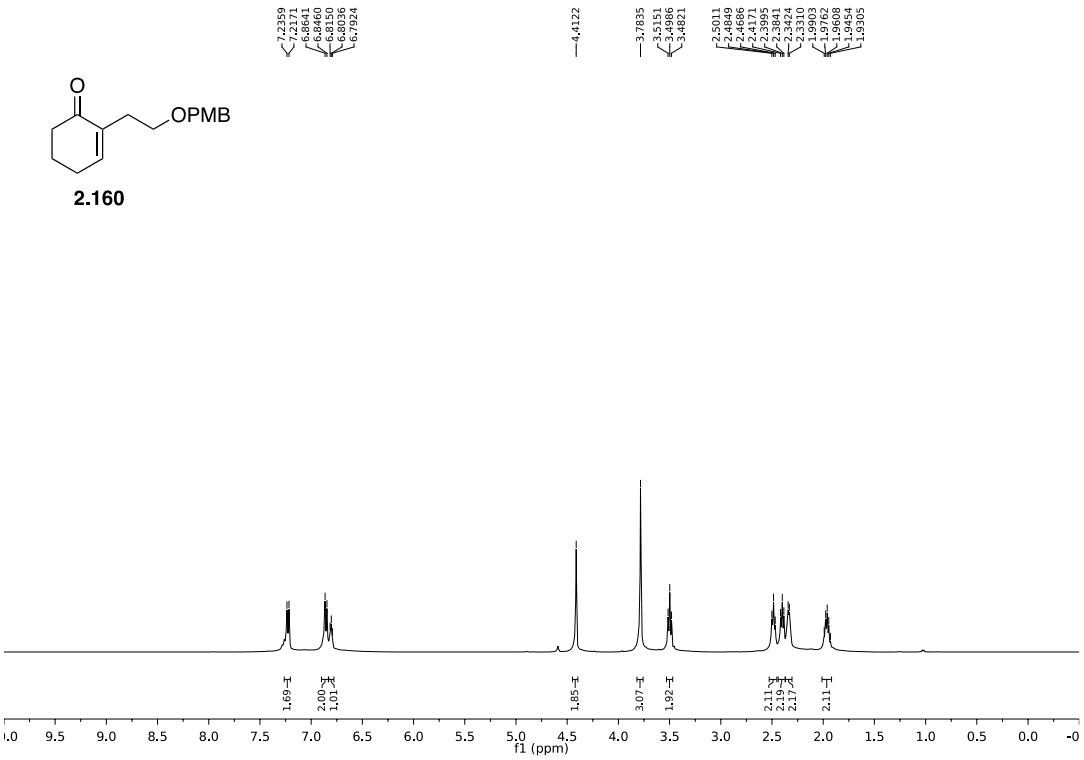

2.161

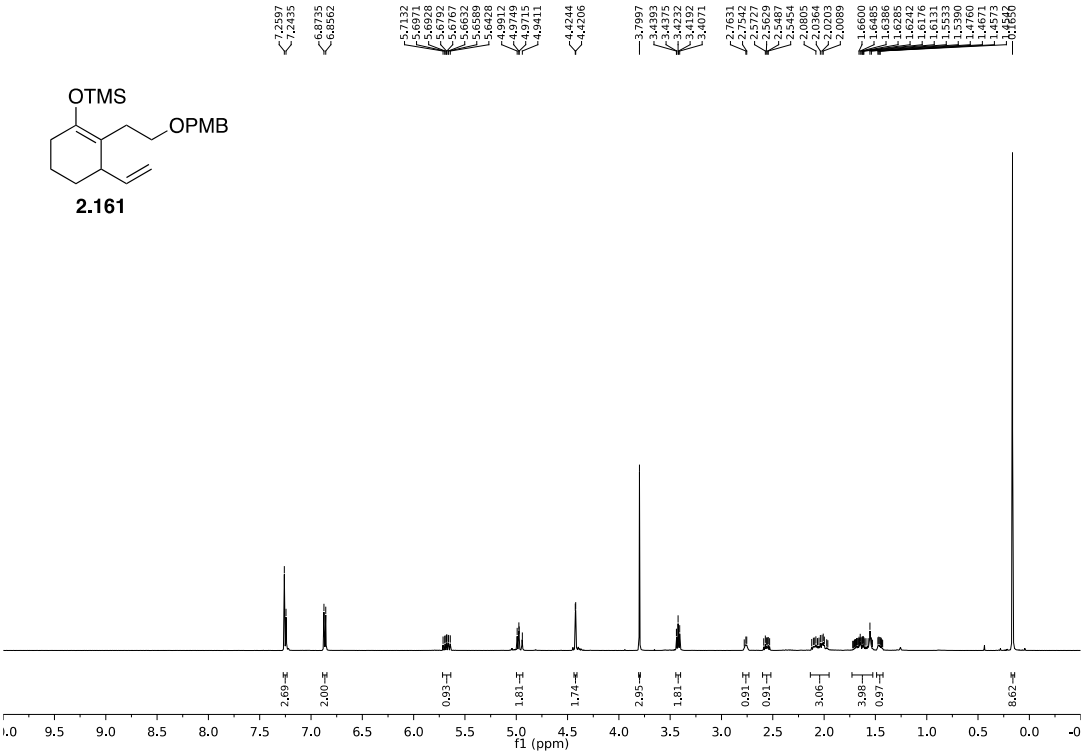

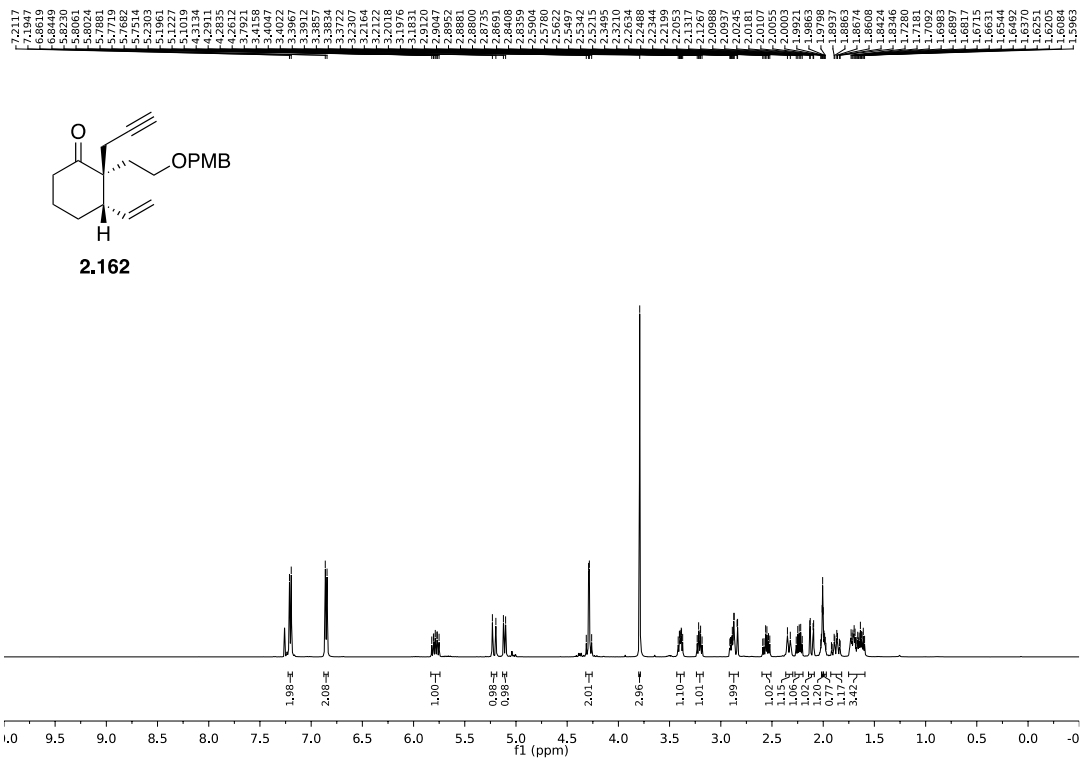
OPMB
H
2.162
f1 (ppm)

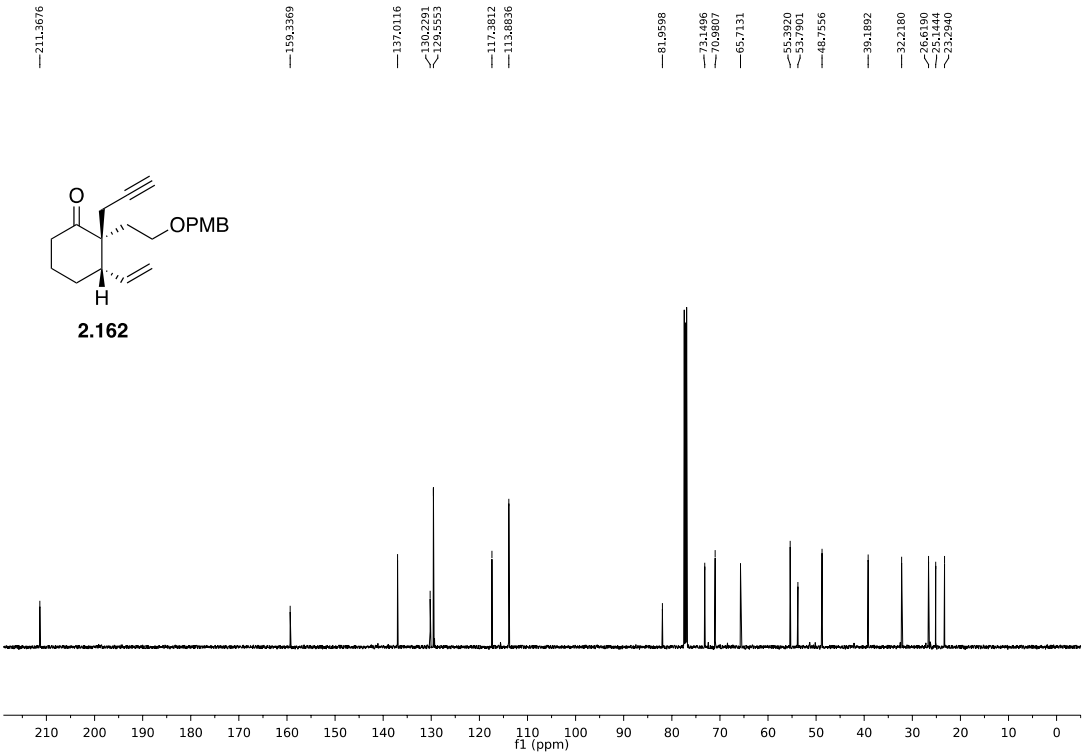
OPMB
H
2.162
f1 (ppm)

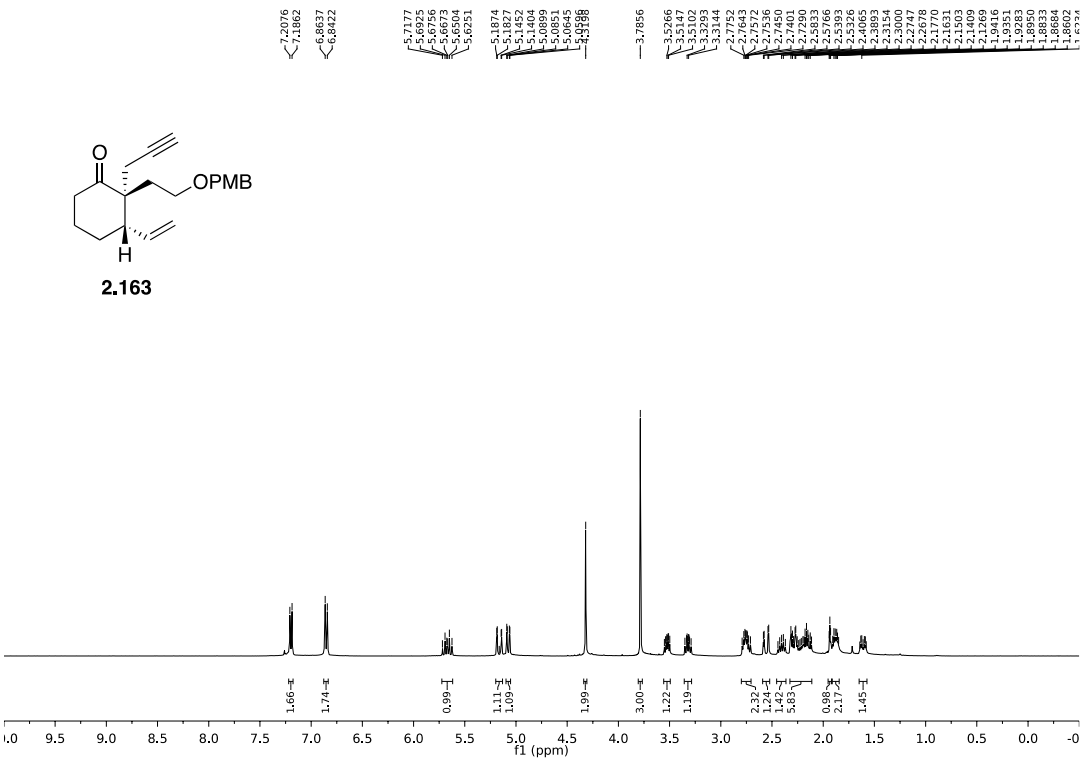

2.163

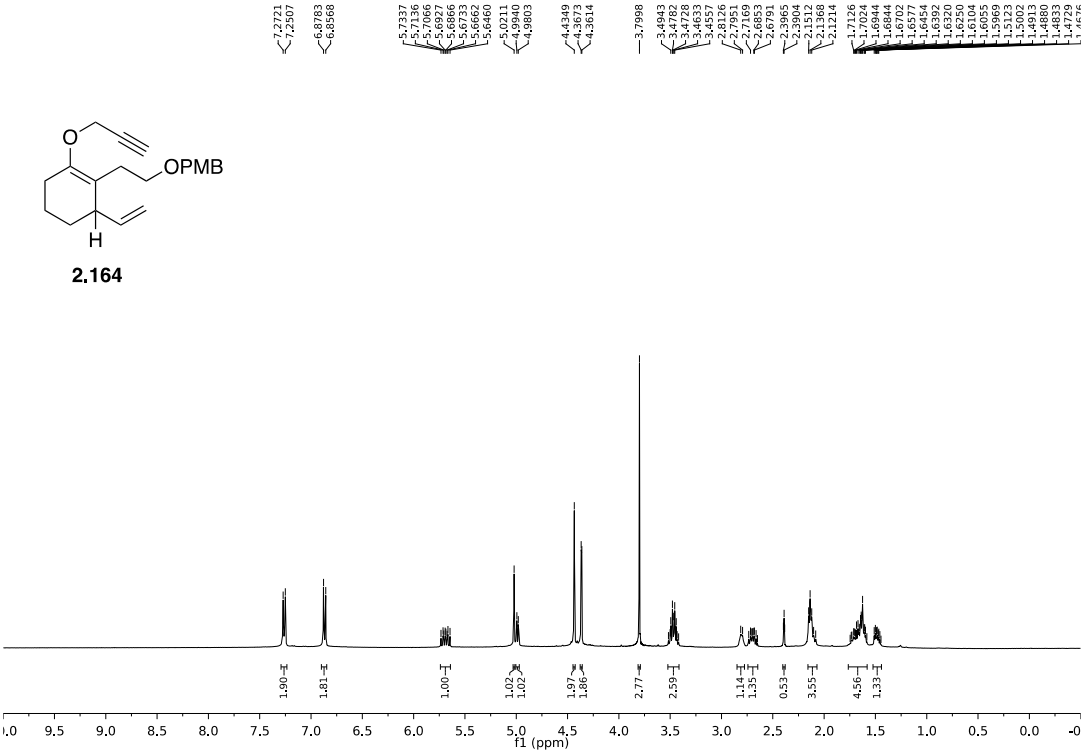

2.164

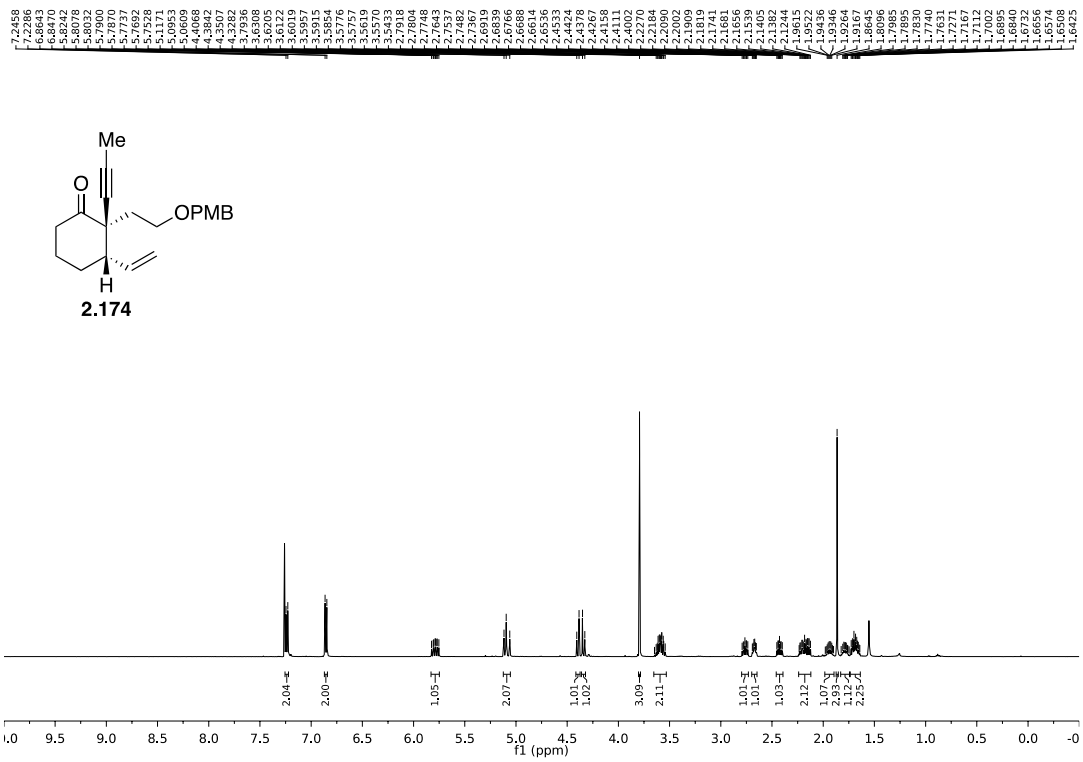
Me
O
OPMB
H
2.174
f1 (ppm)

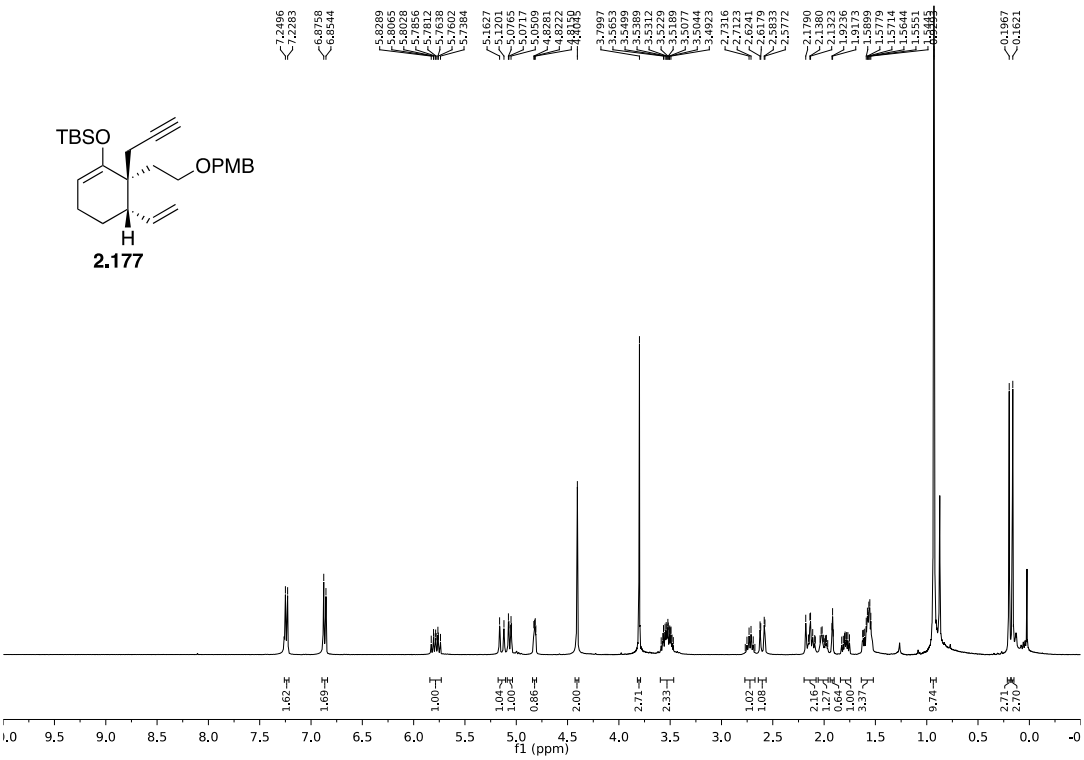
TBSO
OPMB
H
2.177
f1 (ppm)

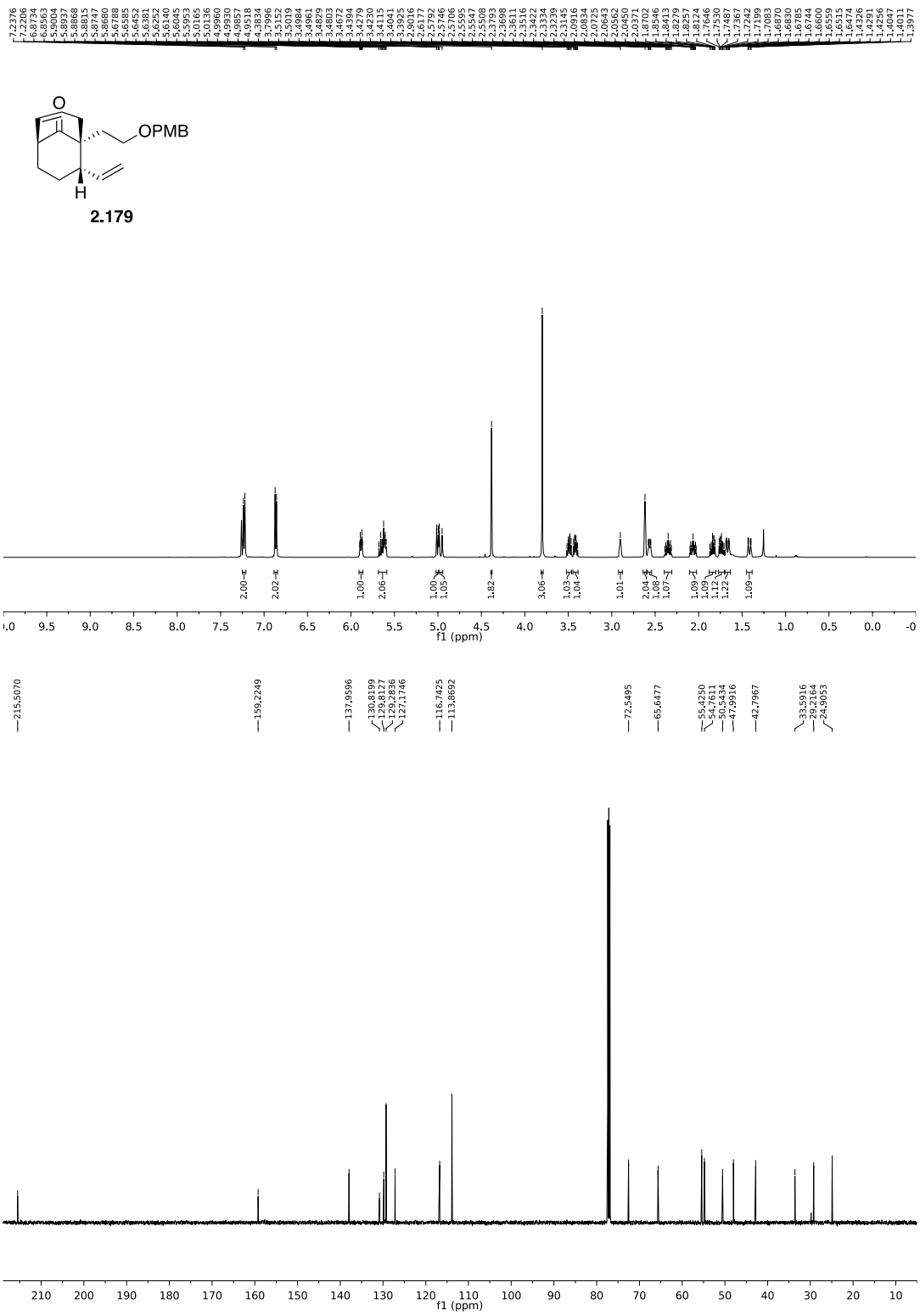
7.2376
7.2096
6.8734
6.8563
5.9004
5.8937
5.8868
5.8815
5.8727
5.8680
5.6788
5.6585
5.6452
5.6381
5.6252
5.6140
5.6045
5.5953
5.0165
5.0136
4.9960
4.9930
4.9857
4.9518
4.3834
3.7996
3.5152
3.5019
3.4984
3.4961
3.4859
3.4803
3.4672
3.4394
3.4279
3.4230
3.4115
3.4041
3.3925
2.9016
2.6177
2.5792
2.5746
2.5706
2.5595
2.5547
2.5508
2.3793
2.3698
2.3611
2.3516
2.3422
2.3334
2.3239
2.3145
2.0916
2.0834
2.0725
2.0643
2.0562
2.0450
2.0371
1.8702
1.8546
1.8413
1.8279
1.8257
1.8124
1.7646
1.7530
1.7487
1.7367
1.7242
1.7199
1.7083
1.6870
1.6830
1.6785
1.6744
1.6660
1.6559
1.6515
1.6474
1.4326
1.4291
1.4256
1.4017
1.4011
1.3977
O
OPMB
H
2.179
2.00
2.02
1.00
2.06
1.00
1.05
1.82
3.06
1.03
1.04
1.01
2.04
1.08
1.07
1.09
1.09
1.12
1.22
1.09
9.5
9.0
8.5
8.0
7.5
7.0
6.5
6.0
5.5
5.0
4.5
4.0
3.5
3.0
2.5
2.0
1.5
1.0
0.5
0.0
f1 (ppm)
215.5070
159.2249
137.9596
130.8199
129.8127
129.2836
127.1746
116.7425
113.8692
72.5495
65.6477
55.4250
54.9511
50.5434
47.9916
42.7967
33.5916
29.2164
24.9053
210
200
190
180
170
160
150
140
130
120
110
100
90
80
70
60
50
40
30
20
10
f1 (ppm)

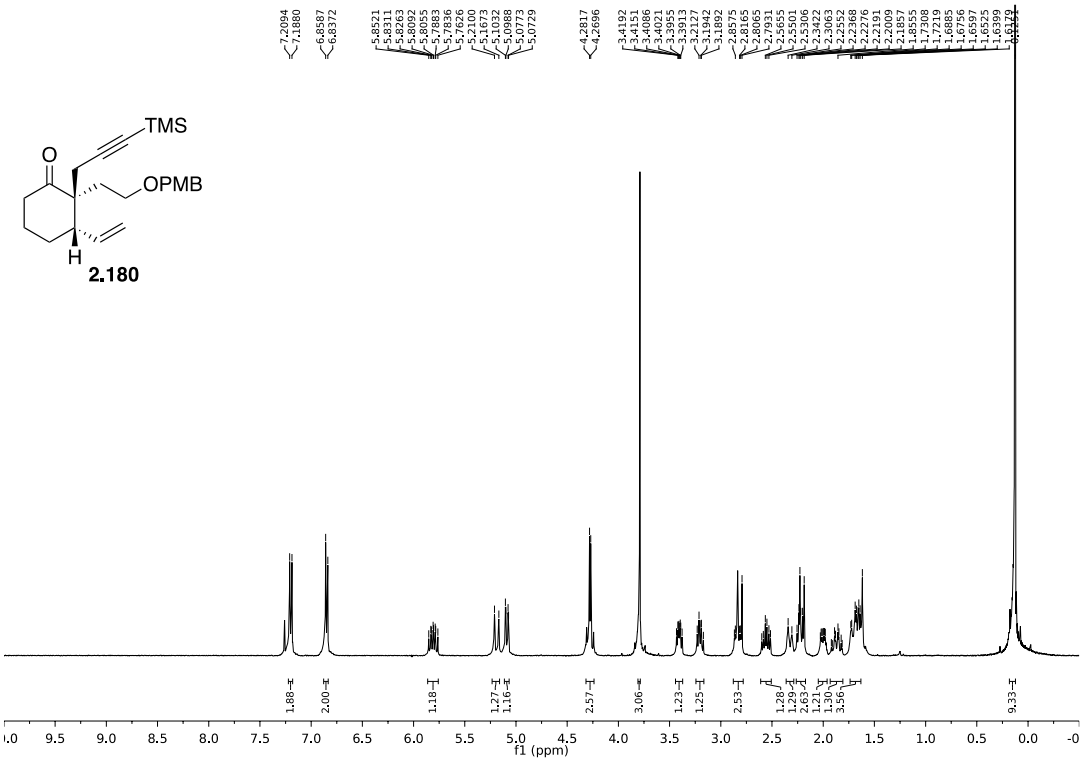
TMS
O
OPMB
H
2.180
f1 (ppm)

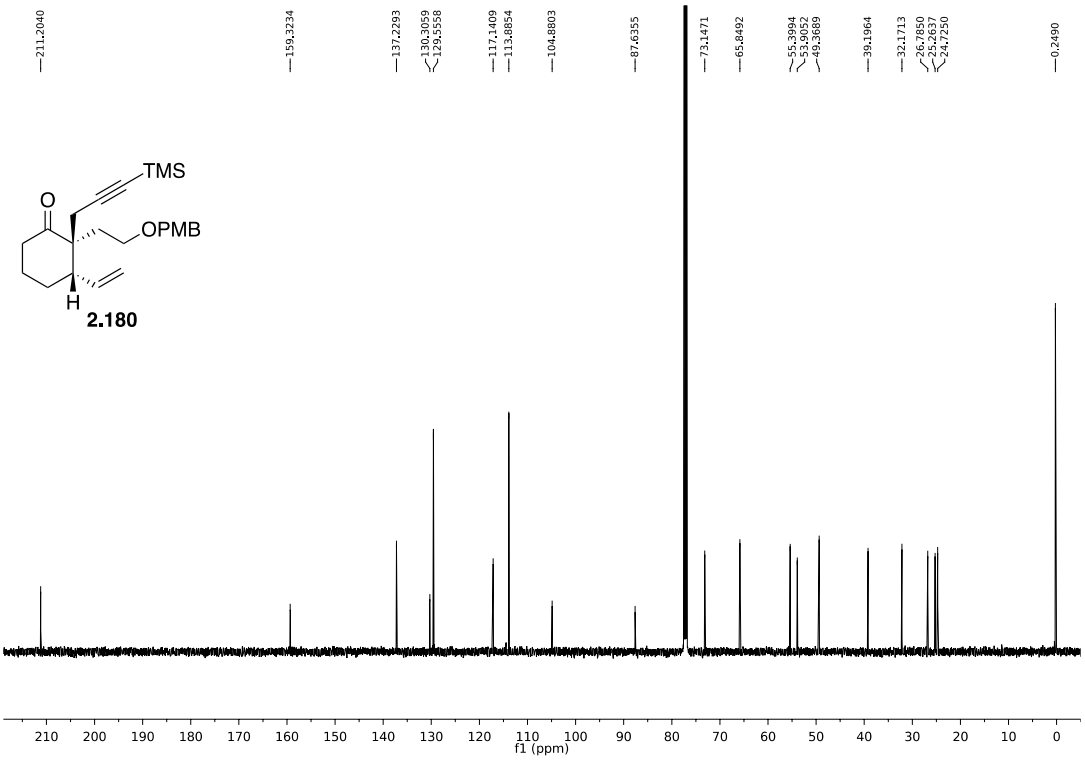
TMS
O
OPMB
H
2.180
f1 (ppm)

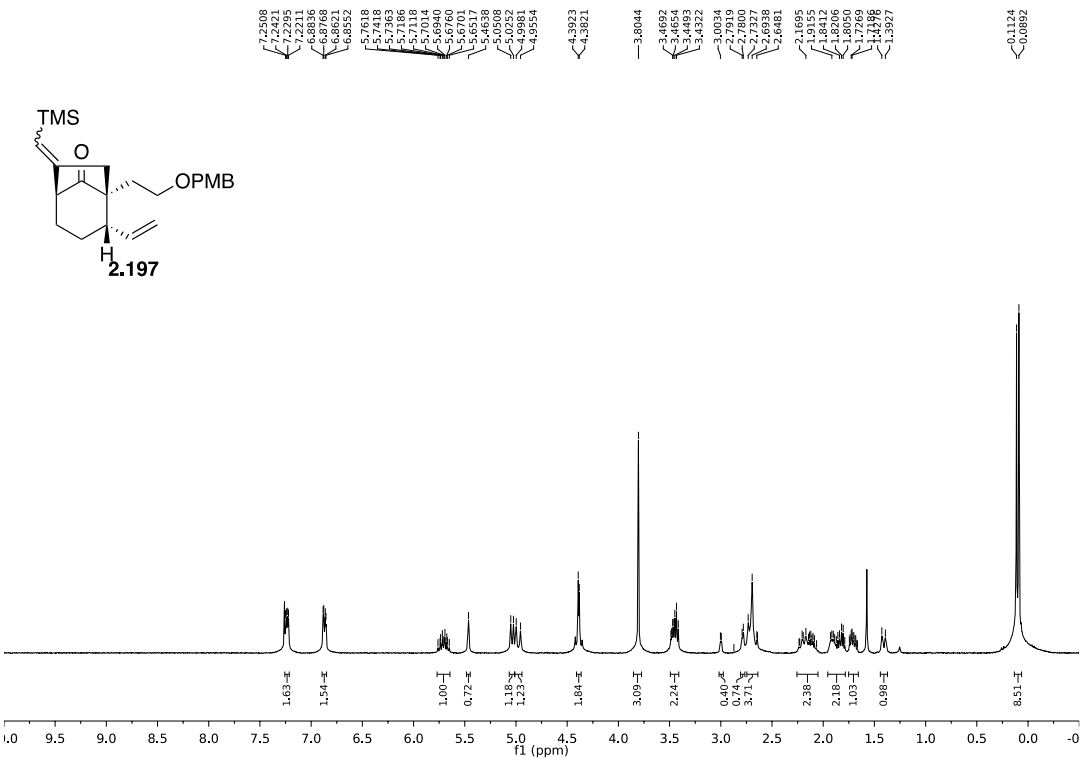
TMS
O
OPMB
H
2.197
f1 (ppm)

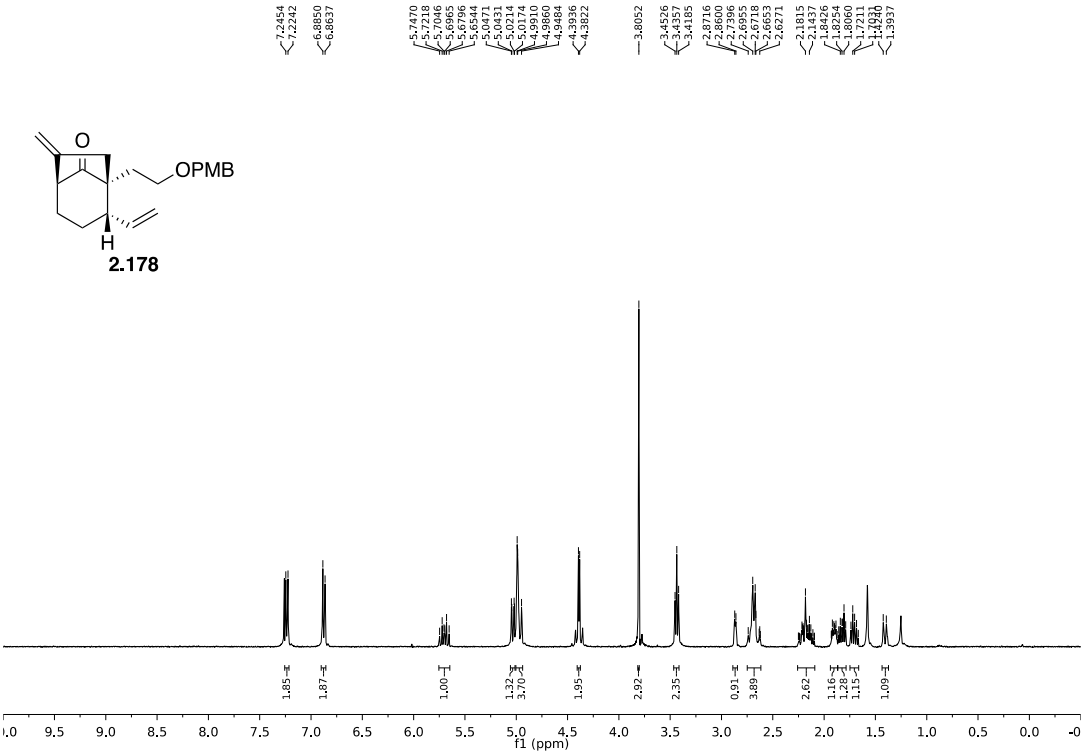
O
OPMB
H
2.178
f1 (ppm)

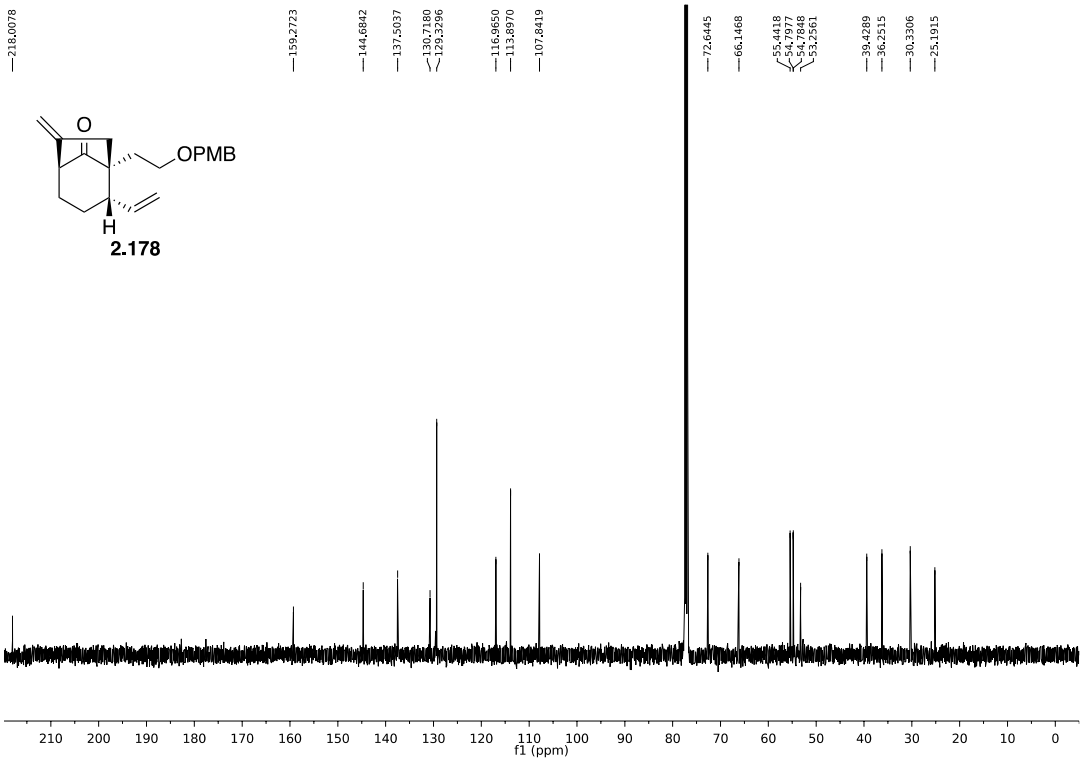
218.0078
159.2723
144.6842
137.5037
130.7180
129.3296
116.9650
113.8970
107.8419
72.6445
66.1468
55.4418
54.7977
54.7848
53.2561
39.4289
36.2515
30.3306
25.1915
O
OPMB
H
2.178
f1 (ppm)

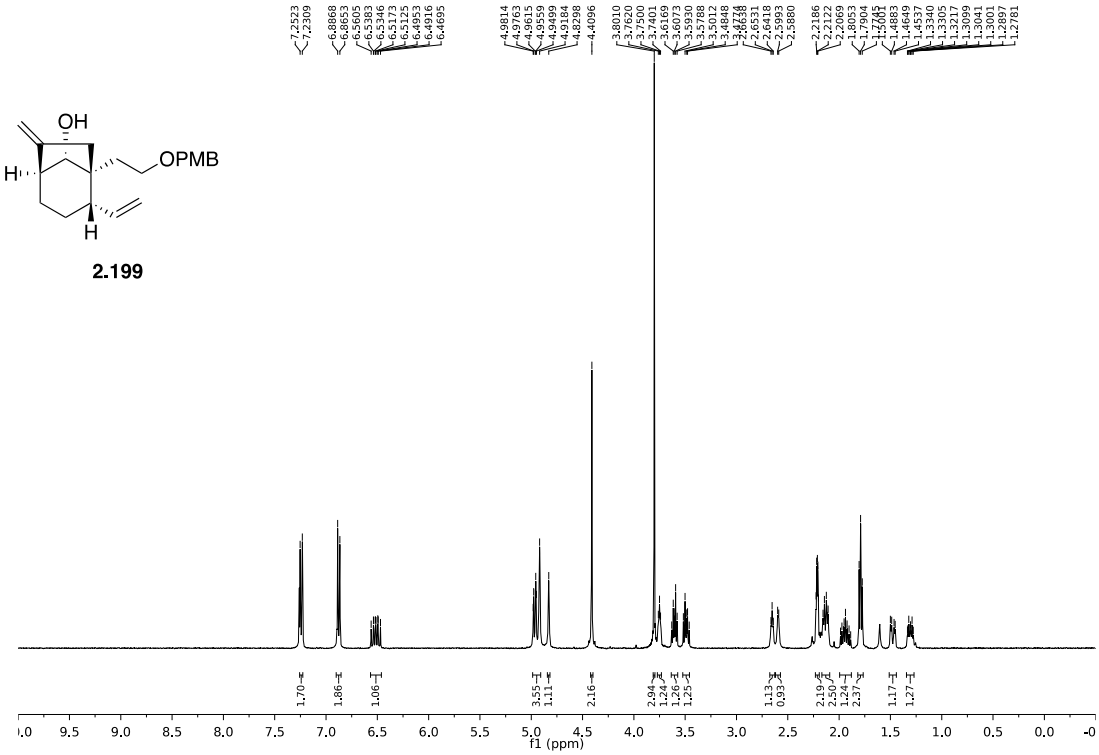
OH
OPMB
H
H
2.199
f1 (ppm)

OH
OPMB
H
H

2.199

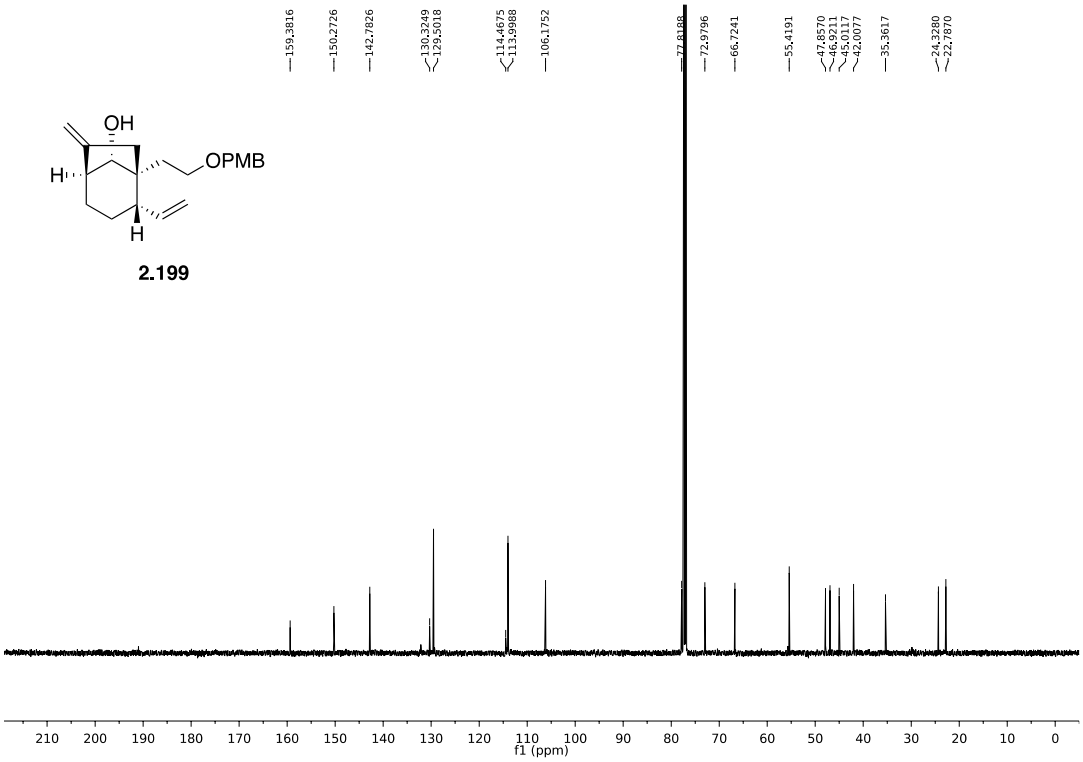
159.3816
150.2726
142.7826
130.3249
129.5018
114.4675
113.9988
106.1752
77.8188
72.9796
66.7241
55.4191
47.8570
46.9211
45.0117
42.0077
35.3617
24.3280
22.7870
f1 (ppm)

O
CO2Et

2.201

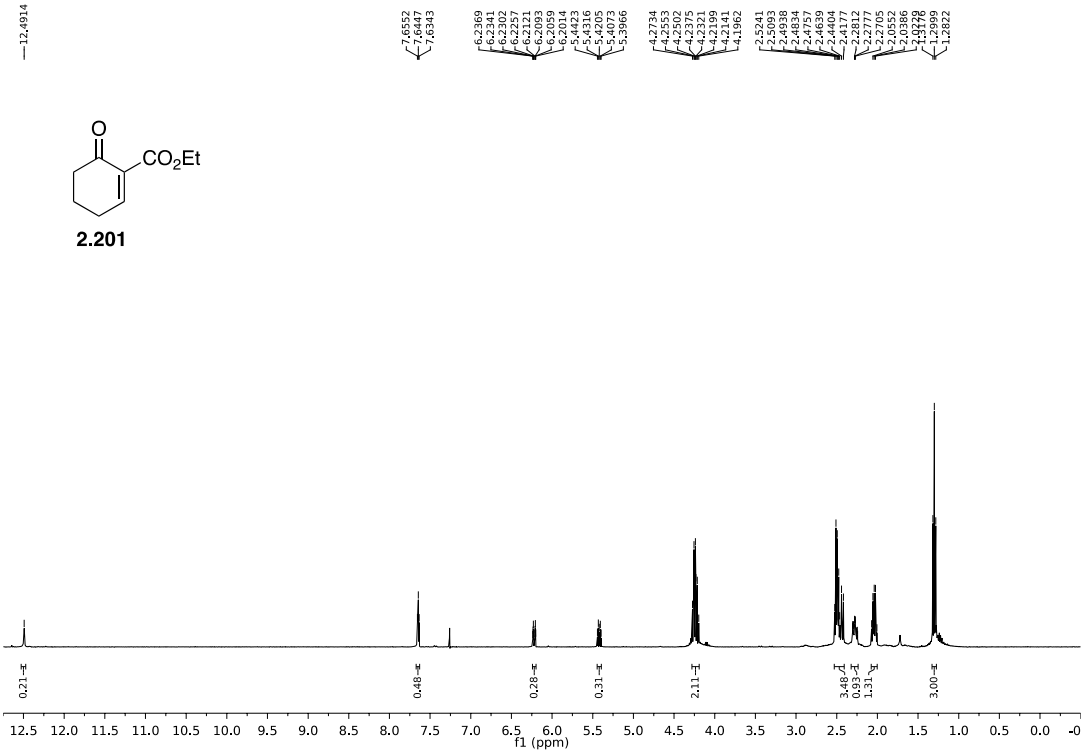
12.4914
7.6552
7.6447
7.6343
6.2369
6.2341
6.2302
6.2257
6.2121
6.2093
6.2059
6.2014
5.4423
5.4316
5.4205
5.4073
5.3966
4.2734
4.2553
4.2502
4.2375
4.2321
4.2199
4.2141
4.1962
2.5241
2.5093
2.4938
2.4834
2.4757
2.4639
2.4404
2.4177
2.2812
2.2777
2.2705
2.0552
2.0386
1.2999
1.2822
0.21
0.48
0.28
0.31
2.11
3.48
0.93
1.31
3.00
f1 (ppm)

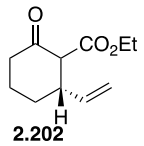

2.202

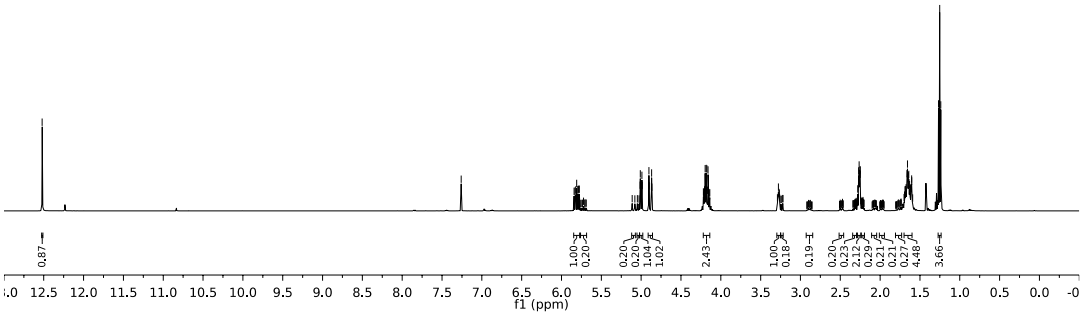

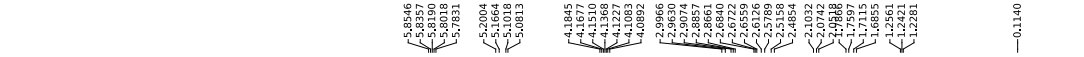

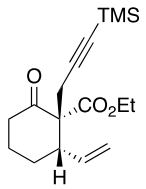

2.203

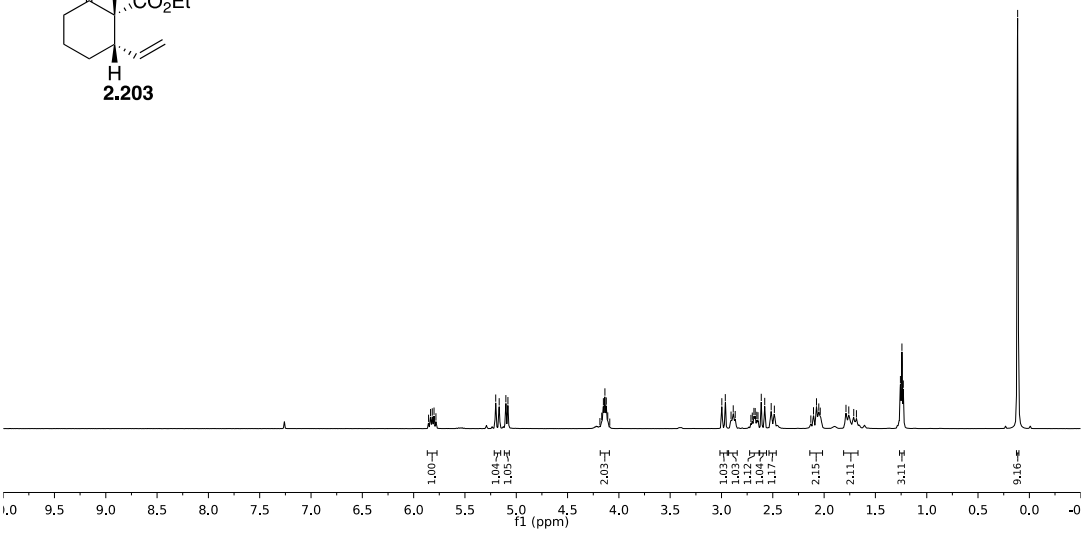

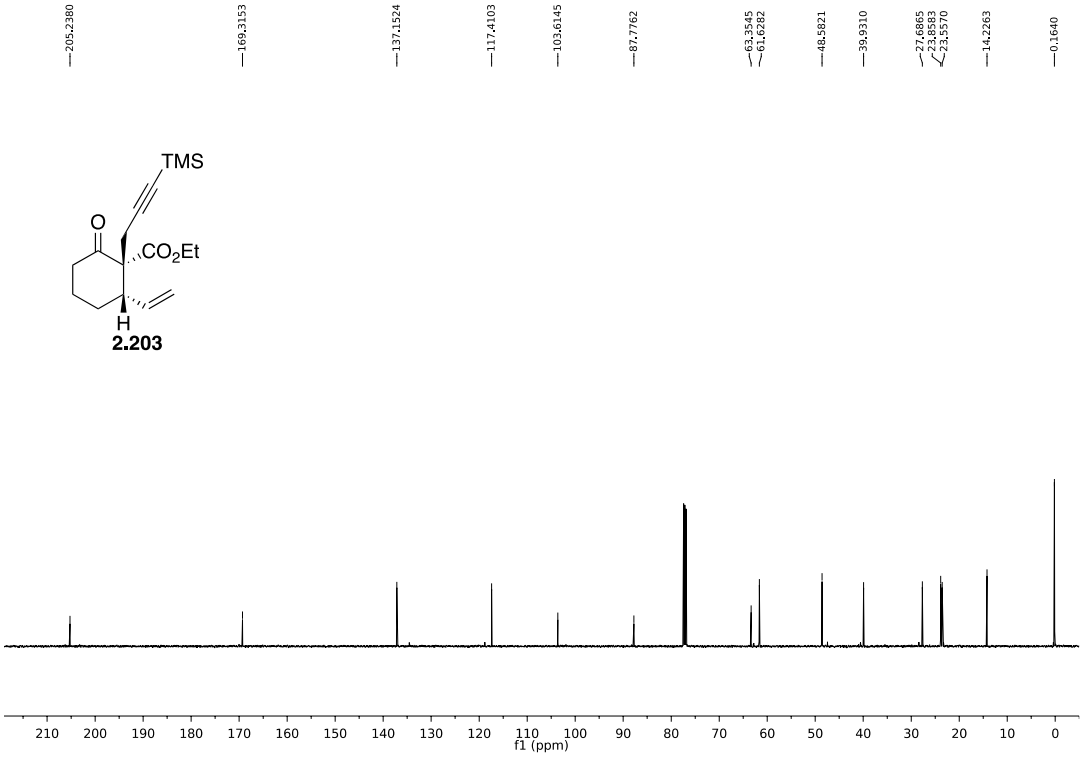
205.2380
169.3153
137.1524
117.4103
103.6145
87.7762
63.3545
61.6282
48.5821
39.9310
27.6865
23.8583
23.5570
14.2263
0.1640
TMS
O
CO2Et
H
2.203
f1 (ppm)

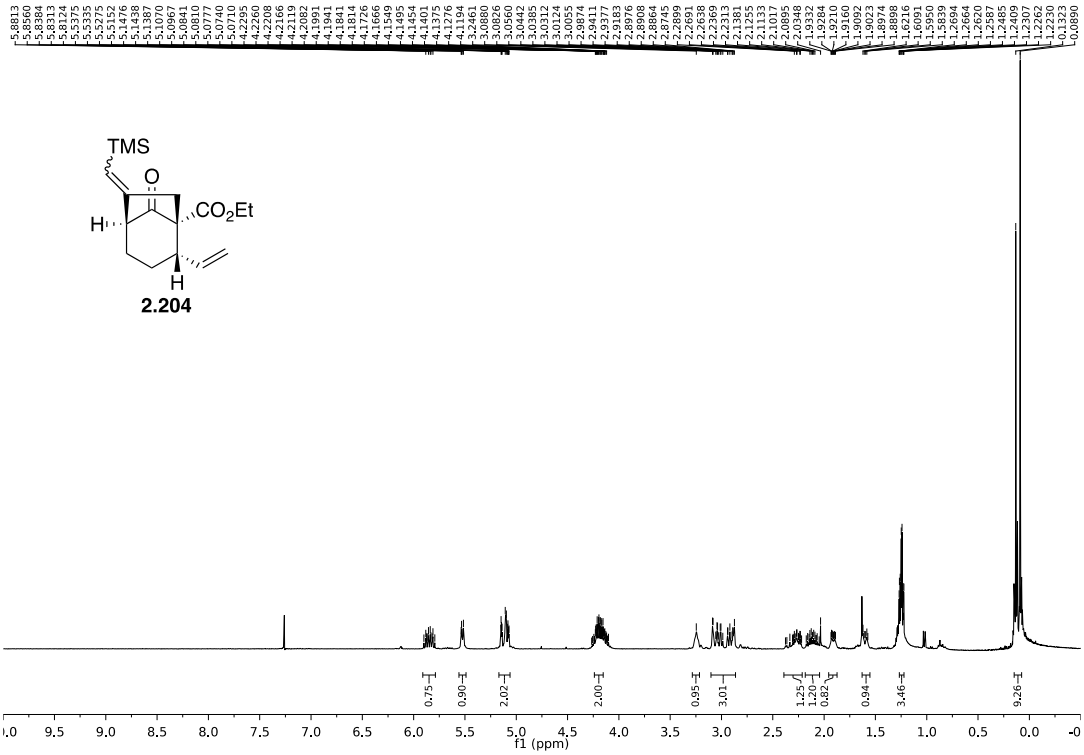
TMS
O
CO2Et
H
H
2.204
0.75
0.90
2.02
2.00
0.95
3.01
1.25
1.20
0.82
0.94
3.46
9.26
f1 (ppm)

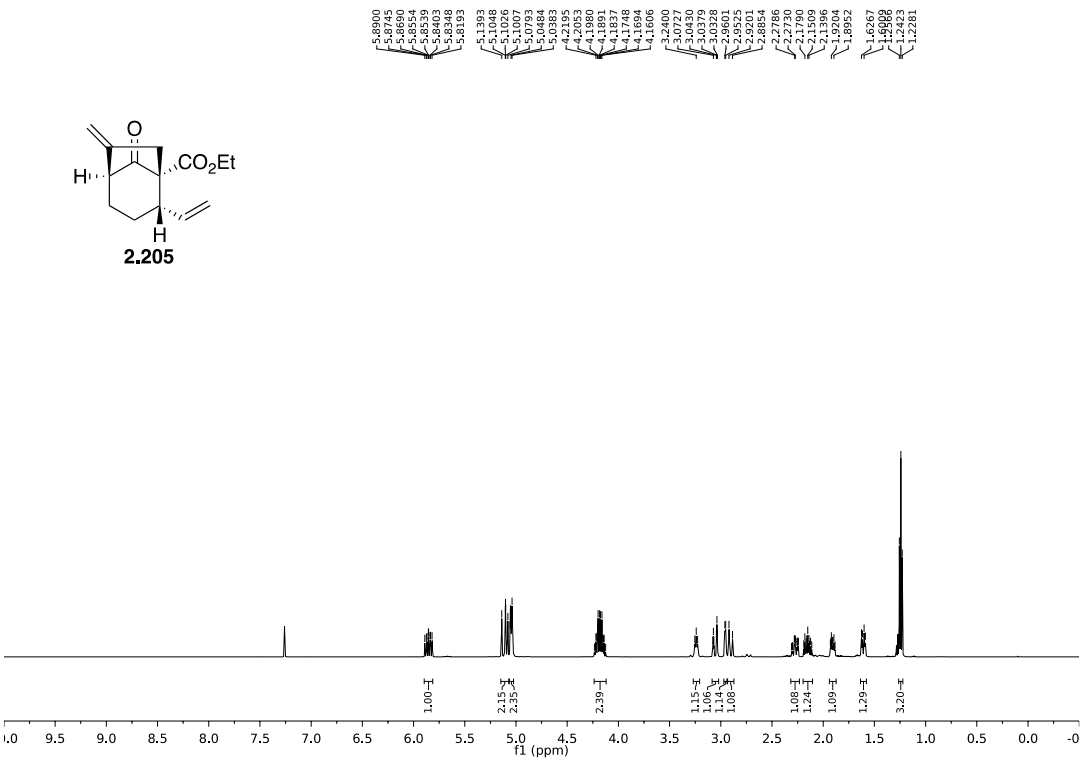
5.8900
5.8745
5.8690
5.8554
5.8539
5.8403
5.8348
5.8193
5.1393
5.1048
5.1026
5.0907
5.0793
5.0484
5.0383
4.2195
4.2053
4.1980
4.1891
4.1837
4.1748
4.1694
4.1606
3.2400
3.0727
3.0430
3.0379
3.0228
3.0201
2.9525
2.9201
2.8854
2.2786
2.2730
2.1790
2.1559
2.1396
1.9204
1.8952
1.6267
1.5969
1.5888
1.2423
1.2281
O
CO2Et
H
H
2.205
1.00
2.15
2.35
2.39
1.15
1.06
1.14
1.08
1.08
1.24
1.09
1.29
3.20
9.5
9.0
8.5
8.0
7.5
7.0
6.5
6.0
5.5
5.0
4.5
4.0
3.5
3.0
2.5
2.0
1.5
1.0
0.5
0.0
f1 (ppm)

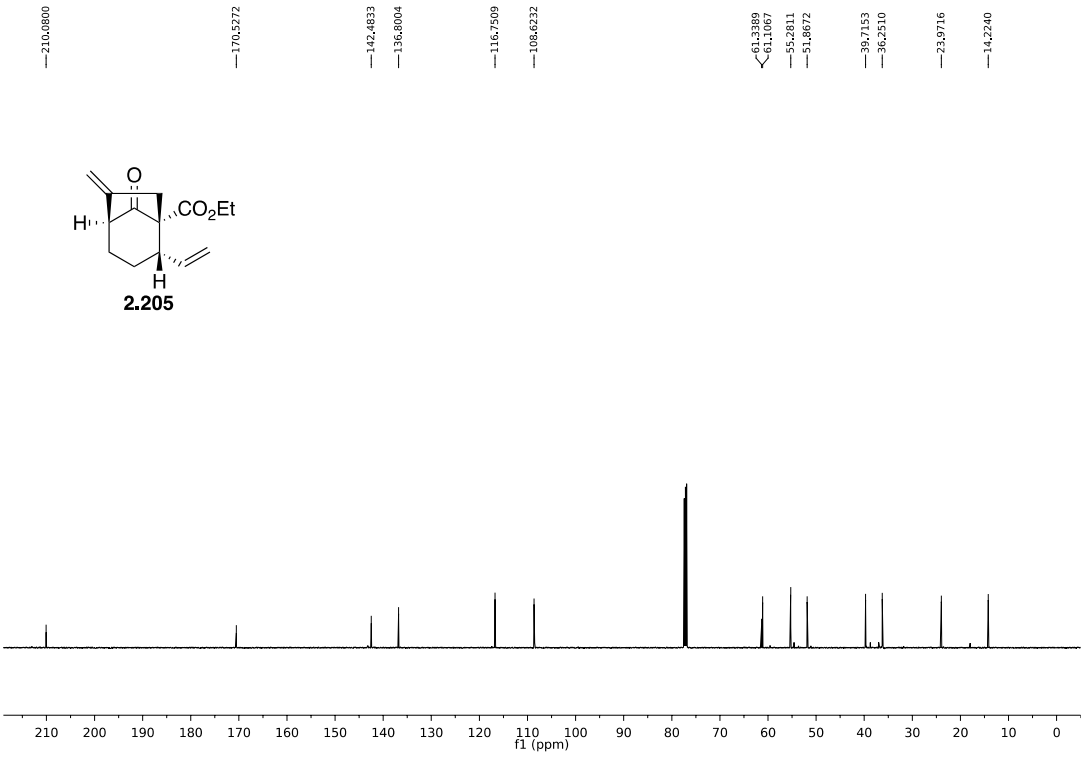
210.0800
170.5272
142.4833
136.8004
116.7509
108.6232
61.3389
61.1067
55.2811
51.8672
39.7153
36.2510
23.9716
14.2240
O
CO2Et
H
H
2.205
210
200
190
180
170
160
150
140
130
120
110
100
90
80
70
60
50
40
30
20
10
0
f1 (ppm)

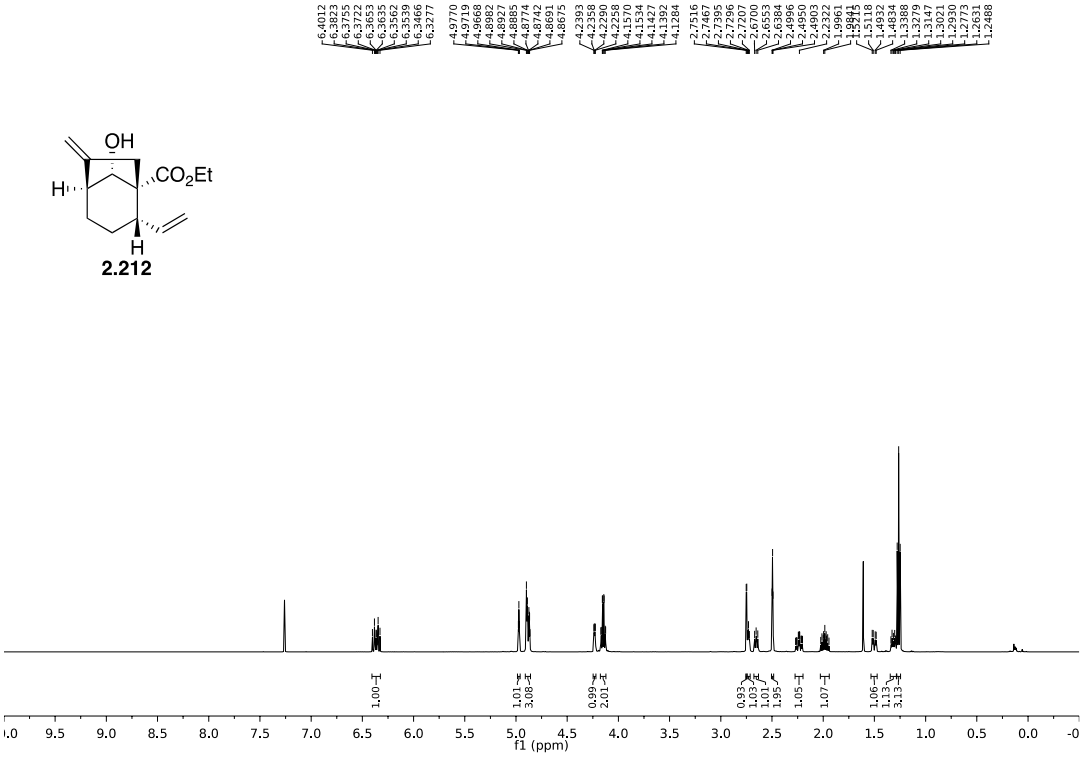
OH
CO2Et
H
H
2.212
f1 (ppm)

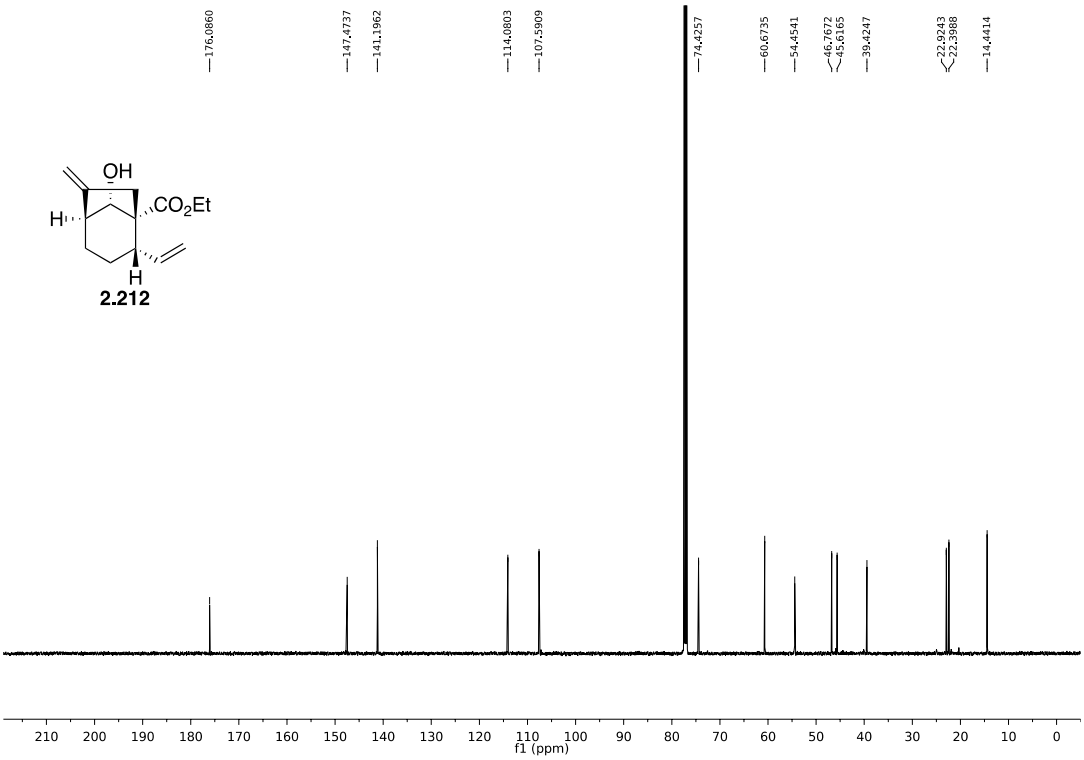
OH
CO2Et
H
H
2.212
f1 (ppm)

2.216

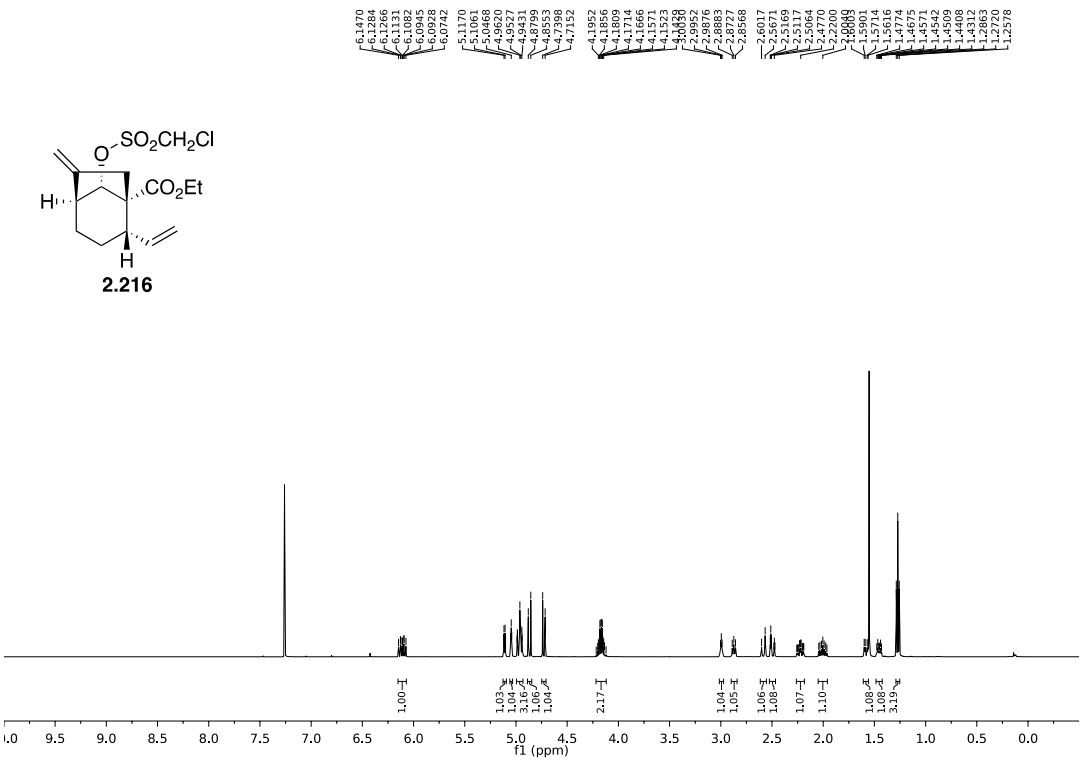

2.211

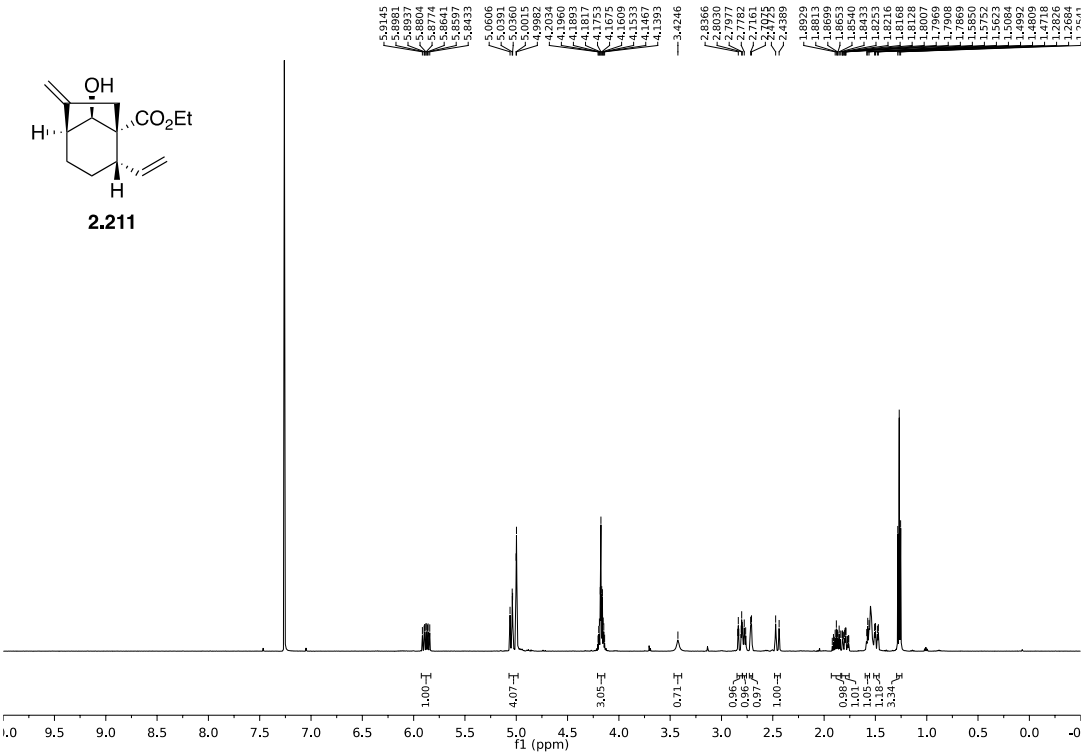

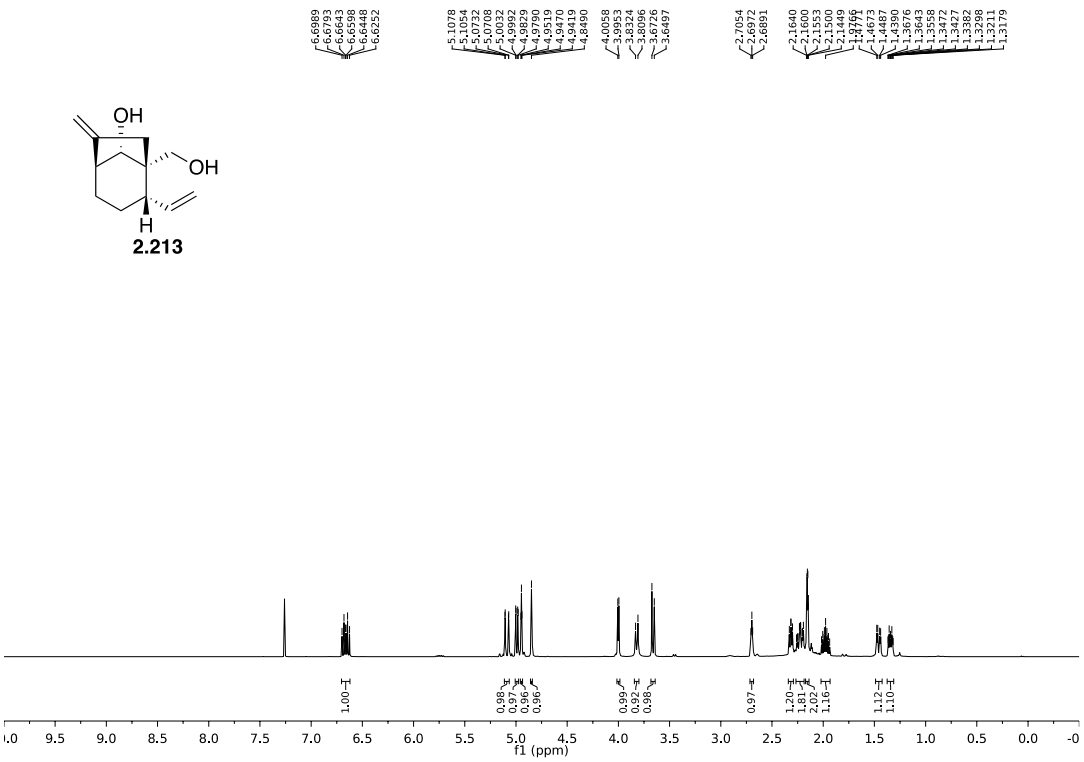
OH
OH
H
2.213
f1 (ppm)

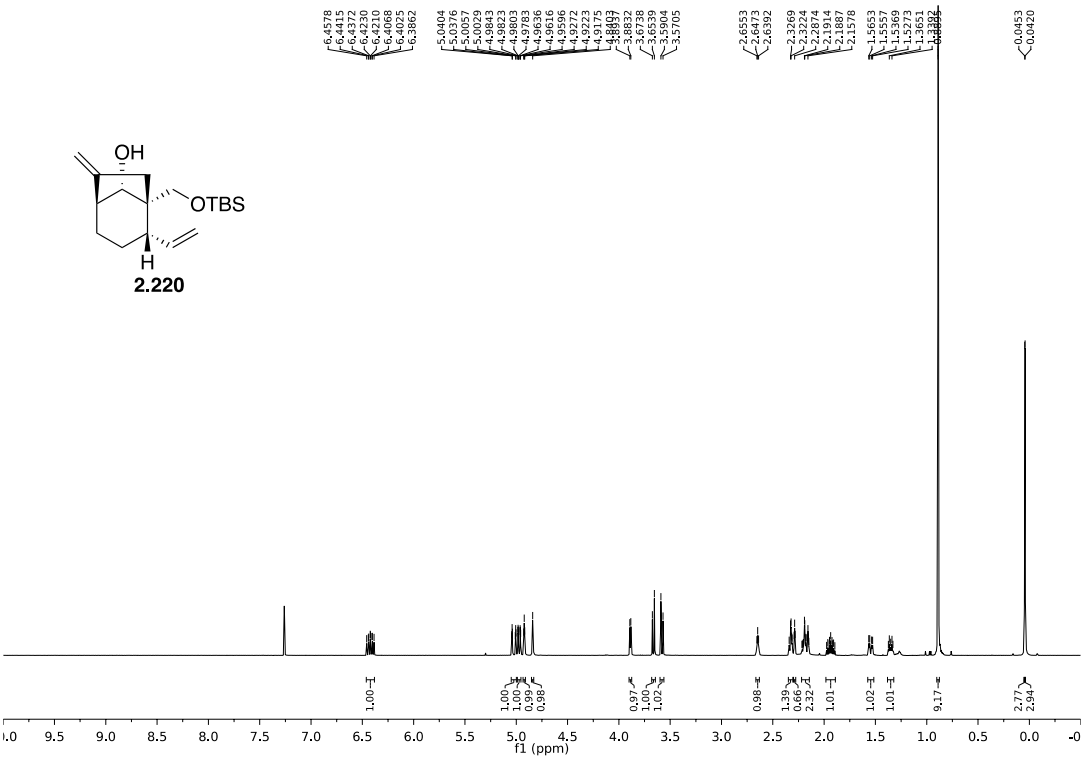
OH
OTBS
H
2.220
f1 (ppm)

S2.1

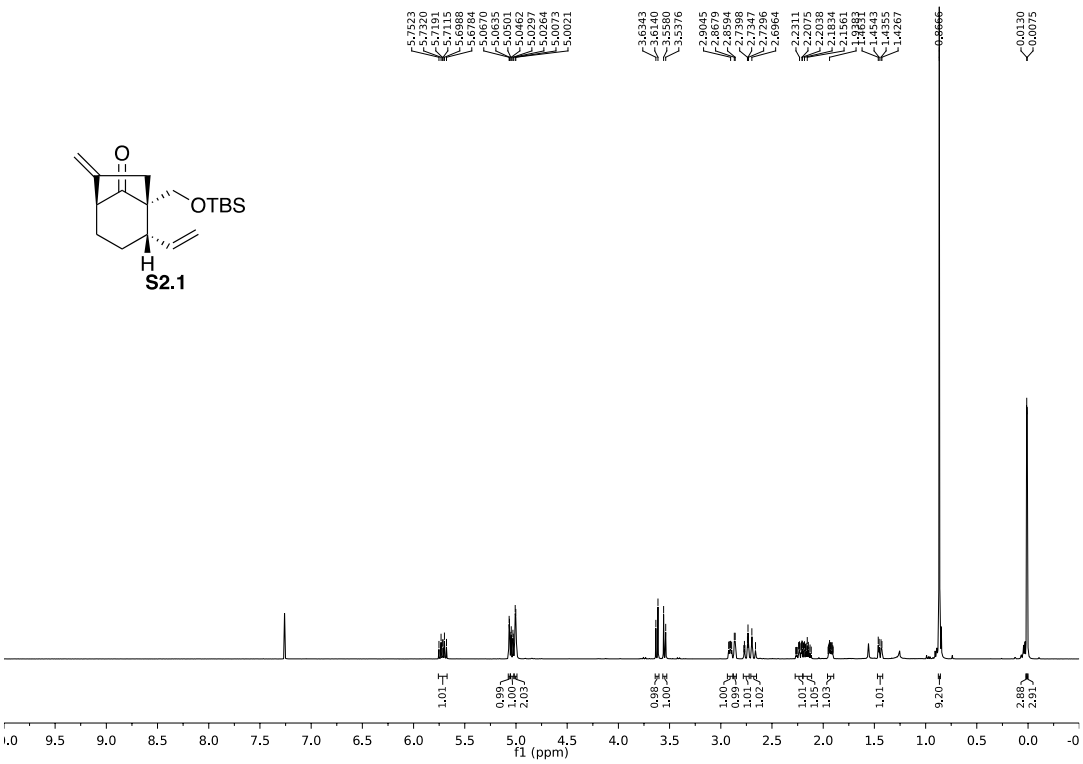

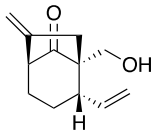

2.218

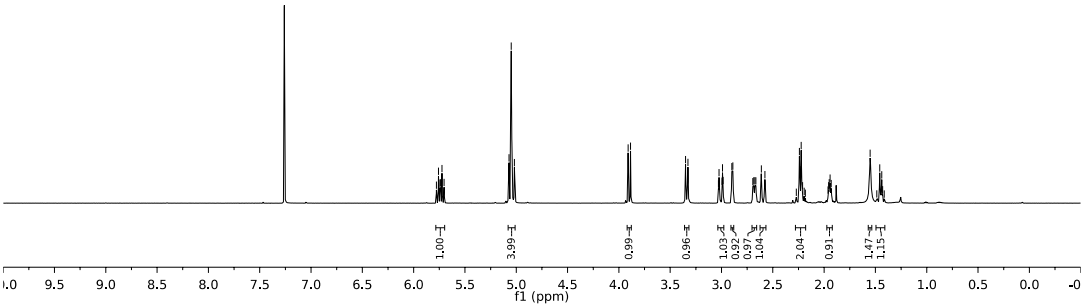

Appendix B. Spectral Data for Chapter 3

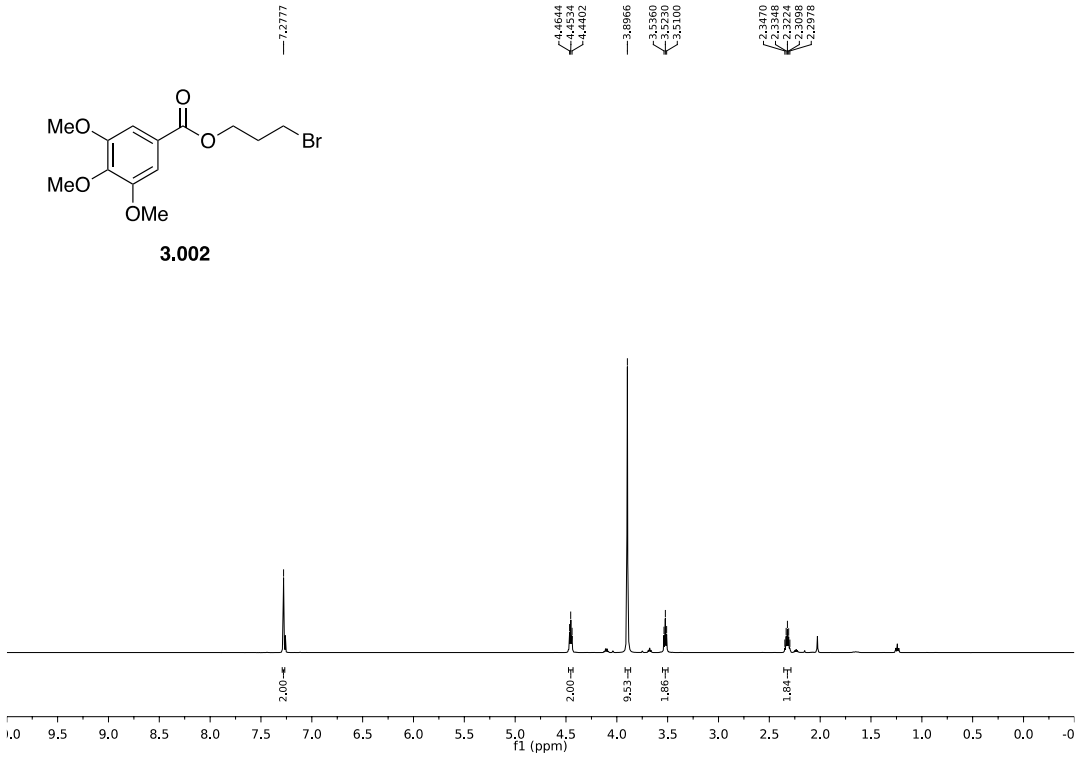

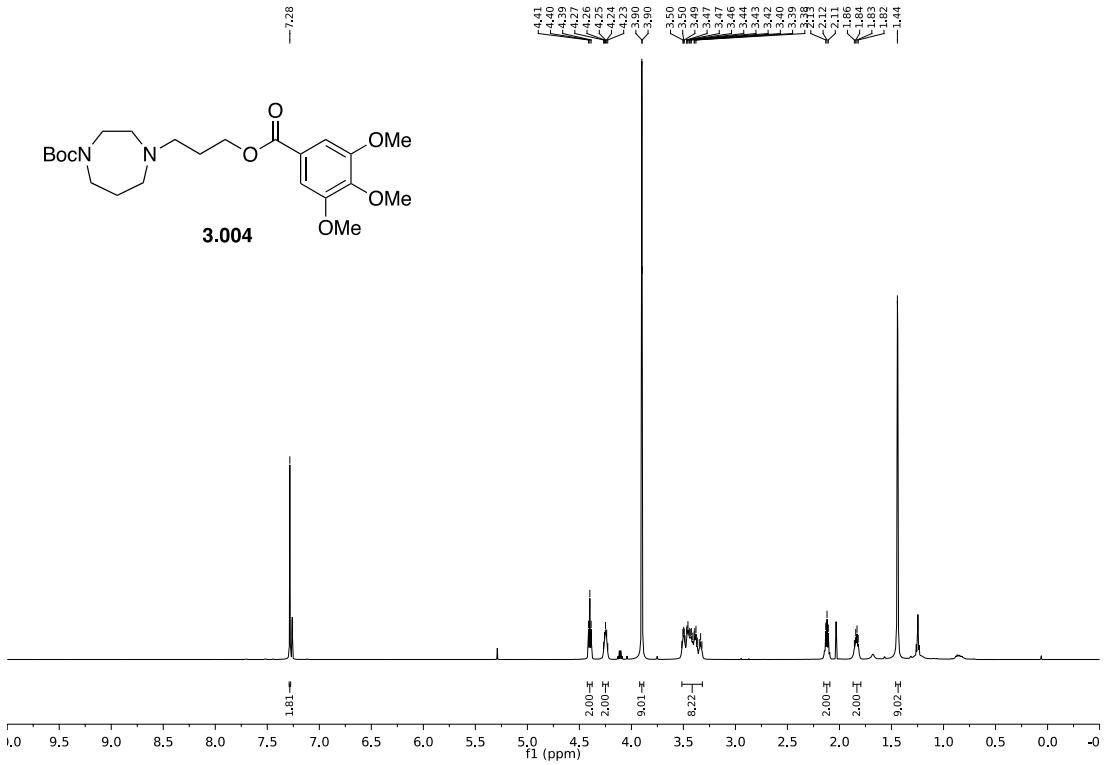

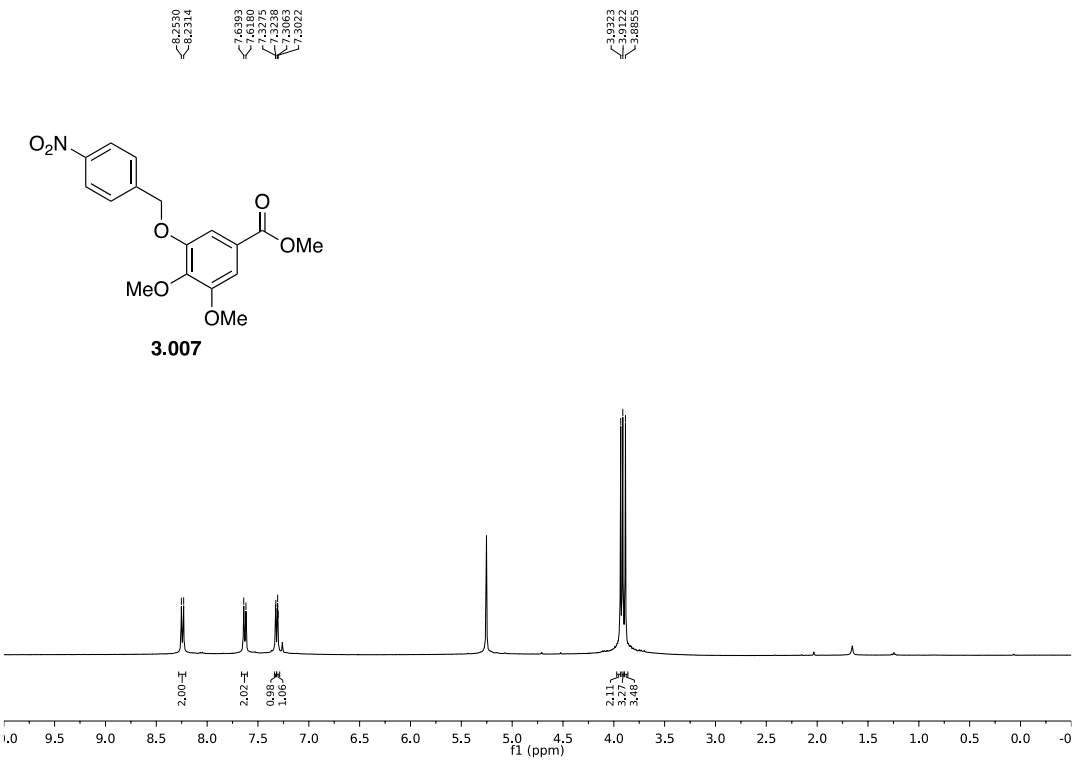
8.2530
8.2314
7.6393
7.6180
7.3275
7.3238
7.3063
7.3022
3.9323
3.9122
3.8895
O2N
O
O
OMe
MeO
OMe
3.007
2.00
2.02
0.98
1.06
2.11
3.27
3.48
f1 (ppm)

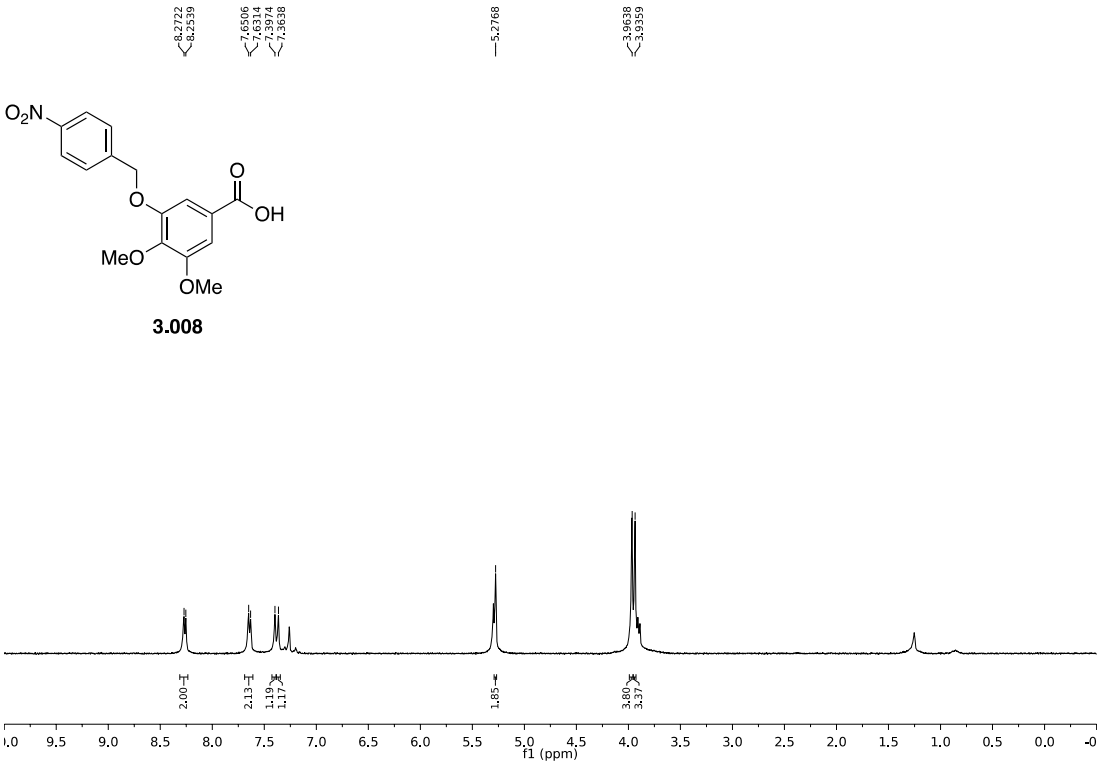
8.2722
8.2539
7.6506
7.6314
7.3914
7.3638
5.2768
3.9638
3.9359
O2N
O
O
OH
MeO
OMe
3.008
2.00
2.13
1.19
1.17
1.85
3.80
3.37
f1 (ppm)

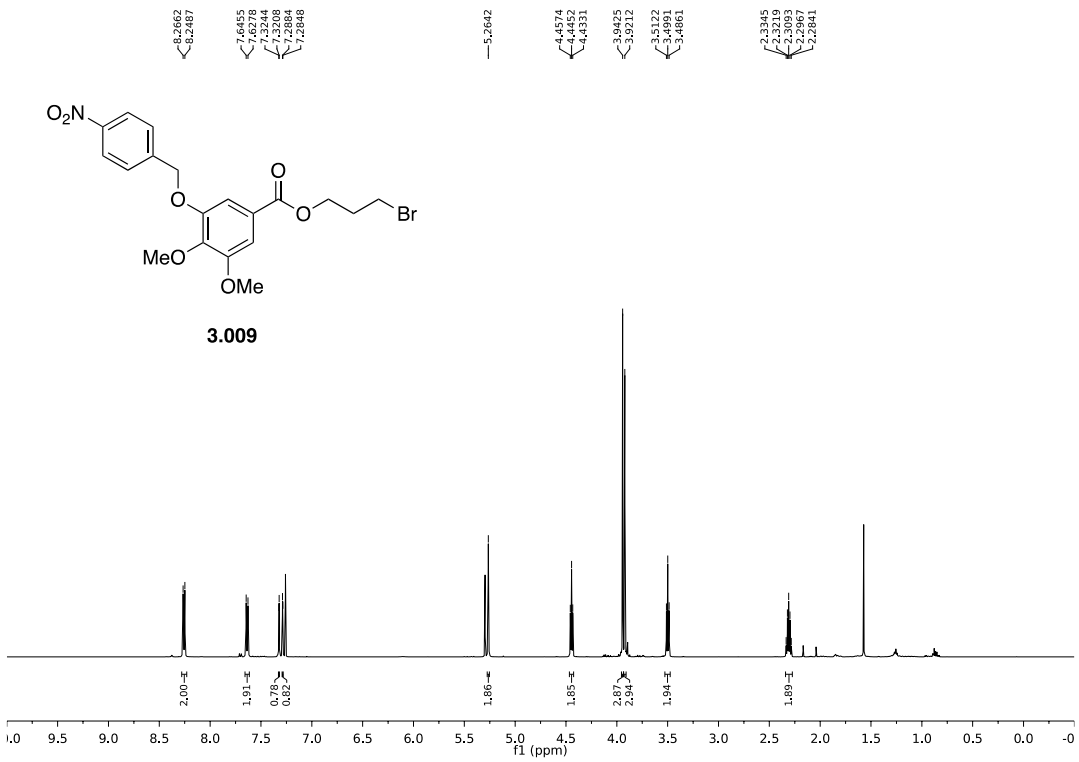
3.009
f1 (ppm)

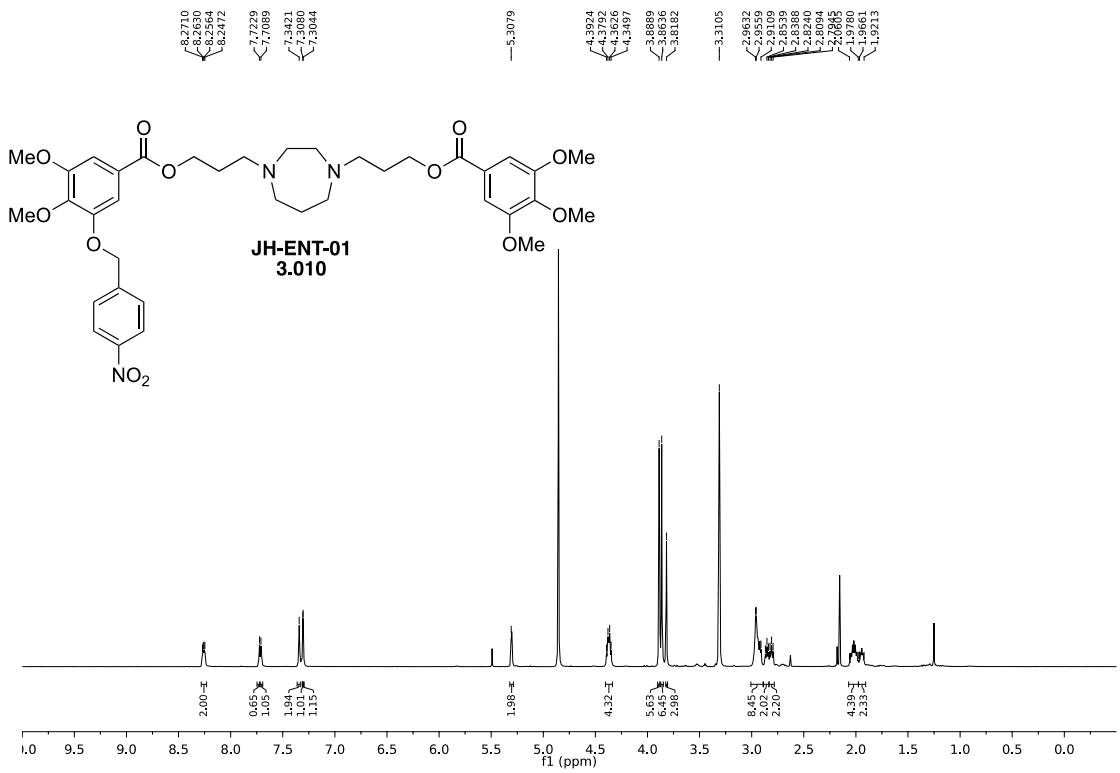
JH-ENT-01
3.010
f1 (ppm)

3.012

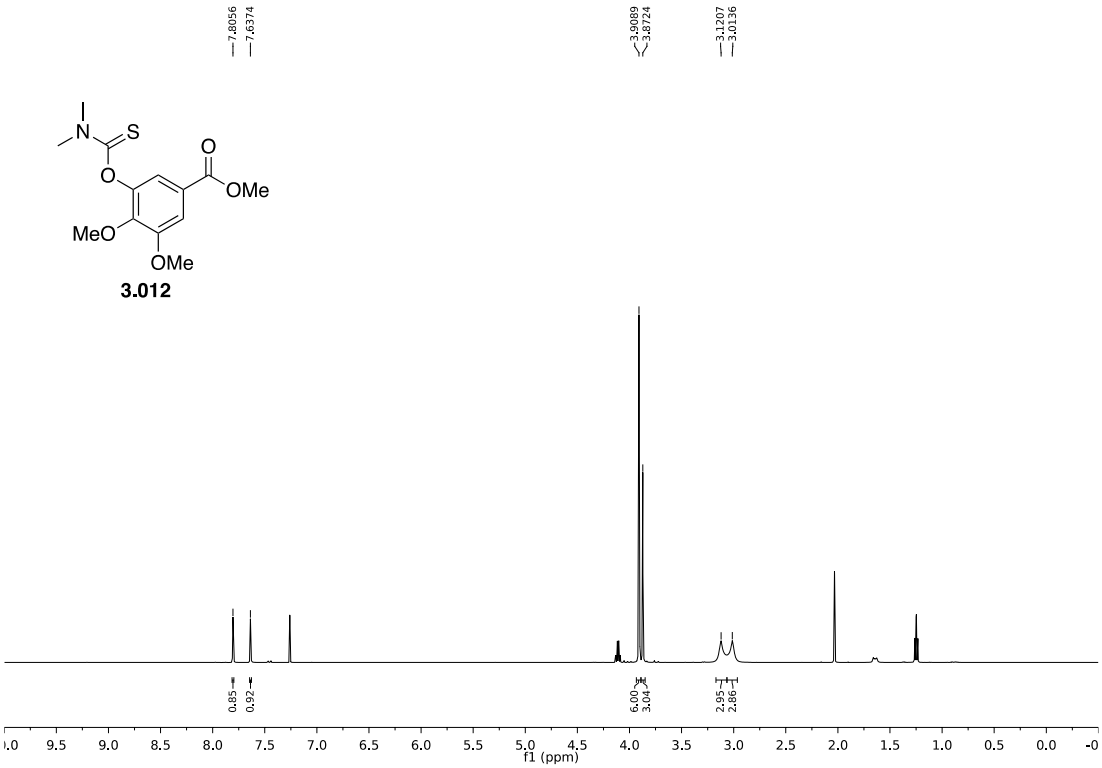
7.8056
7.6374
3.9089
3.8724
3.1207
3.0136
0.85
0.92
6.00
3.04
2.95
2.86
f1 (ppm)

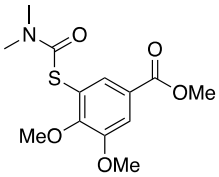

3.013

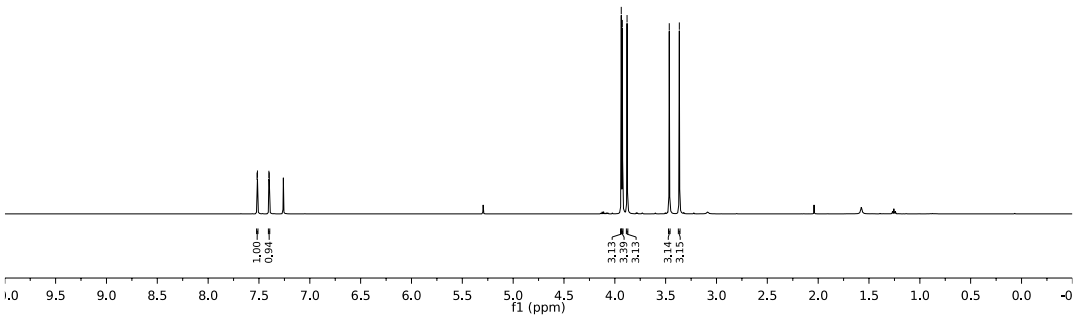
7.5184
7.5148
7.4022
7.3985
3.9366
3.9262
3.8794
3.4643
3.3660
1.00
0.94
3.13
3.39
3.13
3.14
3.15
f1 (ppm)

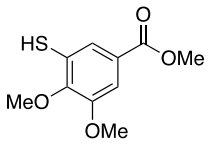

3.014

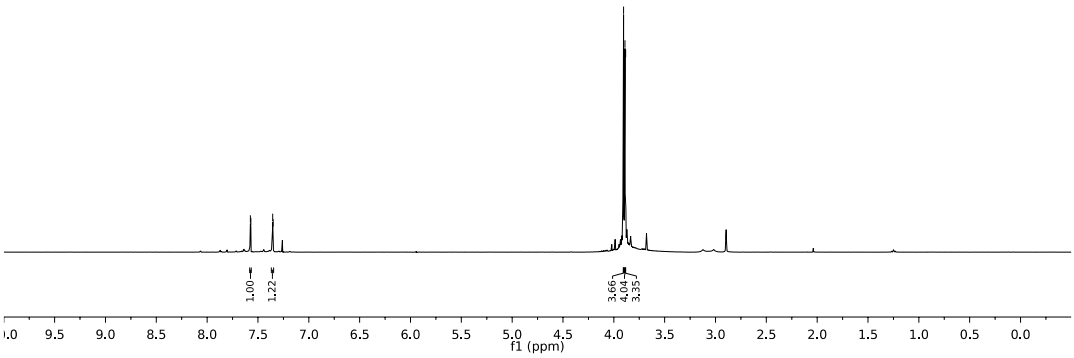
7.5745
7.5702
7.3553
7.3510
3.9043
3.8908
3.8837
1.00
1.22
3.66
4.04
3.35
f1 (ppm)

3.015

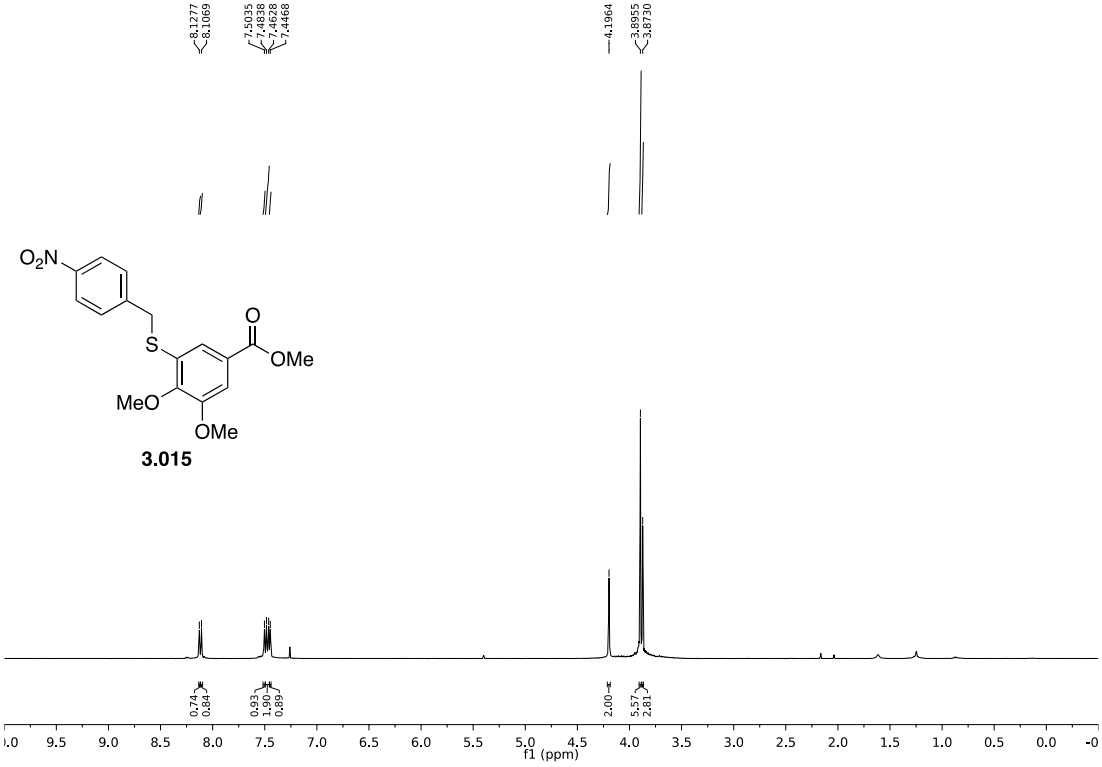
8.1277
8.1069
7.5035
7.4838
7.4628
7.4468
4.1964
3.8955
3.8730
0.74
0.84
0.93
1.90
0.89
2.00
5.57
2.81
f1 (ppm)

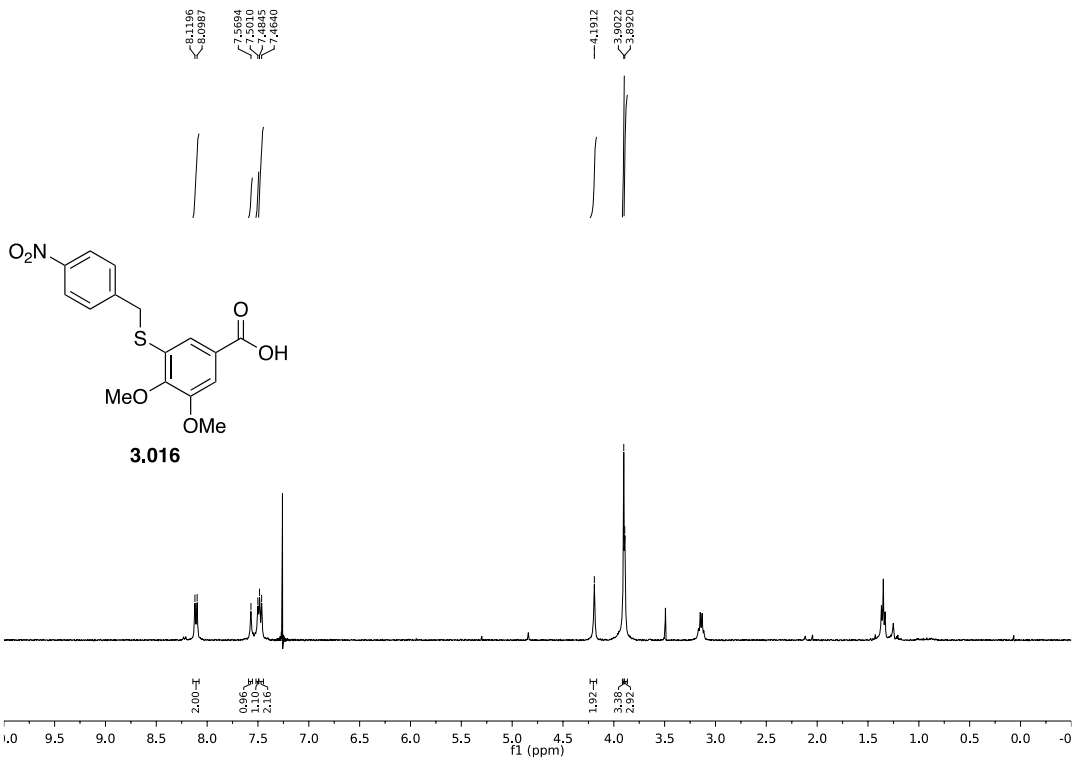
8.1196
8.0987
7.5694
7.5010
7.4845
7.4640
4.1912
3.9022
3.8920
O2N
S
O
OH
MeO
OMe
3.016
2.00
0.96
1.10
2.16
1.92
3.38
2.92
f1 (ppm)

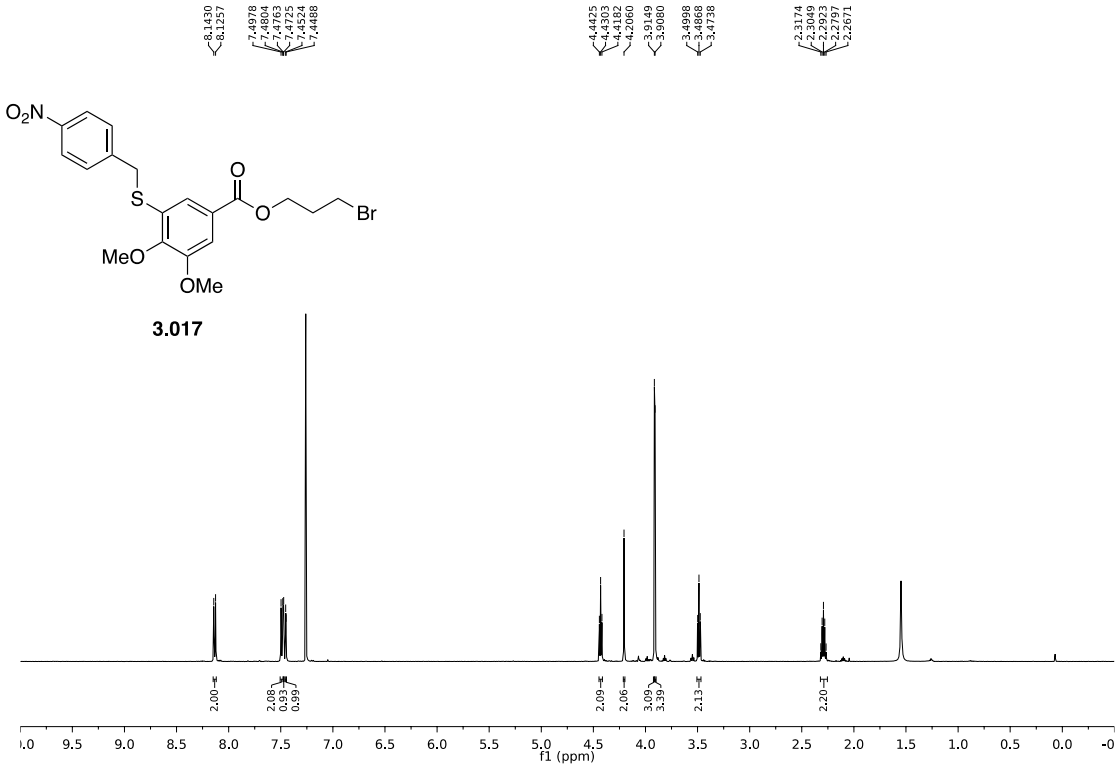
8.1430
8.1257
7.4978
7.4804
7.4763
7.4725
7.4534
7.4488
4.4425
4.4303
4.4182
4.2060
3.9149
3.9080
3.4998
3.4868
3.4738
2.3174
2.3049
2.2923
2.2797
2.2671
O2N
S
O
O
Br
MeO
OMe
3.017
2.00
2.08
0.93
0.99
2.09
2.06
3.09
3.39
2.13
2.20
f1 (ppm)

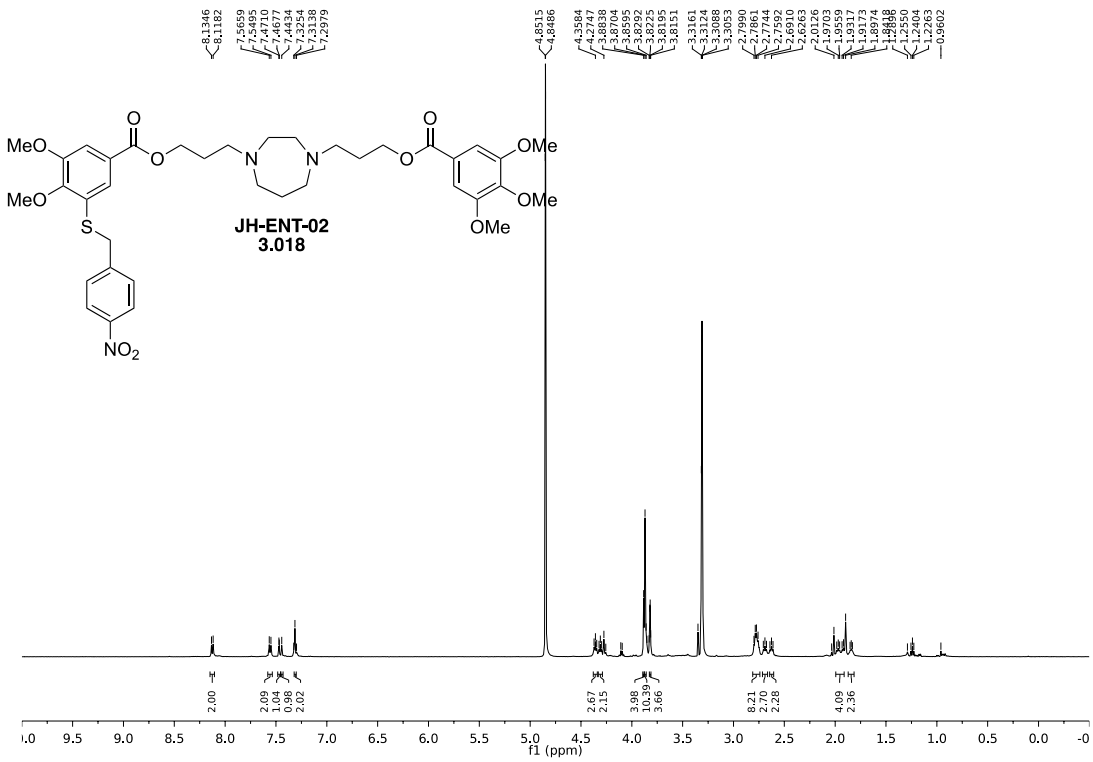
JH-ENT-02
3.018
f1 (ppm)

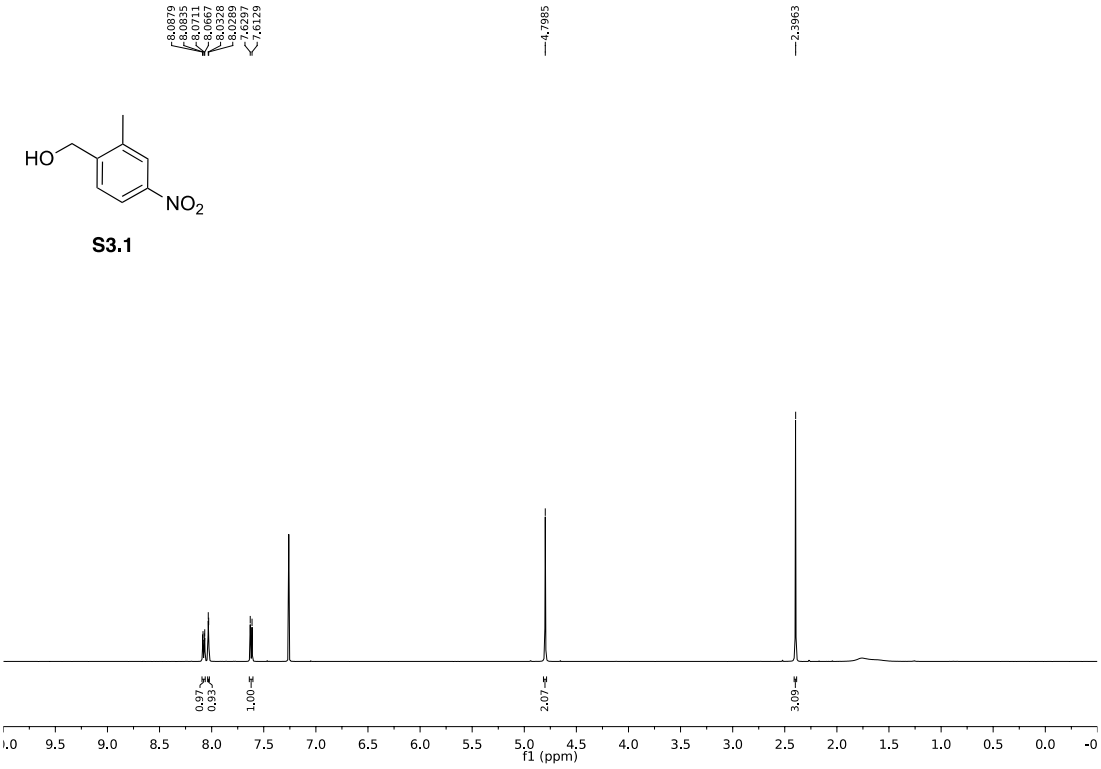
S3.1
f1 (ppm)

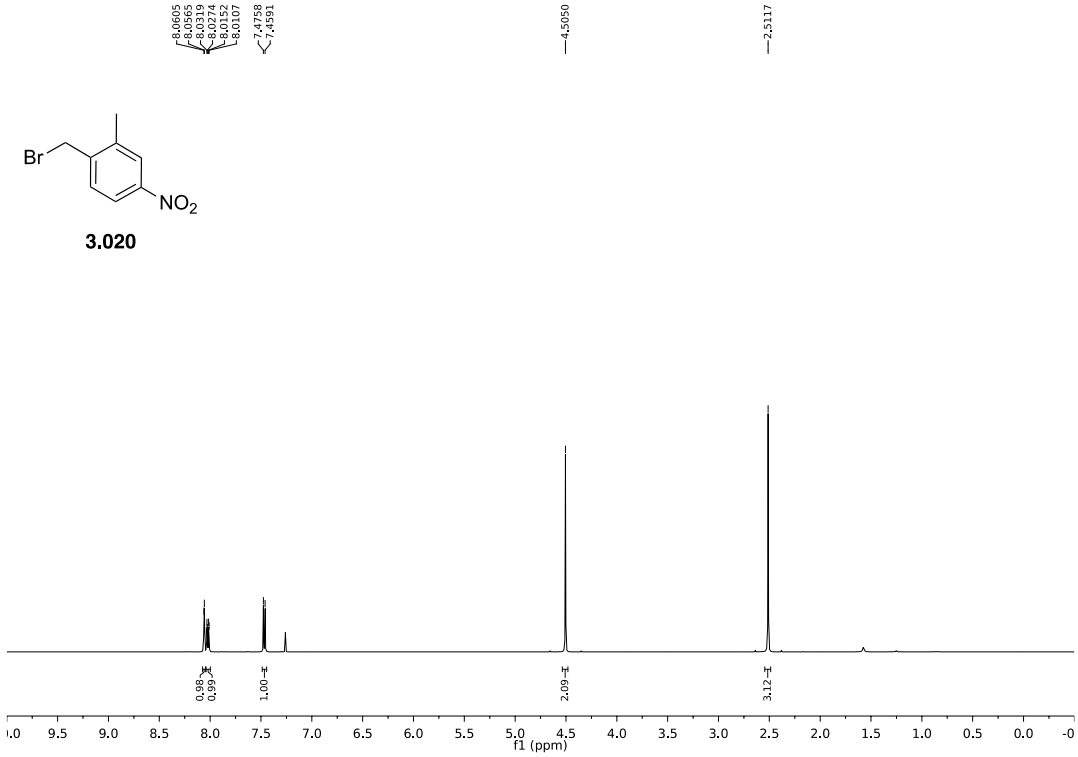
8.0605
8.0565
8.0319
8.0274
8.0152
8.0107
7.4758
7.4591
4.5050
2.5117
Br
NO2
3.020
0.98
0.99
1.00
2.09
3.12
f1 (ppm)

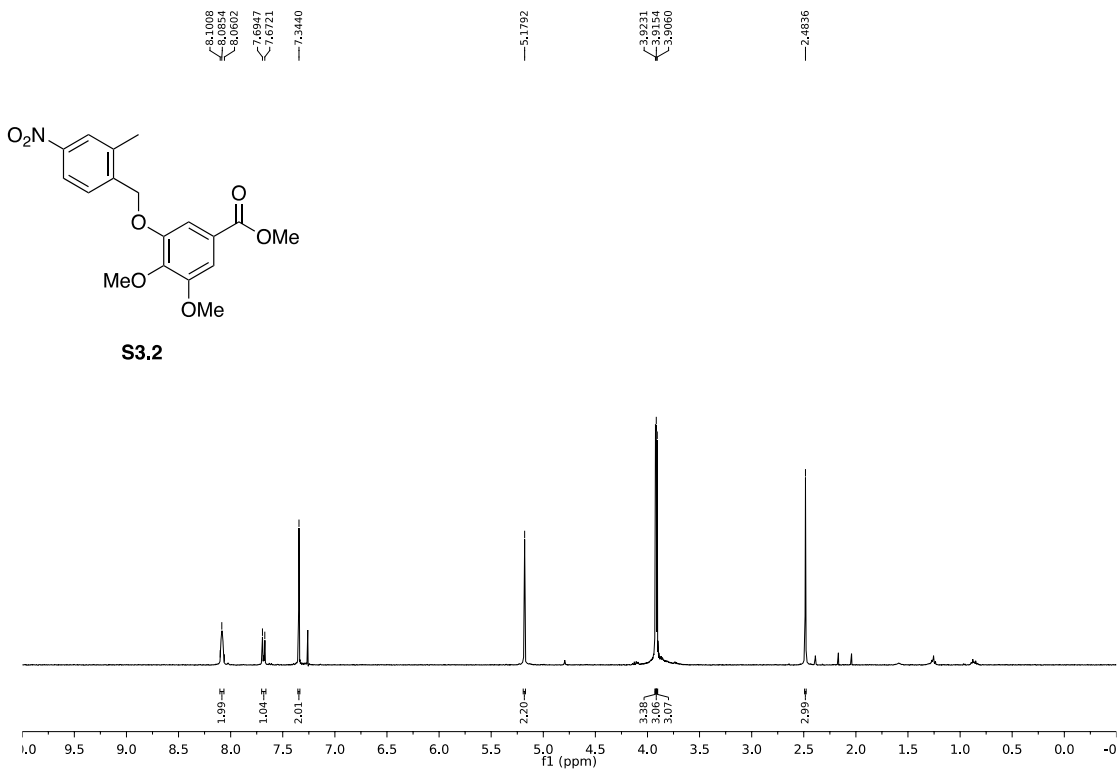
8.1008
8.0854
8.0602
7.6947
7.6721
7.3440
5.1792
3.9231
3.9154
3.9060
2.4836
O2N
O
O
OMe
MeO
OMe
S3.2
1.99
1.04
2.01
2.20
3.38
3.06
3.07
2.99
f1 (ppm)

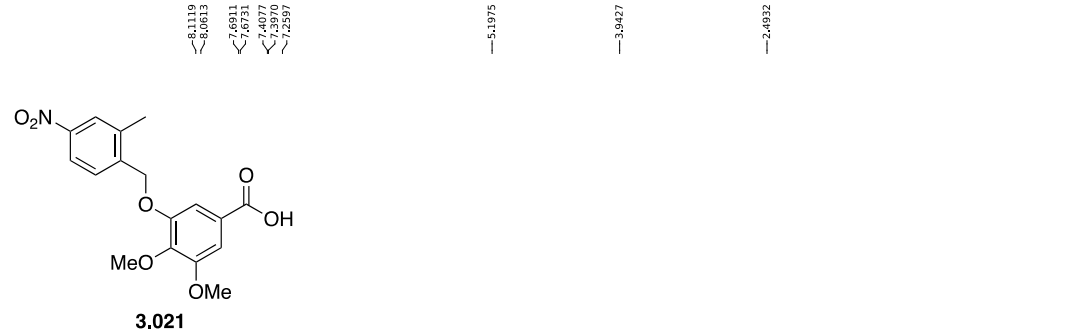
8.1119
8.0613
7.6911
7.6731
7.4077
7.3970
7.2597
5.1975
3.9427
2.4932
O2N
O
O
OH
MeO
OMe
2.00
0.89
0.84
0.88
1.86
5.46
2.74
f1 (ppm)

3.021

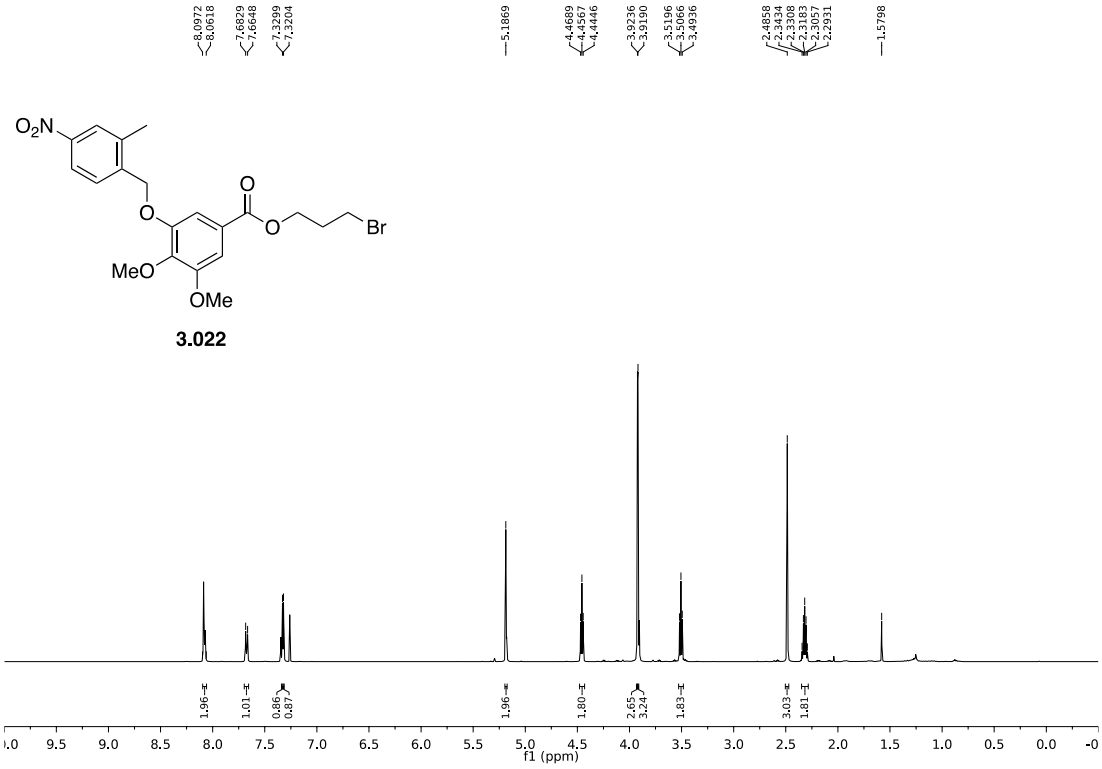
8.0972
8.0618
7.6829
7.6648
7.3299
7.3204
5.1869
4.4689
4.4567
4.4446
3.9236
3.9190
3.5196
3.5066
3.4936
2.4858
2.3434
2.3308
2.3190
2.3133
2.3057
2.2931
1.5798
O2N
O
O
O
Br
MeO
OMe
1.96
1.01
0.86
0.87
1.96
1.80
2.65
3.24
1.83
3.03
1.81
f1 (ppm)

3.022

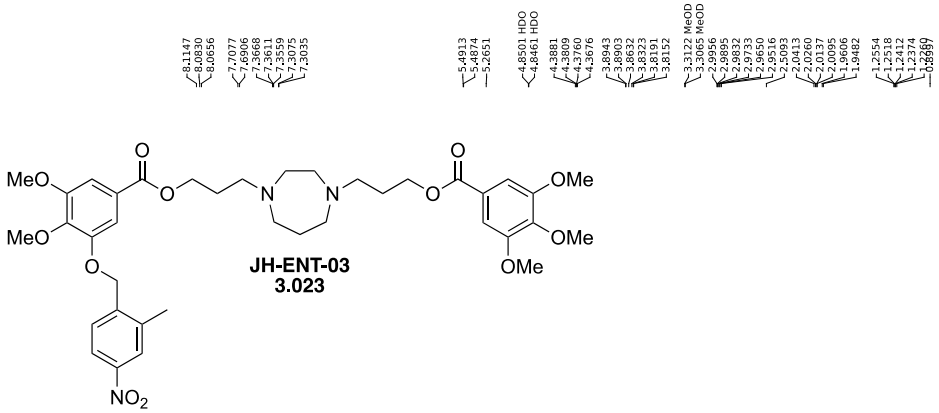
MeO
MeO
O
O
N
N
O
O
OMe
OMe
OMe
O
NO2
JH-ENT-03
3.023

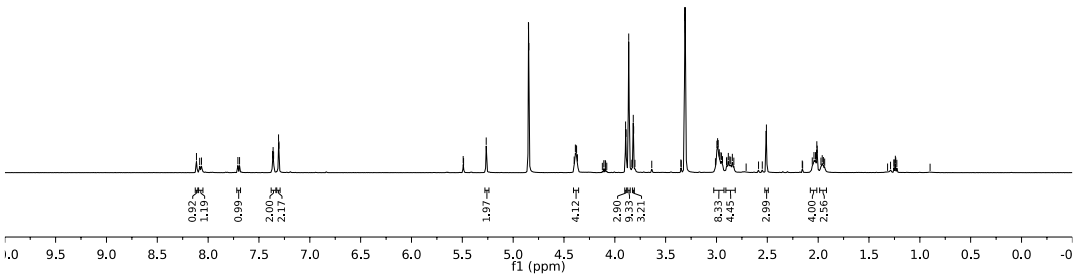
f1 (ppm)

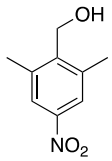
OH
NO2

3.029

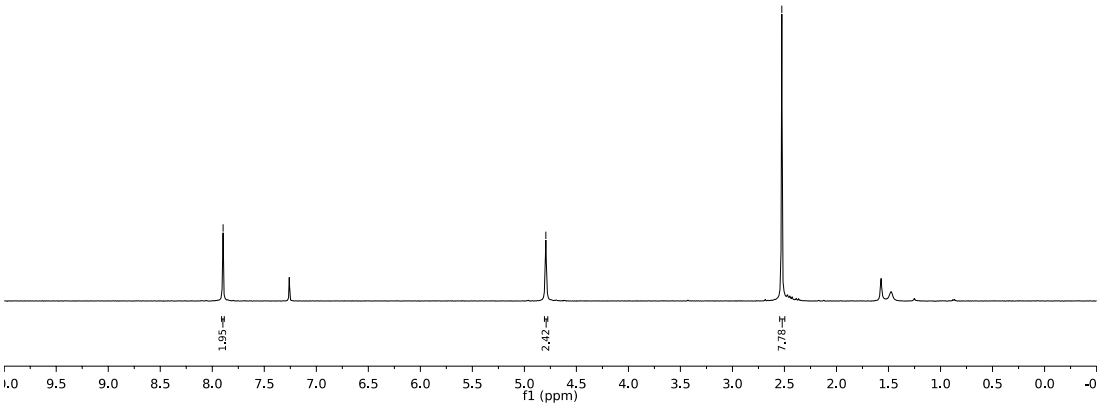
f1 (ppm)

Br
NO2

3.030

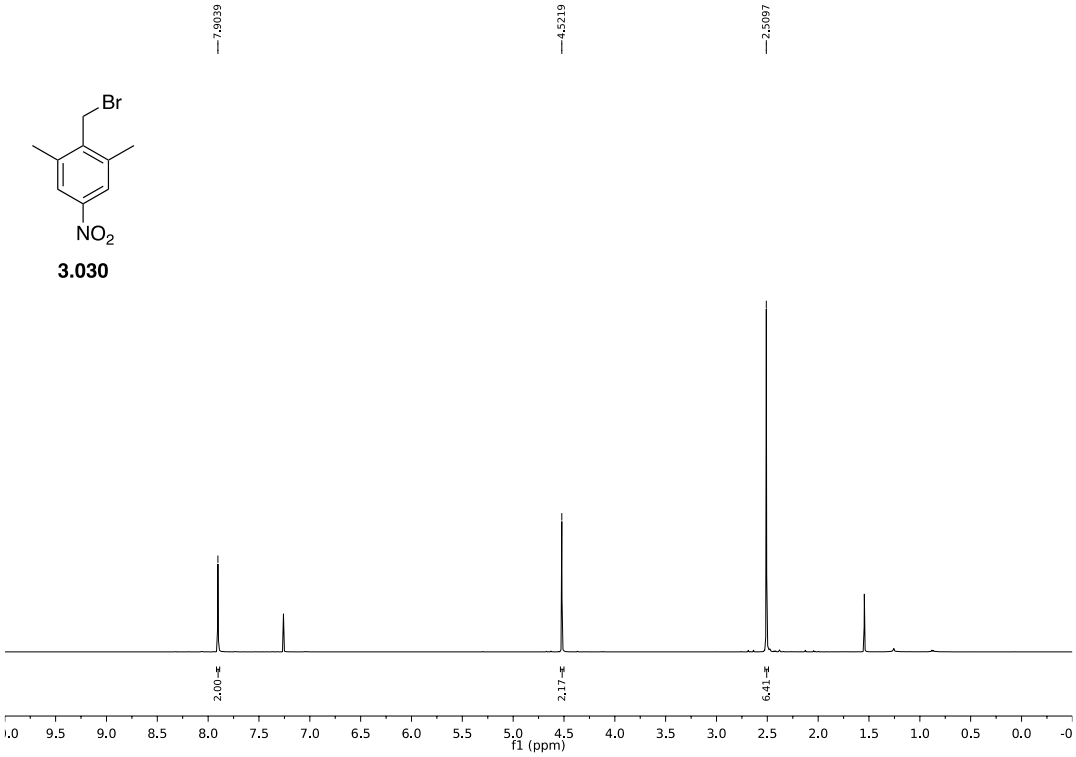
7.9039
4.5219
2.5097
2.00
2.17
6.41
f1 (ppm)

O2N
O
O
OMe
MeO
OMe

S3.4

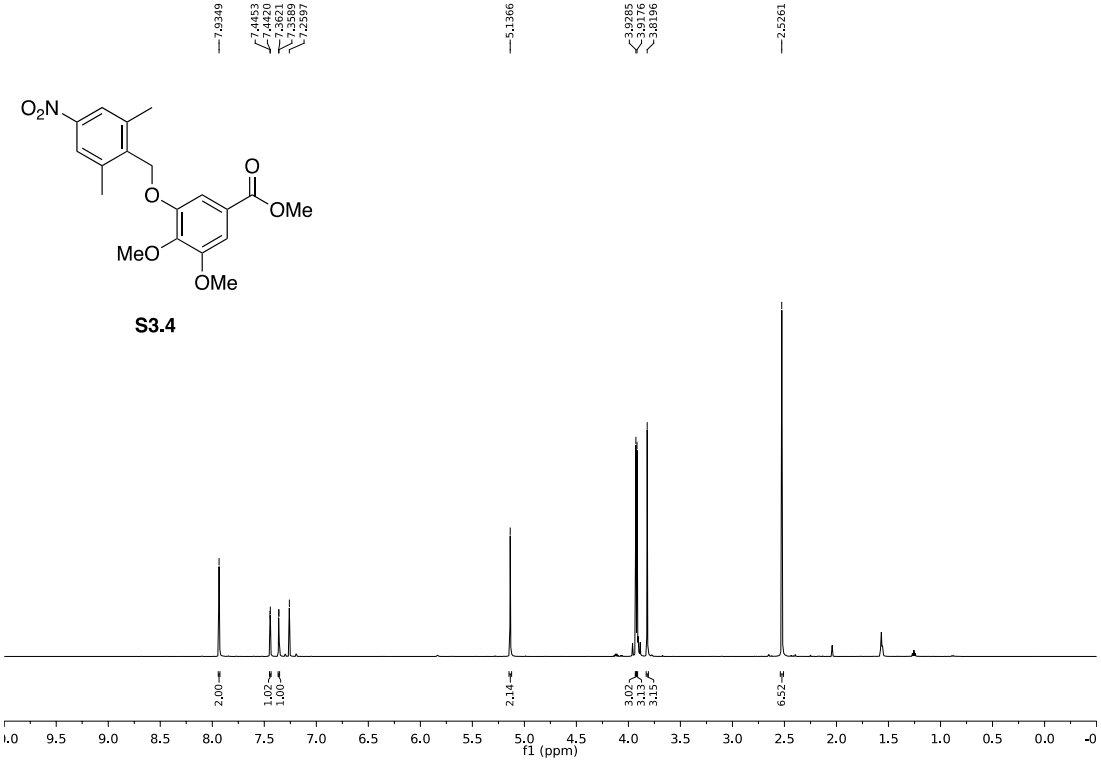
7.9349
7.4453
7.4420
7.3621
7.3589
7.2597
5.1366
3.9285
3.9176
3.8196
2.5261
2.00
1.02
1.00
2.14
3.02
3.13
3.15
6.52
f1 (ppm)

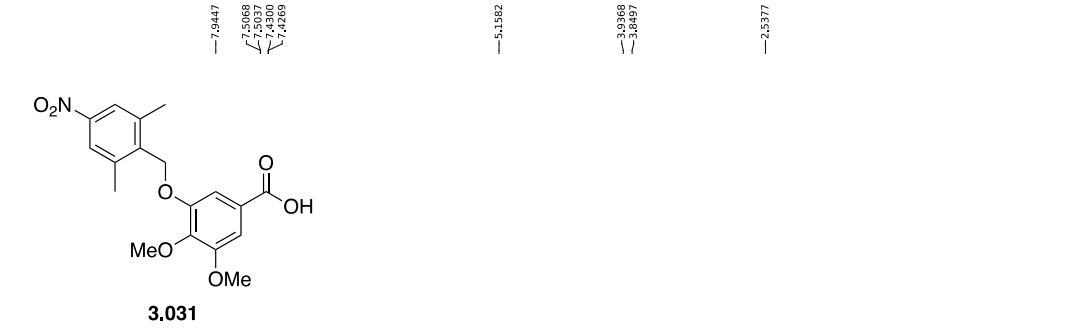
7.9447
7.5068
7.5037
7.4300
7.4269
5.1582
3.9368
3.8497
2.5377
2.00
0.99
1.00
2.00
3.13
3.02
6.15
f1 (ppm)

3.031

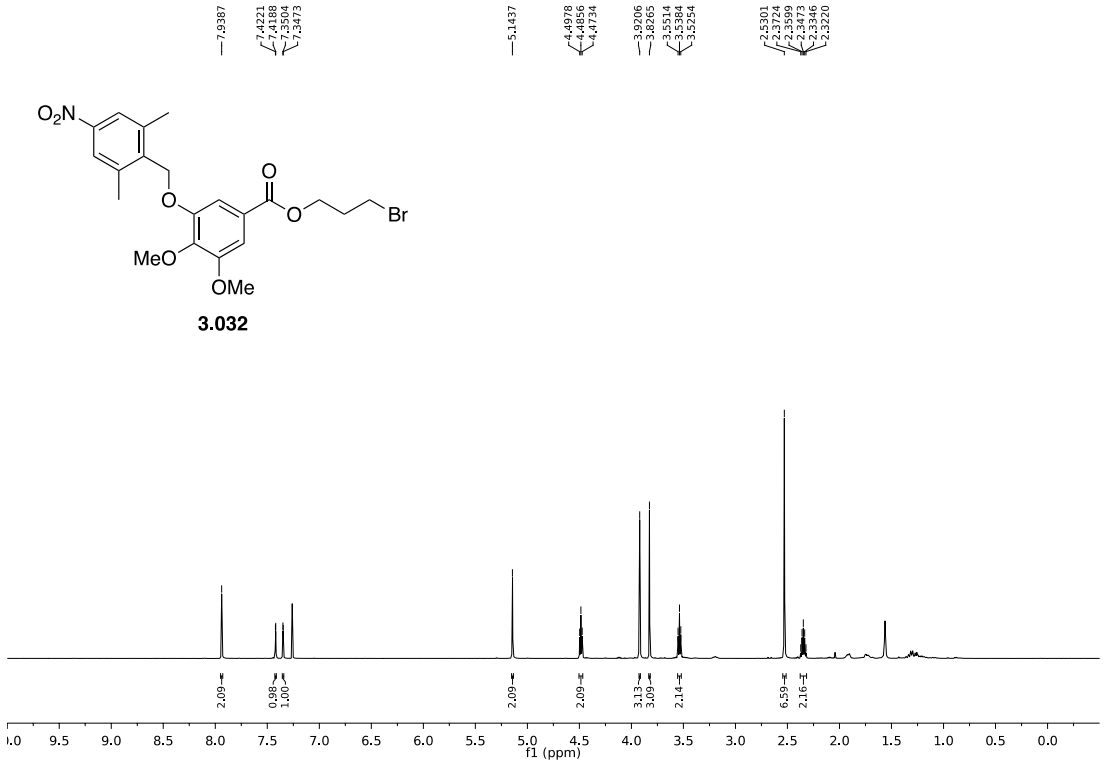
7.9387
7.4221
7.4188
7.3504
7.3473
5.1437
4.4978
4.4856
4.4734
3.9206
3.8265
3.5514
3.5384
3.5254
2.5301
2.3724
2.3599
2.3473
2.3346
2.3220
2.09
0.98
1.00
2.09
2.09
3.13
3.09
2.14
6.59
2.16
f1 (ppm)

3.032

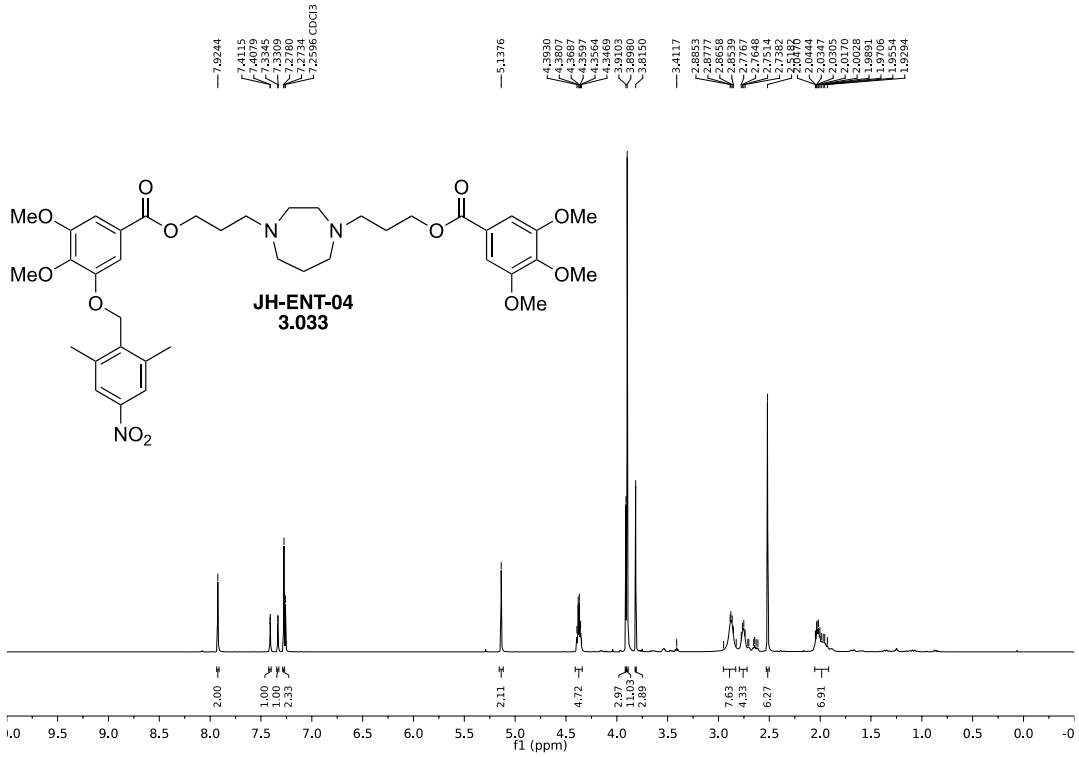
JH-ENT-04
3.033
f1 (ppm)

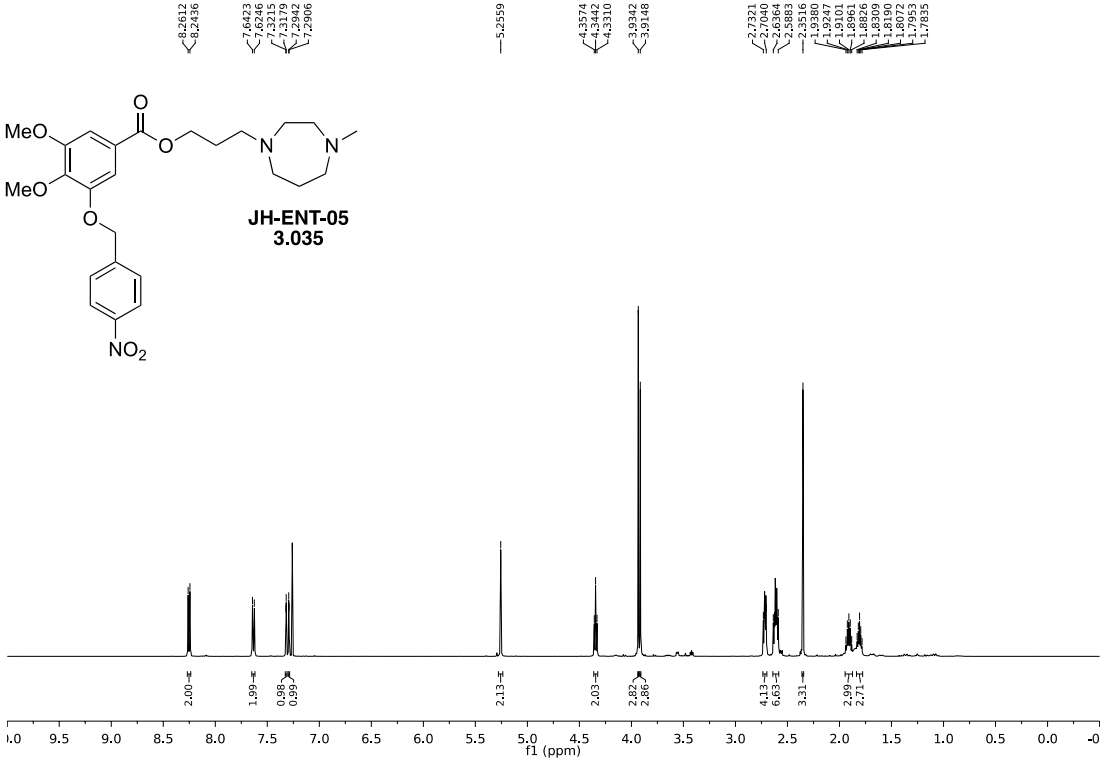
JH-ENT-05
3.035
f1 (ppm)

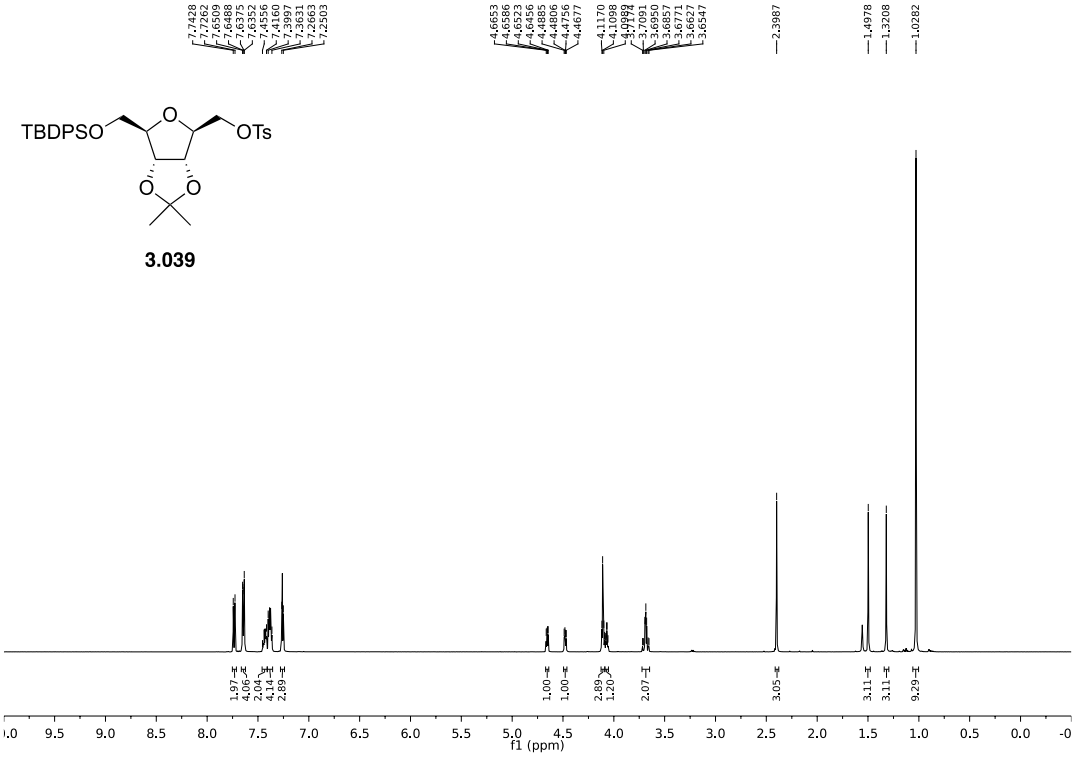
TBDPSO
OTs
O
O
O
3.039
f1 (ppm)

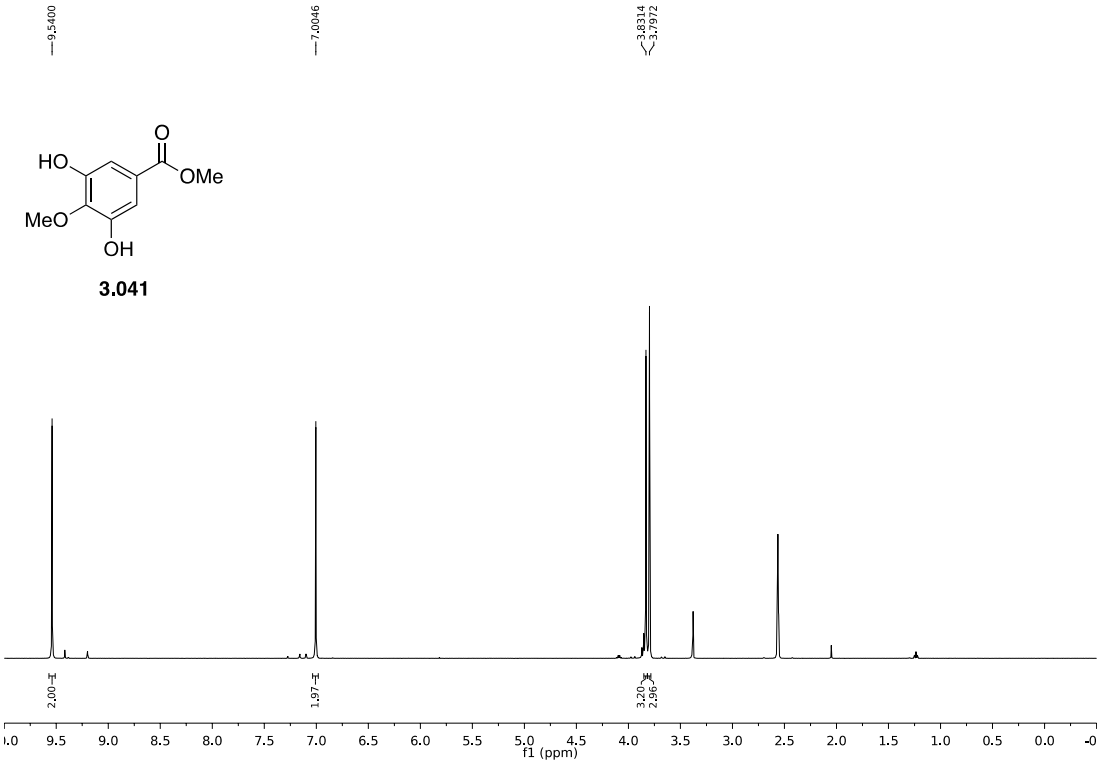
HO
MeO
OH
O
OMe
3.041
f1 (ppm)

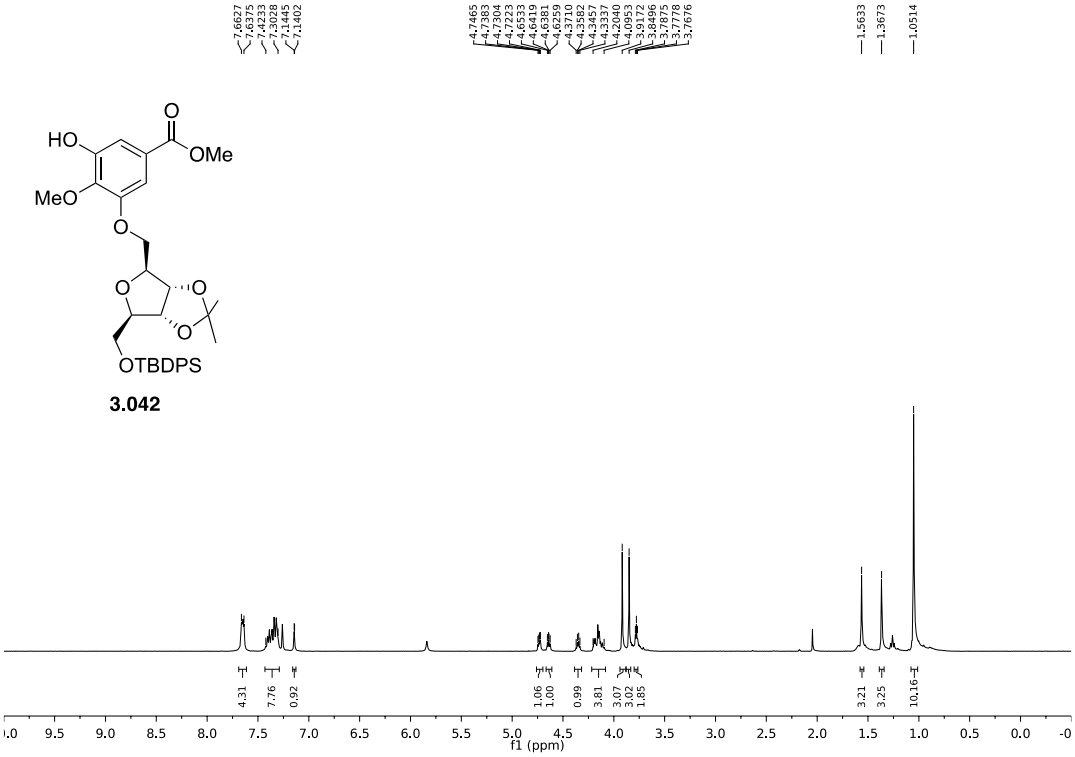
HO
OMe
MeO
O
O
O
O
OTBDPS
3.042
f1 (ppm)

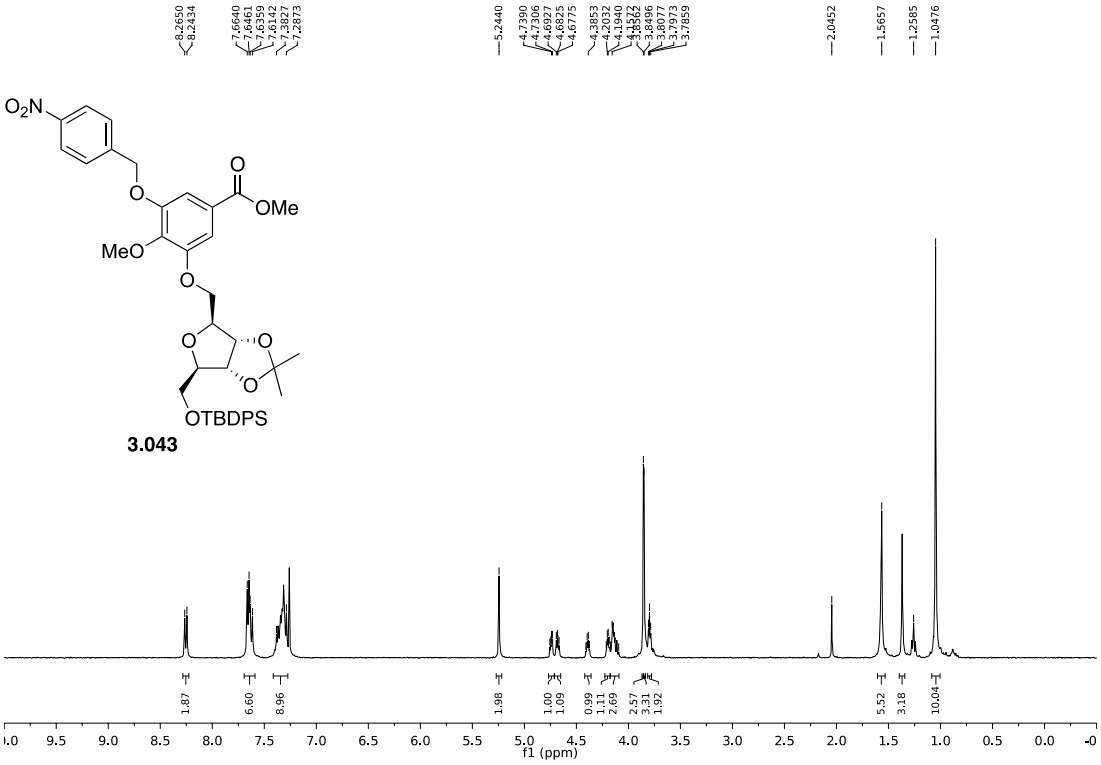
O2N
O
OMe
MeO
O
O
O
O
OTBDPS
3.043
f1 (ppm)

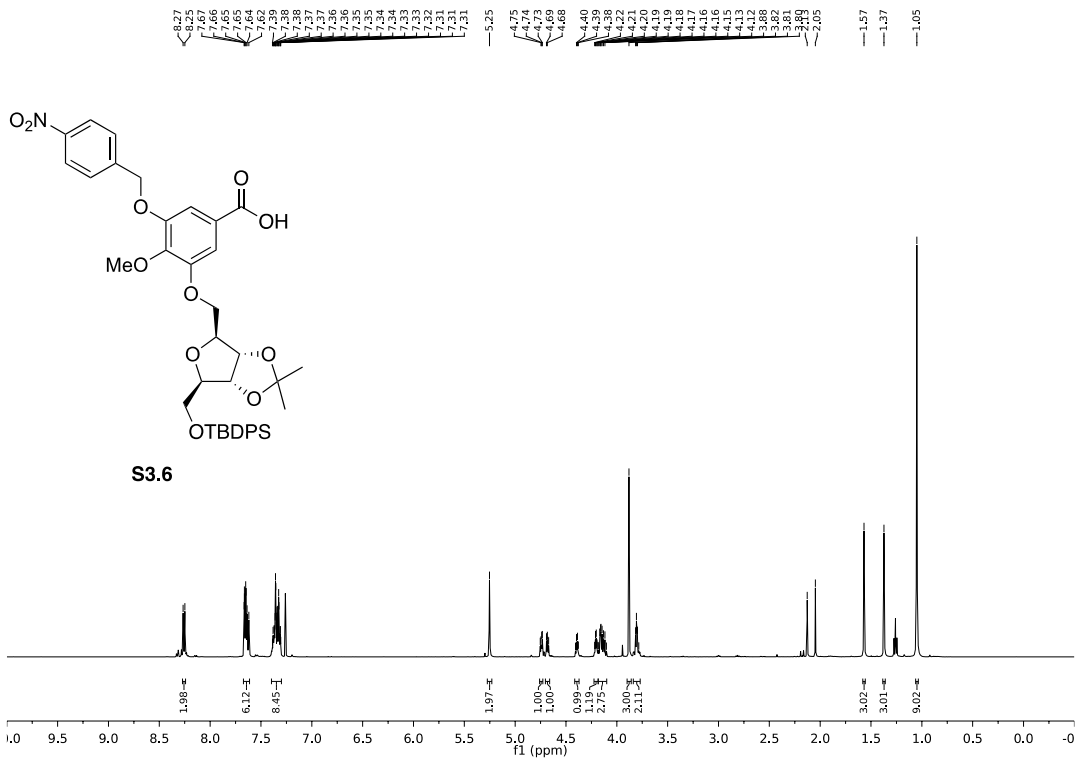
O2N
O
OH
MeO
O
OTBDPS
S3.6
f1 (ppm)

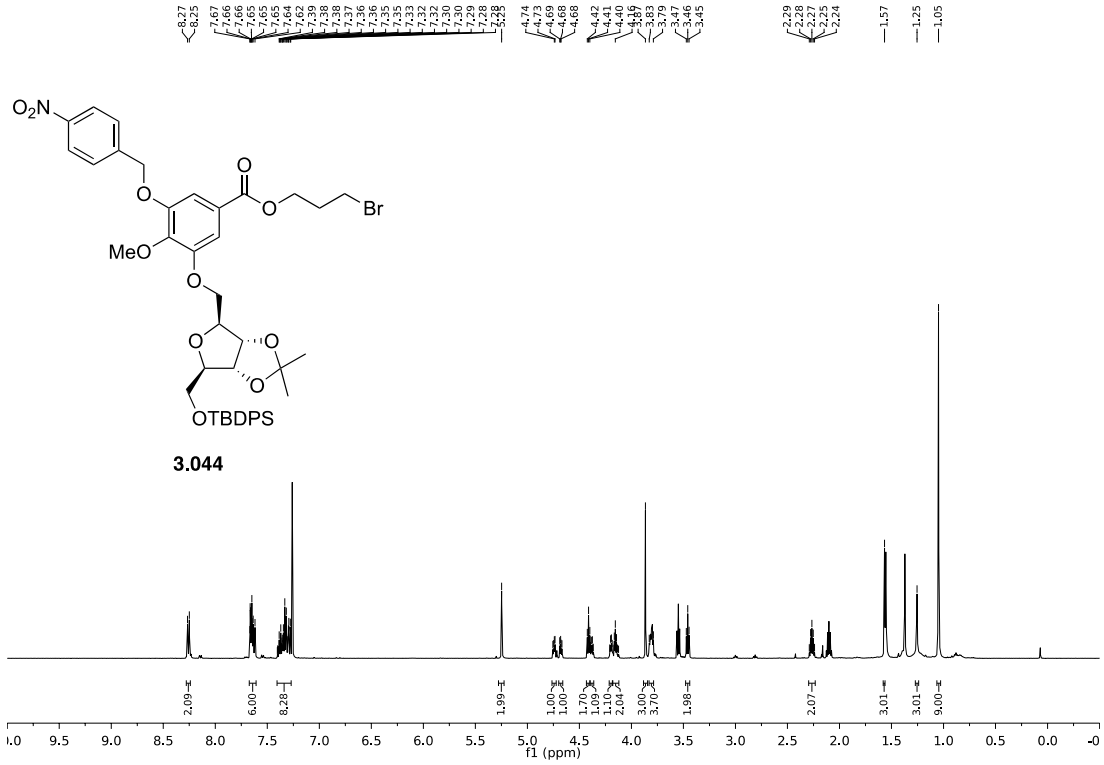
O2N
O
Br
MeO
OTBDPS
3.044
f1 (ppm)

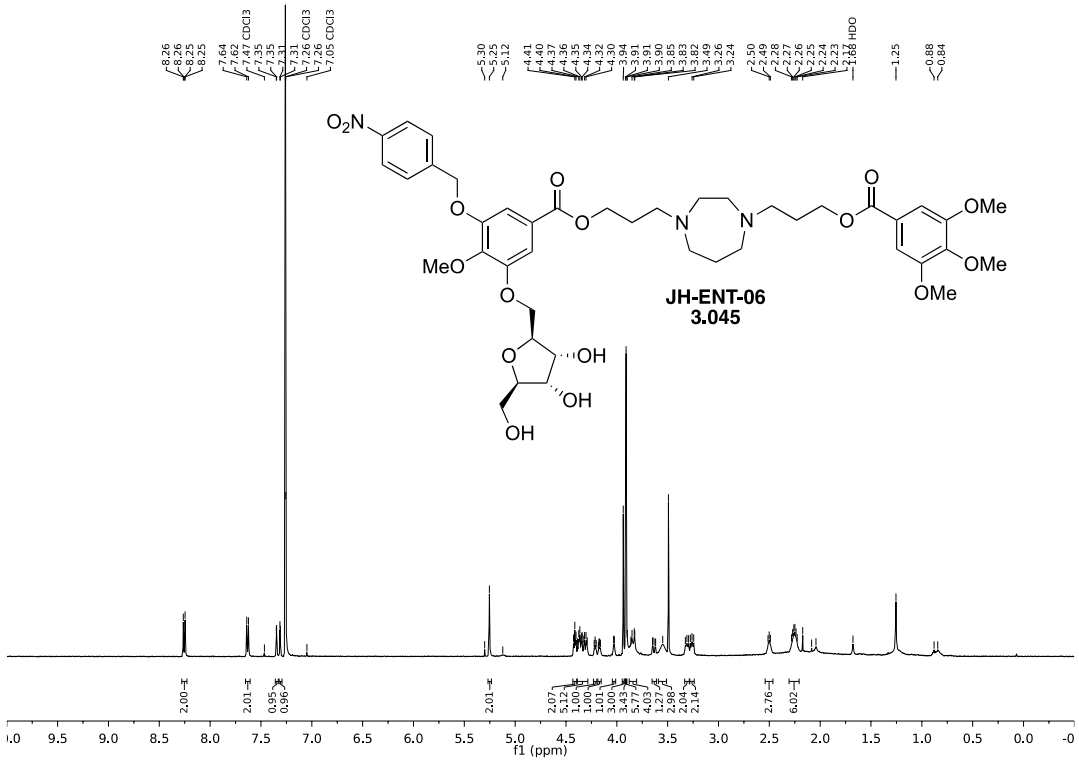
JH-ENT-06
3.045
f1 (ppm)

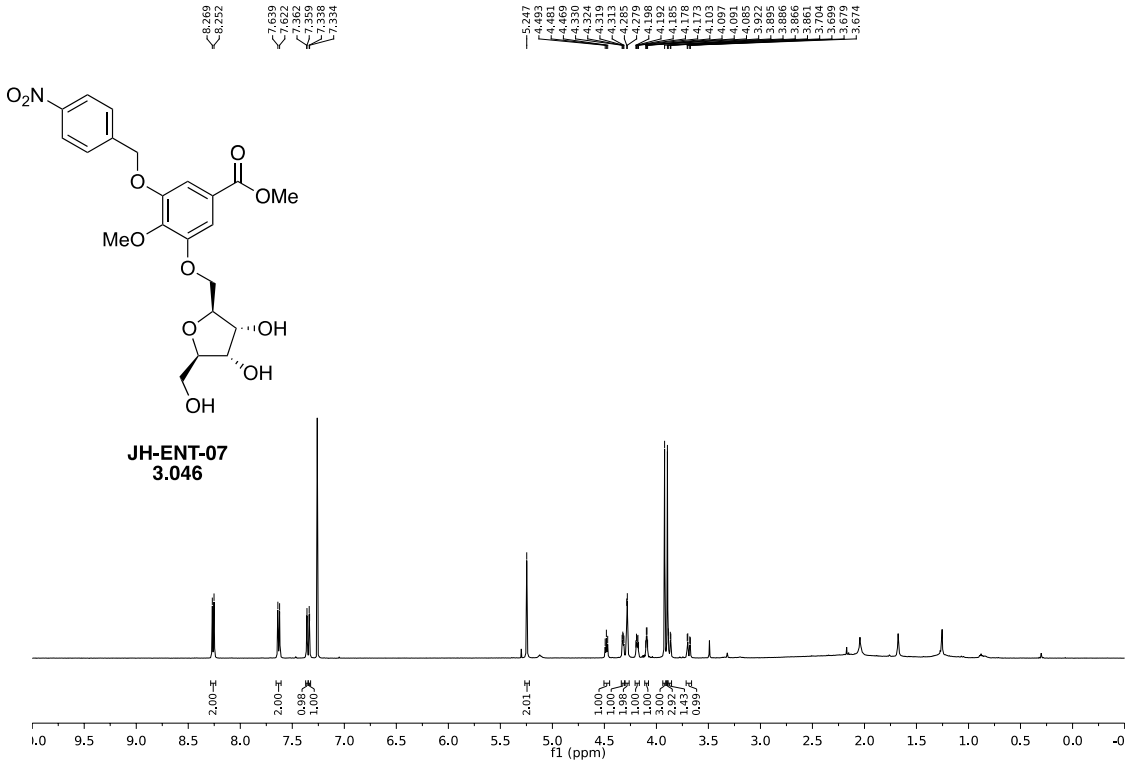
JH-ENT-07
3.046
f1 (ppm)

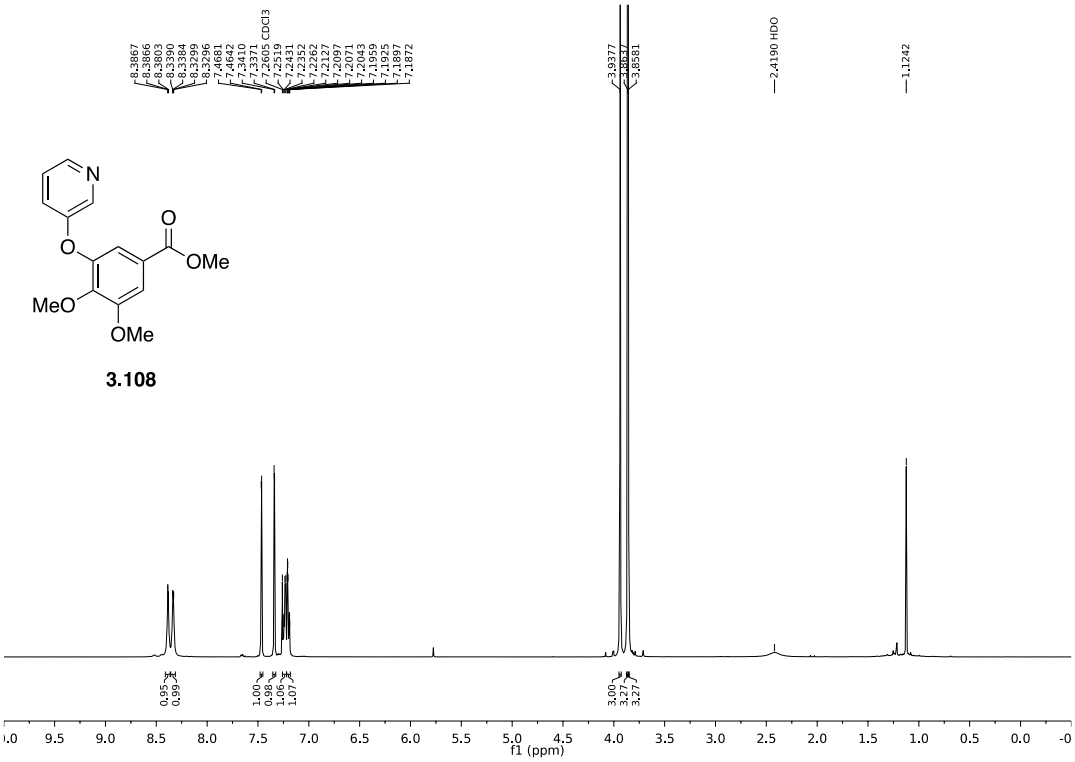
8.3867
8.3866
8.3393
8.3390
8.3384
8.3299
8.3296
7.4681
7.4442
7.3410
7.3371
7.2605 CDCl3
7.2519
7.2431
7.2352
7.2252
7.2227
7.2097
7.2071
7.2043
7.1959
7.1925
7.1897
7.1872
3.9377
3.8547
3.8581
2.4190 HDO
1.1242
0.95
0.99
1.00
0.98
1.06
1.07
3.00
3.27
3.27
f1 (ppm)

N
O
O
OMe
MeO
OMe

3.108

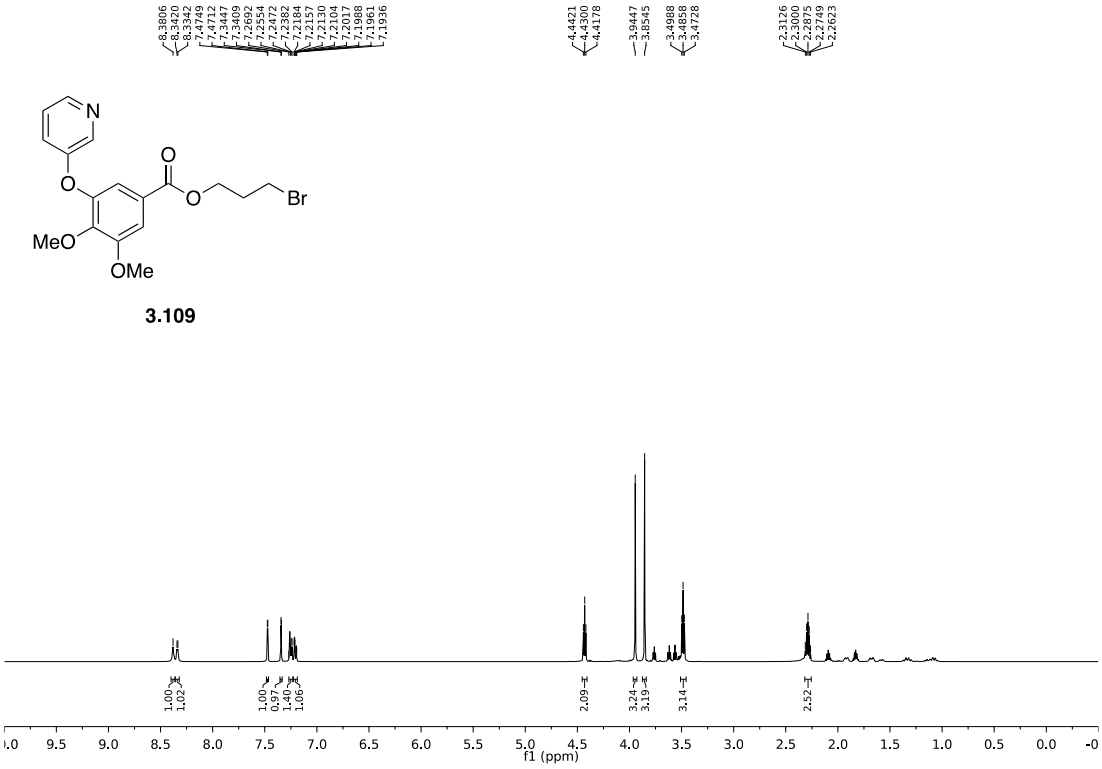
8.3806
8.3420
8.3342
8.3249
7.4712
7.3447
7.3409
7.2692
7.2554
7.2472
7.2282
7.2184
7.2157
7.2130
7.2104
7.2017
7.1988
7.1961
7.1936
4.4421
4.4300
4.4178
3.9447
3.8545
3.4988
3.4858
3.4728
2.3126
2.3000
2.2875
2.2749
2.2623
1.00
1.02
1.00
0.97
1.40
1.06
2.09
3.24
3.19
3.14
2.52
f1 (ppm)

N
O
O
O
Br
MeO
OMe

3.109

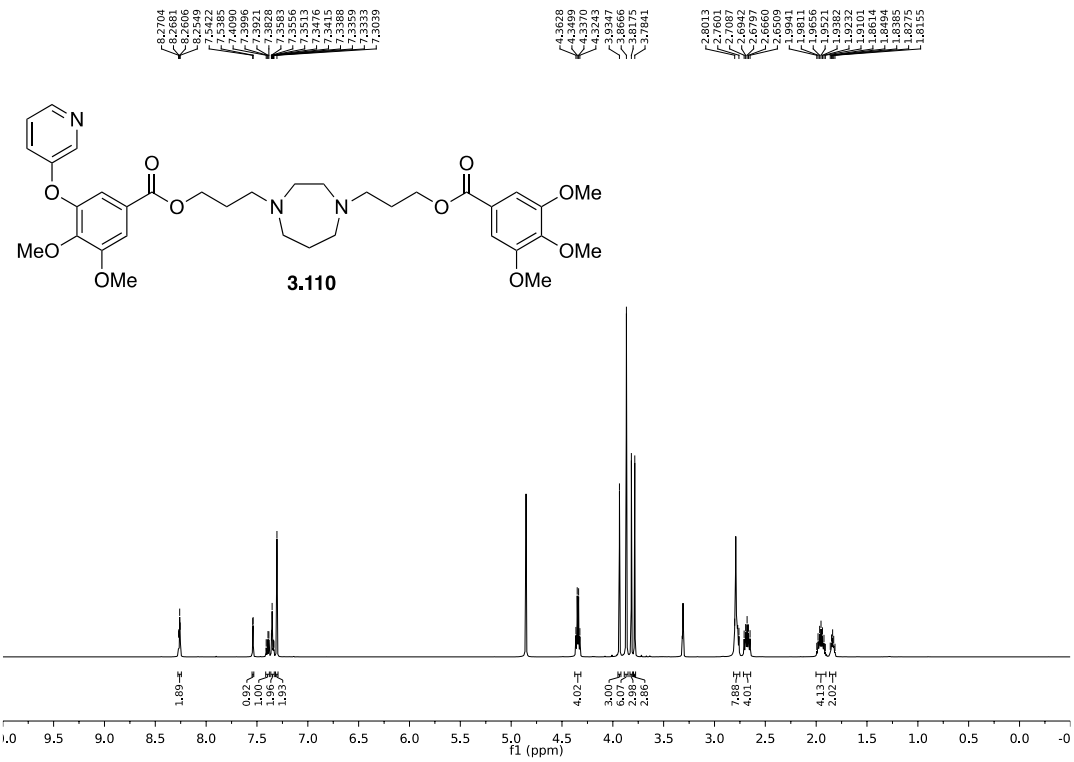
3.110
f1 (ppm)

References

(1) Peirs, C.; Seal, R. P. Neural circuits for pain: Recent advances and current views. *Science* **2016**, *354* (6312), 578-584.

(2) Institute of Medicine Committee on Pain, D.; Chronic Illness, B. In *Pain and Disability: Clinical, Behavioral, and Public Policy Perspectives*, Osterweis, M., Kleinman, A., Mechanic, D. Eds.; National Academies Press (US) Copyright © 1987 by the National Academy of Sciences., 1987.

(3) Pain: Types and Pathways. https://www.lecturio.com/concepts/physiology-of-pain/

(4) Yong, R. J.; Mullins, P. M.; Bhattacharyya, N. Prevalence of chronic pain among adults in the United States. *Pain* **2022**, *163* (2), e328-e332.

(5) Melnikova, I. Pain market. *Nature Reviews Drug Discovery* **2010**, *9* (8), 589-590.

(6) Prevalence of Chronic Pain and High-Impact Chronic Pain Among Adults-United States, 2016. https://www.cdc.gov/mmwr/volumes/67/wr/mm6736a2.htm

(7) Schjerning, A.-M.; McGettigan, P.; Gislason, G. Cardiovascular effects and safety of (non-aspirin) NSAIDs. *Nature Reviews Cardiology* **2020**, *17* (9), 574-584.

(8) Trang, T.; Al-Hasani, R.; Salvemini, D.; Salter, M. W.; Gutstein, H.; Cahill, C. M. Pain and Poppies: The Good, the Bad, and the Ugly of Opioid Analgesics. *The Journal of Neuroscience* **2015**, *35* (41), 13879.

(9) Overdose death rates. https://nida.nih.gov/research-topics/trends-statistics/overdose-death-rates

(10) Florence, C.; Luo, F.; Rice, K. The economic burden of opioid use disorder and fatal opioid overdose in the United States, 2017. *Drug Alcohol Depend* **2021**, *218*, 108350.

(11) Prioritizing pain research in 2022. https://www.nia.nih.gov/research/blog/2022/02/prioritizing-pain-research-2022

(12) Understanding the Epidemic. https://www.cdc.gov/drugoverdose/epidemic/index.html

(13) Yekkirala, A. S.; Roberson, D. P.; Bean, B. P.; Woolf, C. J. Breaking barriers to novel analgesic drug development. *Nature Reviews Drug Discovery* **2017**, *16* (8), 545-564.

(14) Dias, D. A.; Urban, S.; Roessner, U. A historical overview of natural products in drug discovery. *Metabolites* **2012**, *2* (2), 303-336.

(15) Atanasov, A. G.; Zotchev, S. B.; Dirsch, V. M.; Orhan, I. E.; Banach, M.; Rollinger, J. M.; Barreca, D.; Weckwerth, W.; Bauer, R.; Bayer, E. A.; et al. Natural products in drug discovery: advances and opportunities. *Nature Reviews Drug Discovery* **2021**, *20* (3), 200-216.

(16) Newman, D. J.; Cragg, G. M. Natural Products as Sources of New Drugs over the Nearly Four Decades from 01/1981 to 09/2019. *Journal of Natural Products* **2020**, *83* (3), 770-803.

(17) Li, C. H.; Zhang, J. Y.; Zhang, X. Y.; Li, S. H.; Gao, J. M. An overview of grayanane diterpenoids and their biological activities from the Ericaceae family in the last seven years. *Eur J Med Chem* **2019**, *166*, 400-416.

(18) Jansen, S. A.; Kleerekooper, I.; Hofman, Z. L.; Kappen, I. F.; Stary-Weinzinger, A.; van der Heyden, M. A. Grayanotoxin poisoning: 'mad honey disease' and beyond. *Cardiovasc Toxicol* **2012**, *12* (3), 208-215.

(19) Li, Y.; Liu, Y.-B.; Zhang, J.-J.; Liu, Y.; Ma, S.-G.; Qu, J.; Lv, H.-N.; Yu, S.-S. Antinociceptive Grayanoids from the Roots of Rhododendron molle. *Journal of Natural Products* **2015**, *78* (12), 2887-2895.

(20) Hamanaka, N.; Matsumoto, T. Partial Synthesis of Grayanotoxin. *Tetrahedron Letters* **1972**, *13* (30), 3087-3090.

(21) Kan, T.; Hosokawa, S.; Nara, S.; Oikawa, M.; Ito, S.; Matsuda, F.; Shirahama, H. Total Synthesis of (-)-Grayanotoxin III. *The Journal of Organic Chemistry* **1994**, *59* (19), 5532-5534.

(22) Borrelly, S.; Paquette, L. A. Studies Directed to the Synthesis of the Unusual Cardiotoxic Agent Kalmanol. Enantioselective Construction of the Advanced Tetracyclic 7-Oxy-5,6-dideoxy Congener. *Journal of the American Chemical Society* **1996**, *118* (4), 727-740.

(23) Chow, S.; Kreß, C.; Albæk, N.; Jessen, C.; Williams, C. M. Determining a Synthetic Approach to Pierisformaside C. *Organic Letters* **2011**, *13* (19), 5286-5289.

(24) Turlik, A.; Chen, Y.; Scruse, A. C.; Newhouse, T. R. Convergent Total Synthesis of Principinol D, a Rearranged Kaurane Diterpenoid. *Journal of the American Chemical Society* **2019**, *141* (20), 8088-8092.

(25) Yu, K.; Yang, Z.-N.; Liu, C.-H.; Wu, S.-Q.; Hong, X.; Zhao, X.-L.; Ding, H. Total Syntheses of Rhodomolleins XX and XXII: A Reductive Epoxide-Opening/Beckwith–Dowd Approach. *Angewandte Chemie International Edition* **2019**, *58* (25), 8556-8560.

(26) Guo, J.; Li, B.; Ma, W.; Pitchakuntla, M.; Jia, Y. Total Synthesis of (−)-Glaucocalyxin A. *Angewandte Chemie International Edition* **2020**, *59* (35), 15195-15198.

(27) Kong, L.; Yu, H.; Deng, M.; Wu, F.; Jiang, Z.; Luo, T. Enantioselective Total Syntheses of Grayanane Diterpenoids: (−)-Grayanotoxin III, (+)-Principinol E, and (−)-Rhodomollein XX. *Journal of the American Chemical Society* **2022**, *144* (12), 5268-5273.

(28) Lopchuk, J. M.; Green, I. L.; Badenock, J. C.; Gribble, G. W. A Short, Protecting Group-Free Total Synthesis of Bruceollines D, E, and J. *Organic Letters* **2013**, *15* (17), 4485-4487.

(29) Budny, M.; Włodarczyk, J.; Muzioł, T.; Bosiak, M. J.; Wolan, A. Stereoselective synthesis of two potential metabolites of cis-metconazole. *Tetrahedron Letters* **2017**, *58* (45), 4285-4288.

(30) Wang, J.; Sun, B.-F.; Cui, K.; Lin, G.-Q. An Efficient Total Synthesis of (−)-Epothilone B. *Organic Letters* **2012**, *14* (24), 6354-6357.

(31) Zhan, F.; Liang, G. Formation of Enehydrazine Intermediates through Coupling of Phenylhydrazines with Vinyl Halides: Entry into the Fischer Indole Synthesis. *Angewandte Chemie International Edition* **2013**, *52* (4), 1266-1269.

(32) Darwish, A.; Chong, J. M. A Practical One-Pot Synthesis of Vinylstannanes from Ketones. *The Journal of Organic Chemistry* **2007**, *72* (4), 1507-1509.

(33) Lim, B.-Y.; Jung, B.-E.; Cho, C.-G. Ene-hydrazide from Enol Triflate for the Regioselective Fischer Indole Synthesis. *Organic Letters* **2014**, *16* (17), 4492-4495.

(34) Xu, W.; Zhang, X. M.; Mariano, P. S. Single electron transfer promoted photocyclization reactions of (aminoalkyl)cyclohexenones. Mechanistic and synthetic features of processes involving the generation and reactions of amine cation and .alpha.-amino radicals. *Journal of the American Chemical Society* **1991**, *113* (23), 8863-8878.

(35) J.M. Conia, P. L. P. The Thermal Cyclisation of Unsaturated Carbonyl Compounds. *Synthesis* **1975**, 1-19.

(36) Hack, D.; Blümel, M.; Chauhan, P.; Philipps, A. R.; Enders, D. Catalytic Conia-ene and related reactions. *Chemical Society Reviews* **2015**, *44* (17), 6059-6093.

(37) Sladojevich, F.; Michaelides, I. N.; Darses, B.; Ward, J. W.; Dixon, D. J. Expedient Route to the Functionalized Calyciphylline A-Type Skeleton via a Michael Addition–RCM Strategy. *Organic Letters* **2011**, *13* (19), 5132-5135.

(38) Hartrampf, F. W. W.; Furukawa, T.; Trauner, D. A Conia-Ene-Type Cyclization under Basic Conditions Enables an Efficient Synthesis of (−)-Lycoposerramine R. *Angewandte Chemie International Edition* **2017**, *56* (3), 893-896.

(39) Kennedy-Smith, J. J.; Staben, S. T.; Toste, F. D. Gold(I)-Catalyzed Conia-Ene Reaction of β-Ketoesters with Alkynes. *Journal of the American Chemical Society* **2004**, *126* (14), 4526-4527.

(40) Huwyler, N.; Carreira, E. M. Total Synthesis and Stereochemical Revision of the Chlorinated Sesquiterpene (±)-Gomerone C. *Angewandte Chemie International Edition* **2012**, *51* (52), 13066-13069.

(41) Chan, J.; Jamison, T. F. Enantioselective Synthesis of (−)-Terpestacin and Structural Revision of Siccanol Using Catalytic Stereoselective Fragment Couplings and Macrocyclizations. *Journal of the American Chemical Society* **2004**, *126* (34), 10682-10691.

(42) Barabé, F.; Bétournay, G.; Bellavance, G.; Barriault, L. Gold-Catalyzed Synthesis of Carbon-Bridged Medium-Sized Rings. *Organic Letters* **2009**, *11* (18), 4236-4238.

(43) O'Neil, S. V.; Quickley, C. A.; Snider, B. B. Synthesis of (±)-Gymnomitrol. Mn(OAc)3-Initiated Free-Radical Cyclization of Alkynyl Ketones. *The Journal of Organic Chemistry* **1997**, *62* (7), 1970-1975.

(44) Amat, M.; Arioli, F.; Pérez, M.; Molins, E.; Bosch, J. Preparation and Double Michael Addition Reactions of a Synthetic Equivalent of the Nazarov Reagent. *Organic Letters* **2013**, *15* (10), 2470-2473.

(45) Singh, A. K.; Bakshi, R. K.; Corey, E. J. Total synthesis of (.+-.)-atractyligenin. *Journal of the American Chemical Society* **1987**, *109* (20), 6187-6189.

(46) Szostak, M.; Spain, M.; Procter, D. J. Recent advances in the chemoselective reduction of functional groups mediated by samarium(ii) iodide: a single electron transfer approach. *Chemical Society Reviews* **2013**, *42* (23), 9155-9183.

(47) Zeror, S.; Collin, J.; Fiaud, J.-C.; Zouioueche, L. A. Enantioselective ketoester reductions in water: a comparison between microorganism- and ruthenium-catalyzed reactions. *Tetrahedron: Asymmetry* **2010**, *21* (9), 1211-1215.

(48) Germain, N.; Alexakis, A. Formation of Contiguous Quaternary and Tertiary Stereocenters by Sequential Asymmetric Conjugate Addition of Grignard Reagents to 2-Substituted Enones and Mg–Enolate Trapping. *Chemistry – A European Journal* **2015**, *21* (23), 8597-8606.

(49) Magrez, M.; Le Guen, Y.; Baslé, O.; Crévisy, C.; Mauduit, M. Bidentate Hydroxyalkyl NHC Ligands for the Copper-Catalyzed Asymmetric Allylic Substitution of Allyl Phosphates with Grignard Reagents. *Chemistry – A European Journal* **2013**, *19* (4), 1199-1203.

(50) Westmeier, J.; Pfaff, C.; Siewert, J.; von Zezschwitz, P. First Tandem Asymmetric Conjugate Addition of Alkenyl Nucleophiles and Silyl Trapping of the Intermediate Enolates. *Advanced Synthesis & Catalysis* **2013**, *355* (13), 2651-2658.

(51) Helmchen, G.; Wegner, G. Asymmetric synthesis of β-substituted alcanoic acids via highly stereoselective conjugate additions of organocopper compounds to chiral enoates. *Tetrahedron Letters* **1985**, *26* (49), 6051-6054.

(52) Urban, E.; Richs, G.; Knühl, G. Enantiomerically Pure 6-Substituted 2-Oxo-cyclohexanecarboxylates by Conjugate Addition of Cuprates to Asymmetric Shielded 2-Oxo-cyclohexenecarboxylates. *Tetrahedron* **1995**, *51* (41), 11149-11164.

(53) Denmark, S. E.; Rivera, I. Asymmetric Carboalkoxyalkylidenation with a Chiral Horner-Wadsworth-Emmons Reagent. *The Journal of Organic Chemistry* **1994**, *59* (23), 6887-6889.

(54) Rehan, S.; Shahid, S.; Salminen, T. A.; Jaakola, V. P.; Paavilainen, V. O. Current Progress on Equilibrative Nucleoside Transporter Function and Inhibitor Design. *SLAS Discov* **2019**, *24* (10), 953-968.

(55) Young, J. D.; Yao, S. Y.; Sun, L.; Cass, C. E.; Baldwin, S. A. Human equilibrative nucleoside transporter (ENT) family of nucleoside and nucleobase transporter proteins. *Xenobiotica* **2008**, *38* (7-8), 995-1021.

(56) Perez-Torras, M. P.-A. a. S. Emerging Roles of Nucleoside Transporters. *Frontiers in pharmacology* **2018**, *9* (606), 1-8.

(57) Boswell-Casteel, R. C.; Hays, F. A. Equilibrative nucleoside transporters—A review. *Nucleosides, Nucleotides & Nucleic Acids* **2017**, *36* (1), 7-30.

(58) Wright, N. J.; Lee, S.-Y. Toward a Molecular Basis of Cellular Nucleoside Transport in Humans. *Chemical Reviews* **2021**, *121* (9), 5336-5358.

(59) Zhou, M.; Wu, J.; Chang, H.; Fang, Y.; Zhang, D.; Guo, Y. Adenosine signaling mediate pain transmission in the central nervous system. *Purinergic Signalling* **2022**.

(60) Zylka, M. J. Pain-relieving prospects for adenosine receptors and ectonucleotidases. *Trends Mol Med* **2011**, *17* (4), 188-196.

(61) Maes, S. S.; Pype, S.; Hoffmann, V. L.; Biermans, M.; Meert, T. F. Antihyperalgesic activity of nucleoside transport inhibitors in models of inflammatory pain in guinea pigs. *Journal of pain research* **2012**, *5*, 391.

(62) Vlachodimou, A.; Ijzerman, A. P.; Heitman, L. H. Label-free detection of transporter activity via GPCR signalling in living cells: A case for SLC29A1, the equilibrative nucleoside transporter 1. *Scientific Reports* **2019**, *9* (1), 13802.

(63) Governo, R. J.; Deuchars, J.; Baldwin, S. A.; King, A. E. Localization of the NBMPR-sensitive equilibrative nucleoside transporter, ENT1, in the rat dorsal root ganglion and lumbar spinal cord. *Brain Res* **2005**, *1059* (2), 129-138.

(64) Choca, J. I.; Proudfit, H. K.; Green, R. D. Identification of A1 and A2 adenosine receptors in the rat spinal cord. *J Pharmacol Exp Ther* **1987**, *242* (3), 905-910.

(65) Choca, J. I.; Green, R. D.; Proudfit, H. K. Adenosine A1 and A2 receptors of the substantia gelatinosa are located predominantly on intrinsic neurons: an autoradiography study. *J Pharmacol Exp Ther* **1988**, *247* (2), 757-764.

(66) Keil, G. J., 2nd; Delander, G. E. Time-dependent antinociceptive interactions between opioids and nucleoside transport inhibitors. *J Pharmacol Exp Ther* **1995**, *274* (3), 1387-1392.

(67) Merskey, H.; Hamilton, J. T. An open label trial of the possible analgesic effects of dipyridamole. *J Pain Symptom Manage* **1989**, *4* (1), 34-37.

(68) Kvien, T. K.; Fjeld, E.; Slatkowsky-Christensen, B.; Nichols, M.; Zhang, Y.; Prøven, A.; Mikkelsen, K.; Palm, Ø.; Borisy, A. A.; Lessem, J. Efficacy and safety of a novel synergistic drug candidate, CRx-102, in hand osteoarthritis. *Ann Rheum Dis* **2008**, *67* (7), 942-948.

(69) Wright, N. J.; Lee, S.-Y. Structures of human ENT1 in complex with adenosine reuptake inhibitors. *Nature Structural & Molecular Biology* **2019**, *26* (7), 599-606.

(70) Isamu Shiina, R. M. 2,6-dimethyl-4-nitrobenzoic anhydride (DMNBA): An effective coupling reagent for the synthesis of carboxylic esters and lactones. *Heterocycles* **2008**, *76* (2), 1313-1328.

(71) Morelli, C. F.; Monica, M.; Veronese, A. C. A new route to the synthesis of pyrazole and pyrimidine C-nucleoside derivatives. *Tetrahedron* **1999**, *55* (35), 10803-10814.

(72) Owen, D. J.; Thomson, R. J.; von Itzstein, M. A convenient synthesis of C-galactofuranosylic compounds (C-galactofuranosides). *Carbohydrate Research* **2002**, *337* (21), 2017-2022.

(73) Wei, C. W.; Lee, C. Y.; Lee, D. J.; Chu, C. F.; Wang, J. C.; Wang, T. C.; Jane, W. N.; Chang, Z. F.; Leu, C. M.; Dzhagalov, I. L.; et al. Equilibrative Nucleoside Transporter 3 Regulates T Cell Homeostasis by Coordinating Lysosomal Function with Nucleoside Availability. *Cell Rep* **2018**, *23* (8), 2330-2341.

(74) Zhang, Q.; Zhong, Y.; Yan, L.-N.; Sun, X.; Gong, T.; Zhang, Z.-R. Synthesis and preliminary evaluation of curcumin analogues as cytotoxic agents. *Bioorganic & Medicinal Chemistry Letters* **2011**, *21* (3), 1010-1014.

(75) Antilla, J. C.; Baskin, J. M.; Barder, T. E.; Buchwald, S. L. Copper−Diamine-Catalyzed N-Arylation of Pyrroles, Pyrazoles, Indazoles, Imidazoles, and Triazoles. *The Journal of Organic Chemistry* **2004**, *69* (17), 5578-5587.

Biography

Caroline Webster earned her Bachelor of Arts in Chemistry from Syracuse University in 2016. She began her graduate career at Duke University in the fall of 2017 and received her Doctor of Philosophy in organic chemistry in September of 2022. Caroline was awarded the C.R. Hauser Memorial Fellowship in 2020 and participated in the Pharmacological Sciences Training Program from 2018- 2020.